

# **ELEMENTS OF SOLID STATE PHYSICS**

**SECOND EDITION**

**J.P. SRIVASTAVA**

Former Professor of Physics  
Aligarh Muslim University  
Aligarh

**PHI Learning Private Limited**

New Delhi-110001  
2009

## Contents

<i>Preface</i>	xiii
<i>Preface to the First Edition</i>	xv
<b>1. THE CRYSTALLINE STATE</b>	<b>1–31</b>
1.1 Basis of Crystal Structure 1	
1.2 Unit Cell—Primitive Cell Structures 3	
1.3 Symmetry Operations 7	
1.3.1 Translation Operations 7	
1.3.2 Point Operations 8	
1.3.3 Hybrid Operations 10	
1.4 Crystal Types 11	
1.4.1 Two-dimensional Crystal Lattices 12	
1.4.2 Three-dimensional Crystal Lattices 13	
1.5 Indices of a Lattice Direction and a Lattice Plane 15	
1.6 Crystal Point Groups and Space Groups 17	
1.6.1 Point Groups 17	
1.6.2 Space Groups 17	
1.7 Common Crystal Structures 20	
1.7.1 The Simplest Crystal 20	
1.7.2 The CsCl Structure 20	
1.7.3 Crystals of Alkali Metals 21	
1.7.4 Crystals of Noble Metals 21	
1.7.5 The NaCl Structure 21	
1.7.6 Close-packed Structures 22	
1.7.7 Hexagonal Close-packed Structure (HCP) 23	
1.7.8 Diamond Structure 27	
1.8 Quasicrystals 29	
Summary 29	
Problems 30	
Suggested Further Reading 31	
<b>2. ATOMIC COHESION AND CRYSTAL BINDING</b>	<b>32–62</b>
2.1 Cohesion of Atoms 32	
2.2 Primary Bonds 34	
2.2.1 The Covalent Bond 34	
2.2.2 The Metallic Bond 34	
2.2.3 The Ionic Bond 35	
2.2.4 Mixed Bonding 35	

2.3	Secondary Bonds	36
2.3.1	The van der Waals Bond	37
2.3.2	The Hydrogen Bond	37
2.4	The Cohesive Energy	39
2.4.1	Ionic Crystals	40
2.4.2	Noble Gas Crystals	43
2.5	Atomic Radii vs Lattice Constants	45
2.6	Elastic Constants of Crystals	47
2.6.1	Elastic Stress	48
2.6.2	Elastic Strain	48
2.6.3	Dilation	51
2.7	Elastic Compliance and Stiffness Constants	51
2.7.1	Elastic Energy Density	52
2.7.2	Application to Cubic Crystals	53
2.7.3	Bulk Modulus and Compressibility	54
2.8	Elastic Waves in Cubic Crystal	55
2.8.1	Propagation of Waves in the [100] Direction	57
2.8.2	Propagation of Waves in the [110] Direction	57
<i>Summary</i>		59
<i>Problems</i>		60
<i>Suggested Further Reading</i>		62
<b>3.</b>	<b>RECIPROCAL LATTICE AND DETERMINATION OF CRYSTAL STRUCTURE</b>	<b>63–97</b>
3.1	Reciprocal Lattice	63
3.2	Bragg Law	66
3.3	Laue's Interpretation of X-ray Diffraction by Crystals	68
3.4	Construction of Reciprocal Lattice	70
3.5	Relationships between $a$ , $b$ , $c$ and $a^*$ , $b^*$ , $c^*$	71
3.6	Application to Some Crystal Lattices	73
3.7	Analysis of X-ray Diffraction Patterns from Crystals	76
3.8	Measurement of Diffraction Pattern of Crystals	81
3.8.1	The Ewald Construction	82
3.8.2	Experimental Methods	82
3.9	Determination of Lattice Constants	87
3.10	Selection of Incident Beam	91
3.11	Field Ion Microscopy (FIM)	93
<i>Summary</i>		94
<i>Problems</i>		95
<i>Suggested Further Reading</i>		97
<b>4.</b>	<b>LATTICE VIBRATIONS</b>	<b>98–119</b>
4.1	The 'Balls and Springs' Model of a Harmonic Crystal	98
4.2	Normal Modes of a One-dimensional Monatomic Chain	100
4.2.1	The Periodic Boundary Condition	101
4.2.2	Salient Features of the Dispersion Curve	103
4.3	Normal Modes of One-dimensional Diatomic Chain	104
4.3.1	Salient Features of the Dispersion Curves	106

4.4	The Reststrahlen Band	108	
4.5	General Theory of Harmonic Approximation	109	
4.6	Normal Modes of Real Crystals	112	
4.7	Quantization of Lattice Vibrations	113	
4.8	Measurement of Phonon Dispersion by Inelastic Neutron Scattering	115	
	<i>Summary</i>	116	
	<i>Problems</i>	117	
	<i>Suggested Further Reading</i>	119	
<b>5.</b>	<b>THERMAL PROPERTIES OF SOLIDS</b>		<b>120–144</b>
5.1	Classical Lattice Heat Capacity	120	
5.2	Quantum Theory of Lattice Heat Capacity	121	
5.2.1	Average Thermal Energy of a Harmonic Oscillator	122	
5.2.2	Einstein Model	124	
5.2.3	Phonon Density of States	125	
5.2.4	Debye Continuum Model	127	
5.3	Anharmonic Effects	131	
5.3.1	Thermal Expansion	132	
5.3.2	Phonon Collision Processes	134	
5.3.3	Phonon Thermal Conductivity	136	
	<i>Summary</i>	142	
	<i>Problems</i>	143	
	<i>Suggested Further Reading</i>	144	
<b>6.</b>	<b>FREE ELECTRON THEORY OF METALS</b>		<b>145–182</b>
6.1	The Drude Model	146	
6.1.1	Electrical Conductivity of Metals	146	
6.1.2	Thermal Conductivity of Metals	150	
6.2	Lorentz Modification of the Drude Model	153	
6.3	The Fermi–Dirac Distribution Function	155	
6.4	The Sommerfeld Model	157	
6.4.1	The Density of States	160	
6.4.2	The Free Electron Gas at 0 K	162	
6.4.3	Energy of Electron Gas at 0 K	163	
6.5	The Electron Heat Capacity	163	
6.6	The Sommerfeld Theory of Electric Conduction in Metals	167	
6.6.1	The Hall Coefficient ( $R_H$ )	172	
6.7	Matthiessen's Rule	174	
6.8	Thermoelectric Effects	176	
6.8.1	Thermoelectric Power	176	
6.8.2	The Thomson Effect	177	
6.8.3	The Peltier Effect	178	
6.8.4	Kelvin (Thomson) Relations	179	
	<i>Summary</i>	179	
	<i>Problems</i>	181	
	<i>Suggested Further Reading</i>	182	

---

<b>7. ELECTRON ENERGY BANDS</b>	<b>183–210</b>
7.1 Consequences of Periodicity 183	
7.1.1 Proof of the Bloch Theorem 185	
7.1.2 The Periodicity of the Bloch Functions and Their Eigenvalues 186	
7.2 Wave Mechanical Interpretation of Energy Bands 187	
7.3 The Kronig–Penney Model 187	
7.4 The Nearly Free Electron Model 190	
7.5 Zone Schemes for Energy Bands 193	
7.6 Energy Bands in a General Periodic Potential 194	
7.6.1 Solution near the Zone Boundary 196	
7.7 Insulators, Semiconductors and Metals 197	
7.8 The Tight-binding Approximation 199	
7.9 The Wigner–Seitz Cellular Method 204	
7.9.1 Estimation of Cohesive Energy 207	
7.10 Methods of Band Structure Calculation in Use: A Qualitative View 207	
<i>Summary</i> 209	
<i>Problems</i> 209	
<i>Suggested Further Reading</i> 210	
<b>8. MOBILE ELECTRONS AND FERMI SURFACES</b>	<b>211–239</b>
8.1 Concept of Holes 211	
8.2 Effective Mass 214	
8.3 Construction of the Fermi Surfaces 217	
8.4 Electrons in a Uniform Magnetic Field 222	
8.4.1 Free Electrons 222	
8.4.2 Bloch Electrons 224	
8.5 Anomalous Skin Effect 226	
8.6 Cyclotron Resonance 227	
8.6.1 Semiconductors 227	
8.6.2 Metals 229	
8.7 Closed Orbits and Open Orbits 230	
8.8 de Haas–van Alphen Effect 232	
<i>Summary</i> 237	
<i>Problems</i> 239	
<i>Suggested Further Reading</i> 239	
<b>9. SEMICONDUCTORS</b>	<b>240–291</b>
9.1 Classification of Semiconductors 240	
9.2 Examples of Band Structure 242	
9.2.1 Silicon and Germanium 242	
9.2.2 Gallium Arsenide 244	
9.2.3 Determination of Band Gap 246	
9.3 Intrinsic Carrier Densities 247	
9.4 General Features of Extrinsic Semiconductors 253	
9.4.1 The <i>n</i> -type Semiconductors 253	
9.4.2 The <i>p</i> -type Semiconductors 256	

9.5 Population of Donor and Acceptor Levels in the State of Thermal Equilibrium	257
9.6 Extrinsic Carrier Densities	259
9.7 Temperature Dependence of Electrical Conductivity	263
9.8 Hall Effect and Magnetoresistance	266
9.9 The <i>p-n</i> Junction	269
9.10 Examples of <i>p-n</i> Junction-Based Devices	273
9.10.1 The Tunnel Diode	273
9.10.2 The Injection Laser	276
9.11 Thermoelectric Effects	278
9.12 Integral Quantum Hall Effect (IQHE)	282
<i>Summary</i>	288
<i>Problems</i>	289
<i>Suggested Further Reading</i>	291
<b>10. THEORY OF DIELECTRICS: APPLICATIONS TO PLASMONS, Polaritons and Polarons</b>	
	<b>292–328</b>
10.1 Polarization	292
10.2 Dielectric Constant	294
10.3 Local Electric Field	296
10.4 Dielectric Polarizability	299
10.5 Sources of Polarizability	300
10.5.1 Theory of Electronic Polarizability and Optical Absorption	300
10.5.2 Ionic Polarization	303
10.5.3 Polarization from Dipole Orientation	305
10.6 Dielectric Losses	308
10.7 Optical Phenomena	309
10.8 Application to Plasma	311
10.8.1 Plasma Oscillations	311
10.8.2 Transverse Optical Modes in Plasma	317
10.9 Application to Optical Phonon Modes in Ionic Crystals	319
10.9.1 The Longitudinal Optical Mode	320
10.9.2 The Transverse Optical Mode	320
10.10 The Interaction of Electromagnetic Waves with Optical Modes	321
10.11 Application to the Motion of Electrons in Polar Crystals	324
<i>Summary</i>	325
<i>Problems</i>	327
<i>Suggested Further Reading</i>	328
<b>11. FERROELECTRIC CRYSTALS</b>	
	<b>329–353</b>
11.1 Representative Crystal Types of Ferroelectrics	330
11.1.1 Properties of Rochelle Salt	332
11.1.2 Properties of BaTiO <sub>3</sub>	333
11.2 Theory of the Ferroelectric Displacive Transitions	335
11.2.1 Polarization Catastrophe	335
11.2.2 'Frozen in' Transverse Optical Phonons	339

---

11.3	Thermodynamic Theory of the Ferroelectric Transition	340
11.3.1	Second-order Transitions	342
11.3.2	First-order Transitions	344
11.4	Ferroelectric Domains	345
11.5	Antiferroelectricity	347
11.6	Piezoelectricity	347
11.7	Electrostriction	349
11.8	Applications of Piezoelectric Crystals	351
<i>Summary</i>	352	
<i>Problems</i>	352	
<i>Suggested Further Reading</i>	353	

**12. IMPERFECTIONS IN CRYSTALS** 354–386

12.1	Point Imperfections or Point Defects	355
12.2	Line Imperfections: Dislocations	371
12.2.1	Shear Strength and Processes of Plastic Flow	372
12.2.2	Dislocation Types	375
12.3	Stress Fields of Dislocations	377
12.4	Planar Imperfections: Grain Boundaries	379
12.5	Role of Dislocations in Crystal Growth	381
12.6	Strength of Alloys	382
<i>Summary</i>	384	
<i>Problems</i>	385	
<i>Suggested Further Reading</i>	386	

**13. DIAMAGNETISM AND PARAMAGNETISM** 387–429

13.1	Langevin's Theory of Diamagnetism	388
13.2	Langevin's Theory of Paramagnetism	391
13.3	Theory of Atomic Magnetic Moment	394
13.3.1	Hund's Rules	396
13.4	Quantum Theory of Magnetic Susceptibility: A Quantum Mechanical Formulation	397
13.4.1	Diamagnetism	400
13.4.2	Paramagnetism	400
13.4.3	Application to Magnetic Ions in Solids: Effect of the Crystal Field	403
13.5	van Vleck Paramagnetism	404
13.6	Pauli Paramagnetism	406
13.7	Nuclear Paramagnetism	409
13.8	Cooling by Adiabatic Demagnetization	410
13.9	Magnetic Resonance	414
13.9.1	Electron Spin Resonance (ESR)	415
13.9.2	Nuclear Magnetic Resonance (NMR)	418
13.9.3	Spin Relaxation	419
13.9.4	Line Width and Line Shape	421
<i>Summary</i>	424	
<i>Problems</i>	426	
<i>Suggested Further Reading</i>	429	

<b>14. FERROMAGNETISM, ANTIFERROMAGNETISM AND FERRIMAGNETISM</b>	<b>430–467</b>
14.1 Weiss Theory of Ferromagnetism 430	
14.2 The Exchange Interaction 436	
14.3 The Heisenberg Model 438	
14.4 Ferromagnetic Domains 440	
14.4.1 Technical Magnetization Curve 441	
14.4.2 Anisotropy Energy 442	
14.4.3 The Bloch Wall 444	
14.4.4 Origin of Domains 446	
14.5 Néel Model of Antiferromagnetism 447	
14.6 Néel Model of Ferrimagnetism 450	
14.7 Spin Waves 453	
14.7.1 Magnons in Ferromagnets 454	
14.7.2 The Bloch $T^{3/2}$ Law 456	
14.7.3 Magnons in Antiferromagnets 459	
14.8 Determination of Magnetically Ordered Structures 460	
14.9 Novel Magnetic Materials: GMR–CMR Materials 462	
<i>Summary</i> 465	
<i>Problems</i> 466	
<i>Suggested Further Reading</i> 467	
<b>15. SUPERCONDUCTIVITY</b>	<b>468–518</b>
15.1 Phenomena without Observable Quantization 470	
15.1.1 Zero Resistance and Persistent Currents 470	
15.1.2 Perfect Diamagnetism: Meissner Effect 471	
15.1.3 London Equations 475	
15.1.4 Critical Field: Type I and Type II Superconductors 478	
15.1.5 Thermodynamic Properties 479	
15.2 Energy Gap 483	
15.3 Properties Dependent on Energy Gap 484	
15.3.1 Heat Capacity 484	
15.3.2 Thermal Conductivity 485	
15.3.3 Absorption of Electromagnetic Radiation 486	
15.3.4 Normal Tunnelling 487	
15.4 Isotope Effect 488	
15.5 BCS Theory: A Qualitative Approach 490	
15.5.1 Cooper Pair Formation 490	
15.5.2 BCS Ground State 491	
15.6 Important Predictions of the BCS Theory and Comparison with Experiment 493	
15.6.1 Critical Temperature 494	
15.6.2 Energy Gap 495	
15.6.3 Critical Field 495	
15.6.4 Heat Capacity 497	
15.6.5 Acoustic Attenuation 497	

---

15.7	Ginzburg–Landau Theory	498
15.7.1	Magnetic Flux Quantization	499
15.7.2	Coherence Length	500
15.7.3	Type II Superconductivity	502
15.7.4	Josephson Tunnelling	504
15.8	High Temperature Superconductors (HTS)	511
15.8.1	Rare-earth Cuprates: Structural Aspect	511
15.8.2	Bi-based and Tl-based Cuprates: Structural Aspect	511
15.8.3	Significant Properties of Cuprate HTS	512
15.8.4	Fullerenes	514
15.9	Applications	515
<i>Summary</i> 515		
<i>Problems</i> 517		
<i>Suggested Further Reading</i> 518		
<b>16.</b>	<b>NANOMATERIALS</b>	<b>519–552</b>
16.1	Introduction	519
16.2	Nanoparticles	521
16.2.1	Metal Nanoclusters	521
16.2.2	Semiconductor Nanoparticles	523
16.2.3	Other Nanoparticles	524
16.3	Nanostructures	524
16.3.1	Carbon Clusters	524
16.3.2	Carbon Nanotubes	526
16.3.3	Quantum Nanostructures	529
16.3.4	Nanostructured Crystals	534
16.4	Porous Silicon	538
16.5	Physical Techniques of Fabrication	541
16.5.1	Photolithography	541
16.5.2	Scanning Probe Microscopy (SPM)	543
16.6	The Present and Future of Nanotechnology	546
<i>Summary</i> 548		
<i>Questions</i> 551		
<i>Suggested Further Reading</i> 552		
<i>Appendix A</i>	<i>van der Waals Interaction</i>	553–555
<i>Appendix B</i>	<i>Photoconductivity</i>	556–559
<i>Appendix C</i>	<i>Luminescence</i>	560–566
<i>Appendix D</i>	<i>Mössbauer Effect</i>	567–574
<i>Appendix E</i>	<i>Magnetoconductivity</i>	575–578
<i>Index</i>		579–587

# The Crystalline State

The solidification of elements and their chemical compounds from liquid and gaseous states is generally understood in terms of the combined effect of attractive and repulsive forces among the constituent particles (atoms/molecules). The details of this process are far from simple to picturize as this requires us to know mainly the nature of response of valence electrons in atoms to the presence of other atoms. The solidification or freezing of matter may lead to the formation of an ordered or disordered state. The ordered state is commonly called the *crystalline* state whereas the disordered one is termed the *amorphous* state.

The crystalline state refers to an infinite array of atoms or a group of atoms. The regularity in the arrangement or the periodicity extends over the whole volume of a crystalline matter or crystal. The whole volume of a crystal can be constructed by moving a building block of the smallest acceptable size along its edges. This block consisting of atoms or a group of atoms is called a *unit cell*.

Even with the complete available knowledge of the laws of atomic packing and geometrical considerations for a certain material, it is generally not possible to predict the material's crystal structure. Predictions turn out to be wrong as often as right. Various crystal structures existing in nature can be understood by systematically exploring all the possible ways of arranging atoms in periodic arrays. This process involves the visualization of motional operations performed on atoms within a unit cell such that the operations leave the unit cell unchanged. These operations, called 'Symmetry Operations', form the most vital component of Geometrical Crystallography. Every crystal structure satisfies the requirements of a specific group (combination) of certain symmetry operations. Different combinations of symmetry operations result in different crystal structures. Thus the knowledge of the symmetry operations helps us in making a complete list of possible crystal structures and in classifying crystals.

We take up below the relationship between the geometrical symmetry and the constituent particles of a crystal. This helps us in appreciating the meaning of unit cell, defined earlier. Further, the fact that the unit cell design is not always unique is very crucial in the theory of crystalline solids. The illustration of these ideas needs to be carried out in the immediate continuation of our discussion as it will equip us better to give an adequate account of symmetry operations.

## 1.1 BASIS OF CRYSTAL STRUCTURE

An infinite periodic array of points in space is called a *lattice*. In more general terms it is known as the *space lattice*. The arrangement of points defines the lattice symmetry. When an atom or an identical group of atoms is attached to every lattice point, we obtain a crystal structure. The attached atom or the group of atoms, called *basis*, is identical for every lattice point in terms of composition, relative orientation and separation. These features are explained in Fig. 1.1. The number of atoms in the basis of an inorganic crystal may approach 100 whereas it is known to be as large as a few thousands in organic crystals like protein.

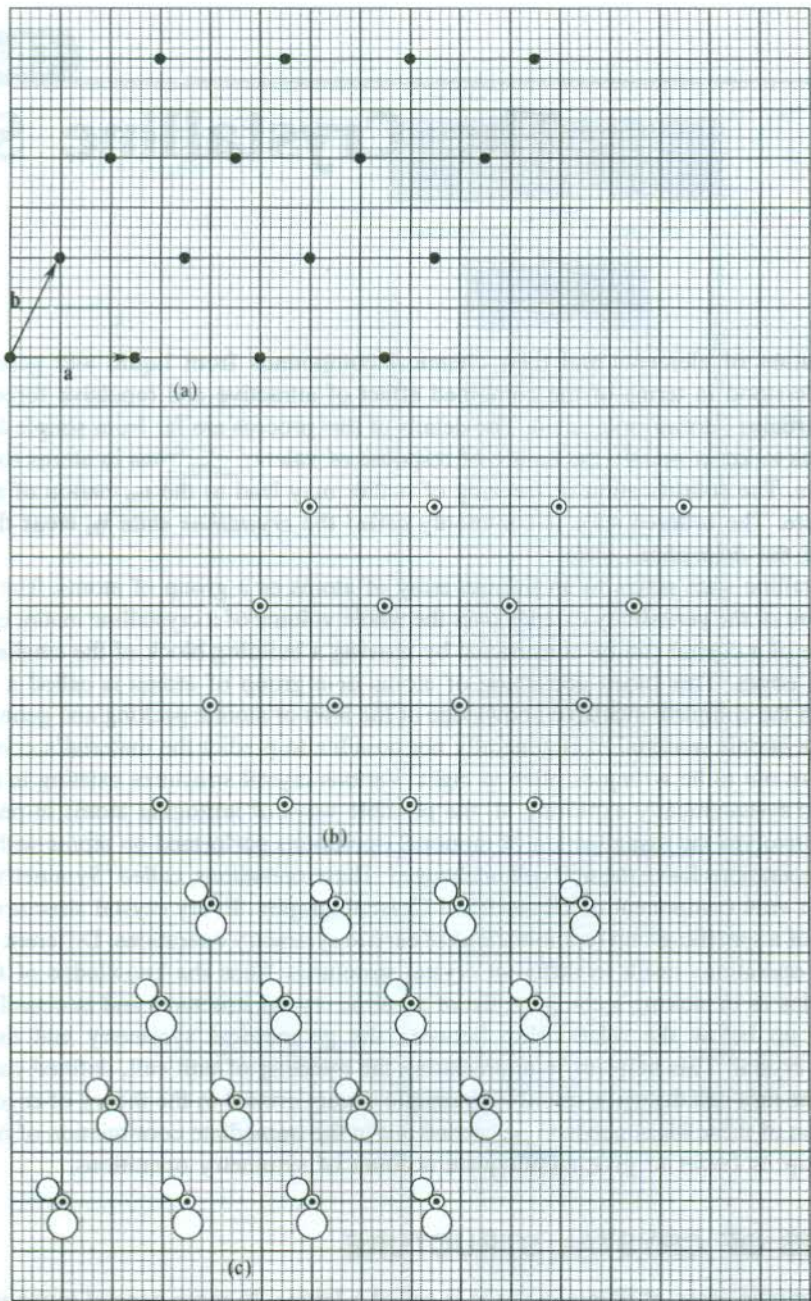


**FIG. 1.1** (a) A regular arrangement of points on a plane forming a two-dimensional space lattice. The points are called *lattice points*. Vectors  $a$  and  $b$  define the symmetry and size of the lattice. (b) A two-dimensional crystal formed when an atom is placed at each lattice point of the space lattice shown in (a). All atoms are identical (of the same element). The single atom forms the *basis* of the crystal structure. The basis of the crystal structure is one. (c) A crystal structure with the space lattice (a) and the basis of three atoms, all of different elements. The relative positions and orientations of atoms in the basis are identical for all lattice points which may now be taken as imaginary points.

In Fig. 1.1(a), **a** and **b** represent vectors that determine the size of a unit cell. Since a unit cell is another name for the smallest structural unit that may be used as the building block of a crystal, a few words about its acceptable size are very much in order. Examine the structure of the following two-dimensional crystal.

The unit cell shown in Fig. 1.2 is represented by  $\mathbf{a}_2$ ,  $\mathbf{b}_2$  and not by  $\mathbf{a}_1$ ,  $\mathbf{b}_1$ . This takes us closer to the introduction of symmetry and symmetry operations in crystals. Figure 1.2 can be used to describe the simplest of the symmetry operations—the translation. In this structure the translation of the unit cell represented by  $\mathbf{a}_2$  and  $\mathbf{b}_2$  vectors is able to map the infinite pattern of the crystal whereas it is not possible with  $\mathbf{a}_1$  and  $\mathbf{b}_1$  as the translation by these vectors takes the smaller atom to the position of the bigger atom and vice versa. Thus in the present case the size of the smallest structural unit representing the unit cell is given by  $\mathbf{a}_2$ ,  $\mathbf{b}_2$ .

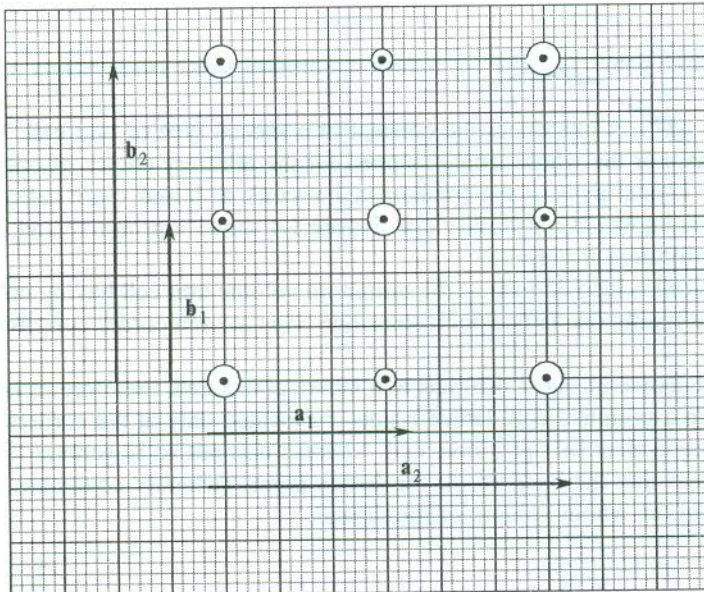


**FIG. 1.2** Identifying the periodicity of the crystal structure to determine the primitive translation vectors ( $\mathbf{a}_2$  and  $\mathbf{b}_2$ ).

## 1.2 UNIT CELL—PRIMITIVE CELL STRUCTURES

The translations along the crystal axes **a**, **b** and **c** are the simplest of many translations that may map the crystal lattice completely. These translations are actually the various combinations of **a**, **b** and **c**, naturally, with certain restrictions. These restrictions are closely linked with the structural aspects of a unit cell which are discussed below.

A proper description of the subject may be carried out by referring to the three-dimensional space lattices. Draw a vector **t** connecting two lattice points  $P_1$  and  $P_2$  (Fig. 1.3) represented by the position vectors  $\mathbf{r}_1$  and  $\mathbf{r}_2$ , respectively. Then, the vector **t** is given by the relation

$$\mathbf{r}_2 = \mathbf{r}_1 + \mathbf{t} \quad (1.1)$$

such that

$$\mathbf{t} = n_1\mathbf{a} + n_2\mathbf{b} + n_3\mathbf{c} \quad (1.2)$$

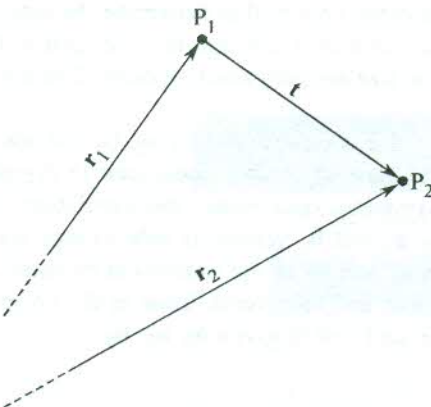


FIG. 1.3 Two lattice points  $P_1$  and  $P_2$  of a three-dimensional lattice connected by a translation vector  $t$ .

The interpretation of (1.2) introduces the concept of a special type of unit cell. When all the lattice points can be located or the whole lattice mapped for the arbitrary choice of only integral values of  $n_1$ ,  $n_2$  and  $n_3$ , the crystal axes or the fundamental vectors  $\mathbf{a}$ ,  $\mathbf{b}$  and  $\mathbf{c}$  are called *primitive* and the resulting unit cell is known as a *primitive cell*. Figure 1.4 shows a primitive and a non-primitive cell belonging to two different materials.

The primitive cell is also defined as the minimum volume unit cell having only one lattice point. In Fig. 1.4(a) there is only one lattice point since one point at each corner contributes  $1/8$ th of a point to the cell.

The other cell shown in Fig. 1.4(b) has two lattice points and, therefore, it is non-primitive. We can also say that in a primitive cell, lattice points are located only at the corners of the cell. All the lattice points are equivalent in a primitive cell, whereas it is not so in general [Fig. 1.4(b)]. But we must not forget here that the basis of all the lattice points (whether equivalent or non-equivalent) remains identical in the whole volume of the crystal.

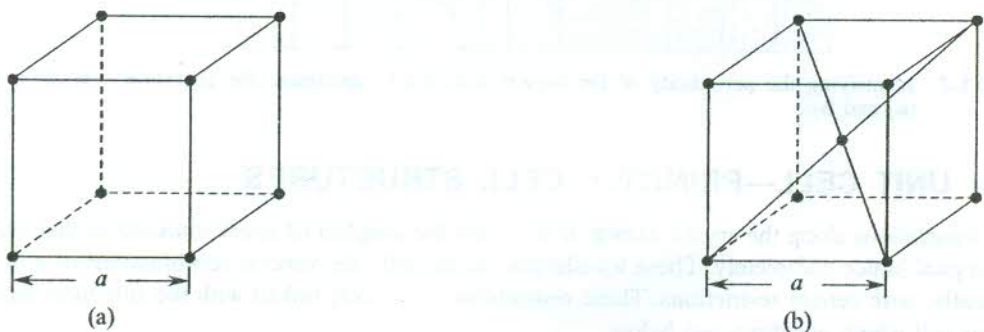
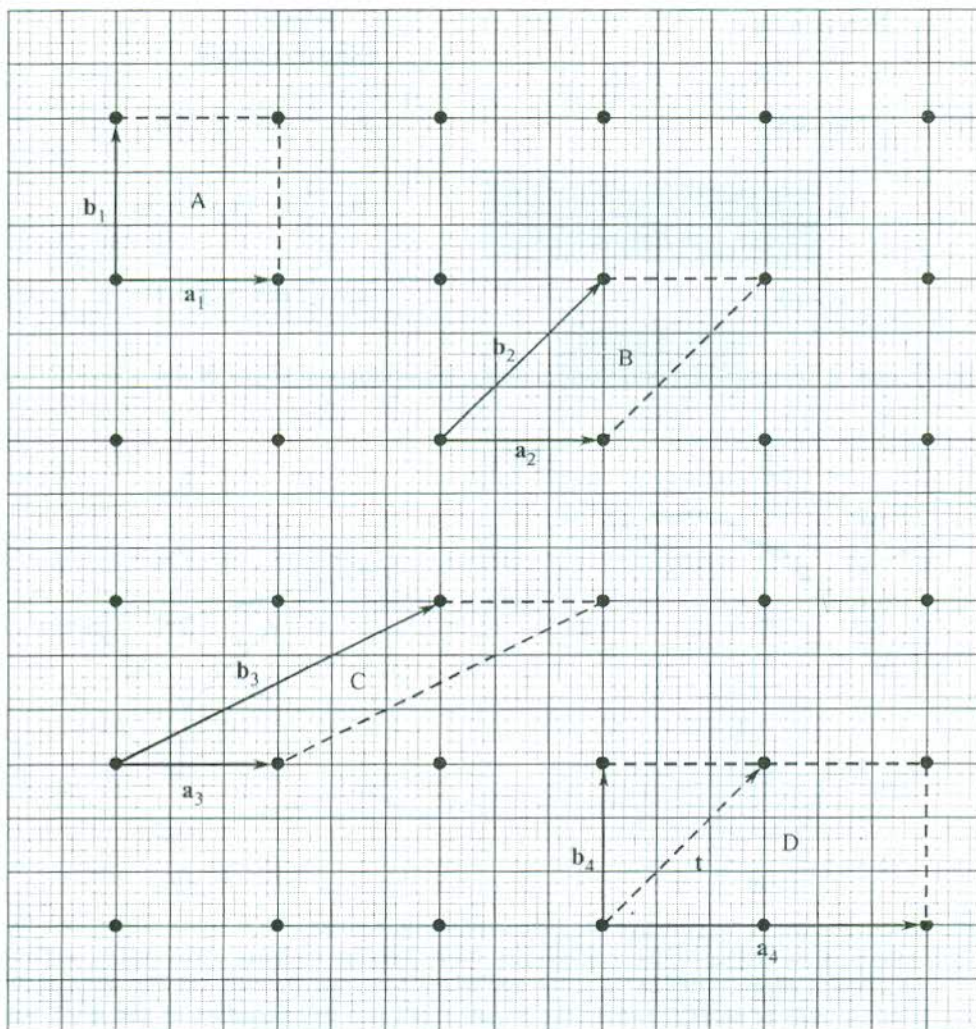


FIG. 1.4 (a) A primitive cell. There is one lattice point in the cell. A point at the corner of the cube contributes the fraction  $(1/8)$ . (b) A non-primitive cell with two lattice points per cell.

It is desirable to mention here that there can be more than one choice for the primitive cell of a given crystal. All of these primitive cells are equally acceptable as each of them has the same volume. This property can be easily demonstrated in a two-dimensional space lattice.

Figure 1.5 shows that all acceptable primitive cells for a square lattice have a common value of the area enclosed.



**FIG. 1.5** Choices for the primitive cell of a square lattice. The choice D is not acceptable since all lattice points cannot be mapped with integral values of  $n_1$  and  $n_2$  in the vector,  $\mathbf{t} = n_1\mathbf{a}_4 + n_2\mathbf{b}_4$ .

The use of a primitive cell or a non-primitive unit cell for the study of a crystalline material is purely a matter of convenience. There is no hard and fast rule in this respect. Figure 1.6(a) shows the non-primitive and primitive cells for the three-dimensional space lattice pictured in Fig. 1.4(b).

The space lattice of the unit cell shown in Fig. 1.6(a) is the body centred cubic (BCC). But the same structure has a rhombohedral symmetry for the design of its primitive cell [Fig. 1.6(a)]. The edges of the unit cell in the two cases are as follows:

Non-primitive  
(BCC)

$$\mathbf{a} = a\hat{\mathbf{x}}$$

$$\mathbf{b} = a\hat{\mathbf{y}}$$

$$\mathbf{c} = a\hat{\mathbf{z}}$$

(1.3)

Primitive  
(Rhombohedral)

$$\mathbf{a} = \frac{1}{2} a(\hat{\mathbf{x}} + \hat{\mathbf{y}} - \hat{\mathbf{z}})$$

$$\mathbf{b} = \frac{1}{2} a(-\hat{\mathbf{x}} + \hat{\mathbf{y}} + \hat{\mathbf{z}})$$

$$\mathbf{c} = \frac{1}{2} a(\hat{\mathbf{x}} - \hat{\mathbf{y}} + \hat{\mathbf{z}})$$

(1.4a)

where  $\hat{\mathbf{x}}$ ,  $\hat{\mathbf{y}}$  and  $\hat{\mathbf{z}}$  represent the unit vectors along the orthogonal edges of the non-primitive cell.

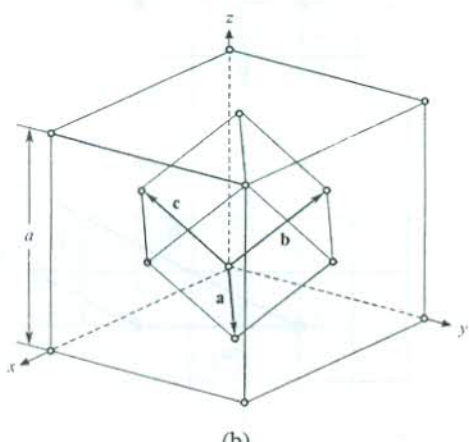
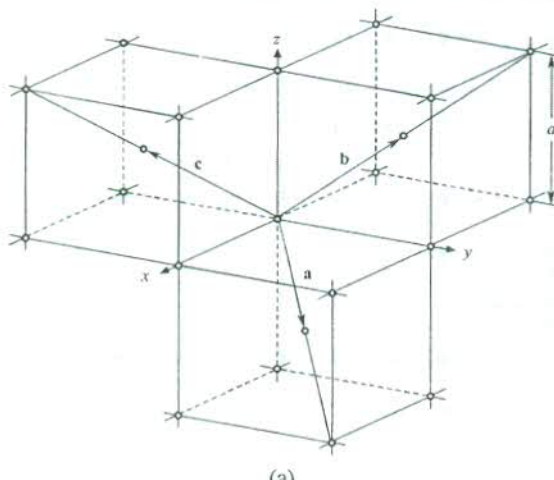


**FIG. 1.6** (a) Orientations of the primitive translation vectors ( $\mathbf{a}$ ,  $\mathbf{b}$ ,  $\mathbf{c}$ ) for a BCC lattice. These form the edges of the primitive cell having the rhombohedral shape. The edge measures  $\sqrt{3}a/2$  and the angle between the adjacent edges is  $109^\circ 28'$  ( $a$  is the size of the non-primitive cell). (b) The non-primitive and primitive cells of an FCC lattice. The primitive cell is a rhombohedron of size  $a/\sqrt{2}$  with axes inclined at  $60^\circ$  to each other.

An alternative primitive cell, known as Wigner–Seitz cell, is of historic importance in the theory of Solid State Physics. The first proper electron energy bands calculation was made by Wigner and Seitz using this design of the primitive cell. The method of construction is as follows.

A lattice point is joined to all the nearby lattice points with the help of lattice vectors. Then, a plane perpendicular to each of these vectors, connecting the central lattice point, is drawn at the mid-point of the vector. The planes form a completely closed polyhedron which contains only one lattice point at its centre. The polyhedron serves as an ideal primitive cell and is named after Wigner and Seitz who are credited with having given the philosophy of its construction. Figure 1.7 shows the pictures of Wigner–Seitz cell of a two-dimensional lattice. It should be noticed that the Wigner–Seitz cell of BCC lattice can in effect be constructed by chopping off all the corners of its lattice cube halfway along a diagonal from the centre to a corner point. In this construction the lattice vectors connecting the lattice point at the centre and the next nearest lattice points are also involved. The resulting polyhedron turns out to be a truncated octahedron.

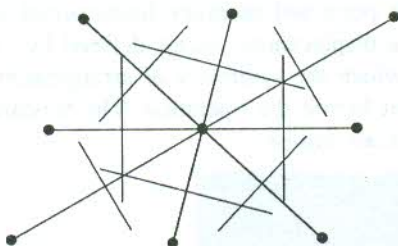


**FIG. 1.7** The construction of the Wigner–Seitz cell for a two-dimensional space lattice.

Another common space lattice to which structures of many solids correspond is the FCC lattice. Its conventional unit cell has four lattice points and the three edge vectors are represented as for the BCC lattice (1.3). The primitive cell is again a rhombohedron with primitive translation vectors as depicted in Fig. 1.6(b). It is straightforward to check that they can be expressed as

$$\begin{aligned} \mathbf{a} &= \frac{1}{2} a(\hat{\mathbf{x}} + \hat{\mathbf{y}}) \\ \mathbf{b} &= \frac{1}{2} a(\hat{\mathbf{y}} + \hat{\mathbf{z}}) \\ \mathbf{c} &= \frac{1}{2} a(\hat{\mathbf{z}} + \hat{\mathbf{x}}) \end{aligned} \quad (1.4b)$$

It thus becomes obvious that in order to make a list of various types of crystal structures, we must know how many types of unit cells are possible. The task involves the compilation of knowledge of the symmetries of unit cells or symmetry operations under which a unit cell remains unchanged. The importance of symmetry operations, as already emphasized in the beginning of this chapter, has now become amply evident. An attempt to give a simple description of the symmetry operations is made below.

### 1.3 SYMMETRY OPERATIONS

An operation that takes the crystal into itself is called a symmetry operation. Imagine an observer placed inside a crystal. He is asked to close his eyes and then an operation is performed on the crystal. If the observer opens eyes after the operation is completed and does not find any change in his surroundings, the performed operation will be called a symmetry operation.

Symmetry operations may be grouped into three classes:

1. Translation operations
2. Point operations
3. Hybrid operations

#### 1.3.1 Translation Operations

As already stated, these are the simplest of the symmetry operations. A translation operation is defined as the displacement of a crystal parallel to itself by a crystal translation vector.

The translation operation is permitted in every fundamental space lattice of crystals when a lattice point is moved through a displacement vector defined by (1.2). The final point of journey is another lattice point around which the symmetry of arrangement of lattice points is identical to that around the first lattice point before the operation. The fundamental space lattice of a crystal is commonly known as the *Bravais lattice*.

### 1.3.2 Point Operations

Point operations described below are performed at a point within a Bravais lattice or a crystalline matter. A simple description of these operations is given below.

#### **The mirror reflection**

In this operation, the reflection of a structure at a mirror plane  $m$  passing through a lattice point leaves the crystal unchanged. The mirror plane is composed of the atoms lying on the concerned imaginary plane. Two different mirror planes in a structure are demonstrated in Fig. 1.8.

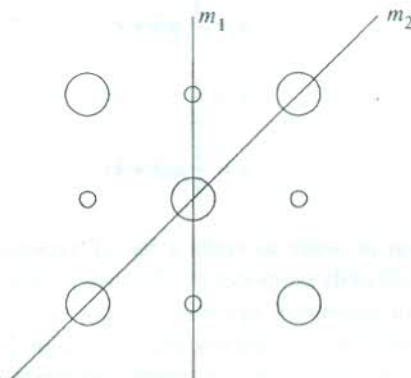


FIG. 1.8 Examples of two mirror planes in a two-dimensional crystal.

#### **The inversion**

Let the position vector of a lattice point be represented by  $\mathbf{r}$ , the origin being another lattice point (Fig. 1.9). If the crystal lattice has a lattice point with the position vector  $-\mathbf{r}$ , we say that the crystal has the inversion symmetry and the origin taken in the example is called the *centre of inversion* represented by symbol  $i$ . The inversion operation shows that the inversion of the lattice point  $A$  at the centre of inversion  $O$  (another lattice point) keeps the lattice unchanged. In this operation the point  $A$  goes to the point  $A'$  which is also a lattice point. After studying Section 1.4, the readers must verify that every Bravais lattice has inversion symmetry.

#### **The rotation**

It is a well-known fact that objects can be repeated by rotation. An object can be rotated about an axis through a certain angle so as to give the unchanged picture of the object to a stationary observer. The axis is called the *rotation axis*. If the angle  $\theta$ , for which this condition is met, be given by

$$\theta = \frac{2\pi}{n} \quad \text{with } n = 1, 2, 3, \dots \quad (1.5)$$

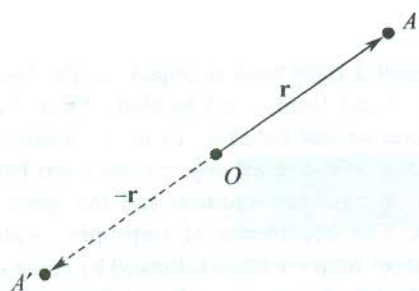


**FIG. 1.9** The illustration of the inversion operation.

then the axis of rotation is termed  $n$ -fold. This implies that such  $n$  rotations of an object about its  $n$ -fold axis bring the object back to its identical configuration. This shows that every object has 1-fold axis of rotation.

These axes of rotation, also known as *symmetry axes*, are very common in the crystalline state of matter. The location of a 4-fold and a 6-fold axis is shown in Fig. 1.10 in two different crystals.

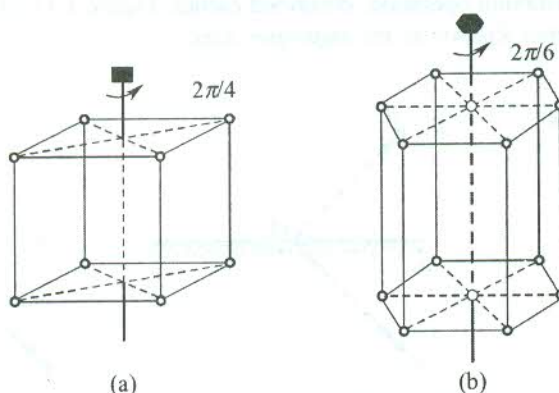


**FIG. 1.10** (a) A 4-fold axis of rotation. (b) A 6-fold axis of rotation.

The symmetry axes most commonly observed in crystals are 1-fold, 2-fold, 3-fold, 4-fold, and 6-fold. The evidence for a 5-fold rotational symmetry is encountered in the structural studies of some materials, classified as quasicrystals (see Section 1.8). The lack of conviction in getting a periodic structure by arranging units with pentagonal faces is strongly supported by the absence of 5-fold symmetry in all generally talked about crystals.

The rotations discussed above always produce a congruent set and are known as proper rotations. But our discussion on rotational symmetry remains incomplete without making a reference to a very special type of rotation. The rotations that repeat a right-handed object from a left-handed one are quite frequent in crystals. They are known as *improper rotations*. A combination of such a rotation with the reflection operation takes a crystal into itself (the congruent set). It can be identified as a *rotoreflection* operation. It is one of the several hybrid symmetry operations which are required to explain or account for the structure of many crystals.

### 1.3.3 Hybrid Operations

The rotations discussed above repeat a right-handed object (or the basis of structure) from a right-handed object and a left-handed object from a left-handed object. Such a rotation resulting in a congruent set is called a *proper rotation* and the axis of rotation a *proper rotation axis*. On the other hand, there are rotations that repeat a right-handed object from a left-handed object (incongruent set) and vice versa. These are known as *improper rotations* and the operation is referred to as rotation about an *improper rotation axis*. The occurrence of improper rotation axes in crystals is well documented in literature. An improper rotation when followed by some other operation like reflection or translation sometimes leads to the congruence. It must be noticed that none of these two operations is independently a symmetry operation of the crystal whereas their combination is. Similarly, a reflection may combine with a translation to produce congruence in some crystals. The combined symmetry operation in these cases is named as a hybrid symmetry operation. Some of the hybrid symmetry operations that frequently occur in crystals are described below.

#### *The rotoreflection*

It is the combination of an  $n$ -fold rotation and a reflection at the plane, perpendicular to the rotation axis. Its general representation is  $n/m$  with  $n = 1, 2, 3, 4, 6$ . It can be shown that the rotoreflection  $2/m$  is equivalent to the inversion operation, described earlier. Figure 1.11 explains this. The axis of rotation in this case is better known as the *improper axis*.

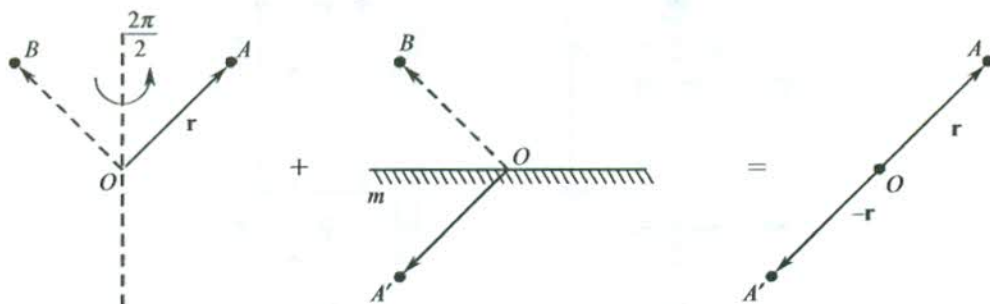


FIG. 1.11 The illustration of a rotoreflection  $2/m$ ; it is equivalent to an inversion operation.

#### *The rotoinversion*

This operation includes an  $n$ -fold rotation followed by an inversion. Its common representation is  $\bar{n}$ , where  $n = 1, 2, 3, 4, 6$ . Thus a rotoinversion composed of a 3-fold rotation and an inversion is depicted as  $\bar{3}$ . The axis of rotation is again an *improper axis*.

#### *The screw translation*

Similar to the two operations explained above, an operation combining an  $n$ -fold rotation with a translation parallel to the rotation axis is found to be permitted by the symmetry of several crystals. Such an operation with a screw diad axis, denoted by  $2_1$  is demonstrated in Fig. 1.12.

#### *The glide reflection*

We can also combine a reflection with a translation parallel to the reflection plane to achieve congruence in some crystals. This combination is called a *glide reflection*. The translation component

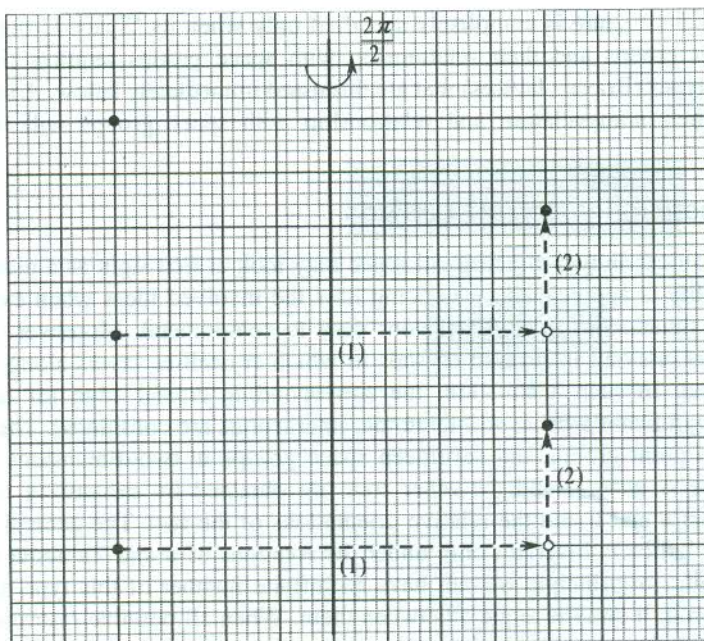


FIG. 1.12 The illustration of a screw translation operation,  $2_1$ .

of a glide reflection is expressed as the combination of translations by fractions of repeat distances in a crystal. For example, the translation in a diagonal glide may be written as

$$\mathbf{t} = \frac{1}{2} \mathbf{a} + \frac{1}{2} \mathbf{b}, \quad \frac{1}{2} \mathbf{b} + \frac{1}{2} \mathbf{c} \quad \text{or} \quad \frac{1}{2} \mathbf{c} + \frac{1}{2} \mathbf{a}$$

The list of symmetry operations is not without a very special symmetry operation, known as the *identity operation*. This operation means doing no operation on the crystal or keeping the crystal undisturbed. Thus every crystal has the identity operation. It is generally denoted by the symbol  $I$ . In the context of symmetry operations the identity operation appears irrelevant at the first instance. But this has to be included in the list to meet the mathematical requirements of Group Theory which arms us with the quickest methods of making a quantitative calculation of many physical properties of crystals.

## 1.4 CRYSTAL TYPES

In order to have a complete list of different types of crystals, we basically require to know the number of fundamental space lattices, referred to as Bravais lattices. The number of these lattices is obtained by imposing restrictions on  $\mathbf{a}$ ,  $\mathbf{b}$  and  $\mathbf{c}$  and getting different arrangements of lattice points each of which is represented by the respective unit cell. The point symmetry operations of a Bravais lattice may be combined in different ways such that each of the combinations represents a different structure in terms of symmetry. Each combination which is a collection of certain symmetry operations is called a 'Point Group'. A symmetry operation in this reference is given another name 'Symmetry Element'. For example, we say that the centre of inversion  $i$  is a symmetry element of the octahedral point group  $O_h$  [see Table 1.2(b)]. It may, however, be remarked that the

symmetry of a crystal structure is completely specified only when its 'Space Group' is known. The description of point groups and their relationship with space groups requires the knowledge of fundamental lattice types (Bravais lattices) that are discussed immediately below. A suitable discussion on point groups, their nomenclature and relationship with space groups will be undertaken in Section 1.6.

### 1.4.1 Two-dimensional Crystal Lattices

The discussion on lattices in two-dimensional space may look at first sight as a matter of theoretical concern. But its utility is appreciated on noticing how the involved ideas when extended make the relatively complex situation in three-dimensions easy to comprehend. Moreover, two-dimensional lattices become most relevant in layered crystals in which crystalline layers along one crystal edge are largely separated. In such a situation, the corresponding crystal edge (or lattice parameter) becomes almost insignificant whenever interatomic interactions are considered. There are in all five Bravais lattices, ten point groups and seventeen space groups in two-dimensions. Out of the five Bravais lattices, one is general and the other four are obtained by exhausting the feasible axial relationships between  $\mathbf{a}$  and  $\mathbf{b}$  and the relative orientations of the two. The general lattice is termed *oblique lattice*. The lattice is invariant only under the rotations of  $\pi$  and  $2\pi$  about the axes passing through a lattice point. In principle we can have an infinite number of this type of lattice as there are no restrictions on  $\mathbf{a}$ ,  $\mathbf{b}$  and the angle  $\gamma$  between them. When all possible restrictions are imposed on  $\mathbf{a}$ ,  $\mathbf{b}$  and  $\gamma$ , we get four special types of two-dimensional Bravais lattice [Fig. 1.13]. All these lattices are primitive except the second of the two derived from the same centred rectangular arrangement of lattice points.

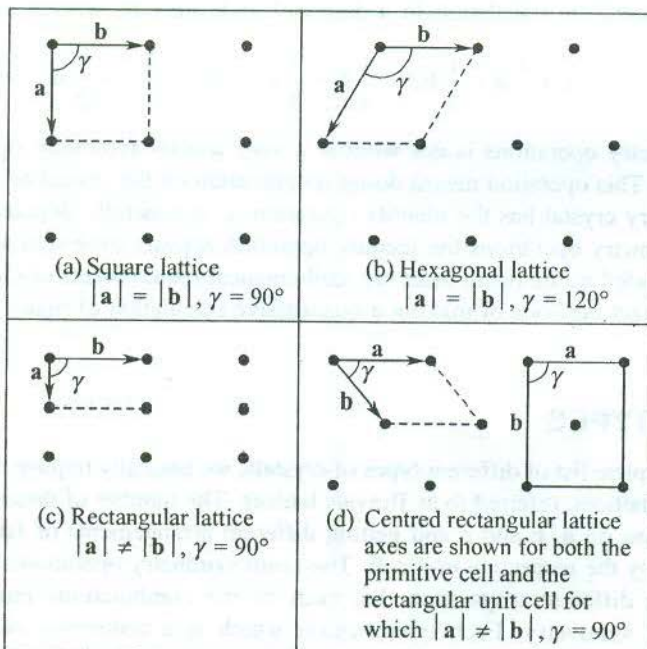
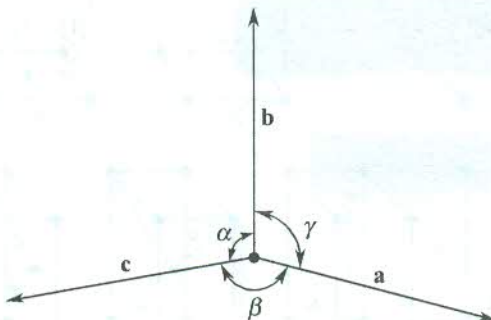


FIG. 1.13 The types (Bravais lattices) of two-dimensional lattices.

### 1.4.2 Three-dimensional Crystal Lattices

A three-dimensional unit cell is defined by vectors **a**, **b** and **c** representing its edges or crystal axes and the angles  $\alpha$ ,  $\beta$  and  $\gamma$  as defined in Fig. 1.14.



**FIG. 1.14** Notation for angles between the crystal axes.

The number of Bravais lattices is 14 with 32 point groups and 230 space groups. Based on relationships between **a**, **b** and **c** in terms of magnitude and relative orientation ( $\alpha$ ,  $\beta$  and  $\gamma$ ), the 14 types of unit cells are grouped in seven different classes of crystal lattices: triclinic, monoclinic, orthorhombic, tetragonal, cubic, trigonal and hexagonal. A description of the 14 Bravais lattices of three-dimensions along with the axial relationship for the class of crystal lattices to which each belongs is entered in Table 1.1. The shapes are shown in Fig. 1.15.

**Table 1.1** The Bravais lattices in three dimensions

Class	Lattice type	No. of lattices	Axial relationship
Triclinic	P	1	$a \neq b \neq c$ $\alpha \neq \beta \neq \gamma$
Monoclinic	P, B	2	$a \neq b \neq c$ $\alpha = \gamma = 90^\circ \neq \beta$
Orthorhombic	P, B, F, C	4	$a \neq b \neq c$ $\alpha = \beta = \gamma = 90^\circ$
Tetragonal	P, C	2	$a = b \neq c$ $\alpha = \beta = \gamma = 90^\circ$
Cubic	P, F, C	3	$a = b = c$ $\alpha = \beta = \gamma = 90^\circ$
Trigonal	P or R	1	$a = b = c$ $\alpha = \beta = \gamma < 120^\circ, \neq 90^\circ$
Hexagonal	P	1	$a = b \neq c$ $\alpha = \beta = 90^\circ$ $\gamma = 120^\circ$

Representation of symbols: P—primitive, B—base centred, C—body centred, F—face centred.

The number of lattice points in unit cell can be calculated by appreciating the following:

Contribution of the lattice point at the corner = 1/8th of the point

Contribution of the lattice point at the face = 1/2 of the point

Contribution of the lattice point at the centre = 1 of the point

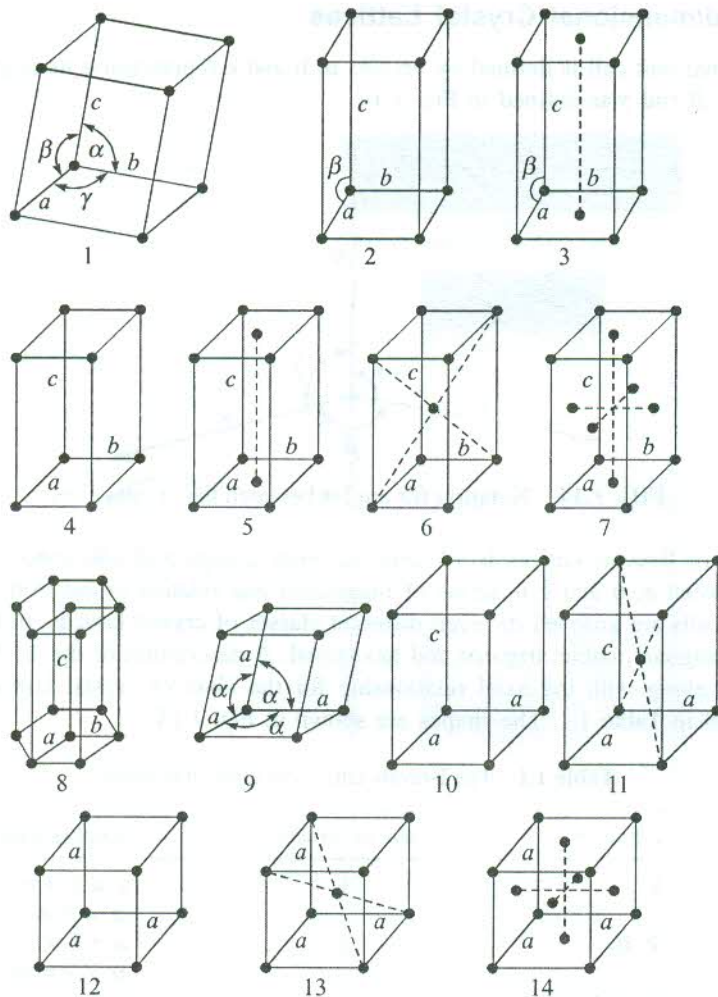


**FIG. 1.15** The three-dimensional lattices; 1: Triclinic, 2–3: Monoclinic, 4–7: Orthorhombic, 8: Hexagonal, 9: Trigonal, 10–11: Tetragonal, 12–14 Cubic.

Every type of unit cell is characterized by the number of lattice points (not the atoms) in it. For example, the number of lattice points per unit cell for simple cubic (SC), body centred cubic (BCC) and face centred cubic (FCC) lattices are one, two and four, respectively. Our knowledge about unit cell may not be complete without having a quantitative estimate of its volume. It can be calculated using the relation

$$V_c = \mathbf{a} \cdot [\mathbf{b} \times \mathbf{c}] \quad (1.6)$$

where  $V_c$  stands for the volume of the cell. The  $\mathbf{a}$ ,  $\mathbf{b}$  and  $\mathbf{c}$ , defined so far as the measure of unit cell edges, are more popularly known as *lattice parameters*.

## 1.5 INDICES OF A LATTICE DIRECTION AND A LATTICE PLANE

The exercise of describing a crystal structure essentially amounts to locating the positions of different atoms in the unit cell. But the study of many physical properties of crystals becomes more meaningful and complete with the knowledge of directions and various atomic planes visualized within their crystalline medium. These are identified by using the index systems discussed below.

### *Indices of a lattice direction*

A vector is drawn along (or parallel to) the desired direction from the origin fixed for the axes system. The components of this vector along the crystal axes are determined and reduced to smallest integers. These integers when written within square brackets represent the indices of the direction in question. Some of the prominent directions in a cubic unit cell are shown in Fig. 1.16.

A bar on an index means that the respective component of the vector is negative.

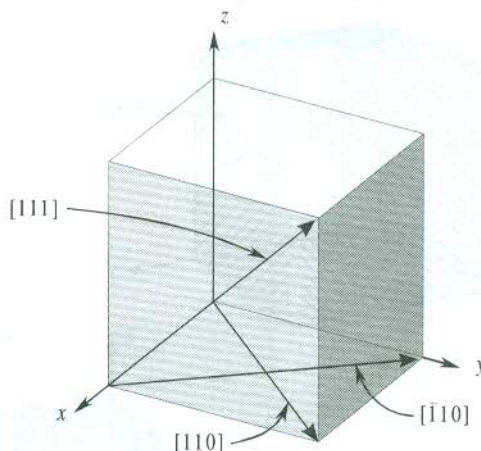


FIG. 1.16 Some prominent directions in a cubic crystal.

### *Indices of a lattice plane*

Every crystal plane is identified by its orientation which is characterized by plane's intercepts with the crystal axes. The equation of a plane having intercepts  $p$ ,  $q$  and  $r$  with  $x$ ,  $y$ ,  $z$  axes is given by

$$\frac{x}{p} + \frac{y}{q} + \frac{z}{r} = 1 \quad (1.7)$$

The form of this equation has been exploited by Miller to develop an index system, for whom the indices are named—Miller indices. The Miller indices of a plane are determined by the following procedure.

Let the intercepts of a plane with **a**, **b** and **c** measure as  $pa$ ,  $qb$  and  $rc$ , respectively. Reduce the set  $\frac{1}{p}, \frac{1}{q}, \frac{1}{r}$  to the three integers  $h, k, l$  having the same ratio as  $\frac{1}{p}, \frac{1}{q}, \frac{1}{r}$ . This set of indices, when written in parentheses as  $(h k l)$  gives the Miller indices of the plane. For example, take a plane

having the intercepts of lengths  $2a$ ,  $b$  and  $2c$  with the three crystal axes. In order to find its Miller indices, first take the reciprocals of 2, 1 and 2 getting  $\frac{1}{2}, 1, \frac{1}{2}$  and then find the integers that are in the same ratio as  $\frac{1}{2}, 1, \frac{1}{2}$ . This gives the Miller indices (121).

Some prominent planes of a cubic unit cell can be seen in Fig. 1.17. If a plane intersects a certain crystal axis on its negative side, a bar is put over the corresponding Miller index. For example, (123) and ( $\bar{1}23$ ) are two parallel planes, their intercepts with the  $b$  axis being on the two sides of the origin. Examine planes (110), (220) and (330) in Fig. 1.17. They are parallel to each other and lie on the same side of the origin. In rare situations we need to distinguish them and generally they are represented by the smallest common indices obtained by dividing through with the largest common factor. Thus all these three planes may be represented by (110).

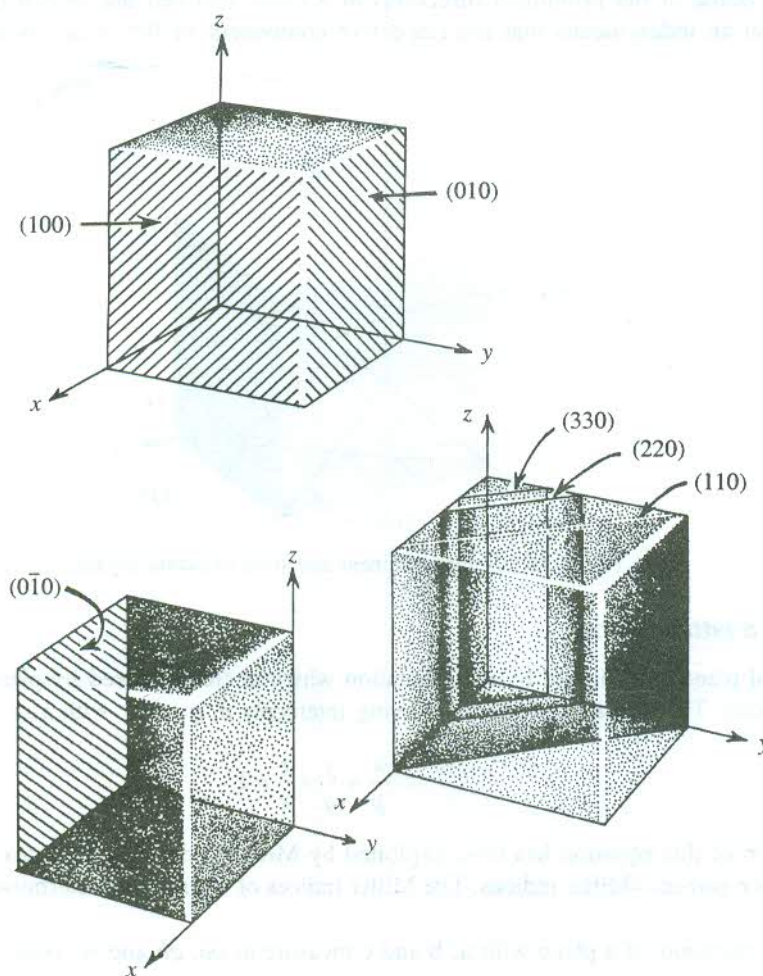


FIG. 1.17 Some prominent planes of a cubic crystal.

## 1.6 CRYSTAL POINT GROUPS AND SPACE GROUPS

### 1.6.1 Point Groups

In continuation with the discussion on crystal types initiated in Section 1.4, we would like to repeat that the symmetry elements may be combined with one another in different ways. In the converse sense, this means that every crystal structure may be described by a combination of symmetry elements (symmetry operations). But the symmetry elements in each such combination are required to satisfy certain conditions. For example, when one symmetry operation  $A$  is followed by another operation  $B$ , the resultant effect is capable of being produced by a third symmetry operation  $C$ , that is  $A * B = C$ , where  $A$ ,  $B$  and  $C$  are members of a combination of certain symmetry elements, permitted by the symmetry of the concerned crystal lattice. Furthermore, the symmetry elements in a combination should also satisfy the following mathematical conditions:

$$(A \times B) \times C = A \times (B \times C) \quad (\text{the associative law}) \\ A \times I = A \quad (1.8)$$

where  $I$  is the identity operation.

$$A^{-1} \times A = I$$

where  $A^{-1}$  is an operation which is the reverse of operation  $A$ .

A set of symmetry elements that satisfies the above conditions is said to form a group, commonly known as the 'point group', since all the operations contained in the group are performed at a point in the crystal lattice. There are in total 32 distinct combinations of symmetry operations performed at a point in various crystals. This number exhausts all the possible ways of combining the symmetry elements such that the symmetry elements in each combination meet the requirements imposed by the mathematical conditions (1.8). This gives 32 point groups in three-dimensional lattices. Twenty-seven of these are non-cubic and five are cubic point groups. There exist two standard nomenclature systems for point group—the Schönflies and international. The Schönflies symbols are most common in group theoretical and spectroscopic illustrations. The composition of these groups together with their symbols in both the nomenclature systems is described in Table 1.2.

It is an established practice in crystallography to represent the point groups by the so-called stereographic projections developed essentially to obtain a systematic classification of the exposed surfaces of naturally grown crystals. The points of intersection of surface normals with a sphere are marked. These points are projected on to the plane that is perpendicular to the highest order symmetry axis. Points referring to the points of intersection on the upper-half of the sphere are indicated by dark full circles and those corresponding to intersections below the plane are represented with cross marks or open circles. Thus the highest order symmetry axis passes through the centre in a systematic representation of point groups. As an example, the stereographic projection of point group  $D_{3d} \equiv \bar{3} \frac{2}{m}$  is shown in Fig. 1.18.

### 1.6.2 Space Groups

The information about a crystal structure is complete only when its point group and space group both are known. The precise knowledge about the composition and the symmetry of the basis of atoms attached to a lattice point is a prerequisite to the determination of the space group of a crystal

**Table 1.2(a)** Twenty-seven (27) non-cubic crystal point groups

Schönlies	International	Meaning in terms of symmetry elements	Number
$C_n$	$n$	These groups have only an $n$ -fold axis of rotation ( $n = 1, 2, 3, 4, 6$ ).	5
$C_{nv}$	$n m m$ ( $n$ even) $n m$ ( $n$ odd)	The groups have an $n$ -fold rotation axis, a mirror plane containing the rotation axis, and as many additional mirror planes as may be required by the presence of the $n$ -fold axis ( $n = 2, 3, 4, 6$ ).	4
$C_{nh}$		In addition to the $n$ -fold rotation axis, there is a single mirror plane perpendicular to the rotation axis.	
	$\left(\frac{n}{m}\right)$	$n = 2, 4, 6$ (even)	
	$\bar{n}$	$n = 1, 3$ (odd)	5
$S_n$	$\bar{n}$	These groups have only an $n$ -fold rotoreflection axis ( $n = 2, 4, 6$ ).	3
$D_n$	$n 2 2$ ( $n$ even) $n$ ( $n$ odd)	These groups contain an $n$ -fold axis of rotation, a 2-fold rotation axis perpendicular to the $n$ -fold axis, and as many additional 2-fold axes as the presence of the $n$ -fold axis demands ( $n = 2, 3, 4, 6$ ).	4
$D_{nh}$	$\frac{n}{m} \frac{2}{m} \frac{2}{m}$	In addition to all the elements of $D_n$ , there is a mirror plane perpendicular to the $n$ -fold rotation axis.	4
	$\left(\frac{n}{mmm}\right)$	$n = 2, 4, 6$ (even)	
	$\bar{n} 2 m$	$n = 3$ (odd)	
$D_{nd}$		In addition to all the elements of $D_n$ , there are mirror planes containing the $n$ -fold rotation axis such that the planes bisect the angles between the 2-fold axes of rotation.	2
	$\bar{n} 2 m$	$n = 2$ (even)	
	$\bar{n} \frac{2}{m}$	$n = 3$ (odd)	

structure whose point group is known. For a given crystal system there can be a certain number of point groups, i.e. the number of different combinations of the symmetry elements of the system. The group of atoms comprising the basis can have any of these point group symmetries. One point group symmetry for the basis gives a space group for each of the possible Bravais lattices of the crystal system. For example, there are five point groups and three Bravais lattices (P, F and C) for a cubic system [see Tables 1.1 and 1.2(b)]. So, five different symmetries for the basis are possible in this case. With these possibilities of symmetry for the basis in each of the three Bravais lattices, 15 different crystal structures can occur, represented by 15 different space groups.

Following the procedure described above, the total number of space groups for real crystals have been determined. In considering these combinations, one must be reminded that symmetry elements

Table 1.2(b) The five (5) cubic crystal point groups

Schönlies	International	Meaning in terms of symmetry elements
$T$	$2 \ 3$	The tetrahedral point group (in a crystal the alternate corners of the cube are vacant). It contains three mutually perpendicular 2-fold axes, plus four 3-fold axes, angles between which are bisected by the 2-fold axes.
$T_d$	$\bar{4} \ 3 \ m$	In addition to all the elements of $T$ , there is a mirror plane through each pair of 3-fold axes (i.e. two mutually perpendicular mirror planes through each 2-fold axis). In all, there are thus six mirror planes.
$T_h$	$\frac{2}{m} \ \frac{\bar{3}}{m}$ ( $m \ 3$ )	The group has all symmetry elements of $T$ , plus a centre of inversion $i$ .
$O$	$4 \ 3 \ 2$	The octahedral point group. It contains three mutually perpendicular 4-fold axes and four 3-fold axes which have the same orientation with respect to one another as the 2-fold and 3-fold axes of the tetrahedral point group.
$O_h$	$\frac{4}{m} \ \frac{\bar{3}}{m} \ \frac{2}{m}$ ( $m \ 3 \ m$ )	The group has all symmetry elements of $O$ , plus a centre of inversion $i$ .

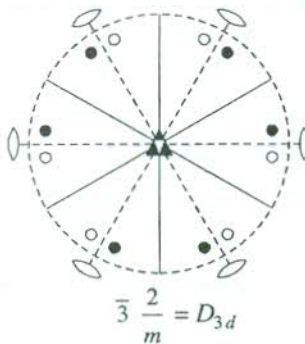


FIG. 1.18 Stereographic projection of the symmetry elements of point group  $D_{3d} \equiv \bar{3} \frac{2}{m}$ . The symbols  $\circlearrowleft$  and  $\blacktriangle$  denote 2- and 3-fold axes of rotation, respectively. The full lines represent mirror planes. If the plane of the figure were to be a mirror plane, the outer circle would be shown as a continuous circle.

permitted for a space lattice can have translational components as well. This demands that in addition to thirty-two point groups, the symmetry groups with identical angular relationships but having screw axes in place of proper rotation axes and glide planes in place of pure reflection planes should also be taken into account. With the inclusion of these groups, the total number of ways in which the symmetry groups may be combined with space lattices in three dimensions are found to be 230. This gives the total number of space groups for real crystals. It should surprise none that this number would be mere 14 for structures with a completely (spherically) symmetric basis (e.g. a monatomic basis). The space group of a crystal is usually represented on a plane by a repetitive pattern of the allowed point symmetry elements, by using standard symbols for different symmetry elements. Both the nomenclature systems, Schönlies and International are used. Readers interested in more details may consult Buerger's *Elementary Crystallography* (Wiley, 1963).

## 1.7 COMMON CRYSTAL STRUCTURES

### 1.7.1 The Simplest Crystal

The simplest crystal structure that we can think of is that of simple cubic symmetry with a basis of one atom. Polonium is the lone known example of this class in nature. The atoms are positioned at the corners of a cube. Thus the crystal has just one atom per primitive cell.

### 1.7.2 The CsCl Structure

The structure of a CsCl crystal is shown in Fig. 1.19. There is an atom at the centre of the cube surrounded by eight atoms of the other type at the corners. The space lattice is simple cubic (SC) and the primitive cell has one formula unit. The basis is composed of two atoms situated at 000 and  $\frac{1}{2} \frac{1}{2} \frac{1}{2}$ , positions being measured in units of the lattice parameter. Notice that this structure cannot be interpreted as body centred cubic (BCC). If the cube centre is treated as the second lattice point,

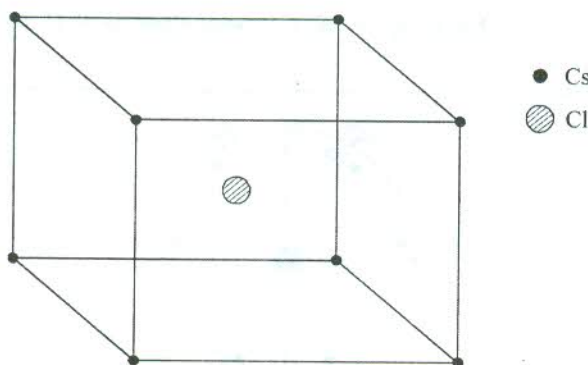


**FIG. 1.19** The unit cell structure of CsCl crystal.

its basis is found to be different from the one at the corner which is not permitted, since every lattice point is required to have an identical basis in a crystal. The nearest neighbours are the atoms of the other element and their number, also known as the *coordination number*, is eight. The lattice parameter of some ionic crystals having this structure is given below:

Crystal	Lattice parameter ( $\text{\AA}$ ) ( $\text{\AA} = 10^{-10} \text{ m}$ )
CsCl	4.11
CsBr	4.29
CsI	4.56
TlCl	3.84
TlBr	3.97
TlI	4.18

### 1.7.3 Crystals of Alkali Metals

Crystals of alkali metals (Li, Na, K, Rb, Cs) are typical representatives of the body centred cubic (BCC) structure. The unit cell is non-primitive with two lattice points and the basis of one atom.

The positions of atoms at the two non-equivalent lattice points are 000 and  $\frac{1}{2} \frac{1}{2} \frac{1}{2}$ . The coordination number is eight. As stated earlier, its primitive cell is rhombohedral [see Fig. 1.6(a)] and its edges in vector form are expressed by (1.4a).

Crystal	Lattice parameter ( $\text{\AA}$ )	
Li	3.50	
Na	4.28	at room temperature
K	5.33	
Rb	5.62	at 92 K
Cs	6.05	

### 1.7.4 Crystals of Noble Metals

The crystalline noble metals (Cu, Ag, Au) represent another important structure, the face centred cubic (FCC). The unit cell has four lattice points with the basis of one atom. The positions of the atoms in the unit cell are:

$$000, \frac{1}{2} \frac{1}{2} 0, \frac{1}{2} 0 \frac{1}{2}, 0 \frac{1}{2} \frac{1}{2}$$

The coordination number is 12. It will become clear later when close-packed structures are discussed. One of the two close-packed structures has FCC symmetry. The primitive cell of an FCC crystal is a rhombohedron with primitive translation vectors as already shown in Fig. 1.6(b).

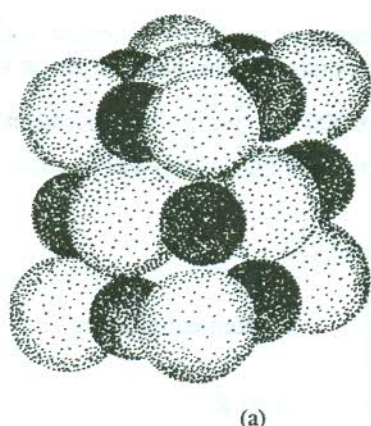
Crystal	Lattice parameter ( $\text{\AA}$ )
Cu	3.61
Ag	4.08
Au	4.07

### 1.7.5 The NaCl Structure

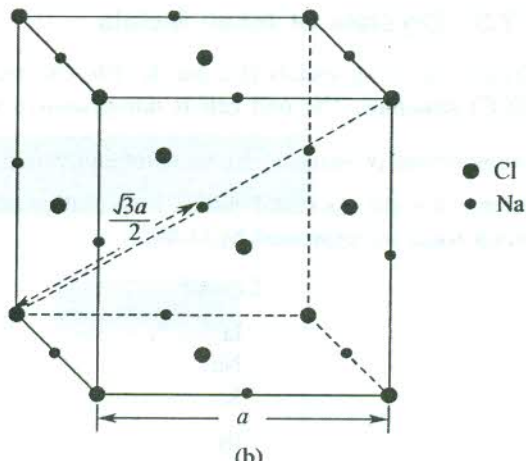
The space lattice of the NaCl crystal is FCC. The arrangement of Na and Cl atoms on this lattice is shown in Fig. 1.20(a). Notice that none of the sodium atoms is located at any lattice point. One of them is at the centre and the others are at the mid-points of the 12 edges of the cube. An atom on the edge contributes 1/4th of the atom. Thus the unit cell gets three sodium atoms from those on the edges ( $12/4 = 3$ ) and one from that at the centre. This gives four sodium atoms in the cell. Similarly, the contribution of chlorine atoms to the unit cell comes to four [ $(8/8) + (6/2) = 4$ ]. A single unit cell accommodates four formula unit cells of NaCl. The positions of atoms in the unit cell are:

$$\text{Na: } \frac{1}{2} \frac{1}{2} \frac{1}{2} \quad 00\frac{1}{2} \quad 0\frac{1}{2}0 \quad \frac{1}{2}00$$

$$\text{Cl: } 000 \quad \frac{1}{2} \frac{1}{2} 0 \quad \frac{1}{2} 0 \frac{1}{2} \quad 0 \frac{1}{2} \frac{1}{2}$$



(a)



(b)

**FIG. 1.20** (a) The arrangement of Na and Cl (shown bigger) atoms on the unit cell of NaCl crystal. (b) Locations of Na and Cl (shown bigger) atoms in the cube representing the unit cell. The separation between the basis partners is half the length of the body diagonal  $\sqrt{3}a/2$ .

The basis is composed of two atoms (Na and Cl) which are separated by half the length of the body diagonal,  $\sqrt{3}a/2$ , where  $a$  represents the length of the cube edge. The basis partner of each of the chlorine atoms at the corners is the sodium atom located at the centre whereas each of those at the face centres has partners in sodium atoms lying on two such edges as the distance between Na and Cl atoms in the basis remains  $\sqrt{3}a/2$  [Fig. 1.20(b)]. This shows that 1/8th of a formula unit is associated with the lattice point at the corner and 1/2 that at the face centre, explaining the distribution of four formula units among four lattice points of the FCC lattice. In this structure the nearest neighbours are the atoms of different type and their number is six.

Some of the crystals, representative of NaCl arrangement, along with their lattice parameter (cube edge) are included in the following table.

Crystal	Lattice parameter (Å)
NaCl	5.63
LiH	4.08
KBr	6.50
RbI	7.33
NH <sub>4</sub> I	4.37
NiO	4.17
UO	4.92
PbS	5.92

### 1.7.6 Close-packed Structures

The term *close-packing* needs a careful discussion. We may talk of the close-packed structure of a crystal of specific symmetry by referring to the structure with the smallest possible unit cell. Thus for every type of unit cell, there can be a maximum degree of closeness to which the atoms may be packed. The degree of closeness is represented by ‘Packing Fraction’, expressed as

$$\text{Packing fraction} = \frac{\text{Volume of the unit cell actually occupied by atoms}}{\text{Total volume of the unit cell}}$$

Considering unit cells having the basis of one atom, one can easily calculate the packing fraction of the closest-packed cells of different symmetries. Figure 1.21 shows the picture of a closest-packed BCC cell. Calculations show that the packing fraction is the highest in hexagonal and FCC unit cell and it has the same value (0.74) for both of these structures. This reveals that the packing in hexagonal and FCC structures can be made ideally the closest. But conventionally these two are referred to as the close-packed structures in literature. This point must be clearly borne in mind while using this nomenclature.

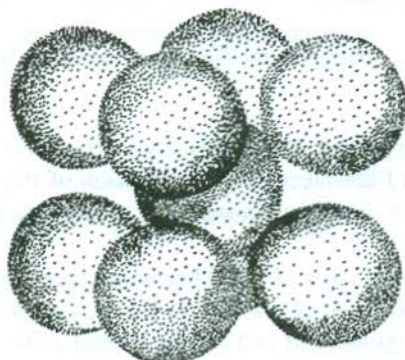


**FIG. 1.21** The arrangement of atoms in the closest-packed BCC crystal.

It is desirable to appreciate that the ideas mentioned just above can be visualized if one tries to arrange identical balls in all possible regular arrays. We observe that the closest-packed hexagonal and FCC patterns maximize the packing fraction.

While giving a description of the hexagonal close-packed structure, the way of arranging identical balls to get a close-packed FCC structure is explained. The main feature of the close-packed FCC structure is that the two atoms on the corners along the face diagonal touch the face centred atom. With this information its packing fraction can be easily calculated and this is left as an exercise for the reader.

### 1.7.7 Hexagonal Close-packed Structure (HCP)

When we try to make the closest arrangement of identical balls by placing them on a plane surface, we find that the largest number of balls that can touch a certain ball is six. This forms the layer A in Fig. 1.22. In arranging the closest packing of balls above this layer, we observe that a ball of layer A is in contact with three balls of the new layer, marked as B. Similarly, we can visualize in a layered structure like this that a ball of layer A will be in contact with three balls of the layer just below the layer A. It shows that in the closest-packed arrangement of identical atoms, an atom touches 12 atoms. This means that the maximum number of the nearest neighbours that is possible in the resulting crystalline structure is 12. If the building of layers is continued, we have two ways of arranging balls in the third layer C above the layer B. One way is to place balls above holes left in the layer A and not occupied in the layer B. The repetition of this arrangement of layers (ABC ABC ABC ...) produces an FCC structure in which the layer A forms its (111) plane. The other way

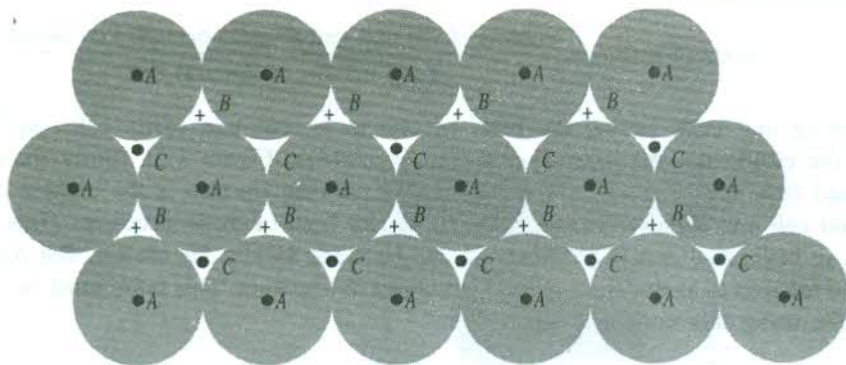


**FIG. 1.22** Three successive layers of the close-packed structure of identical spheres. The points *A*, *B*, *C* represent the centres of spheres in the first layer, second layer (in the middle) and third layer, respectively.

of arranging the third layer is to place balls exactly above the centres of balls in layer *A*. Thus the third layer becomes the replica of the layer *A*: The repetition of this arrangement of layers (*AB AB AB ...*) results in an HCP structure. In this structure, layer *A* serves as the basal plane of the hexagonal unit cell.

The HCP structure is shown in Fig. 1.23. The atomic positions do not represent the lattice points. The structure's basis consists of two identical atoms, i.e. two identical atoms are associated with each lattice point. The hexagonal unit cell can be treated as the combination of three rhombus based right prism shape unit cells. The position of the atom lying within a rhombohedron in layer *B* can be determined on the basis of simple geometrical considerations of the closest packing. Its height above the base is  $c/2$ . The picture of the arrangement of the atoms *P*, *Q*, *R*, *S* and *M* of Fig. 1.23(b) looks as shown in Fig. 1.24(a).

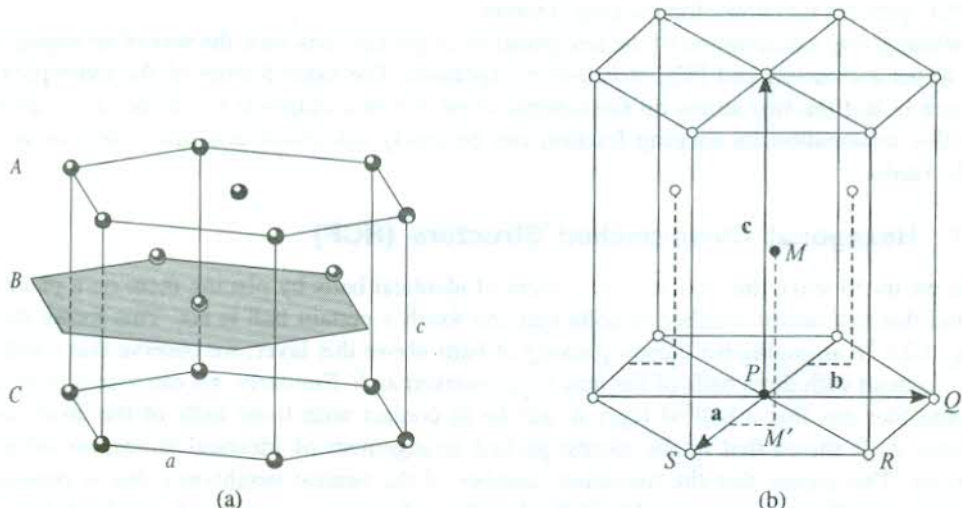


**FIG. 1.23** (a) The hexagonal close-packed structure. (b) The primitive axes of the HCP crystal. The *c* is normal to the plane of *a* and *b*. The two atoms of one basis are shown as solid circles.

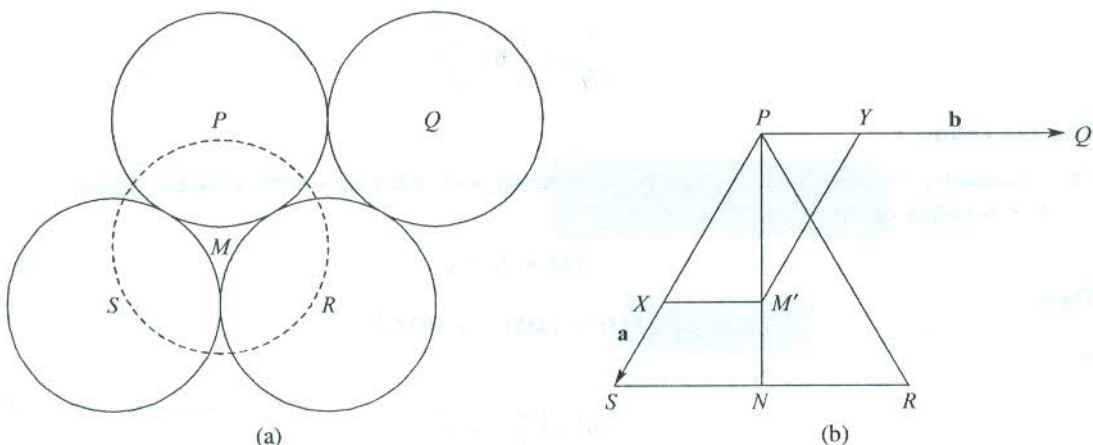


**FIG. 1.24** The atoms in the basal plane (centred at  $P, Q, R, S$ ) and the atom in the mid-plane (centred at  $M$ ) of the primitive HCP structure.

The point  $M'$  is the foot of the perpendicular dropped from  $M$  on the plane  $PRS$  and coincides with the centroid of the equilateral triangle  $PRS$  [Fig. 1.24(b)]. Thus

$$PM' = \frac{2}{3} PN = \frac{2}{3} \times \frac{\sqrt{3}a}{2} = \frac{a}{\sqrt{3}}$$

Therefore,

$$\begin{aligned} PX &= \frac{2}{3} PS \quad (\because XM' \parallel SN) \\ &= \frac{2}{3} a \end{aligned}$$

From  $\Delta PM'X$ ,

$$\begin{aligned} (XM')^2 &= (PX)^2 - (PM')^2 \\ &= \left(\frac{2}{3}a\right)^2 - \left(\frac{a}{\sqrt{3}}\right)^2 \\ &= \frac{a^2}{9} \end{aligned}$$

or

$$XM' = \frac{a}{3}$$

This gives the position of  $M$ , the other atom in the basis as

$$\left(\frac{2}{3}a, \frac{1}{3}a, \frac{c}{2}\right)$$

with respect to the origin at  $P$ , the first atom in the basis. The position vector of  $M$  can be expressed as

$$\frac{2}{3}\mathbf{a} + \frac{1}{3}\mathbf{b} + \frac{1}{2}\mathbf{c}$$

### The $c/a$ ratio

The relationship between  $a$  and  $c$  can be determined with the help of the adjacent figure.

If  $r$  is radius of the atom, then

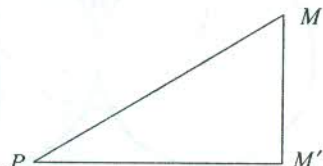
$$PM = 2r = a$$

Then

$$(PM)^2 = (MM')^2 + (PM')^2$$

or

$$a^2 = \left(\frac{c}{2}\right)^2 + \frac{a^2}{3}$$



or

$$\frac{c}{a} = \left(\frac{8}{3}\right)^{1/2} = 1.633$$

This value is the ideal value for the HCP structure composed of identical atoms whose shape is assumed as exactly spherical. The ratio departs from this theoretical value in crystals as can be seen from the table given below:

HCP crystal	$a$ (Å)	$c$ (Å)	$c/a$
Be	2.28	3.59	1.574
Mg	3.20	5.20	1.625
$\alpha$ -Co	2.51	4.11	1.637
Zn	2.65	4.93	1.860

### Packing fraction

The packing fraction can be easily calculated by using the primitive cell of the HCP structure. The primitive cell is a rhombus based right prism. Three such primitive cells combine to produce the non-primitive hexagonal unit cell. There are two atoms in a primitive cell.

$$\text{Packing fraction} = \frac{\text{Volume of two atoms}}{\text{Volume of the primitive cell}}$$

$$= \frac{2 \times \frac{4}{3} \pi r^3}{[\mathbf{a} \times \mathbf{b}] \cdot \mathbf{c}}$$

$$= \frac{\pi}{3\sqrt{2}} \quad (\text{use } a = 2r)$$

$$= 0.743$$

It can be shown that the closest-packed FCC structure has the same packing fraction as well. This value for some other standard crystal types is as under:

<i>Crystal type</i>	<i>Packing fraction</i>
Simple cubic	0.52
BCC	0.68
Diamond	0.34

The above data indicates that the HCP and the close-packed FCC structures have the closest-packing. Approximately, two-third of the metals crystallize either in HCP or in FCC structure. Most of the remaining one-third that are not close-packed are alkali metals and transition metals. They tend to solidify in a BCC symmetry. In common terminology the two closest-packed structures are referred to only as close-packed structures. The diamond structure, to be described in the following section, appears as the most empty lattice. The basis of these unique phenomena will be discussed in Chapter 2.

### 1.7.8 Diamond Structure

The space lattice of the diamond structure has FCC symmetry. Its unit cell has in all eight atoms with a basis of two atoms located at  $000, \frac{1}{4} \frac{1}{4} \frac{1}{4}$ . From this structure it is impossible to derive a

primitive cell whose basis may be composed of only one atom. The structure may be visualized as a combination of two FCC lattices with one being displaced from the other along the body diagonal by one-fourth of its length. The arrangement of atoms as projected on a face of the unit cell is shown

in Fig. 1.25. The dark shaded atoms are positioned at  $\frac{1}{4} \frac{1}{4} \frac{1}{4}, \frac{3}{4} \frac{3}{4} \frac{1}{4}, \frac{3}{4} \frac{1}{4} \frac{3}{4}$  and  $\frac{1}{4} \frac{3}{4} \frac{3}{4}$  and each of them makes a tetrahedral bond with one atom at the nearest neighbour and three centred on the nearest faces (Fig. 1.26). Thus the coordination number is four and not 12 as in the closest-packed structure with a maximum of only 34 per cent of the total volume being actually occupied by atoms.

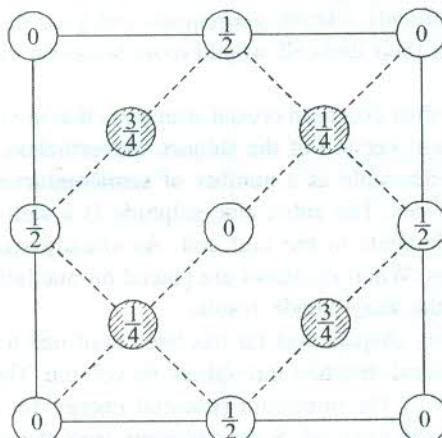
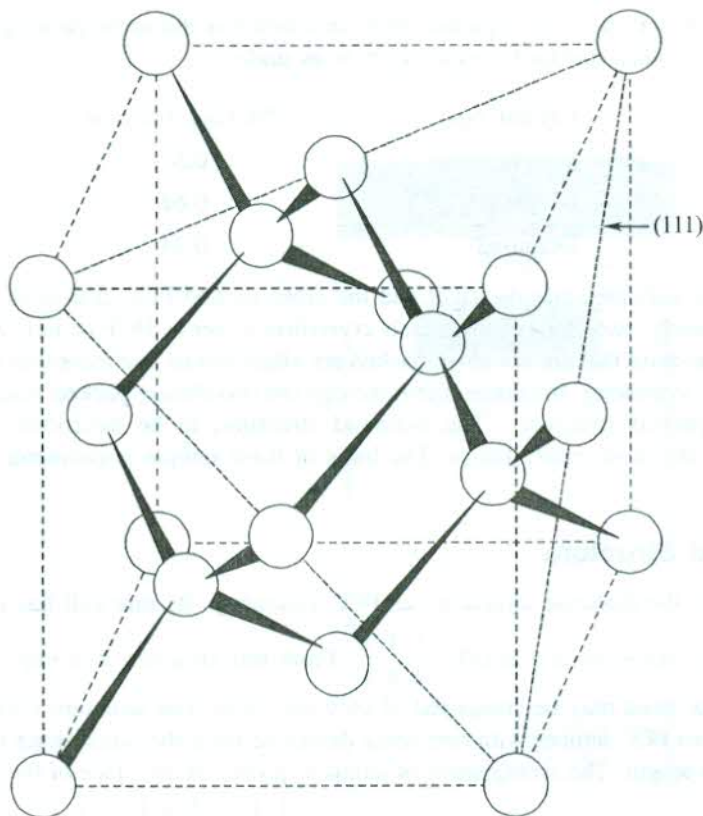


FIG. 1.25 Projection of atomic arrangement on a cube face in a diamond unit cell. The unit cell consists of two similar FCC lattices, displaced along the body diagonal of the cell by one-fourth of its length. The positions 0 and  $\frac{1}{2}$  refer to atoms on one lattice while  $\frac{1}{4}$  and  $\frac{3}{4}$  give positions of atoms on the second lattice.



**FIG. 1.26** The bonding model of the diamond structure.

Figure 1.26 shows that the diamond structure can be described as a stacking of sheets made up of continuously linked plucked hexagonal rings of atoms parallel to (111) planes of the cubic crystal. Crystals of carbon (diamond), silicon, germanium and grey tin are well known examples of diamond structures. The edge of their unit cell around room temperature measures as 3.56, 5.43, 5.65 and 6.46 Å, respectively.

The description of several other common crystal structures that are important crystallographically cannot find a place in the present version of the subject. Nevertheless, a brief reference to the zinc blende structure is very much desirable as a number of semiconductors having this structure form the basis of certain current devices. The cubic zinc sulphide is a well-known representative of this structure with atoms of two elements in the unit cell. As already stated, the diamond lattice is a combination of two FCC lattices. When Zn atoms are placed on one lattice and S atoms on the other, the conventional unit cell of the zinc blende results.

The whole discussion in this chapter thus far has been confined to ideal crystals. But in reality no crystal of finite size has the ideal structure throughout its volume. Thermodynamic considerations, such as the requirement of having the minimum potential energy for a configuration to be stable, control the arrangement of atoms in a crystal. Some departure from the crystallographically prescribed structure is observed in every crystal. These deviations are called imperfections. In no way we should

infer that the presence of imperfections always affects the usefulness of a crystal adversely. In many applications some of the imperfections prove as a boon and make the material in question extremely useful for applications. The study of various imperfections and their effect on the properties of crystals will be taken up in Chapter 12.

## 1.8 QUASICRYSTALS

Some materials diffract electrons like single crystals but have point group symmetry that is inconsistent with lattice translations. This structure was discovered by Shechtman et al.<sup>1</sup> in 1984 in grains of size up to 2  $\mu\text{m}$  of rapidly cooled alloys of Al with 10–14 atomic% Mn, Fe or Cr. It has long-range orientational order. The translational order is, however, not periodic and the structure does not have a rotational point symmetry. Materials showing this new structure have many of the properties of crystals and hence are classified as quasi periodic crystals or simply quasicrystals, in short. Unlike in crystals, the basis of structure (a group of atoms/molecules) does not repeat periodically in a quasicrystal. The repeating basis in this case is called the *unit cell*. An ideal quasicrystal is constructed by the infinite repetition in space of two or more unit cells.

The structure of aluminium alloys that forms the signature of quasicrystals is identified with the icosahedral<sup>1,2</sup> phase with the point group symmetry  $m \bar{3} \bar{5}$ . The icosahedra\* are the packing unit with Mn, Fe or Cr atom at the centre surrounded by twelve Al atoms located like the corners of an icosahedron. Although the icosahedral symmetry is an approximate representation of the site symmetry in these structures, the aperiodic lattice translations do not permit it to survive. Quasicrystals cannot and do not exhibit the point group symmetry. For example, the icosahedral phase under discussion shows five-fold axes of symmetry together with others only over a selected area when the specimen is rotated through angles of the icosahedral group. The observation must be read with the indications of elementary crystallography<sup>3</sup> that five-fold axes are inconsistent with translational orders.

The crystal structure analyses confirm that the symmetry of the fundamental space lattice of a quasicrystal belongs to none of the Bravais lattices (five in two dimensions and fourteen in three dimensions) that are used to describe the symmetry of crystals. The symmetries are instead intermediate to those for a crystal and for a liquid. The quasicrystals, discovered so far, are intermetallic alloys and show nearly insulating behaviour. They are also of great academic interest, as they enlarge the concept of crystal lattice.

## SUMMARY

### 1. Crystal = Space lattice + Basis

Space lattice: An infinite periodic array of points in space

Basis: An atom or an identical group of atoms attached to every lattice point. It is identical for every lattice point in terms of composition, relative orientation and separation.

1. D. Shechtman, L. Blech, D. Gratias and J.W. Cahn, *Phys. Rev. Lett.* **53**, 1951 (1984).

2. D. Levine and Paul J. Steinhardt, *Phys. Rev. Lett.* **53**, 2477 (1984).

\* Icosahedron is a polyhedron with twenty faces.

3. M.J. Burger, *Elementary Crystallography* (MIT Press, Cambridge, 1978).

2. Lattice points are connected to each other by the translation vector  $\mathbf{t} = n_1\mathbf{a} + n_2\mathbf{b} + n_3\mathbf{c}$ , where  $n_1, n_2, n_3$  are integers and  $\mathbf{a}, \mathbf{b}, \mathbf{c}$  are primitive translation vectors (the axes of a primitive cell).

3. Primitive cell: A minimum volume unit cell having only one lattice point.

4. Crystal types	Bravais lattices	Point groups	Space groups
Two-dimensional crystals	5	10	17
Three-dimensional crystals	14	32	230

5. Identical atoms may crystallize into the closest-packed structure either with HCP or with FCC symmetry, having the pattern of layers as:

HCP: AB AB AB AB ...

FCC: ABC ABC ABC ...

For both the structures:

- (i) The number of nearest neighbours (coordination number) = 12
- (ii) The packing fraction = 0.743

## PROBLEMS

- 1.1 Determine the lattice constant of NaCl crystal. The molecular weight of NaCl is 58.44 and the density is 2.167 g cm<sup>-3</sup>.

- 1.2 It is given that the primitive basis vectors of a lattice are:

$$\mathbf{a} = 3\hat{\mathbf{x}}, \quad \mathbf{b} = 3\hat{\mathbf{y}} \quad \text{and} \quad \mathbf{c} = \frac{3}{2}(\hat{\mathbf{x}} + \hat{\mathbf{y}} + \hat{\mathbf{z}})$$

What is the Bravais lattice?

- 1.3 In a simple hexagonal lattice,  $c/a = \sqrt{8/3}$ . Determine the volume of its direct primitive cell in terms of  $a$ .

- 1.4 (a) Show that every edge of the Wigner–Seitz cell for the BCC lattice has the length  $\sqrt{2}a/4$ , where  $a$  is the lattice constant of the BCC structure.

- (b) Show that the two diagonals on each face of the Wigner–Seitz cell for the FCC lattice are in the ratio  $\sqrt{2}:1$ .

- 1.5 Show that, for the closest packing of atoms, the densities of the FCC, BCC, SC and diamond monatomic lattices are approximately in the ratio 1.4 : 1.3 : 1.0 : 0.65.

- 1.6 The angles between the tetrahedral bonds of diamond are the same as the angles between the body diagonals of a cube. Determine the value of the angle using elementary vector analysis.

- 1.7 (a) What will be the indices of (100) and (001) planes of a conventional FCC lattice when referred to the primitive axes?

- (b) Prove that in a crystal of cubic symmetry, a direction  $[h k l]$  is perpendicular to the plane  $(h k l)$  with the same indices. Assume that the primitive basis vectors of the lattice are given.

- 1.8** Show geometrically that the face centred tetragonal structure is equivalent to a body centred tetragonal structure.
- 1.9** (a) Show that the Wigner–Seitz cell for any two-dimensional Bravais lattice is either a hexagon or a rectangle.  
 (b) Prove that the hexagonal faces of the BCC Wigner–Seitz cell are all regular hexagons.
- 1.10** Sodium metal transforms from BCC to HCP structure at about 23 K. Calculate the lattice constant in the hexagonal phase. Take the value of the lattice constant as 4.23 Å in the cubic phase and assume that the density remains unchanged during the transition and the ratio  $c/a$  is close to the ideal value.

## SUGGESTED FURTHER READING

- Buerger, M.J., *Introduction to Crystal Geometry* (McGraw-Hill, 1971).
- Fujiwara, T. and T. Ogawa (Eds.), "Quasicrystals", *Springer Ser. Solid State Sci.*, Vol. 93 (Springer, 1990).
- Megaw, H.D., *Crystal Structures: A Working Approach* (Saunders, 1973).
- Philips, F.C., *An Introduction to Crystallography*, 4th ed. (Wiley, 1971).

## EMOTA RO MOSEBHOQ

Emota ro mosebhoo is a short story by Yashpal and P. Bhagat. It is a simple story with a moral. It is a story of a boy who is very fond of playing with his kite. He has a very good kite which he likes very much. One day, while he is flying his kite, he sees a kite flying in the sky. It is a very beautiful kite with many colours. He wants to catch it, but he fails. He asks his mother for help, but she says that it is a kite of a rich person. She tells him that if he wants to catch it, he must work hard and earn money. The boy listens to his mother and starts working hard. After some time, he earns enough money to buy a kite like the one he saw. He is very happy and goes to fly his kite again. He catches the kite and flies it happily.



Emota ro mosebhoo is a short story by Yashpal and P. Bhagat. It is a simple story with a moral. It is a story of a boy who is very fond of playing with his kite. He has a very good kite which he likes very much. One day, while he is flying his kite, he sees a kite flying in the sky. It is a very beautiful kite with many colours. He wants to catch it, but he fails. He asks his mother for help, but she says that it is a kite of a rich person. She tells him that if he wants to catch it, he must work hard and earn money. The boy listens to his mother and starts working hard. After some time, he earns enough money to buy a kite like the one he saw. He is very happy and goes to fly his kite again. He catches the kite and flies it happily.

# Atomic Cohesion and Crystal Binding

## Cohesive Forces in Crystals

As discussed in Chapter 1, the symmetry and the structure of a crystal depend on the nature of the binding forces acting between the constituent atoms or particles. The analyses of crystal structure revealed the important fact that there is no essential difference between the forces which bind a chemical molecule and those which hold the atoms in a crystal together. This has proved to be of tremendous help to physicists in studying the nature of the binding forces in crystals by suitably extending the ideas of chemists. The present chapter is devoted to the description of various kinds of binding forces that result in different types of crystals. Other related properties will also be discussed.

### 2.1 COHESION OF ATOMS

Consider two atoms kept at a finite separation. The nature of the forces between atoms or the binding energy depends primarily on the distribution of positive charge over the inner ion core and of negative charge over the outer space within the atoms. Their potential energy is zero when the atoms are infinite distance apart. When they are brought closer to a finite separation, there will be a potential energy for the system whose sign depends on the relative order of magnitude of the repulsive and attractive forces. The attractive part of the potential energy is conventionally treated as negative since the atoms themselves do the work of attraction. The positive sign for the repulsive potential energy comes from the concept that in binding the atoms closer, the work is done against the repulsive force by an external agency. The total potential energy may be represented by a general potential of the form

$$U(r) = -\frac{A}{r^n} + \frac{B}{r^m} \quad (2.1)$$

where  $r$  is the interatomic distance, and  $A$  and  $B$  are constants. The net force is expressed as

$$\mathbf{F}(r) = -\frac{dU(r)}{dr} = -\frac{nA}{r^{n+1}} + \frac{mB}{r^{m+1}} \quad (2.2)$$

The first term represents the attractive force and the second the repulsive. The variation of potential energy and force as a function of the interatomic separation is traced in Fig. 2.1. The net force at the separation  $r_0$ , when the atoms are in stable equilibrium forming a diatomic molecule, is zero [Fig. 2.1(b)]. Obviously, the potential energy at this position is minimum with the negative sign

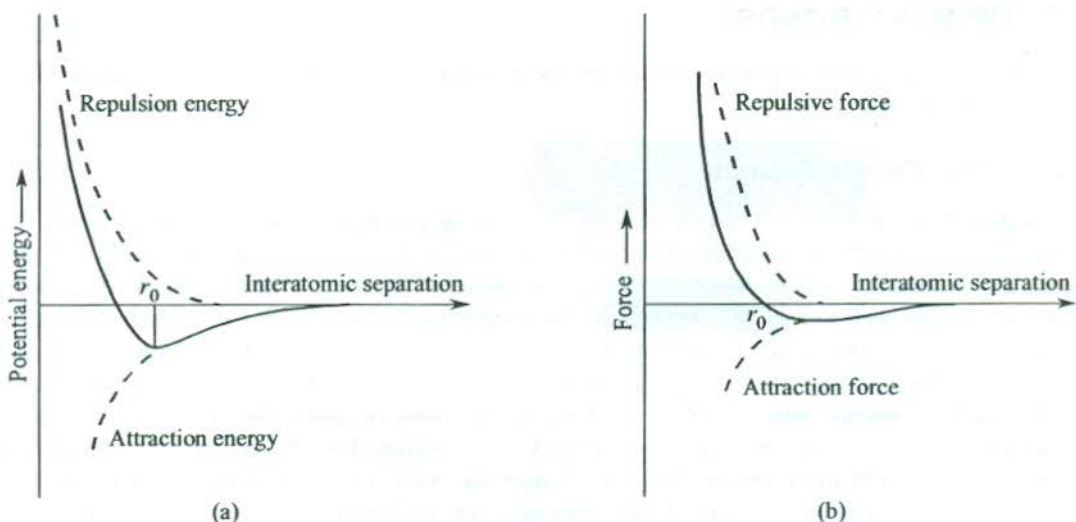


**FIG. 2.1** (a) Potential energy of a system of two atoms as a function of their interatomic separation. (b) Force between two atoms as a function of their interatomic separation.  $r_0$  denotes the separation at which the bond formation occurs.

[Fig. 2.1(a)]. It is also evident that as the atoms are brought closer, the repulsive force increases faster than the attractive force at short distances. When the two atoms stay in stable equilibrium at a certain separation they are said to have formed a chemical bond between them. The atoms spend a part of their energy in bond formation or we can say that a bond stores a part of the energy of the atoms. Therefore, the electron energy of atoms decreases when a large number of them collect together to form a solid. This suggests that when a solid is heated to break it finally into isolated atoms. How strongly the atoms are bound together in a solid is represented by its cohesive energy (or binding energy). A proper discussion on cohesive energy will be taken up later in this chapter after dealing with the types of binding in solids. When on solidification a pronounced lowering of electron energies takes place, the bonds formed are strong and called *primary bonds*. On the other hand if the lowering of electron energies is small, weak bonds are formed and referred to as *secondary bonds*.

The quantum mechanical interpretation of the probability function comes handy in understanding why some bonds are strong and directional while the others are weak and non-directional. It can be done qualitatively by acquiring information about the energies and the locations of the bonding electrons with respect to the positively charged ion cores. The probability that an electron, confined in the small volume  $dV$ , may lie in the orbital  $\psi$  is given by  $|\psi|^2 dV$ . For the large value of the probability amplitude  $|\psi|^2$  in a certain direction, the bond formed is strong and concentrated along this direction and it behaves as directional. The small values of  $|\psi|^2$  correspond to the weaker non-directional bonds. Furthermore, if  $|\psi|^2$  is spherically symmetric non-directional bonds result. The spherical symmetry means that the chance of finding a bonding electron in all directions is equal and an atom can approach the other atom from any direction over the solid angle  $4\pi$  for making the bond. Such a bonding gives rise to close packing exhibited by metals.

Now, we set out to outline the description of various forms of binding mechanisms in solids. Based on their comparative strength, the bonds formed in various binding processes may broadly be classified as (a) primary bonds and (b) secondary bonds.

## 2.2 PRIMARY BONDS

The three limiting cases of primary bonds are identified as (a) covalent bonds, (b) metallic bonds, and (c) ionic bonds.

### 2.2.1 The Covalent Bond

A covalent bond involves the mutual sharing of a pair of electrons between a pair of atoms. The spins of the two electrons are oriented in opposite directions. In solid state, the most stable covalent bonds are formed between non-metallic atoms like those of N, O, C, F and Cl. Some of the other elements that are well known to form covalent-bonded crystals include Si, Ge, As and Se. But, the nature of bonds in these solids is only partly covalent. Strong covalent bonds are formed when each atom has at least one-half filled orbital. In such a situation only will there be a substantial lowering in the electrons energy when each of the bonding electrons occupies the orbitals of two atoms simultaneously. The lowering of electrons energy is proportional to the degree of overlap of the bonding orbitals. The more the overlap, the stronger the bond. Either the electrostatic repulsion or the Pauli exclusion principle controls the overlap. The molecular hydrogen offers itself as the simplest candidate for the explanation of the covalent bonding. Hydrogen has a single electron which occupies the 1s orbital in the ground state. The orbital is half-filled and the Pauli principle allows it to accommodate one more electron with the opposite spin. Thus when two hydrogen atoms are brought close, their electron charge distributions overlap and the covalent bond is formed by having the two electrons with opposite spins in the 1s orbital belonging to both the atoms. This configuration, being lower in energy than the one in which the second electron went to the 2s orbital with the possibility of the same spin orientation, belongs to the hydrogen molecule in the ground state.

The effect of repulsive interaction as a compulsion of Pauli principle is best demonstrated in rare gas solids whose atoms have completely filled orbitals with little chance of overlap. This results in a large interatomic distance (3.76 Å in Ar) compared to the bond length in a covalent-bonded molecule such as Cl<sub>2</sub> (2 Å). There is a deficiency of one electron in the outermost shell of chlorine (3p<sup>5</sup>) to saturate it. Because of this the outermost orbital of a chlorine atom has the tendency to overlap with that of the neighbouring chlorine atom in search of the deficit electron. Since this forms the basis of the covalent bond formation, the covalent bond is also known as a *saturable bond*.

The discussion on the covalent binding remains incomplete without a few remarks on elements in group IV of the periodic table (C, Si, Ge and grey Sn). These are extremely covalent elements and crystallize in the tetrahedrally coordinated diamond structure (see Fig. 1.26). Each atom participates in four covalent bonds with its four neighbours. These bonds are extremely directional and difficult to tilt. This provides the material with unusual strength and hardness. The wide use of diamond for making cutting tools is a well-acknowledged fact. Also, the strong directional nature of the covalent bonds rules out close packing and increases emptiness in covalent bonded crystals. For example, the fraction of volume of a diamond crystal actually occupied by atoms is a mere 0.34 which is 46 per cent of the value for the close-packed FCC and HCP structures. In view of this fact, the diamond lattice is called the *empty lattice*.

### 2.2.2 The Metallic Bond

In the modern theory of metals the valence electrons, being loosely bound to the respective parent atoms, are treated as common to the whole assembly of atoms comprising the metal. The valence electrons, generally one or two per atom, are considered free and, therefore, allowed to move freely

over the whole volume of the metal. The metal is pictured as an assembly of positive metal ions embedded in a sea of the free electron gas. The attraction between the metal ions and the electron gas gives rise to a strong cohesive force. The free electron gas serves as the glue. The concept of free electrons contributes significantly to the success of this model in explaining most of the properties of metals such as high electrical and thermal conductivities, high reflectivity and opacity. In reality the motions of valence electrons, also called *conduction electrons* with reference to metals, are affected, no matter how slightly, because of the presence of other particles including the fellow electrons. A complete theory does take care of this effect which is of crucial advantage in explaining some of the dramatic properties (e.g. superconductivity) of solids in general.

Since the metallic bonds involve loosely-bound electrons, there can be a relatively large number of probable orientations for a metal bond. In other words, the bonds are weak and non-directional. This characterizes metals as having the tendency to crystallize in relatively close-packed structures with a large number of nearest neighbours. This fact is in agreement with the observed structures of metals—HCP, FCC and BCC. In all these structures, the metallic bond is not saturated. For example, in the BCC structure of lithium, each bond has only 1/4th of an electron since the only outermost electron ( $3s^1$ ) is involved in eight bonds with atoms at the corners of the cube. Still the modern picture assumes that the metallic bond is more closely related to the electron-pair or covalent bond than to an ionic-type bond, which is discussed next.

### 2.2.3 The Ionic Bond

The formation of an ionic bond is based on an electrostatic attraction between the positive and negative ions that are derived from the free atoms by the loss or gain of electrons. The ionic bond is responsible for the binding of salts that comprise the combinations of the elements located on the right- and left-hand sides of the periodic table. Alkali halides are the typical representatives of such salts. The electronic configurations of the alkali and halogen atoms are nearly closed-shell configurations. The bond formation is facilitated by the ease with which the alkali atom loses one electron and the halogen atom accepts it to acquire closed-shell configurations. In another way, we say that the origin of binding lies in the low ionization energy of the alkali atom and the high electron affinity of the halogen atom. Take the example of NaCl in which the sodium atom has one electron more ( $1s^2 2s^2 2p^6 3s^1$ ) than the neon ( $1s^2 2s^2 2p^6$ ) and the chlorine atom is one electron short ( $1s^2 2s^2 2p^6 3s^2 3p^5$ ) of the argon configuration ( $1s^2 2s^2 2p^6 3s^2 3p^6$ ). This shows how Na and Cl atoms get bonded when brought close because of their easy ionization to  $\text{Na}^+$  and  $\text{Cl}^-$  ions. Each ion has the tendency of being surrounded by as many ions of the opposite type as possible. The coordination number and the nearest neighbour distance are governed jointly by the geometrical factors and the repulsive interaction between the like ions. But the tendency of one type of ions to surround an ion of the opposite type binds a continuous network of ions to form the crystal instead of forming small discrete molecules.

Ionic bonds are neither saturable nor directional. Even then they are strong enough as is confirmed by the hardness, high melting point and low coefficient of expansion of ionic crystals.

### 2.2.4 Mixed Bonding

The discussion on primary bonds remains inconclusive without commenting on the purity of bonds in crystals. The mixture of bonding types has been discussed by Pauling\* in great detail. In particular it is a matter of general observation that the bonding in most of the covalent-bonded crystals has

\* L. Pauling, *The Nature of the Chemical Bond*, Cornell Univ. Press (1960).

a small component of ionic bonding. Ashcroft and Mermin\* elucidate it for GaAs by picturizing the electron density of Ga and As ions in the crystal. Phillips\*\* developed a semiempirical theory of fractional covalent or ionic character of bonds in a dielectric crystal. His calculations show that bonds in Ge and Si are purely covalent. But the bonding in most of the binary crystals turns out to be of mixed nature. LiF, NaCl and RbF are found to be almost purely ionic as the fraction of ionic character in them turns out to be 0.92, 0.94 and 0.96, respectively.

The ionic character of a solid may be determined by analyzing its x-ray scattering data. This is an effective tool as the scattering power depends on the number of electrons possessed by the constituent ions. For example, in ionic-bonded KCl each of the ions,  $K^+$  and  $Cl^-$ , has 18 electrons. Hence the scattering power for  $K^+$  and  $Cl^-$  is found to be equal. The electron density distribution in the basal plane of NaCl, as derived by G. Schoknecht† is shown in Fig. 2.2.

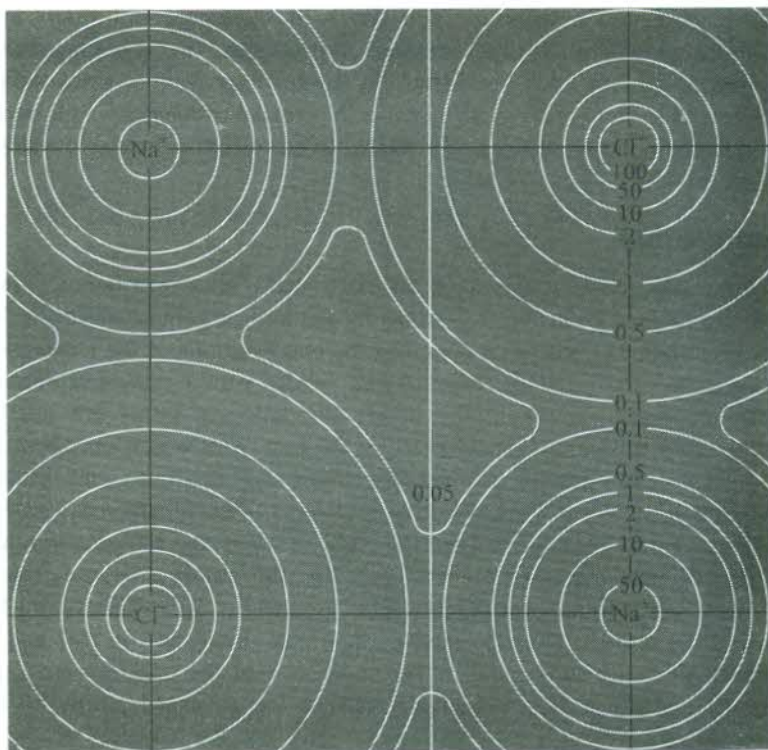


**FIG. 2.2** Electron density distribution in the basal plane of NaCl. The numbers of contours express the relative electron density. [From Kittle, C., *An Introduction to Solid State Physics*, 6th ed., p. 65, John Wiley (1986).]

### 2.3 SECONDARY BONDS

The limiting cases of secondary bonds are not easily separable. van der Waals and hydrogen bonds will be discussed in this category. The electric dipole-dipole interaction forms the basis of these bonds.

\* N.W. Ashcroft and N.D. Mermin, *Solid State Physics*, Saunders College (1988).

\*\* J.C. Phillips, *Bonds and Bands in Semiconductors*, Academic Press (1973).

† In C. Kittle, *Introduction to Solid State Physics*, 6th ed., p. 65, John Wiley (1986).

### 2.3.1 The van der Waals Bond

We may be curious to know why neutral molecules or noble gases should undergo liquefaction and crystallization. Consider noble gas atoms which have close-shell structure and are represented as spherical rigid charge distributions. Such electron distributions are reluctant to overlap when any two atoms are brought close to each other. But there must be some attractive forces between atoms bringing about the cohesion and finally the solidification. Of these forces, one is the van der Waals force we are interested in. These are weak forces arising out of the attractive interaction between fluctuating electric dipoles. By chance, for a fraction of the second, there could be more number of electrons on one side of the nucleus than on the other. This destroys the spherical symmetry of the electron charge distribution and momentarily displaces the centre of the negative charge (the electrons) from the centre of the positive charge (the nucleus). Thus an atom becomes a tiny electric dipole which is capable of inducing an electric dipole moment in the neighbouring atom. The two dipoles attract each other, though weakly, resulting in the van der Waals binding. As the electron charge distribution keeps fluctuating, the electric dipoles in question are called *fluctuating dipoles*.

Suppose we have two atoms 1 and 2 of a noble gas separated by distance  $r$ . As described above, when atom 1 acquires an instantaneous electric dipole moment  $\mathbf{p}_1$ , an instantaneous electric dipole moment  $\mathbf{p}_2$  may be induced in atom 2 because of the polarization caused by the electric field  $\mathbf{E}$  of the atomic dipole 1 at atom 2. It is now a trivial exercise in electrostatics (refer to Problem 2.2) to show that the interaction energy of two dipoles  $\mathbf{p}_1$  and  $\mathbf{p}_2$  ( $= - \mathbf{p}_2 \cdot \mathbf{E}$ ) varies with separation as  $1/r^6$ . This interaction energy is essentially the van der Waals binding energy of the two atoms.

An alternative explanation of van der Waals interaction is the quantum mechanical basis in which the creation of the electric dipole is attributed to the zero point electronic motion. In fact, the van der Waals interaction more completely identified as the van der Waals–London interaction turns out to be a quantum effect. The quantum mechanical calculation confirms  $1/r^6$  dependence of the interaction. The interaction is expressed as  $A/r^6$  (for derivation see Appendix A), where  $A$  is a constant involving the Planck constant. This implies that the interaction vanishes when the Planck constant is taken as zero, proving that the van der Waals interaction has its proper explanation in quantum physics.

It must be noticed that the van der Waals bonds are neither saturable nor directional. Barring helium, all the noble gases crystallize in the close-packed FCC structure. These weakly-bound crystals are transparent insulators and characterized by low melting points.

### 2.3.2 The Hydrogen Bond

A number of covalently-bonded molecules behave as permanent electric dipoles. HF and  $\text{H}_2\text{O}$  are the two most talked about examples. The attraction between the positive end of one dipole and the negative end of the neighbouring dipole forms clusters or large aggregates of molecules on cooling when the crystallization may take place. The mechanism of bond formation involves the attraction of a hydrogen atom to two strongly electronegative atoms. These bonds are called *hydrogen bonds*. These bonds have the directional property and are stronger than the van der Waals bonds. This is endorsed by the observation that supermolecules like  $\text{H}_2\text{F}_2$ ,  $\text{H}_3\text{F}_3$ , . . . are formed even in the gaseous phase.

In an effort to understand the mechanism of hydrogen bonding clearly, we take up ice crystals which exhibit some unusual behaviour. The outer electron configuration of the oxygen atom in  $\text{H}_2\text{O}$  is represented by four  $\text{sp}^3$  hybrid orbitals. Figure 2.3 shows that two of these are involved in covalent bonds to the hydrogen atoms and the rest two are doubly occupied by oxygen electrons. Out of the

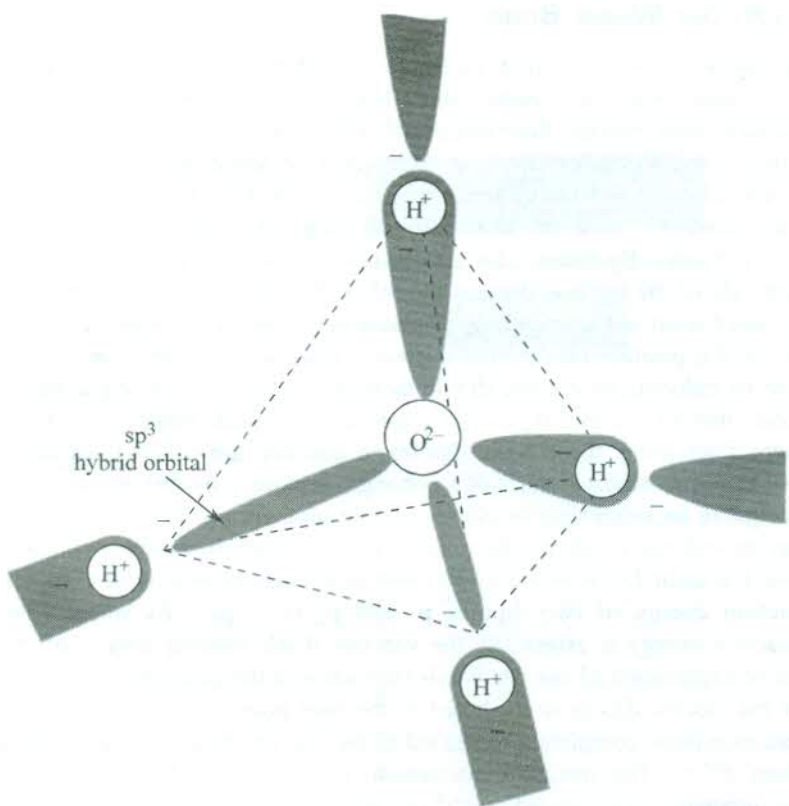


**FIG. 2.3** The tetrahedral covalent bonding in ice involving the  $sp^3$  hybrid orbitals of  $H_2O$ .

six outer oxygen electrons, two are engaged in bonding and the other four find a place in spare orbitals. This bonding pattern gives a tetrahedral shape to bonded molecules in ice. Two vertices of a tetrahedron are occupied by hydrogen atoms which are essentially the localized protons. The other two vertices exhibit relatively diffused negative charges.

The negligible small size of the proton is responsible for the peculiar structure of ice crystals as it practically sits on the oxygen ions, something impossible for any other positive ion to do. One of the many phases of ice crystals as shown in Pauling's book\* is pictured in Fig. 2.4. Two oxygen atoms are bound by a proton that is localized close to one oxygen atom along the line joining it to one of its neighbouring oxygen atoms. There are two protons close to each oxygen atom, giving a large number of ways to attach a proton to either end of the bond. This is reflected in the irregular positions of protons which are very well accounted by the observed large residual entropy of ice crystals at low temperatures. Lastly, a word about the floating property of ice. The molecular clusters of water are smaller and less stable in liquid state than they are in ice because of which they are on the average more closely packed in this state. This increases the density of water and ice floats when immersed in it.

\* L. Pauling, *The Nature of the Chemical Bond*, Cornell Univ. Press (1960).

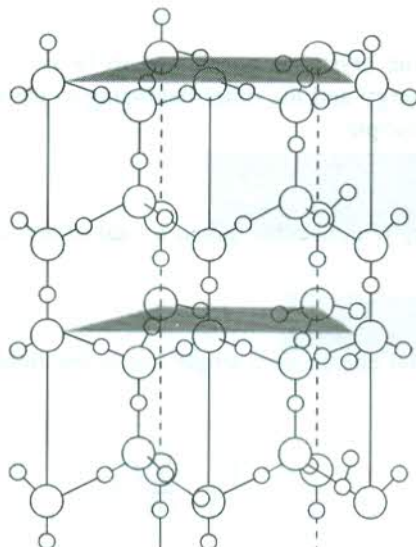


**FIG. 2.4** The hydrogen bonding in ice. The large circles denote oxygen ions and the small circles protons.

## 2.4 THE COHESIVE ENERGY

As stated earlier, the cohesive energy of a crystal is the measure of how strongly its constituent atoms or particles are bound. It may be defined as the energy required to break the crystal into its isolated neutral constituent parts. By constituent parts we precisely mean atoms or molecules. For example, it sounds more reasonable to define the cohesive energy of solid nitrogen as the energy required to disassemble it into isolated nitrogen molecules instead of atoms. The two definitions are, however, interconvertible. In the early development of the solids classification, the theory based itself heavily on the nature of cohesion. The role of spatial electronic arrangement was almost sidelined. But with the increasing need to study the non-equilibrium properties for the development of devices, the concern for cohesive energy has ceased to be of any significant note.

Now, we present here a brief sketch of the classical theory to discuss the cohesive energy of crystals at 0 K. Calculations are made in the static lattice approximation which treats the atoms to be at rest at equilibrium sites. It neglects the zero point motion which relates to one of the basic tenets (the uncertainty principle) of quantum theory. The resulting error for most of the crystals turns out to be 1 per cent or less. But there may be a question mark against this approximation while treating the lighter noble gases as they have the origin of their cohesion in the zero point motion. This is not to suggest that the noble gases cannot be handled with a simplified theory, like the one under discussion. Surprisingly, the theory which is reasonably simple in this case enjoys a high degree of success.

The oversimplified theory discussed above is applied to ionic crystals with maximum ease as the dominating long-range attractive interaction between the oppositely charged ions renders other interactions of little concern. On the other hand, it is difficult to have a simple theory for calculating the cohesive energy of covalent and metallic crystals. The electronic configurations in crystals have far more distorted forms than what they are in isolated atoms or ions. This makes it imperative to calculate the energy by treating the valence electrons in the field of the periodic crystal potential. It leads to the problem of band structure calculation complicating the whole procedure. The level of the present book cannot accommodate the theory of covalent and metallic crystals. The description of simple methods of calculating the cohesive energy of ionic and noble gas crystals would suffice.

### 2.4.1 Ionic Crystals

The potential energy of an ionic crystal is considered to be composed of two components, one representing the electrostatic energy and the other belonging to the repulsive overlap which has its origin in the Pauli exclusion principle.

#### *The electrostatic energy*

Consider an ionic crystal having  $N$  molecules, given a total of  $2N$  ions. The electrostatic energy of the crystal can be written as

$$U_e = NU_i \quad (2.3)$$

where  $U_i$  is the average potential energy of a single ion in the field of the other remaining ions. Also

$$U_i = \sum_{i=1}^{2N-1} U_{ij} \quad (2.4)$$

with

$$U_{ij} = \pm \frac{1}{4\pi \epsilon_0} \frac{q^2}{|\mathbf{r}_{ij}|}; \quad \mathbf{r}_{ij} = \mathbf{r}_i - \mathbf{r}_j \quad (2.5)$$

Here  $U_{ij}$  represents the electrostatic interaction energy in SI units between two ions bearing an equal charge  $q$  and their positions being given by the vectors  $\mathbf{r}_i$  and  $\mathbf{r}_j$ . Taking the origin of the coordinate system at the position of one of the positive ions, we have

$$\begin{aligned} \mathbf{r}_{ij} &= (\hat{i}n_1 + \hat{j}n_2 + \hat{k}n_3)r \\ |\mathbf{r}_{ij}| &= (n_1^2 + n_2^2 + n_3^2)^{1/2} r \end{aligned} \quad (2.6)$$

where  $n_1, n_2, n_3$  represent the number of units of the nearest neighbour distance  $r$  along the  $x, y, z$  axes of the crystal. Having a positive ion at the origin, we observe that  $(n_1, n_2, n_3) r$  represents the location of

a negative ion, if  $(n_1 + n_2 + n_3)$  is an odd integer

a positive ion, if  $(n_1 + n_2 + n_3)$  is an even integer.

The Coulomb energy between the ion at the origin and any other ion located at  $\mathbf{r}_j$  will be

$$U_{ij} = \frac{(-1)^{n_1+n_2+n_3}}{4\pi \epsilon_0} \frac{q^2}{(n_1^2 + n_2^2 + n_3^2)^{1/2} r} \quad (2.7)$$

or

$$U_i = \frac{\alpha q^2}{4\pi \epsilon_0 r} \quad (2.8)$$

where  $\alpha$  is a constant known as the *Madelung constant*, expressed by the following relation:

$$\alpha = \sum_{n_1=0}^{2N-1} \sum_{n_2=0}^{2N-1} \sum_{n_3=0}^{2N-1} (-1)^{n_1+n_2+n_3} (n_1^2 + n_2^2 + n_3^2)^{-1/2} \quad (2.9)$$

$(n_1, n_2, n_3) \neq (0, 0, 0)$

For a NaCl crystal, the first term is  $-6/\sqrt{1}$  that is contributed by the six nearest neighbours of the opposite type located at  $(\pm 1, 0, 0)$ ,  $(0, \pm 1, 0)$  and  $(0, 0, \pm 1)$  in units of the nearest neighbour distance. The second term  $12/\sqrt{2}$  comes from the 12 nearest neighbours of the same type, located at  $(\pm 1, \pm 1, 0)$ ,  $(0, \pm 1, \pm 1)$  and  $(\pm 1, 0, \pm 1)$  and at a distance of  $\sqrt{2}r$  from the origin. The sum in (2.9) can be made to converge rapidly using some tricky mathematical method. The calculations yield the value of Madelung constant as  $-1.7476$  for a NaCl crystal. For some other important ionic crystals such as CsCl, zinc blende (ZnS) and wurtzite (ZnS), the values are  $-1.7627$ ,  $-1.6381$  and  $-1.641$ , respectively. A detailed account of the method of calculation has been provided by Born and Huang.\*

### The repulsive overlap energy

An approximate analytical form of the potential energy for a pair of ions as originally introduced by Born and Mayer\*\* is given by

$$U_{ij}^{(r)} = \lambda_{ij} \exp\left(\frac{-|\mathbf{r}_{ij}|}{\rho}\right) \quad (2.10)$$

where  $\lambda_{ij}$  and  $\rho$  are the empirical parameters which depend on the nature of the ions  $i$  and  $j$  but are independent of the distance between them.

The repulsive term is representative of the fact that the overlap between the electron configurations of neighbouring ions is resisted. The constants  $\lambda$  and  $\rho$  stand for the strength and the range of interaction, respectively, and can be determined with the knowledge of the experimental values of the lattice constant and compressibility. The range  $\rho$  is defined as the value of  $|\mathbf{r}_{ij}|$  for which the interaction is reduced to  $1/e$  of the interaction  $\lambda_{ij}$  when the two ions are in contact, treating them as ideal point charges.

Thus the total potential energy of the ions at  $\mathbf{r}_i$  and  $\mathbf{r}_j$  can be written as the sum of the attractive potential energy  $U_{ij}^{(a)}$  and the repulsive potential energy  $U_{ij}^{(r)}$  such that

$$\begin{aligned} U_{ij}^{(t)} &= U_{ij}^{(a)} + U_{ij}^{(r)} \\ &= -\frac{1}{4\pi\epsilon_0} \frac{q^2}{|\mathbf{r}_{ij}|} + \lambda_{ij} \exp\left(\frac{-|\mathbf{r}_{ij}|}{\rho}\right) \end{aligned} \quad (2.11)$$

The total potential energy of a crystal of NaCl structure will then be written as

$$U = N \left( -\frac{\alpha q^2}{4\pi\epsilon_0 r} + 6\lambda_{+-} \exp\left(\frac{-\sqrt{1}r}{\rho}\right) + 12\lambda_{++} \exp\left(\frac{-\sqrt{2}r}{\rho}\right) + \dots \right) \quad (2.12)$$

\* M. Born and K. Huang, *Dynamical Theory of Crystal Lattice*, Oxford Univ. Press (1954).

\*\* M. Born and J.E. Mayer, *Z. Physik*, **75**, 1 (1932).

The subscripts on  $\lambda$  in (2.12) indicate that its value is different with reference to the interaction between the like ions and that between the unlike ions.

If we consider the repulsion only between the nearest neighbours, the relation (2.12) assumes the general form

$$U = N \left( -\frac{\alpha q^2}{4\pi\epsilon_0 r} + z \lambda e^{-r/\rho} \right) \quad (2.13)$$

where  $z$  stands for the number of nearest neighbours (six in the NaCl structure). To ensure that (2.13) applies to a stable crystal,  $\alpha$  is assigned the positive sign in the relation.

Since the cohesive energy is referred to as the minimum value of the potential energy, we can achieve the objective by expressing (2.13) in terms of the nearest neighbour distance for which the minimum of potential energy occurs. For  $U$  to be minimum,

$$\frac{dU}{dr} = 0$$

From (2.13), we get

$$\frac{dU}{dr} = N \left( \frac{\alpha q^2}{4\pi\epsilon_0 r^2} - \frac{z\lambda}{\rho} e^{-r/\rho} \right)_{r=r_0} = 0$$

where  $r_0$  is the nearest neighbour distance at equilibrium. This condition gives

$$z \lambda e^{-r_0/\rho} = \frac{\alpha q^2 \rho}{4\pi\epsilon_0 r_0^2} \quad (2.14)$$

From (2.13) and (2.14), we get

$$U_0 = \frac{-N\alpha q^2}{4\pi\epsilon_0 r_0} \left( 1 - \frac{\rho}{r_0} \right) \quad (2.15)$$

As an exercise, we apply (2.15) to a NaCl crystal. The potential energy of a single ion in the crystal is given by

$$U_{\text{ion}} = - \frac{\alpha q^2}{4\pi\epsilon_0 r_0} \left( 1 - \frac{\rho}{r_0} \right) \quad (2.16)$$

For NaCl,  $\alpha = 1.748$ ,  $r_0 = 2.81 \text{ \AA}$  and  $\rho$  is generally found to be  $r_0/9$ . (A small value of  $\rho$  shows the short range of repulsive interaction.)

Substituting these values in (2.16), we get

$$U_{\text{ion}} = -7.97 \text{ eV}$$

This is not the correct energy of a single ion as every ion is counted twice while taking the pair

interaction. Therefore, the true potential energy of an ion is  $-7.97/2$  eV = -3.99 eV, which is essentially the contribution of a single ion to the potential energy. With reference to ionic crystals the quantity, 7.97 eV, is referred to as the lattice energy which is only the cohesive energy per ion pair. This is in excellent agreement with the measured value of 7.96 eV.

The cohesive energy per atom may as well be calculated easily. The ionization potential of Na is 5.14 eV and the electron affinity of Cl is -3.61 eV. In the formation of  $\text{Na}^+ - \text{Cl}^-$  ion pair, the energy spent in the electron transfer is equal to  $(5.14 - 3.61)$  eV, i.e. 1.53 eV, meaning thereby that each atom contributes 0.77 eV to the cohesive energy. Thus the cohesive energy/atom of NaCl

$$\begin{aligned} &= (-3.99 + 0.77) \text{ eV} \\ &= -3.22 \text{ eV} \end{aligned}$$

The success of the underlined theory is further emphasized by the closeness of the measured value (3.28 eV/atom).

## 2.4.2 Noble Gas Crystals

The discussion under Section 2.3.1 needs extension for obtaining a complete picture of interactions in noble gas crystals. The repulsive potential energy is conventionally expressed in the form of an empirical power law as  $B/r^{12}$ . The total potential energy of a pair of atoms at the separation  $r$  is generally represented by

$$U(r) = -\frac{A}{r^6} + \frac{B}{r^{12}} \quad (2.17a)$$

and this is known as the Lennard-Jones potential. The constants  $A$  and  $B$  are empirical parameters.

On the requirement that the repulsive force increases faster than the attractive force at short distances, the exponent in the repulsive term has to be more than 6. In addition, if the analytic simplicity is taken into account the choice falls on 12. Further, with this choice the theoretical estimates of several physical properties of noble gases, exclusive of  $\text{He}^3$  and  $\text{He}^4$ , are found to be in excellent accord with the experiment. A satisfactory explanation for the disagreement in the case of helium is not possible at this stage to avoid digression. However, it should suffice to remark that helium is identified as a unique quantum matter in the solid state theory which has developed provisions for dealing with it especially. Finally, it must be emphasized that the van der Waals interaction is present in all the three states of every material. Being weak in nature it is not the main cause of cohesion in many crystals where other strong interactions are present and the crystal bindings are named after them.

Equation [2.17(a)] is usually expressed as

$$U(r) = 4\epsilon \left[ \left( \frac{\sigma}{r} \right)^{12} - \left( \frac{\sigma}{r} \right)^6 \right] \quad (2.17b)$$

where

$$\sigma = \left( \frac{B}{A} \right)^{1/6} \quad \text{and} \quad \epsilon = \frac{A^2}{4B}$$

The Lennard-Jones potential in the form of relation (2.17b) is shown in Fig. 2.5. Suitable values of the parameters and  $\sigma$  have been obtained by fitting the theoretically calculated values of certain

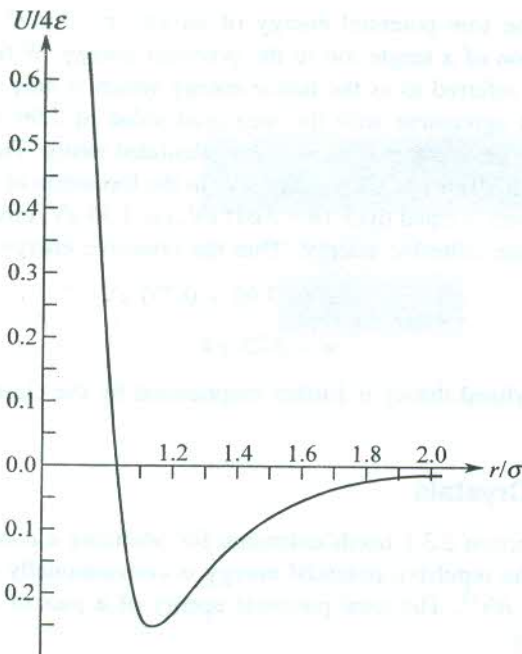


FIG. 2.5 The Lennard-Jones potential as given by equation (2.17b).

physical properties involving these parameters with those experimentally observed in the gaseous phase. In principle, these values cannot be used for solids where the interaction is not a sum of pair potentials on account of high densities. The values of parameters serve as a measure of the strength of attraction and the radius of the repulsive core.

The hydrogen crystals are among the weakest bonded crystals with a cohesive energy of 0.01 eV per molecule which is one-tenth of that of methane's (0.1 eV per molecule). The cohesive energies of a number of crystals of different types are given in Table 2.1 for the purpose of a comparative study. For a thorough study the reader may consult the book by Ashcroft and Mermin\* which gives a more comprehensive view of the subject and treasures large data on the related physical quantities of molecular and ionic crystals in particular.

It must now be abundantly clear that the calculations we have discussed in this section are closely linked with lattice constants (or lattice parameters) of crystals. Let us briefly comment on the involvement of lattice constants in a few other important physical properties. The pressure required to maintain a certain volume can be determined by calculating the rate of variation of cohesive energy with lattice constants. In effect, we succeed in reproducing the experimental value of the equilibrium lattice constant maintainable at zero pressure. Similarly, it is possible to study the change in volume caused by a change in pressure and calculate the compressibility. The significance of the lattice constant and compressibility must be emphasized in view of their utility in estimating the empirical parameters  $\lambda$  and  $\rho$  of (2.13). As the lattice constants have a close relationship with the bond length and the atomic radii, we propose to give a short account of the same in the following section.

\* N.W. Ashcroft and N.D. Mermin, *Solid State Physics*, Saunders College (1988).

**Table 2.1** Cohesive energy of crystals

Crystal	Binding type	Cohesive energy	Melting point (K)
LiF	Ionic	10.31 eV/ion	1143
NaCl	Ionic	7.96 eV/ion pair 3.28 eV/atom	1074
RbI	Ionic	6.17 eV/ion pair	915
Diamond	Covalent	7.37 eV/atom	> 3773
Si	Covalent	4.63 eV/atom	1687
SiC	Covalent	12.04 eV/molecule	2873 (subl.)
Na	Metallic	1.11 eV/atom	371
Cu	Metallic	3.49 eV/atom	1358
Au	Metallic	3.81 eV/atom	1338
Ne	van der Waals	0.02 eV/atom	24.6
H <sub>2</sub>	van der Waals	0.01 eV/molecule	14
CH <sub>4</sub>	van der Waals	0.10 eV/molecule	90
Ice (H <sub>2</sub> O)	Hydrogen	0.51 eV/molecule	273
HF	Hydrogen	0.30 eV/molecule	180.7

## 2.5 ATOMIC RADII vs LATTICE CONSTANTS

The atomic and ionic radii have been compiled by Pearson.\* An examination of this data shows that on ion formation the size of a positive ion is smaller and that of a negative ion larger than the size of the neutral atom. The best examples illustrating this fact are the radii of C (0.72 Å), C<sup>4+</sup> (0.15 Å) and C<sup>4-</sup> (2.60 Å). This can be understood by taking simple examples of Na and Cl. The Na atom, whose radius is 1.86 Å, loses one electron in becoming the Na<sup>+</sup> ion of radius of 0.96 Å. On losing this outermost electron (3s<sup>1</sup>) which is loosely bound, the atom assumes a more tightly bound configuration of Na<sup>+</sup> ion with the reduced size. This is one of the best examples to state, as the Na<sup>+</sup> ion turns out to be smaller than even the isoelectronic Ne atom of the preceding period. Similarly, the bigger size of the Cl<sup>-</sup> ion makes sense on the ground that the Cl atom is readily willing to turn into a Cl<sup>-</sup> ion whose electronic configuration is identical with the rigid spherical charge distribution of the nearest (the next in the same period) noble gas atom (Ar).

The extent of charge clouds of a constituent ion in any crystal is generally referred to as the *crystal ionic radius*. It needs to be distinguished from the free ion radius. According to the quantum mechanical interpretation, the free ion radius may be defined as the radius at which the probability amplitude  $|\psi|^2$  for the outermost electrons to be in the orbital represented by the wavefunction  $\psi$  is maximum. The wavefunction  $\psi$  is then a solution of the Schrödinger wave equation whose hamiltonian includes the ordinary Coulomb potential. The boundary condition requires that the magnitude and the derivative of the wavefunction  $\psi$  vanish at infinitely large distances. In contrast, for an ion in the crystal the magnitude and derivative of the wavefunction must be zero at the

\* W.B. Pearson, *Crystal Chemistry and Physics of Metals and Alloys*, Wiley-Interscience (1972).

boundary of the ion on the demand of the boundary condition. The potential in this case is not Coulomb but of the type shown in Fig. 2.1(a).

The above discussion indicates that the ionic radii may be calculated by solving one-electron Schrödinger wave equation. This is usually done by the Hartree–Fock self-consistent field method, treated in great detail by Slater.\* Some semi-empirical methods of calculating the ionic radii in crystals are also in practice. For example, the distance between two atoms shown as  $r_0$  (the nearest neighbour distance in a crystal) in Fig. 2.1 is approximately equal to the sum of the radii of the two neighbouring atoms. This property is known as the additive rule. The diffraction method is the standard way at present to measure lattice constants. From the diffraction pattern it is possible to determine the radius ratio of any two types of atoms from which the radii of other atoms comprising the crystal can be determined. Goldschmidt\*\* was the first to initiate calculations based on the experimental data. Later Pauling<sup>†</sup> used his own theory to calculate the ionic radii in crystals. His results are very well accounted in literature because of their amazing success in explaining most of the related physical properties of solids.

Using the additive rule of atomic radii it is possible to predict the bond lengths or the interatomic separations in a crystal. This is successfully done for crystalline phases even before they are crystallized. But we must be aware that the charge distribution is not rigid and spherically symmetric in every atom. This may introduce an appreciable error in our estimate. Therefore, it is a *must* to know accurately the average of charge clouds of the constituent atoms in a crystal for making any estimates.

At first instance the knowledge of atomic radii can be used to determine the coordination of an atom and suggest the probable arrangement of atoms in the crystal. Though this point has more relevance to Chapter 1, it is worth digressing to emphasize the role of atomic radii being discussed here. Beiser<sup>††</sup> has excellently explained the threefold coordination for a binary ionic crystal. It is shown that the coordination is stable (bonds formed) only when the positive ion  $A^+$  touches all the surrounding negative ions  $B^-$ . The mutual contact among the three  $B^-$  ions is not the necessary requirement for the coordination to crystallize. A simple geometrical calculation shows that the minimum ionic radius ratio  $r_A/r_B$  for this coordination to materialize is 0.155. We calculate below this ratio for the fourfold coordination in a similar ionic crystal.

In the fourfold coordination, the  $A^+$  ion positioned at the centre of a cube is surrounded by four  $B^-$  ions located at the alternate corners of the cube (Fig. 2.6) whose edge is  $a$ . For stable coordination, all the four  $B^-$  ions should touch the  $A^+$  ion. Two  $B^-$  ions on every face are also in contact with each other, the distance between their centres being equal to the length of the face diagonal ( $\sqrt{2}a$ ). Let  $\theta$  be the angle between the line joining a  $B^-$  ion to an  $A^+$  ion and the line joining the two  $B^-$  ions.

From Fig. 2.6, we have

$$\cos \theta = \frac{\sqrt{2}a/2}{\sqrt{3}a/2} \quad (\text{length of the body diagonal} = \sqrt{3}a)$$

$$= \sqrt{\frac{2}{3}}$$

\* J.C. Slater, *Quantum Theory of Atomic Structure*, Vols. I and II, McGraw-Hill Book Company Inc. (1960).

\*\* V.M. Goldschmidt, *Skrifter Norske Videnskaps Akad.*, No. 2 (1926); No. 8 (1927).

† L. Pauling, *The Nature of Chemical Bond*, Cornell Univ. Press (1960).

†† A. Beiser, *Perspective of Modern Physics*, pp. 426–427, McGraw-Hill, Kogakush Ltd. (1969).

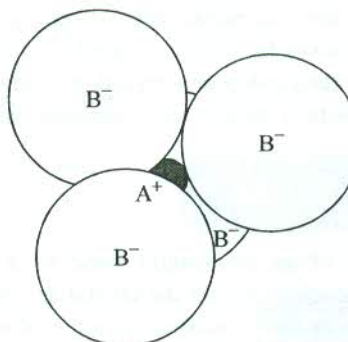


**FIG. 2.6** The fourfold coordination: The smaller ion  $A^+$  at the centre of a cube is surrounded by four  $B^-$  ions located at the alternate corners of the cube. The minimum value of  $r_A/r_B$  for the coordination is 0.225.

Also

$$\cos \theta = \frac{r_B}{r_A + r_B} = \sqrt{\frac{2}{3}} = 0.816$$

This gives  $r_A/r_B = 0.225$ , which is the minimum value for the fourfold coordination to be stable. These calculations show that for the formation of a stable threefold coordination, the ion radius ratio must lie between 0.155 and 0.225.

Finally, we demonstrate how successfully the bond lengths and the lattice constants are reproduced with the knowledge of the self-consistent atomic/ionic sizes. The degree of success achieved can be perceived by the data in Table 2.2.

**Table 2.2** Data on the nearest neighbour separation and lattice constant, predicted from the radii of the constituent ions/atoms, for some crystals

Crystal	Radius of the constituent ions/atoms (Å)	Predicted nearest neighbour separation, $d$ (Å)	Relation between $d$ and $a$ (lattice constant)	Lattice constant $a$ (Å)	
				Predicted	Observed
NaF	$\text{Na}^+$ (0.97) $\text{F}^-$ (1.63)	2.33	$a = 2d$	4.66	4.62
NaCl	$\text{Na}^+$ (0.97) $\text{Cl}^-$ (1.81)	2.78	$a = 2d$	5.56	5.63
Diamond	C (0.72)	1.54	$a = \frac{4d}{\sqrt{3}}$	3.56	3.56
Ne	Ne (1.58)	3.16	$a = \sqrt{2}d$	4.47	4.46

## 2.6 ELASTIC CONSTANTS OF CRYSTALS

The crystal binding discussed thus far in this chapter strongly controls the elastic behaviour of solids. The nature of binding forces in a solid is often reflected in its elastic response. The study

of elastic properties is essential for the interpretation of several properties of solids. For example, certain elastic constants relate themselves to thermal properties, like the Debye temperature. In this section we discuss the stress-strain relationship in a crystal, treating it as a homogeneous continuous elastic medium. Effectively, the crystal's picture as a periodic array of atoms is replaced with a homogeneous elastic continuum.

### 2.6.1 Elastic Stress

Consider the uniform deformation of an elementary cube of a crystal. Under the action of a deforming force, an internal force develops within the crystal as a reaction to the applied force. The internal force acting on the unit area of the crystal is defined as the stress. For the present treatment it is assumed that the applied force is not large and the Hooke's law remains valid (stress  $\propto$  strain). The stress acting on the six faces of the cube is expressed by nine components:  $\sigma_{xx}$ ,  $\sigma_{xy}$ ,  $\sigma_{xz}$ ,  $\sigma_{yx}$ ,  $\sigma_{yy}$ ,  $\sigma_{yz}$ ,  $\sigma_{zx}$ ,  $\sigma_{zy}$ ,  $\sigma_{zz}$ . The first subscript denotes the direction of the applied force and the second subscript gives the direction of the normal to the face on which the force is applied. The stress is a tensor of second rank and denoted by a  $(3 \times 3)$  matrix

$$[\sigma_{\alpha\beta}] = \begin{bmatrix} \sigma_{xx} & \sigma_{xy} & \sigma_{xz} \\ \sigma_{yx} & \sigma_{yy} & \sigma_{yz} \\ \sigma_{zx} & \sigma_{zy} & \sigma_{zz} \end{bmatrix} \quad (2.18)$$

with  $\alpha, \beta = x, y, z$ .

The components  $\sigma_{xx}$ ,  $\sigma_{yy}$ ,  $\sigma_{zz}$  denote the normal stress components acting on the  $yz$ ,  $zx$ , and  $xy$  faces, respectively. The remaining six components represent the tangential stress (two components on each of the three pairs of the faces). If the cube is in the state of static equilibrium and it does not rotate under the influence of tangential stress components,  $\sigma_{\alpha\beta}$  and  $\sigma_{\beta\alpha}$  would produce equal and opposite rotations. Hence  $\sigma_{\alpha\beta} = \sigma_{\beta\alpha}$  and the nine stress components reduce to six independent components. Figure 2.7 shows a normal component  $\sigma_{yy}$  and a tangential component  $\sigma_{yz}$  acting on the respective faces of a cube. The stress components have the dimensions of force per unit area or energy per unit volume.

### 2.6.2 Elastic Strain

Let three orthogonal unit vectors  $\hat{\mathbf{i}}, \hat{\mathbf{j}}, \hat{\mathbf{k}}$  be safely embedded in an unstrained crystal. Suppose on straining the crystal by a small deforming force these vectors are transformed to non-orthogonal vectors  $\mathbf{l}, \mathbf{m}, \mathbf{n}$ , respectively, with individual magnitudes differing from unity. We treat the two sets of vectors as the new and old coordinate axes. The new coordinate axes may be expressed as

$$\begin{aligned} \mathbf{l} &= (1 + \varepsilon_{xx}) \hat{\mathbf{i}} + \varepsilon_{xy} \hat{\mathbf{j}} + \varepsilon_{xz} \hat{\mathbf{k}} \\ \mathbf{m} &= \varepsilon_{yx} \hat{\mathbf{i}} + (1 + \varepsilon_{yy}) \hat{\mathbf{j}} + \varepsilon_{yz} \hat{\mathbf{k}} \\ \mathbf{n} &= \varepsilon_{zx} \hat{\mathbf{i}} + \varepsilon_{zy} \hat{\mathbf{j}} + (1 + \varepsilon_{zz}) \hat{\mathbf{k}} \end{aligned} \quad (2.19)$$

where  $\varepsilon_{\alpha\beta}$  define the deformation. These coefficients are dimensionless and very small ( $\ll 1$ ) for a small strain.

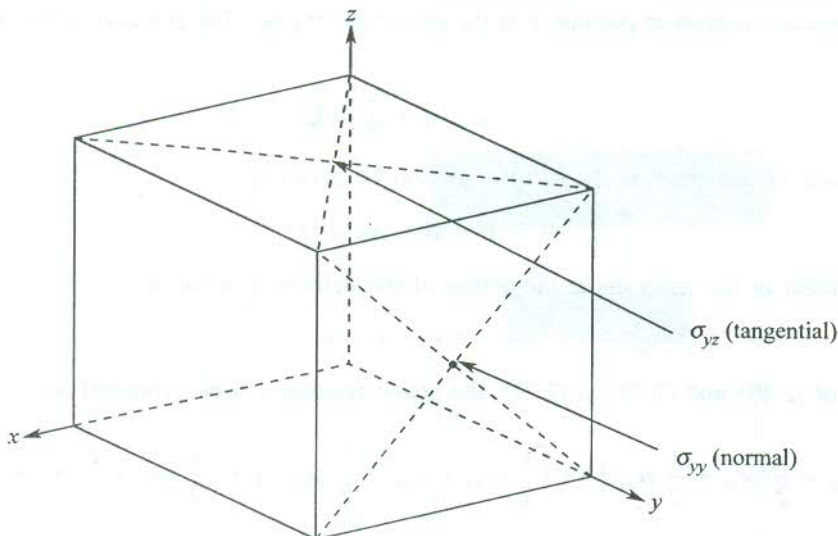


**FIG. 2.7** The normal stress component,  $\sigma_{yy}$ , produced by a force applied in the  $+y$  direction on the  $xz$  face (with normal along the  $+y$  direction) of a cube. The tangential stress component,  $\sigma_{yz}$ , produced by a force applied in the  $+y$  direction on the  $xy$  face (with normal along the  $+z$  direction) of a cube.

By taking the dot products  $\mathbf{l} \cdot \mathbf{l}$ ,  $\mathbf{m} \cdot \mathbf{m}$ ,  $\mathbf{n} \cdot \mathbf{n}$ , we can easily show that the magnitude of each of the three new vectors is different from unity. Also, the dot products  $\mathbf{l} \cdot \mathbf{m}$ ,  $\mathbf{m} \cdot \mathbf{n}$ ,  $\mathbf{n} \cdot \mathbf{l}$  do not vanish indicating that  $\mathbf{l}$ ,  $\mathbf{m}$  and  $\mathbf{n}$  are not orthogonal vectors.

The strain components  $e_{\alpha\beta}$  are defined in terms of  $\varepsilon_{\alpha\beta}$  as

$$e_{xx} = \varepsilon_{xx}, \quad e_{yy} = \varepsilon_{yy}, \quad e_{zz} = \varepsilon_{zz} \quad (2.20a)$$

and

$$\begin{aligned} e_{xy} &= \mathbf{l} \cdot \mathbf{m} \simeq \varepsilon_{yx} + \varepsilon_{xy} \\ e_{yz} &= \mathbf{m} \cdot \mathbf{n} \simeq \varepsilon_{zy} + \varepsilon_{yz} \\ e_{zx} &= \mathbf{n} \cdot \mathbf{l} \simeq \varepsilon_{xz} + \varepsilon_{zx} \end{aligned} \quad (2.20b)$$

In relations (2.20b) the sign  $\simeq$  may be replaced by the sign  $=$ , if the terms of order  $\varepsilon^2$  are neglected ( $\varepsilon_{\alpha\beta} \ll 1$ ). It is to be noticed that the strain components in (2.20b) are defined in terms of the changes in angle between the axes. Therefore, for a rigid rotation in which angles do not change,  $e_{xy} = e_{yz} = e_{zx} = 0$  and  $\varepsilon_{xy} = -\varepsilon_{yx}$ ;  $\varepsilon_{yz} = -\varepsilon_{zy}$ ;  $\varepsilon_{zx} = -\varepsilon_{xz}$ .

If we do not consider pure rotations since they are not deformation, we may always take

$$\varepsilon_{xy} = \varepsilon_{yx}, \quad \varepsilon_{yz} = \varepsilon_{zy} \quad \text{and} \quad \varepsilon_{zx} = \varepsilon_{xz} \quad (2.21)$$

Using (2.21) in (2.20b), we get

$$\begin{aligned} \varepsilon_{xy} &= \varepsilon_{yx} = \frac{1}{2} e_{xy} \\ \varepsilon_{yz} &= \varepsilon_{zy} = \frac{1}{2} e_{yz} \\ \varepsilon_{zx} &= \varepsilon_{xz} = \frac{1}{2} e_{zx} \end{aligned} \quad (2.22)$$

Now, consider an atom at position  $\mathbf{r}$  in the unstrained crystal. The position vector is expressed as

$$\mathbf{r} = x\hat{\mathbf{i}} + y\hat{\mathbf{j}} + z\hat{\mathbf{k}} \quad (2.23)$$

Let the position of this atom in the strained crystal be given by

$$\mathbf{r}' = xl + ym + zn \quad (2.24)$$

The displacement of the atom under the action of the deforming force is

$$\Delta(\mathbf{r}) = \mathbf{r}' - \mathbf{r} \quad (2.25)$$

Making use of (2.19) and (2.22) to (2.24), the above relation can be expressed as

$$\Delta(\mathbf{r}) = \left( xe_{xx} + \frac{1}{2} ye_{yx} + \frac{1}{2} ze_{zx} \right) \hat{\mathbf{i}} + \left( \frac{1}{2} xe_{xy} + ye_{yy} + \frac{1}{2} ze_{zy} \right) \hat{\mathbf{j}} + \left( \frac{1}{2} xe_{xz} + \frac{1}{2} ye_{yz} + ze_{zz} \right) \hat{\mathbf{k}} \quad (2.26)$$

On rewriting it as

$$\Delta(\mathbf{r}) = u_1 \hat{\mathbf{i}} + u_2 \hat{\mathbf{j}} + u_3 \hat{\mathbf{k}} \quad (2.27)$$

we get

$$\begin{aligned} u_1 &= xe_{xx} + \frac{1}{2} ye_{yx} + \frac{1}{2} ze_{zx} \\ u_2 &= \frac{1}{2} xe_{xy} + ye_{yy} + \frac{1}{2} ze_{zy} \\ u_3 &= \frac{1}{2} xe_{xz} + \frac{1}{2} ye_{yz} + ze_{zz} \end{aligned} \quad (2.28)$$

where  $u_1, u_2, u_3$  are the displacement components along the coordinate axes of the unstrained crystal.

All the six dimensionless strain components can now be defined as follows by taking the partial derivatives of  $u_1, u_2$  and  $u_3$ .

$$\begin{aligned} e_{xx} &= \frac{\partial u_1}{\partial x}; & e_{xy} &= \frac{\partial u_2}{\partial x} + \frac{\partial u_1}{\partial y} \\ e_{yy} &= \frac{\partial u_2}{\partial y}; & e_{yz} &= \frac{\partial u_3}{\partial y} + \frac{\partial u_2}{\partial z} \\ e_{zz} &= \frac{\partial u_3}{\partial z}; & e_{zx} &= \frac{\partial u_1}{\partial z} + \frac{\partial u_3}{\partial x} \end{aligned} \quad (2.29)$$

Relations (2.29) give alternative definitions of strain components. Relations (2.19) and (2.20a) indicate that  $e_{xx}, e_{yy}$  and  $e_{zz}$  represent linear strains, i.e. changes in length per unit length along the three axes.

Each of the other type of three components interprets a combination of two simple shears. Take for example,

$$e_{yz} = \frac{\partial u_3}{\partial y} + \frac{\partial u_2}{\partial z}$$

It describes two shears: One in which the planes normal to  $y$ -axis slide in the  $z$ -direction and the other in which the planes normal to  $z$ -axis slide along the  $y$ -direction. Like stress, strain is also a tensor of second rank. In general, it is described by nine components with the matrix representation as

$$[e_{\alpha\beta}] = \begin{bmatrix} e_{xx} & e_{xy} & e_{xz} \\ e_{yx} & e_{yy} & e_{yz} \\ e_{zx} & e_{zy} & e_{zz} \end{bmatrix} \quad (2.30)$$

with  $\alpha, \beta = x, y, z$ .

### 2.6.3 Dilation

The fractional increase in volume created by deformation is called *dilation*. It is useful in determining some elastic constants such as the bulk modulus.

Volume of a unit cube after the deformation is

$$V' = \mathbf{l} \cdot \mathbf{m} \times \mathbf{n} \quad (2.31)$$

Substituting for  $\mathbf{l}$ ,  $\mathbf{m}$  and  $\mathbf{n}$  from (2.19) into (2.31) and neglecting the product of two strain components ( $e_{\alpha\beta} \ll 1$ ), we get

$$V' = 1 + e_{xx} + e_{yy} + e_{zz} \quad (2.32)$$

Therefore, the dilation  $\delta$  can be expressed as

$$\delta = \frac{V' - V}{V} = e_{xx} + e_{yy} + e_{zz} \quad (2.33)$$

using  $V = 1$  for a unit cube.

## 2.7 ELASTIC COMPLIANCE AND STIFFNESS CONSTANTS

According to Hooke's law, the strain is directly proportional to the stress for sufficiently small deformations. Therefore, for appreciable small elastic deformations of a crystal, the stress tensor components and the strain tensor components are linearly related as

$$\begin{bmatrix} \sigma_{xx} \\ \sigma_{yy} \\ \sigma_{zz} \\ \sigma_{yz} \\ \sigma_{zx} \\ \sigma_{xy} \end{bmatrix} = \begin{bmatrix} C_{11} & C_{12} & C_{13} & C_{14} & C_{15} & C_{16} \\ C_{21} & C_{22} & C_{23} & C_{24} & C_{25} & C_{26} \\ C_{31} & C_{32} & C_{33} & C_{34} & C_{35} & C_{36} \\ C_{41} & C_{42} & C_{43} & C_{44} & C_{45} & C_{46} \\ C_{51} & C_{52} & C_{53} & C_{54} & C_{55} & C_{56} \\ C_{61} & C_{62} & C_{63} & C_{64} & C_{65} & C_{66} \end{bmatrix} \begin{bmatrix} e_{xx} \\ e_{yy} \\ e_{zz} \\ e_{yz} \\ e_{zx} \\ e_{xy} \end{bmatrix} \quad (2.34)$$

Conversely, the strain components can be expressed as the linear functions of the stress components.

$$\begin{bmatrix} e_{xx} \\ e_{yy} \\ e_{zz} \\ e_{yz} \\ e_{zx} \\ e_{xy} \end{bmatrix} = \begin{bmatrix} S_{11} & S_{12} & S_{13} & S_{14} & S_{15} & S_{16} \\ S_{21} & S_{22} & S_{23} & S_{24} & S_{25} & S_{26} \\ S_{31} & S_{32} & S_{33} & S_{34} & S_{35} & S_{36} \\ S_{41} & S_{42} & S_{43} & S_{44} & S_{45} & S_{46} \\ S_{51} & S_{52} & S_{53} & S_{54} & S_{55} & S_{56} \\ S_{61} & S_{62} & S_{63} & S_{64} & S_{65} & S_{66} \end{bmatrix} \begin{bmatrix} \sigma_{xx} \\ \sigma_{yy} \\ \sigma_{zz} \\ \sigma_{yz} \\ \sigma_{zx} \\ \sigma_{xy} \end{bmatrix} \quad (2.35)$$

The coefficients  $C_{11}$ ,  $C_{12}$ , etc. are called *elastic stiffness constants* and represent moduli of elasticity with dimensions of  $\frac{\text{force}}{\text{area}}$  or  $\frac{\text{energy}}{\text{volume}}$ . The other coefficients  $S_{11}$ ,  $S_{12}$ , etc. are called *elastic compliance constants* and have dimensions of  $\frac{\text{area}}{\text{force}}$  or  $\frac{\text{volume}}{\text{energy}}$ .

### 2.7.1 Elastic Energy Density

By analogy with the expression for the energy of a stretched spring (to be discussed in Chapter 4), the elastic energy density  $\phi$  is a quadratic function of strains in the approximation of Hooke's law

$$\phi = \frac{1}{2} \sum_{\mu=1}^6 \sum_{\nu=1}^6 \bar{C}_{\mu\nu} e_{\mu} e_{\nu} \quad (2.36)$$

where the indices 1 to 6 should read as

$$1 \equiv xx; \quad 2 \equiv yy; \quad 3 \equiv zz; \quad 4 \equiv yz; \quad 5 \equiv zx; \quad 6 \equiv xy \quad (2.37)$$

The coefficients  $\bar{C}_S$  are found to be related to  $C_S$  of (2.34), as we will see below. We will exploit the definition (2.36) to show that the 36 coefficients in (2.34) or (2.35) can be reduced in number. The very definition of potential energy allows us to obtain the stress components from the derivative of  $\phi$  with respect to the associated strain component. For example, when the stress  $\sigma_{xx}$  acts on one face of a unit cube and the opposite face is held at rest, we have

$$\sigma_{xx} = \frac{\partial \phi}{\partial e_{xx}} = \frac{\partial \phi}{\partial e_1} = \bar{C}_{11} e_1 + \frac{1}{2} \sum_{\beta=2}^6 (\bar{C}_{1\beta} + \bar{C}_{\beta 1}) e_{\beta} \quad (2.38)$$

An inspection of relation (2.38) reveals that only the combination  $\frac{1}{2}(\bar{C}_{\alpha\beta} + \bar{C}_{\beta\alpha})$  enters the stress-strain relations, implying that the elastic stiffness constants are symmetrical. Thus we have

$$C_{\alpha\beta} = \frac{1}{2} (\bar{C}_{\alpha\beta} + \bar{C}_{\beta\alpha}) = C_{\beta\alpha} \quad (2.39)$$

The above symmetrical property reduces the number of constants from 36 to 21.

## 2.7.2 Application to Cubic Crystals

In accordance with the Neumann's principle, the number of independent elastic stiffness constants decreases as the symmetry of a crystal increases. This number is 21, 13, 5 and 3, respectively, for triclinic, monoclinic, hexagonal and cubic systems. The cubic crystals, being the most symmetric, have the least number of independent elastic stiffness constants. We now indulge in the exercise of deriving this result.

We pronounce that the relation for the elastic energy density of a cubic crystal has the form

$$\phi = \frac{1}{2} C_{11} (e_{xx}^2 + e_{yy}^2 + e_{zz}^2) + \frac{1}{2} C_{44} (e_{yz}^2 + e_{zx}^2 + e_{xy}^2) + C_{12} (e_{yy}e_{zz} + e_{zz}e_{xx} + e_{xx}e_{yy}) \quad (2.40)$$

The above relation does not have the quadratic terms

$$(e_{xx}e_{xy} + \dots); \quad (e_{yz}e_{zx} + \dots); \quad (e_{xx}e_{yz} + \dots); \quad (2.41)$$

The correctness of (2.40) can be confirmed by showing that  $\phi$  is invariant under all symmetry operations permitted in a cubic crystal. The minimum symmetry requirement for cubic symmetry is the presence of four threefold rotation axes along the directions of the four body diagonals of the cube (see Fig. 2.8). Counterclockwise rotations by  $2\pi/3$  about the [111] direction and three other equivalent directions interchange the  $x$ ,  $y$ ,  $z$  axes according to the following four schemes:

$$\begin{aligned} x \rightarrow y \rightarrow z \rightarrow x; & \quad -x \rightarrow z \rightarrow -y \rightarrow -x \\ x \rightarrow z \rightarrow -y \rightarrow x; & \quad -x \rightarrow y \rightarrow z \rightarrow -x \end{aligned} \quad (2.42)$$

It is straightforward to check that the relation for  $\phi$  remains unchanged when  $x$ ,  $y$ ,  $z$  are interchanged in (2.40) according to any one of the four schemes (2.42). But every term appearing in (2.41) is odd in one or more indices. One of the schemes in (2.42) is surely such that its application to (2.40) would change the sign of the term in (2.41) ( $e_{xy} = -e_{x(-y)}$ , for example). This only confirms that the terms included in (2.41) have rightly been excluded from the relation (2.40) for  $\phi$ .

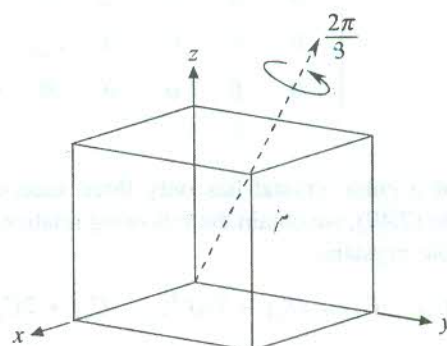


**FIG. 2.8** Rotation of  $2\pi/3$  about the [111] direction (the direction of a body diagonal) in a cubic crystal leaves the crystal unchanged in space by the way of interchange of the orthogonal axes:  $x \rightarrow y \rightarrow z \rightarrow x$ . Thus the [111] direction represents one of the four threefold rotation axes. The rest three are in other three directions that are equivalent to the [111] direction (i.e. the directions of the other three body diagonals).

We may now easily derive the stress components from (2.40). Thus

$$\sigma_{xx} = \frac{\partial \phi}{\partial e_{xx}} = C_{11}e_{xx} + C_{12}(e_{zz} + e_{yy}) \quad (2.43)$$

The corresponding relation given by (2.34) is

$$\sigma_{xx} = C_{11}e_{xx} + C_{12}e_{yy} + C_{13}e_{zz} + C_{14}e_{yz} + C_{15}e_{zx} + C_{16}e_{xy} \quad (2.44)$$

On comparing (2.43) with (2.44), we get

$$C_{12} = C_{13}; \quad C_{14} = C_{15} = C_{16} = 0 \quad (2.45)$$

Further, from (2.40)

$$\sigma_{xy} = \frac{\partial \phi}{\partial e_{xy}} = C_{44}e_{xy} \quad (2.46)$$

The corresponding relation from (2.34) is

$$\sigma_{xy} = C_{61}e_{xx} + C_{62}e_{yy} + C_{63}e_{zz} + C_{64}e_{yz} + C_{65}e_{zx} + C_{66}e_{xy} \quad (2.47)$$

Comparison of (2.46) with (2.47) gives

$$C_{66} = C_{44}; \quad C_{61} = C_{62} = C_{63} = C_{64} = C_{65} = 0 \quad (2.48)$$

Proceeding this way for other stress components, we find that the array of values of the elastic stiffness constants of a cubic crystal may be expressed in the following matrix representation.

$$[C_{\alpha\beta}] = \begin{bmatrix} C_{11} & C_{12} & C_{12} & 0 & 0 & 0 \\ C_{12} & C_{11} & C_{12} & 0 & 0 & 0 \\ C_{12} & C_{12} & C_{11} & 0 & 0 & 0 \\ 0 & 0 & 0 & C_{44} & 0 & 0 \\ 0 & 0 & 0 & 0 & C_{44} & 0 \\ 0 & 0 & 0 & 0 & 0 & C_{44} \end{bmatrix} \quad (2.49)$$

with  $\alpha, \beta = 1, 2, 3, 4, 5, 6$ .

Matrix (2.49) shows that a cubic crystal has only three independent stiffness constants. By evaluating the inverse matrix to (2.49), we obtain the following relationships between the stiffness and compliance constants for cubic crystals.

$$C_{44} = 1/S_{44}; \quad C_{11} - C_{12} = (S_{11} - S_{12})^{-1}; \quad C_{11} + 2C_{12} = (S_{11} + 2S_{12})^{-1} \quad (2.50)$$

### 2.7.3 Bulk Modulus and Compressibility

Let us consider a strained crystal which is uniformly dilated. This refers to the mathematical condition

$$e_{xx} = e_{yy} = e_{zz} = \frac{1}{3} \delta \quad (2.51)$$

From (2.40) we obtain the following relation for the elastic energy density of a cubic crystal.

$$\phi = \frac{1}{6} (C_{11} + 2C_{12}) \delta^2 \quad (2.52)$$

The bulk modulus  $B$  is usually defined by the relation

$$\phi = \frac{1}{2} B \delta^2 \quad (2.53)$$

Comparing (2.52) with (2.53), we express the bulk modulus of a cubic crystal as

$$B = \frac{1}{3} (C_{11} + 2C_{12}) \quad (2.54)$$

The inverse of  $B$  has been interpreted as another useful elastic property called the *compressibility*  $K$ . The compressibility of a cubic crystal is accordingly given by

$$K = \frac{3}{C_{11} + 2C_{12}} \quad (2.55)$$

## 2.8 ELASTIC WAVES IN CUBIC CRYSTAL

Consider an elementary cube of edges  $\Delta x = \Delta y = \Delta z$  within the volume of a cubic crystal. The cube edges are in the directions of the  $x$ -,  $y$ - and  $z$ -axes. When the cube is strained, let the stress  $\sigma_{xx}(x)$  act on the face at  $x$ . Assuming that the variation of  $\sigma_{xx}$  is uniform along the  $x$ -direction, the stress on the face parallel to that at  $x$  can be expressed as  $[\sigma_{xx}(x) + \{\partial\sigma_{xx}/(\partial/\partial_x)\}\Delta x]$  (see Fig. 2.9). The net force on the cube due to  $\sigma_{xx}$  component is equal to  $[\{\partial\sigma_{xx}/(\partial/\partial_x)\}\Delta x] \Delta y \cdot \Delta z$ . The other forces in the  $x$ -direction arise from the variation of  $\sigma_{xy}$  and  $\sigma_{xz}$  across the cube. Therefore, the net force on the cube along the  $x$ -direction is

$$F_x = \left( \frac{\partial\sigma_{xx}}{\partial x} + \frac{\partial\sigma_{xy}}{\partial y} + \frac{\partial\sigma_{xz}}{\partial z} \right) \Delta x \cdot \Delta y \cdot \Delta z \quad (2.56)$$

The above force is actually the restoring force that tends to bring the cube to its unstrained state. As a result, the particles in the crystal are thrown to a motion described by the relevant equation of motion. If  $\rho$  is the density of the crystal, the force per unit volume on the crystal along the  $x$ -direction is  $\rho(\partial^2 u_1 / \partial t^2)$  and the equation of motion in the  $x$ -direction becomes

$$\rho \frac{\partial^2 u_1}{\partial t^2} = \frac{\partial\sigma_{xx}}{\partial x} + \frac{\partial\sigma_{xz}}{\partial z} + \frac{\partial\sigma_{xy}}{\partial y} \quad (2.57)$$

Using (2.34) and (2.49), the above equation is reduced to the following form for a cubic crystal.

$$\rho \frac{\partial^2 u_1}{\partial t^2} = C_{11} \frac{\partial e_{xx}}{\partial x} + C_{12} \left( \frac{\partial e_{yy}}{\partial x} + \frac{\partial e_{zz}}{\partial x} \right) + C_{44} \left( \frac{\partial e_{xy}}{\partial y} + \frac{\partial e_{zx}}{\partial z} \right) \quad (2.58)$$

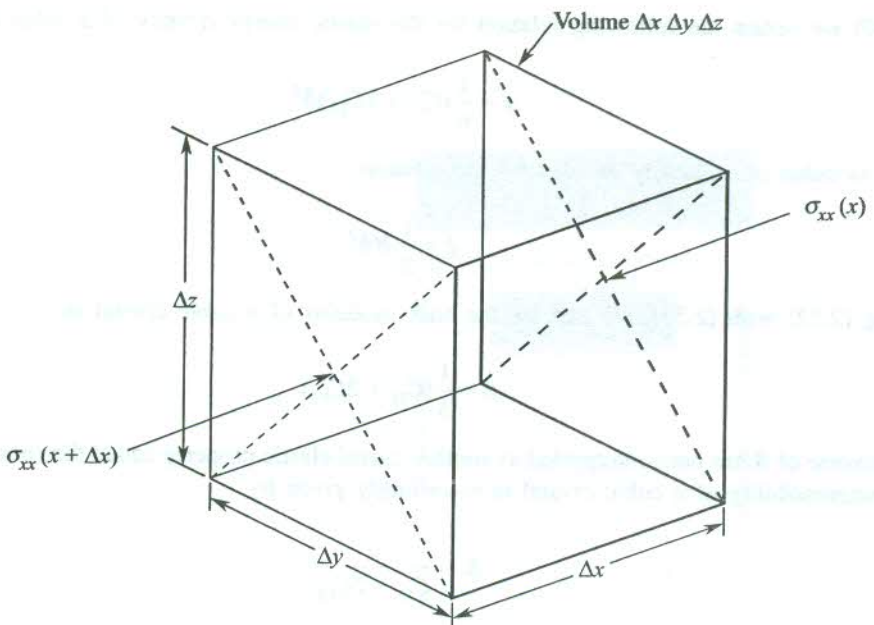


**FIG. 2.9** Variation of a normal stress component ( $\sigma_{xx}$ ) within a cube of volume  $\Delta x \cdot \Delta y \cdot \Delta z$  (with  $\Delta x = \Delta y = \Delta z$ ) along the  $x$ -edge.

On eliminating the strain components with the help of (2.29), the above equation assumes the form

$$\rho \frac{\partial^2 u_1}{\partial t^2} = C_{11} \frac{\partial^2 u_1}{\partial x^2} + C_{44} \left( \frac{\partial^2 u_1}{\partial y^2} + \frac{\partial^2 u_1}{\partial z^2} \right) + (C_{12} + C_{44}) \left( \frac{\partial^2 u_2}{\partial x \partial y} + \frac{\partial^2 u_3}{\partial x \partial z} \right) \quad (2.59)$$

Here  $u_1, u_2, u_3$  are the components of the atomic displacement  $\Delta(\mathbf{r})$  along the axes of the unstrained crystal [see equation (2.27)]. The solution to (2.59) turns out to have a waveform, indicating that waves propagate within the crystal when it is strained in such a way as there exists a non-zero stress on the crystal. These waves are called the *elastic waves* because they are produced here in an elastic continuum by elastic deformation.

Similar to (2.59), there are equations of motion in the  $y$ - and  $z$ -directions. We write them by symmetry on the basis of (2.59):

$$\rho \frac{\partial^2 u_2}{\partial t^2} = C_{11} \frac{\partial^2 u_2}{\partial y^2} + C_{44} \left( \frac{\partial^2 u_2}{\partial x^2} + \frac{\partial^2 u_2}{\partial z^2} \right) + (C_{12} + C_{44}) \left( \frac{\partial^2 u_1}{\partial x \partial y} + \frac{\partial^2 u_3}{\partial y \partial z} \right) \quad (2.60)$$

$$\rho \frac{\partial^2 u_3}{\partial t^2} = C_{11} \frac{\partial^2 u_3}{\partial z^2} + C_{44} \left( \frac{\partial^2 u_3}{\partial x^2} + \frac{\partial^2 u_3}{\partial y^2} \right) + (C_{12} + C_{44}) \left( \frac{\partial^2 u_1}{\partial x \partial z} + \frac{\partial^2 u_2}{\partial z \partial x} \right) \quad (2.61)$$

Now, we proceed to study the solutions of these equations in some common directions in cubic crystals.

### 2.8.1 Propagation of Waves in the [100] Direction

First, consider a longitudinal or compressional wave that propagates along the  $x$ -cube edge. Its propagation constant or wavevector  $k$  is parallel to the particle displacement  $u_1$ , given by

$$u_1 = (u_1)_0 \exp [i(kx - \omega t)] \quad (2.62)$$

where  $k = 2\pi/\lambda$ , and  $\omega$  is the angular frequency. When (2.62) is used as a trial solution of (2.59) and placed in it, we obtain the dispersion relation

$$\omega^2 \rho = C_{11} k^2 \quad (2.63)$$

This gives the velocity of a longitudinal wave in the [100] direction in a cubic crystal as

$$v_l = \frac{\omega}{k} = \left( \frac{C_{11}}{\rho} \right)^{1/2} \quad (2.64)$$

Next, we consider a transverse or shear wave with its wavevector  $k$  along the  $x$ -cube edge and the particle displacement  $u_2$  in the  $y$ -direction. Thus,

$$u_2 = (u_2)_0 \exp [i(kx - \omega t)] \quad (2.65)$$

The substitution of (2.65) into (2.60) gives

$$\omega^2 \rho = C_{44} k^2 \quad (2.66)$$

Therefore, the velocity of a transverse wave in the [100] direction in a cubic crystal is

$$v_s = \frac{\omega}{k} = \left( \frac{C_{44}}{\rho} \right)^{1/2} \quad (2.67)$$

It can be shown that a transverse wave with wavevector along the  $x$ -cube edge and the particle displacement  $u_3$  in the  $z$ -direction moves with the identical velocity. This result asserts that two independent shear waves whose wavevectors point along the [100] direction propagate in a cubic crystal with equal velocities. For a general direction of the wavevector this result is not applicable. The geometry of the longitudinal and transverse waves propagation in the [100] direction in a cubic crystal is shown in Fig. 2.10(a).

### 2.8.2 Propagation of Waves in the [110] Direction

The study of elastic waves propagating in the [110] direction (the direction of a face diagonal) is especially gainful because the three elastic constants can be obtained simply from the three measured propagation velocities.

Let us first consider a shear wave with wavevector  $\mathbf{k} = k_x \hat{\mathbf{i}} + k_y \hat{\mathbf{j}}$  propagating in the  $xy$  plane and causing a particle displacement  $u_3$  in the  $z$ -direction. Thus

$$u_3 = (u_3)_0 \exp [i(k_x x + k_y y - \omega t)] \quad (2.68)$$

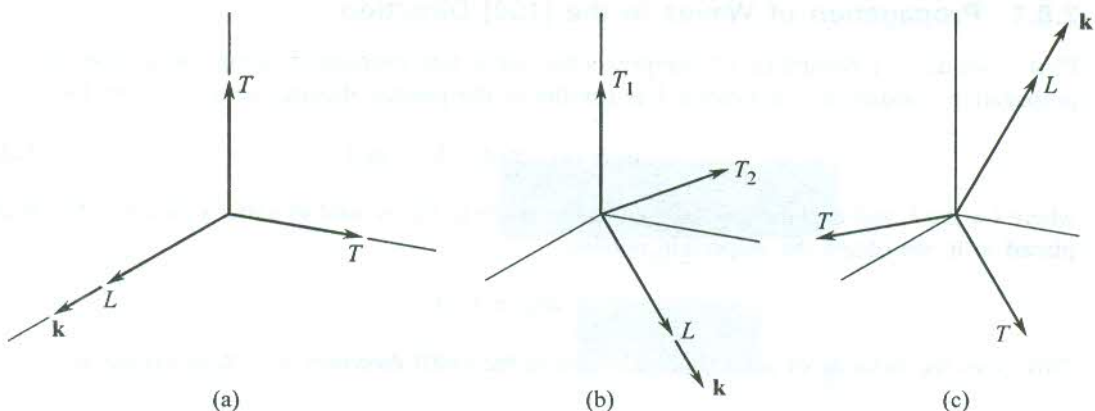


**FIG. 2.10** Propagation of elastic waves in a cubic crystal— $L$  denotes a longitudinal wave and  $T$  denotes a shear wave. (a) Waves in the [100] direction ( $\mathbf{k}$  parallel to  $\hat{\mathbf{i}}$ )—one longitudinal wave with velocity characterized by  $C_{11}$ , two degenerate shear waves with velocity characterized by  $C_{44}$ . (b) Waves in the [110] direction [ $\mathbf{k}$  parallel to  $(\hat{\mathbf{i}} + \hat{\mathbf{j}})$ ]: one longitudinal wave with velocity characterized by  $1/2(C_{11} + C_{12} + 2C_{44})$ , two shear waves with velocities characterized respectively by  $C_{44}$  and  $1/2(C_{11} - C_{12})$ . (c) Waves in the [111] direction [ $\mathbf{k}$  parallel to  $(\hat{\mathbf{i}} + \hat{\mathbf{j}} + \hat{\mathbf{k}})$ ]: one longitudinal wave with velocity characterized by  $1/3(C_{11} + 2C_{12} + C_{44})$ , two degenerate shear waves with velocity characterized by  $1/3(C_{11} - C_{12} + C_{44})$ .  $\hat{\mathbf{i}}, \hat{\mathbf{j}}, \hat{\mathbf{k}}$  denote unit vectors along the cube edges defining the  $x$ -,  $y$ - and  $z$ -coordinate axes.

Substituting (2.68) into (2.61), we obtain

$$\omega^2 = \left( \frac{C_{44}}{\rho} \right) k^2 \quad (2.69)$$

Next, consider the other two waves propagating in the  $xy$  plane with particle velocity in the  $xy$ -plane. Let these be represented as

$$\begin{aligned} u_1 &= (u_1)_0 \exp i(k_x x + k_y y - \omega t) \\ u_2 &= (u_2)_0 \exp i(k_x x + k_y y - \omega t) \end{aligned} \quad (2.70)$$

Placing these solutions in (2.59) and (2.60), we get the following pair of equations:

$$\begin{aligned} \omega^2 \rho u_1 &= (C_{11} k_x^2 + C_{44} k_y^2) u_1 + (C_{12} + C_{44}) k_x k_y u_2 \\ \omega^2 \rho u_2 &= (C_{11} k_y^2 + C_{44} k_x^2) u_2 + (C_{12} + C_{44}) k_x k_y u_1 \end{aligned} \quad (2.71)$$

For a wave in the [110] direction for which  $k_x = k_y = k/\sqrt{2}$ , equations (2.71) have a characteristically simple solution. The solution exists only if the determinant of the coefficients of  $u_1$  and  $u_2$  in (2.71) vanishes. Thus

$$\begin{vmatrix} \frac{1}{2}(C_{11} + C_{44})k^2 - \omega^2 \rho & \frac{1}{2}(C_{12} + C_{44})k^2 \\ \frac{1}{2}(C_{12} + C_{44})k^2 & \frac{1}{2}(C_{11} + C_{44})k^2 - \omega^2 \rho \end{vmatrix} = 0 \quad (2.72)$$

On solving (2.72), we get two dispersion relations

$$\omega^2 = \left( \frac{C_{11} + C_{12} + 2C_{44}}{2\rho} \right) k^2; \quad \omega^2 = \left( \frac{C_{11} - C_{12}}{2\rho} \right) k^2 \quad (2.73)$$

These two roots refer to two different types of waves. We now determine the nature of the waves by finding the direction of the particle displacement caused by the respective waves. When we substitute the first root in the first equation of (2.71) we get  $u_1 = u_2$ . Since the particle displacement occurs in the  $xy$  plane,  $\Delta(\mathbf{r}) = u_1(\hat{\mathbf{i}} + \hat{\mathbf{j}})$ . This shows that the displacement takes place in the [110] direction that represents the direction of  $(\hat{\mathbf{i}} + \hat{\mathbf{j}})$  and happens to be the direction of propagation of the wave [see Fig. 2.10(b)]. Thus we infer that the first root in (2.73) belongs to a longitudinal wave.

Similarly, on substituting the second root in the first equation of (2.71), we obtain  $u_1 = -u_2$ , implying that  $\Delta(\mathbf{r}) = u_1(\hat{\mathbf{i}} - \hat{\mathbf{j}})$ . The direction of the vector  $(\hat{\mathbf{i}} - \hat{\mathbf{j}})$  is indicated as [1̄10] which is perpendicular to the [110] direction, the direction of propagation of the wave. Hence the second root in (2.73) must refer to a shear wave [Fig. 2.10(b)]. The treatment of waves in the [111] direction is relatively lengthy though not so complicated as for other general directions. The main features of propagation may, however, be found in Fig. 2.10(c).

The subject matter of the last section is closely linked to the analysis of normal modes of vibration of crystals. Generally, the direction of particle displacement or the polarization of normal modes may not be exactly parallel or perpendicular to the direction of the wavevector  $\mathbf{k}$ . The analysis becomes easier when  $\mathbf{k}$  is along any symmetry axis of the crystal. A suitable discussion dealing with these aspects is presented in Section 4.6.

## SUMMARY

1. (a) Bonds are broadly classified on the basis of strength as (i) primary bonds and (ii) secondary bonds  
 (b) The three limiting cases of primary bonds are identified as (a) covalent, (b) metallic, and (c) ionic  
 (c) Some primary bonds are of mixed type.  
 (d) van der Waals and hydrogen bonds fall in the category of secondary bonds.
2. van der Waals interaction (induced dipole-dipole interaction) varies with interatomic separation as  $1/r^6$ . It is a quantum effect. The interaction potential vanishes when the Planck constant  $h = 0$ . Example, inert gas solids.
3. The cause of repulsive interaction between atoms lies generally in the electrostatic repulsion of overlapping charge distributions and the Pauli exclusion principle that forces overlapping electrons of parallel spin occupy higher energy states.
4. The potential energy per ion in an ionic crystal is given by

$$U_{\text{ion}} = - \frac{\alpha q^2}{4\pi \epsilon_0 r_0} \left( 1 - \frac{\rho}{r_0} \right)$$

where

$\alpha$  is the Madelung constant

$q$  is the charge on an ion

$\rho$  is an empirical parameter

$r_0$  is the separation in a pair of ions of opposite type at equilibrium.

5. The overlap of charge distributions of antiparallel electron spin gives rise to covalent bonding.
6. There are only three independent elastic stiffness constants for a cubic crystal:  $C_{11}$ ,  $C_{12}$ ,  $C_{44}$ . This number increases with decrease in the crystalline symmetry (21 for triclinic symmetry).

## PROBLEMS

- 2.1** Briefly answer the following questions.

- (a) If positive and negative ions attract each other, why does the structure not collapse?
- (b) Why is it that the cohesive energy of an ionic crystal is almost equal to the attractive Coulomb energy?
- (c) What is the origin of cohesion in metals? Can it be described by interatomic potentials or covalent or any other bonds?

- 2.2** Consider a system of two argon atoms with position of the second atom with respect to the location of the first atom being denoted by vector  $\mathbf{r}$  at certain instant of time. If for a fraction of second the centre of positive charges is shifted from the centre of negative charges (electrons) in the first atom, show that this would lead to an attractive potential of the system expressible as

$$U = - \frac{\alpha_e p^2}{(4\pi\epsilon_0)^2 r^6} (1 + 3\cos^2\theta)$$

where

$\alpha_e$  is the electronic polarizability of the argon atom

$p$  is the instantaneous electric dipole moment of the first atom

$\theta$  is the angle between  $\mathbf{p}$  and  $\mathbf{r}$ .

- 2.3** Show that the Madelung constant for one-dimensional array of ions of alternating sign with a distance  $a$  between successive ions is given by  $2 \ln 2$ .

- 2.4** Calculate the cohesive energy per ion-pair of LiCl and KCl crystals using the following data:

	LiCl	KCl
Madelung constant	1.748	1.748
$\text{Li}^+ - \text{Cl}^-/\text{K}^+ - \text{Cl}^-$ spacing	2.57 Å	3.14 Å
Ionization energy of	5.4 eV	4.34 eV
Li/K		

Assume that the repulsive potential energy is negligibly small.

- 2.5** Assume that the repulsive potential energy of an ion-pair in an ionic crystal arises because of the action of the Pauli exclusion principle and that it can be expressed as

$$U_{\text{rep.}} = \frac{B}{r^n}$$

where  $r$  is the separation between the ions of the opposite sign,  $n$  is a large number and  $B$  is a constant of the crystal.

Show that the total potential energy per ion-pair for equilibrium separation  $r_0$  is

$$U = - \frac{\alpha e^2}{4\pi \epsilon_0 r_0} \left(1 - \frac{1}{n}\right)$$

The observed cohesive energy of LiCl crystal is 6.8 eV per ion-pair. Using the data given in Problem 2.4, evaluate the value of  $n$  in the repulsive potential energy term (refer to the above problem).

- 2.6** Calculate the cohesive energy of hydrogen in kJ per mole using the Lennard-Jones parameters

$$\epsilon = 5 \times 10^{-22} \text{ J} \quad \text{and} \quad \sigma = 2.96 \text{ \AA}$$

Assume that hydrogen molecules are spherical and crystallize into an FCC structure. Compare your result with the measured value (0.751 kJ per mole) and comment.

- 2.7** In a crude model of alkali metals, the charge of each electron is treated as uniformly distributed over the volume of a sphere of radius  $r_s$  centred at each ion. Prove that the electrostatic energy per electron is then given by

$$\begin{aligned} U_{\text{coul}} &= - \frac{9a_0}{5r_s} \text{ rydberg} \\ &= \frac{24.49}{r_s/a_0} \text{ eV} \end{aligned}$$

where  $a_0$  is the Bohr radius.

- 2.8** Symbols  $r^>$  and  $r^<$  represent the radius of the bigger and smaller atom, respectively, in a crystal of diatomic basis. Show that the critical ratio,

$$\frac{r^>}{r^<} = \frac{\sqrt{3} + 1}{2} \text{ for the CsCl structure}$$

$$= 2 + \sqrt{6} \text{ for the zinc blende structure}$$

- 2.9** Show that the longitudinal and shear wave velocities in the [111] direction in a cubic crystal are, respectively, given by

$$v_l = \left[ \frac{C_{11} + 2C_{12} + 4C_{44}}{3\rho} \right]^{1/2}$$

$$v_s = \left[ \frac{C_{11} - C_{12} + C_{44}}{3\rho} \right]^{1/2}$$

- 2.10** Show that in a cubic crystal, the effective elastic constant for a shear across the (110) plane in the  $[1\bar{1}0]$  direction is equal to  $\frac{(C_{11} - C_{12})}{2}$ .

## SUGGESTED FURTHER READING

- Evans, R.C., *An Introduction to Crystal Chemistry* (Cambridge, 1964).
- Horton, G.K., "Ideal Rare Gas Crystals", *Amer. J. Phys.*, **36**, 93(1968).
- Maitland, G., et al., *Intermolecular Forces: Their origin and determination* (Oxford, 1981).
- Pauling, L., *Nature of the Chemical Bond*, 3rd ed. (Cornell, 1960).
- Phillips, J.C., *Covalent Bonding in Crystals, Molecules and Polymers* (The Univ. of Chicago Press, 1969).

# Reciprocal Lattice and Determination of Crystal Structure

This chapter is devoted to the description of principles and experimental methods that form the basis for determining crystal structures. We learnt about crystal structures in Chapter 1 in terms of the lattice symmetry, basis composition, and various intersecting families of planes as visualized in the space defined by the three crystal edges. As we already know, the most common experimental technique employed to investigate crystal structures is the x-ray diffraction method. The crystal photograph as recorded on the x-ray film represents the diffraction pattern of the crystal in which each of the spots corresponds to the diffraction maximum of a different family of parallel planes, with a certain orientation and common spacing. The derivation of the actual crystal structure from this photographic pattern in terms of atomic positions and orientation of planes in the usual three-dimensional space is not straightforward. This is done by having various geometrical constructions in the recorded photograph the details of which can be found in any book on crystallography.

Nevertheless, it is worthwhile to find some correlation between the structure of a crystal and its planar x-ray photograph. A family of parallel planes may as well be represented by their common normal. It is far more easy to visualize the motion of a normal (equivalent to a rod) than that of a plane which is a two-dimensional figure. If a length in some proportion of the common spacing be chosen and signified by a point along the normal, the point acts as a perfect representative of the family of planes under consideration. The theory discussed in this chapter will show that the x-rays diffracted from the family of planes produce the maximum intensity at this point. Further, the analysis shows that the distance of the point from an origin fixed at an arbitrary lattice point on the normal is proportional to the reciprocal of the interplanar spacing. The dimension of the representative position vector is thus the reciprocal of length. It is due to this reason that each of such points is called a *reciprocal lattice point*. These points happen to be arranged in a regular pattern forming a space lattice which is referred to as *the reciprocal lattice*. In this spirit, the regular pattern of spots on the film (Fig. 3.1) may be treated as the two-dimensional map of a three-dimensional reciprocal lattice for a certain incident direction of x-rays in the crystal. An appropriate treatment of the reciprocal lattice is taken up in the following section with the aim to establish the relationship between the direct lattice and the reciprocal lattice of a crystal.

## 3.1 RECIPROCAL LATTICE

The simple interpretation of reciprocal lattice as made above needs a suitable analytical extension for its complete treatment. Let us consider some functions whose values are periodic in the crystal lattice. These could be functions representing physical quantities such as electron charge density, or

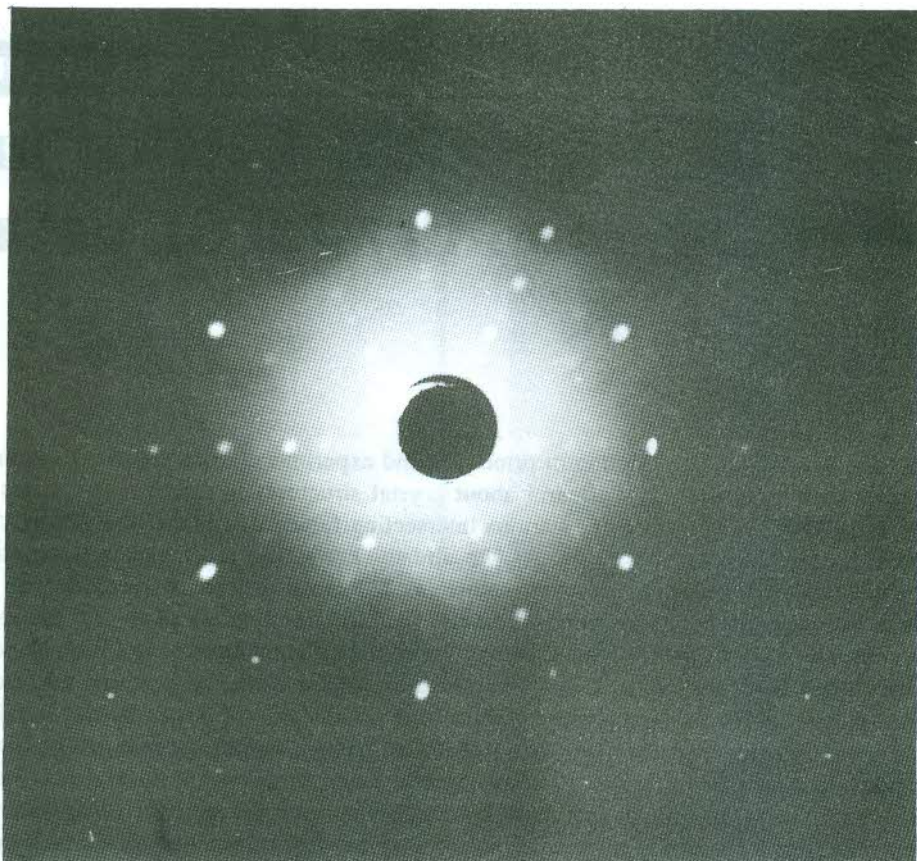


**FIG. 3.1** Laue photograph of CdTe crystal ( $a = 6.48 \text{ \AA}$ ) in [111] orientation. x-rays are incident normally on a (111) plane in [111] direction of the crystal; true for cubic crystals only. (Courtesy B.B. Sharma)

electrostatic crystal potential. We take the example of the crystal potential which is periodic or whose value is the same at all such points that are connected by translation vectors of the lattice. For a monatomic one-dimensional crystal (a linear chain of identical atoms), this potential  $U(x)$  is shown in Fig. 3.2. The periodic character of  $U(x)$  demands

$$U(\mathbf{x} + \mathbf{t}) = U(\mathbf{x}) \quad (3.1)$$

with  $\mathbf{t} = ma$

$U$ , potential energy

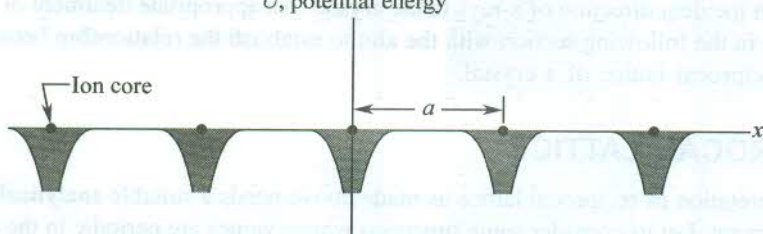


**FIG. 3.2** The periodic potential energy of an electron inside a linear crystal of identical atoms.

where  $m$  is an integer and  $|\mathbf{a}|$  the lattice constant. Since  $U(\mathbf{x})$  is a periodic function, it can be expanded in a Fourier series

$$U(\mathbf{x}) = \sum_n U_n \exp \left( \frac{i2\pi n \mathbf{x}}{\mathbf{a}} \right) \quad (3.2)$$

$n$  being an integer.

This form of  $U(\mathbf{x})$  ensures that its periodic nature expressed by (3.1) remains valid. The series (3.2) is generally expressed in the form

$$U(\mathbf{x}) = \sum_{\mathbf{g}} U_{\mathbf{g}} \exp (i\mathbf{g} \cdot \mathbf{x}) \quad (3.3)$$

where

$$\mathbf{g} = \frac{2\pi n}{\mathbf{a}} \quad (3.4)$$

with  $n = 1, 2, 3, \dots$

The vector  $\mathbf{g}$  has the dimension of the inverse of length vector and it is accordingly identified as the reciprocal vector. The coefficients  $U_{\mathbf{g}}$  are the usual Fourier coefficients. The set of reciprocal vectors given by (3.4) may be viewed as translation vectors of a one-dimensional lattice with the repeat interval of  $2\pi/\mathbf{a}$ . In other words the vectors  $2\pi n/\mathbf{a}$  represent position vectors of the lattice points of a one-dimensional reciprocal lattice. The set of vectors  $2\pi n/\mathbf{a}$  is known as the *reciprocal lattice vectors*. Further, the periodic character of  $U(\mathbf{x})$  requires,

$$\exp (i\mathbf{g} \cdot \mathbf{t}) = 1 \quad (3.5)$$

or

$$\mathbf{g} \cdot \mathbf{t} = \text{an even multiple of } \pi$$

This condition is readily satisfied by the expressions for  $\mathbf{g}$  and  $\mathbf{t}$ . The above treatment may be easily extended to the three dimensions where

$$U(\mathbf{r}) = \sum_{\mathbf{g}} U_{\mathbf{g}} \exp (i\mathbf{g} \cdot \mathbf{r}) \quad (3.6)$$

with the expression for  $\mathbf{g}$  being given by

$$\mathbf{g} = m_1 \mathbf{a}^* + m_2 \mathbf{b}^* + m_3 \mathbf{c}^* \quad (3.7)$$

where

$$\mathbf{a}^* = \frac{2\pi}{\mathbf{a}}, \quad \mathbf{b}^* = \frac{2\pi}{\mathbf{b}} \quad \text{and} \quad \mathbf{c}^* = \frac{2\pi}{\mathbf{c}} \quad (3.8)$$

Here  $\mathbf{a}^*$ ,  $\mathbf{b}^*$  and  $\mathbf{c}^*$  represent the primitive translation vectors of the reciprocal lattice as against  $\mathbf{a}$ ,  $\mathbf{b}$  and  $\mathbf{c}$  for the direct lattice. In other words,  $\mathbf{a}^*$ ,  $\mathbf{b}^*$  and  $\mathbf{c}^*$  form the three edges of the primitive cell of the reciprocal lattice under discussion. But it is customary to use a Wigner–Seitz type primitive cell for the purpose of calculations related to a reciprocal lattice. The method of construction of this cell is the same as in the direct space described in Chapter 1. The Wigner–Seitz cell of a reciprocal lattice is known by a special name—First Brillouin Zone. The first Brillouin zone for a two-dimensional reciprocal lattice is drawn in Fig. 3.3. These zones each of which is a closed figure fill the entire space of the reciprocal lattice. From the nomenclature we may question if there exist second, third or higher

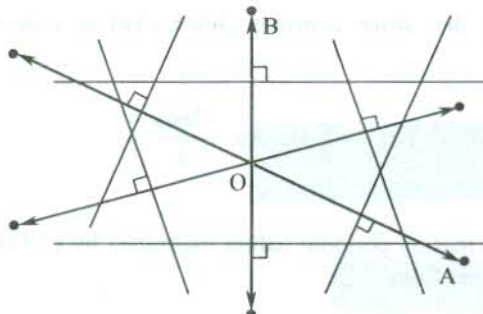
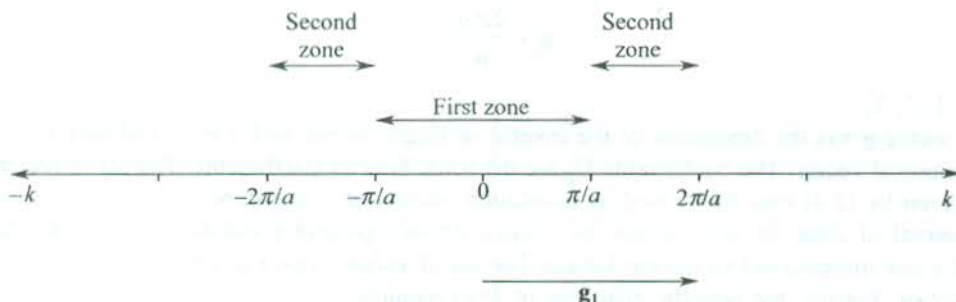


FIG. 3.3 Construction of the first Brillouin zone for a two-dimensional reciprocal lattice.

FIG. 3.4 Brilloin zones of a one-dimensional reciprocal lattice. Note that only the first zone appears as a single piece.  $\mathbf{g}_1$  denotes the shortest reciprocal lattice vector  $2\pi/a$ .

order Brillouin zones as well. The answer is yes. The Brillouin zones for a reciprocal lattice in one dimension are shown in Fig. 3.4.

The concept of reciprocal space may easily gain ground in our mind if we can identify some physical quantities that are measured in this space. One such simple physical quantity is the propagation constant which is more popularly known as wavevector ( $\mathbf{k}$ ) in solid state theory. This vector, having the dimension of the inverse of length ( $|\mathbf{k}| = 2\pi/\lambda$ ;  $\lambda$  is the wavelength), is a reciprocal vector and, therefore, rightly lies in the reciprocal space. On account of this, the reciprocal space is often referred to as the  $k$ -space.

A complete description of the reciprocal lattice cannot be achieved without coming to grips with the basic principles of the theory of x-ray diffraction. There are two parallel approaches to this theory. One is based on the Bragg law and the other is Max von Laue's formulation. But it will be shown that the two in effect are equivalent to one another. The theory succeeds in giving the direction of reciprocal lattice vectors that connect the reciprocal lattice points to the origin in the reciprocal space. A reciprocal lattice point will be found to be along the direction of x-rays reflected by a family of parallel planes with a certain orientation and common interplanar spacing. We discuss below first the Bragg law and then follow it with the Laue's version of x-ray diffraction.

### 3.2 BRAGG LAW

Strong x-ray diffraction produced by crystalline solids is based on Bragg law. Crystals are composed of various intersecting planes each of which itself contains a number of atoms. Since the interatomic

separations in crystals are of the same order of magnitude as the wavelength of x-rays ( $\sim \text{\AA}$ ), crystals act as diffraction gratings and produce diffraction on being irradiated by x-rays. W.H. Bragg and his son W.L. Bragg observed in 1913 such characteristic effects in the x-ray radiation reflected from crystals. In this phenomenon, the crystal planes are believed to act like plane mirrors. Radiations reflected from two successive parallel planes under certain conditions may interfere constructively to produce a diffraction maximum. The Bragg diffraction shown in Fig. 3.5 occurs for specular reflections (angle of incidence = angle of reflection). The constructive interference occurs when the path difference ( $2d \sin \theta$ ) between the interfering rays equals an integral multiple of the x-ray wavelength  $\lambda$ . That is,

$$2d \sin \theta = n\lambda \quad (3.9)$$

where

$d$  is the interplanar spacing

$\theta$  is the angle of the incident radiation with the plane

$n = 1, 2, 3, \dots$  (order of diffraction)

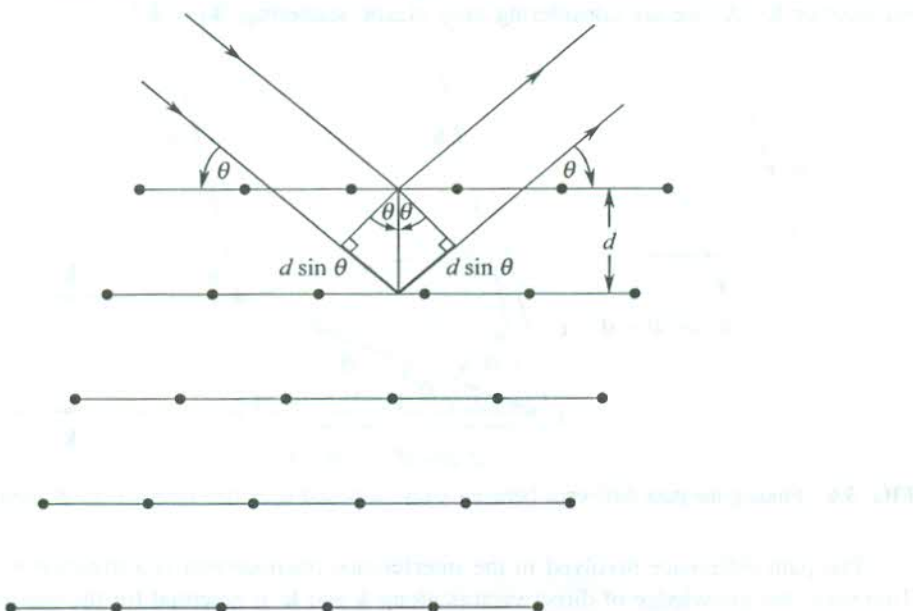


FIG. 3.5 Bragg reflection from a family of planes with interplanar spacing  $d$ . Note that the incident beam is deflected by twice the Bragg angle  $\theta$ .

The relation (3.9), which is a mathematical statement of the Bragg law, shows that the diffraction effects cannot be observed from a family of planes for any arbitrary angle of incidence. Even if monochromatic x-rays are used, the match among  $d$ ,  $\theta$  and  $\lambda$  has to be sought to satisfy (3.9) and get the Bragg diffraction. So, it is clear that Bragg diffraction is very much different from ordinary diffraction which generally puts no restriction on the incident angle.

Further, since  $\sin \theta \leq 1$ ,

$$\lambda \leq 2d \quad (3.10)$$

The condition expressed by (3.10) clearly explains why Bragg diffraction cannot occur for the visible

radiation. The Bragg law as expressed by (3.9) is essentially the consequence of the periodicity with only the elastic scattering of radiation taken into consideration.

### 3.3 LAUE'S INTERPRETATION OF X-RAY DIFFRACTION BY CRYSTALS

Max von Laue is credited for giving the idea that x-rays can produce constructive interference after getting diffracted from crystals. In 1912 two of Laue's colleagues Friedrich and Knipping at Munich did experiments which proved his theory. The Bragg law was established at Cambridge in 1913 with the awareness of the research activity of the Laue's group. In Laue's theory, the crystal is considered to be made up of identical microscopic set of ions or atoms. The x-rays scattered from these individual objects within each plane are believed to interfere constructively.

Let the x-rays of the wavevector  $\mathbf{k}$  be incident on two identical atoms at a separation of  $d$  (Fig. 3.6). The two atoms being identical would scatter x-rays in the direction with a common wavevector  $\mathbf{k}'$ . As we are considering only elastic scattering,  $|\mathbf{k}| = |\mathbf{k}'|$ .

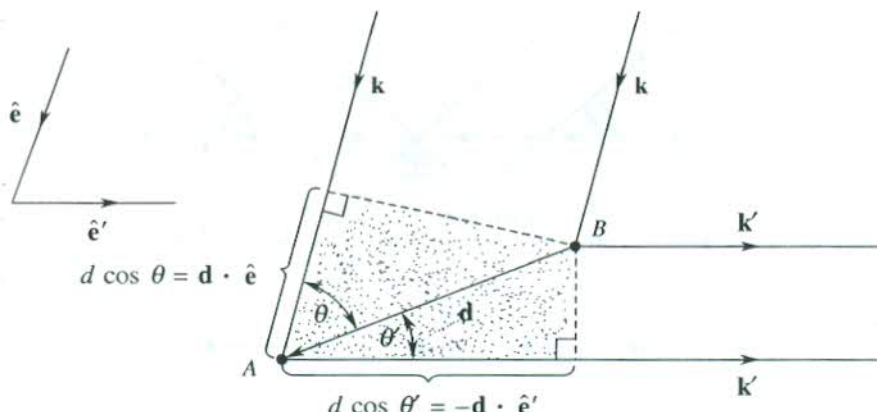


FIG. 3.6 Finding the path difference between x-rays scattered from two points  $A$  and  $B$  separated by distance  $d$ .

The path difference involved in the interference phenomenon is a distance in the direct space. Therefore, the knowledge of direct vectors along  $\mathbf{k}$  and  $\mathbf{k}'$  is essential for the calculation of the path difference between the x-rays scattered by atom  $A$  and those scattered by atom  $B$ . On the assumption of the direct unit vectors  $\hat{\mathbf{e}}$  and  $\hat{\mathbf{e}}'$  along  $\mathbf{k}$  and  $\mathbf{k}'$ , respectively, we solve the problem.

$$\begin{aligned} \text{The path difference} &= d \cos \theta + d \cos \theta' \\ &= \mathbf{d} \cdot \hat{\mathbf{e}} - \mathbf{d} \cdot \hat{\mathbf{e}}' \\ &= \mathbf{d} \cdot (\hat{\mathbf{e}} - \hat{\mathbf{e}}') \end{aligned}$$

The path difference at a point of constructive interference should meet the condition,

$$\mathbf{d} \cdot (\hat{\mathbf{e}} - \hat{\mathbf{e}}') = m\lambda \quad (3.11)$$

where  $m$  is an integer.

Multiplying both sides of (3.11) by  $2\pi/\lambda$ , we get

$$\mathbf{d} \cdot (\mathbf{k} - \mathbf{k}') = 2\pi m \quad (3.12)$$

When we consider the full crystal as an array of scatterers, the vector  $\mathbf{d}$  in (3.12) should be replaced by a general lattice vector  $\mathbf{t}$ , and thus

$$\mathbf{t} \cdot (\mathbf{k} - \mathbf{k}') = 2\pi m \quad (3.13)$$

which can be further transformed to

$$\exp[i(\mathbf{k} - \mathbf{k}')] \cdot \mathbf{t} = 1 \quad (3.14)$$

Comparison of (3.14) with (3.5) suggests that

$$\mathbf{k} - \mathbf{k}' = \mathbf{g} \quad (3.15)$$

where  $\mathbf{g}$  is a reciprocal lattice vector. The relation (3.15) states the Laue condition of diffraction. From (3.15), we have

$$\mathbf{k}' = \mathbf{k} - \mathbf{g}$$

which leads the Laue condition to the following form

$$2\mathbf{k} \cdot \mathbf{g} = \mathbf{g}^2 \text{ (using } |\mathbf{k}| = |\mathbf{k}'| \text{)} \quad (3.16)$$

The Laue condition for a wavevector  $\mathbf{k}$  to produce constructive interference in the diffracted radiation is contained in (3.16). The geometrical relationship between  $\mathbf{k}$ ,  $\mathbf{k}'$  and  $\mathbf{g}$  is demonstrated by Fig. 3.7. The plane perpendicular to the plane of the figure and passing through the horizontal line can be taken as the Bragg plane in Laue's formulation, which is essentially the reflecting plane in the Bragg picture. In this picture, the figure clearly represents the property that the reciprocal lattice vector ( $\mathbf{g}$ ) is perpendicular to the reflecting plane (and hence to the respective family of the reflecting planes).

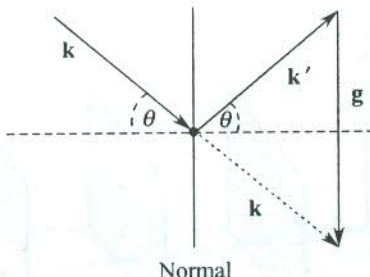


**FIG. 3.7** The geometrical relationship between the wavevector of incident ( $\mathbf{k}$ ) and scattered ( $\mathbf{k}'$ ) x-rays. For elastic scattering  $|\mathbf{k}| = |\mathbf{k}'|$ . The scatterers are two identical atoms.

By analogy with (3.4), the general relation for  $\mathbf{g}$  is

$$\mathbf{g} = \frac{2\pi n}{\mathbf{d}} \quad (3.17)$$

since the repeat distance in the present case is  $d$ .

The shortest  $\mathbf{g}(=\mathbf{g}_1)$  of the set of vectors expressed by (3.17) measures  $(2\pi/d)$ . It is now very simple to derive the Bragg law from the Laue's theory.

From Fig. 3.7, we get

$$\begin{aligned}\mathbf{k} \cdot \mathbf{g} &= kg \cos(90 - \theta) \\ &= kg \sin \theta\end{aligned}\quad (3.18)$$

Using (3.17) and (3.18), Laue condition (3.16) transforms to

$$2d \sin \theta = n\lambda \quad (3.19)$$

The parameters appearing in (3.19) and used in the two formulations independently refer to the same peak in the diffraction pattern of the crystal under consideration. The analysis of geometrical scattering as per Laue's formulation thus proves beyond doubt that the approaches of Bragg and Laue are equivalent. One important point emerging from the theory discussed above is that the reciprocal lattice point, representing a family of parallel planes with a common interplanar spacing, lies along the common normal of planes drawn from the origin in the reciprocal space. This concept is utilized in constructing the reciprocal lattice of a crystal lattice.

### 3.4 CONSTRUCTION OF RECIPROCAL LATTICE

In this section we describe in brief how the reciprocal lattice of a crystal lattice (or direct lattice) can be constructed. First of all, fix the origin at any arbitrary lattice point  $O$  in the direct lattice and then identify the three crystal axes ( $\mathbf{a}$ ,  $\mathbf{b}$ ,  $\mathbf{c}$ ) as shown in Fig. 3.8. Let us now draw a family of  $d_{100}$  planes where  $d$  stands for the interplanar separation and  $(100)$  are the Miller indices. Drop a normal  $\mathbf{OP}$  to these set of planes from the origin  $O$ . The vector  $\mathbf{OP}$  in this case represents the direction of  $\mathbf{a}^*$ . The complete set of reciprocal lattice vectors along this direction is given by

$$\mathbf{g} = \frac{2\pi n^\dagger}{\mathbf{d}_{100}}, \quad (n = 1, 2, 3, \dots) \quad (3.20)$$

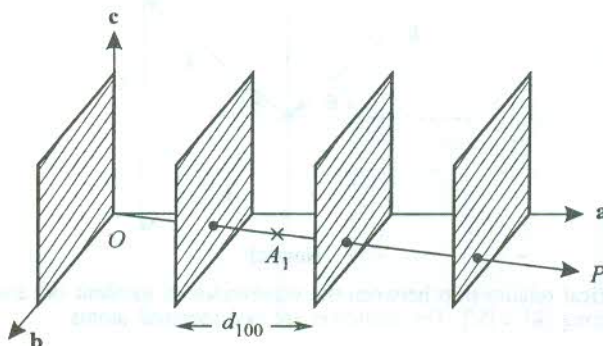


**FIG. 3.8** Construction of the reciprocal lattice.  $\mathbf{a}$ ,  $\mathbf{b}$ ,  $\mathbf{c}$  represent the primitive axes of the direct lattice.  $A_1$  is the reciprocal lattice point referred to  $d_{100}$  planes and lies on the normal to  $d_{100}$  planes. The normal  $\mathbf{OP}$  passing through the origin  $O$  gives the direction of the  $\mathbf{a}^*$  axis of the reciprocal lattice ( $|OA_1| = |\mathbf{a}^*|$ ).

<sup>†</sup> Here  $2\pi$  is called the scale factor or the magnification factor for  $OA_1$  that defines the reciprocal point. The value of this factor is a matter of convenience. Other values commonly used are 1 and  $\lambda$  (the wavelength of radiation).

The tip of these vectors will be located at the respective reciprocal lattice points  $A_1, A_2, A_3, \dots$ . The smallest of these  $\mathbf{OA}_1$ , is denoted by  $\mathbf{a}^*$  and expressed as

$$\mathbf{OA}_1 = \mathbf{a}^* = \frac{2\pi}{d_{100}} = \frac{2\pi\hat{\mathbf{e}}}{d_{100}} \quad (3.21)$$

where  $\hat{\mathbf{e}}$  stands for the unit vector along  $\mathbf{OP}$  or  $\mathbf{a}^*$ .

Thus  $A_1$  represents the reciprocal lattice point corresponding to  $d_{100}$  planes and  $A_2$  will correspond to  $d_{200}$  planes which are parallel to  $d_{100}$  planes with half common spacing.

Therefore, it is reasonable to write

$$\mathbf{OA}_2 = \frac{2\pi}{d_{200}} = \frac{2\pi\hat{\mathbf{e}}}{d_{200}}$$

It is also very clear that a reciprocal lattice point truly symbolizes a family of parallel planes because its position is defined implicitly by the orientation and explicitly by the common spacing of planes. And the general expression for reciprocal lattice vectors along  $\mathbf{a}^*$ , identified as one of the three primitive translation vectors, is

$$\mathbf{g}_{h00} = h\mathbf{a}^*, \quad (h = 1, 2, 3, \dots) \quad (3.22a)$$

We can similarly write vectors along the other two primitive vectors  $\mathbf{b}^*$  and  $\mathbf{c}^*$  as

$$\mathbf{g}_{0k0} = k\mathbf{b}^*, \quad (k = 1, 2, 3, \dots) \quad (3.22b)$$

and

$$\mathbf{g}_{00l} = l\mathbf{c}^*, \quad (l = 1, 2, 3, \dots) \quad (3.22c)$$

Following this procedure for all the planes of a crystal lattice, its reciprocal lattice may be mapped. The general reciprocal lattice vector should read as

$$\mathbf{g} = h\mathbf{a}^* + k\mathbf{b}^* + l\mathbf{c}^* \quad (3.23)$$

### 3.5 RELATIONSHIPS BETWEEN $\mathbf{a}, \mathbf{b}, \mathbf{c}$ AND $\mathbf{a}^*, \mathbf{b}^*, \mathbf{c}^*$

Consider a direct crystal lattice as shown in Fig. 3.9. Draw a normal  $OA$  from  $O$  on the face opposite to  $bc$  face.

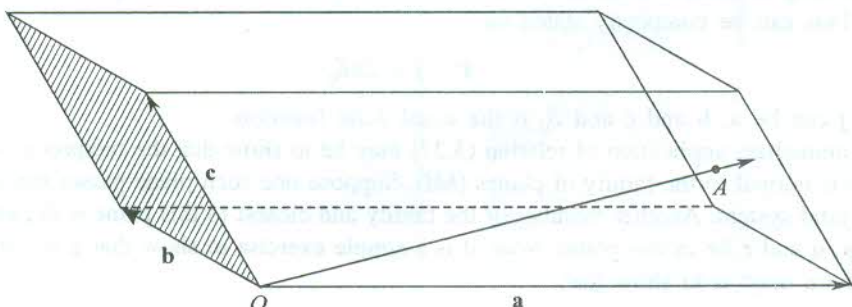


FIG. 3.9 A general direct crystal lattice.

Volume of the unit cell,  $V = \mathbf{a} \cdot (\mathbf{b} \times \mathbf{c})$

$$\begin{aligned} &= OA \times (\text{area of the face } bc) \\ &= OA \times |\mathbf{S}| \end{aligned} \quad (3.24)$$

Therefore,

$$\frac{1}{OA} = \frac{|\mathbf{S}|}{V}$$

or

$$\frac{1}{d_{100}} = \frac{|\mathbf{S}|}{V} \quad (\because OA = d_{100})$$

Thus

$$\frac{\hat{\mathbf{e}}}{d_{100}} = \frac{\mathbf{S}}{V}$$

where  $\hat{\mathbf{e}}$  is the unit vector in the direction of the normal  $OA$ . Therefore, we have

$$\frac{2\pi\hat{\mathbf{e}}}{d_{100}} = \frac{2\pi\mathbf{S}}{V} = 2\pi \frac{\mathbf{b} \times \mathbf{c}}{\mathbf{a} \cdot (\mathbf{b} \times \mathbf{c})} \quad (3.25)$$

Comparing (3.25) with (3.21), we get

$$\mathbf{a}^* = 2\pi \frac{\mathbf{b} \times \mathbf{c}}{\mathbf{a} \cdot (\mathbf{b} \times \mathbf{c})} \quad (3.26a)$$

Similarly, we can show that

$$\mathbf{b}^* = 2\pi \frac{\mathbf{c} \times \mathbf{a}}{\mathbf{a} \cdot (\mathbf{b} \times \mathbf{c})} \quad (3.26b)$$

and

$$\mathbf{c}^* = 2\pi \frac{\mathbf{a} \times \mathbf{b}}{\mathbf{a} \cdot (\mathbf{b} \times \mathbf{c})} \quad (3.26c)$$

It is interesting to observe from (3.26) that each of  $\mathbf{a}^*$ ,  $\mathbf{b}^*$  and  $\mathbf{c}^*$  is orthogonal to two crystal axis vectors. This can be compactly stated as

$$\mathbf{i}^* \cdot \mathbf{j} = 2\pi\delta_{ij} \quad (3.27)$$

where  $\mathbf{i}$ ,  $\mathbf{j}$  can be  $\mathbf{a}$ ,  $\mathbf{b}$  and  $\mathbf{c}$  and  $\delta_{ij}$  is the usual delta function.

The immediate application of relation (3.27) may be to show that the reciprocal vector  $\mathbf{g}$  given by (3.23) is normal to the family of planes  $(hkl)$ . Suppose one such plane passes through the origin  $O$  in a crystal system. Another member of the family and closest to this plane is drawn in Fig. 3.10. Vectors  $\mathbf{p}$ ,  $\mathbf{q}$  and  $\mathbf{r}$  lie in this plane. Now, it is a simple exercise to show that  $\mathbf{g}$  is normal to planes  $(hkl)$ . All we need is to show that

$$\mathbf{g} \cdot \mathbf{t} = 0 \quad \text{with } \mathbf{t} \equiv \mathbf{p}, \mathbf{q}, \mathbf{r}.$$

From the definition of the Miller indices, it follows that the intercepts of the plane, shown in Fig. 3.10, with  $\mathbf{a}$ ,  $\mathbf{b}$  and  $\mathbf{c}$  axis vectors of the direct crystal are vectorially written as  $\mathbf{a}/h$ ,  $\mathbf{b}/k$ , and  $\mathbf{c}/l$ , respectively. This enables us to write

$$\mathbf{p} = \left( \frac{\mathbf{a}}{h} - \frac{\mathbf{b}}{k} \right); \quad \mathbf{q} = \left( \frac{\mathbf{c}}{l} - \frac{\mathbf{b}}{k} \right) \text{ and } \mathbf{r} = \left( \frac{\mathbf{c}}{l} - \frac{\mathbf{a}}{h} \right)$$

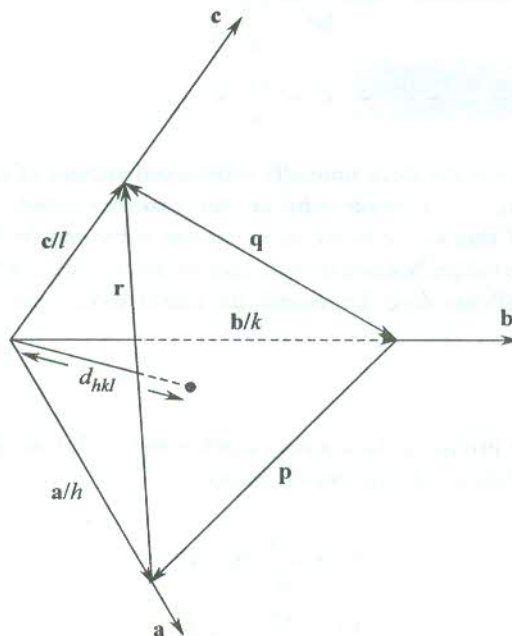


**FIG. 3.10** The figure shows intersections of a plane ( $hkl$ ) with crystal axes  $\mathbf{a}$ ,  $\mathbf{b}$ ,  $\mathbf{c}$  at general orientations. The three intercepts measure  $\mathbf{a}/h$ ,  $\mathbf{b}/k$  and  $\mathbf{c}/l$ , respectively. Vectors  $\mathbf{p}$ ,  $\mathbf{q}$  and  $\mathbf{r}$  lie in the plane ( $hkl$ ).

It can be checked that the scalar product of any of these vectors with  $\mathbf{g}$  vanishes, proving thereby that every reciprocal vector is normal to a family of parallel planes with common interplanar spacing.

One point of caution:  $h$ ,  $k$  and  $l$  in (3.23) need not always represent the Miller indices and in principle they can have a common factor. In view of this fact it is safer to use the form given by (3.7), i.e.

$$\mathbf{g} = m_1 \mathbf{a}^* + m_2 \mathbf{b}^* + m_3 \mathbf{c}^*$$

where  $m_1$ ,  $m_2$  and  $m_3$  are any integers.

### 3.6 APPLICATION TO SOME CRYSTAL LATTICES

We will now apply the relationships obtained above to determine the primitive translation vectors of lattices, reciprocal to certain crystal lattices.

#### *Simple cubic (SC) lattice*

For this lattice,  $|\mathbf{a}| = |\mathbf{b}| = |\mathbf{c}|$  and  $\mathbf{a}$ ,  $\mathbf{b}$  and  $\mathbf{c}$  are mutually orthogonal vectors given by  $a\hat{x}$ ,  $a\hat{y}$  and  $a\hat{z}$ .

respectively, where  $\hat{x}, \hat{y}, \hat{z}$  are unit vectors along the three orthogonal coordinate axes  $x, y$ , and  $z$  directed along the three edges of the lattice.

Therefore, using (3.26)

$$\begin{aligned}\mathbf{a}^* &= \frac{2\pi}{a} \hat{x} \\ \mathbf{b}^* &= \frac{2\pi}{a} \hat{y} \\ \mathbf{c}^* &= \frac{2\pi}{a} \hat{z}\end{aligned}\tag{3.28}$$

The set (3.28) again represents the three mutually orthogonal vectors of equal magnitude  $2\pi/a$ . This shows that the reciprocal lattice of a simple cubic crystal is another simple cubic lattice. We can easily show that the reciprocal of this lattice is the same simple cubic lattice of the direct space.

The six planes, that are the perpendicular bisectors of the vectors  $\pm \mathbf{a}^*$ ,  $\pm \mathbf{b}^*$  and  $\pm \mathbf{c}^*$ , constitute the boundary of the first Brillouin zone. To remind, the first Brillouin zone serves as the primitive cell of the reciprocal lattice.

### BCC lattice

Using (1.4a) (that give the primitive translation vectors) and (3.26) we get the following primitive vectors for the reciprocal lattice of this crystal lattice.

$$\begin{aligned}\mathbf{a}^* &= \frac{2\pi}{a} (\hat{x} + \hat{y}) \\ \mathbf{b}^* &= \frac{2\pi}{a} (\hat{y} + \hat{z}) \\ \mathbf{c}^* &= \frac{2\pi}{a} (\hat{z} + \hat{x})\end{aligned}\tag{3.29}$$

These vectors represent an FCC lattice of lattice constant  $4\pi/a$  [see (1.4b)], showing that an FCC lattice is the reciprocal lattice of the BCC lattice. The rhombohedron formed by  $\mathbf{a}^*, \mathbf{b}^*, \mathbf{c}^*$  represents the primitive cell of volume  $V$  expressed as

$$\begin{aligned}V &= \mathbf{a}^* \cdot (\mathbf{b}^* \times \mathbf{c}^*) \\ &= \frac{16\pi^3}{a^3}\end{aligned}$$

Similarly, it can be shown that the reciprocal lattice of the FCC lattice is a BCC lattice. There are in all 12 shortest vectors for the lattice described by (3.29):

$$\frac{2\pi}{a} (\pm \hat{y} \pm \hat{z}); \quad \frac{2\pi}{a} (\pm \hat{z} \pm \hat{x}); \quad \frac{2\pi}{a} (\pm \hat{x} \pm \hat{y})$$

with the choices of signs being independent.

Planes perpendicular to these vectors at their mid-points enclose the volume of the first Brillouin zone which turns out to be a rhombododecahedron (Fig. 3.11).

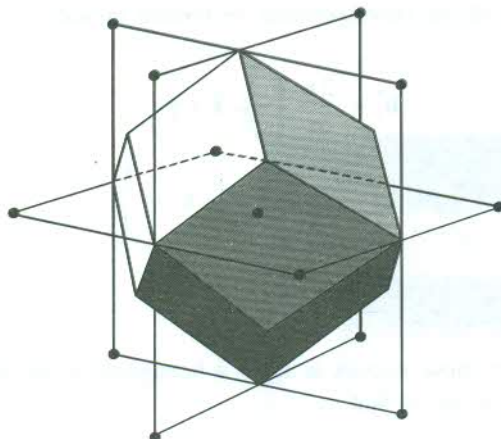


FIG. 3.11 The first Brillouin zone of a BCC crystal. It is rhombododecahedral in shape.

### Hexagonal space lattice

The primitive translation vectors  $\mathbf{b}_1$ ,  $\mathbf{b}_2$  and  $\mathbf{b}_3$  are drawn in Fig. 3.12. In relation to the directions of  $x$ ,  $y$ ,  $z$  axes as shown in the figure, the primitive vectors of the direct lattice are given by

$$\begin{aligned}\mathbf{b}_1 &= \frac{\sqrt{3} a}{2} \hat{\mathbf{x}} + \frac{a}{2} \hat{\mathbf{y}} \\ \mathbf{b}_2 &= -\frac{\sqrt{3} a}{2} \hat{\mathbf{x}} + \frac{a}{2} \hat{\mathbf{y}} \\ \mathbf{b}_3 &= c \hat{\mathbf{z}}\end{aligned}\quad (3.30)$$

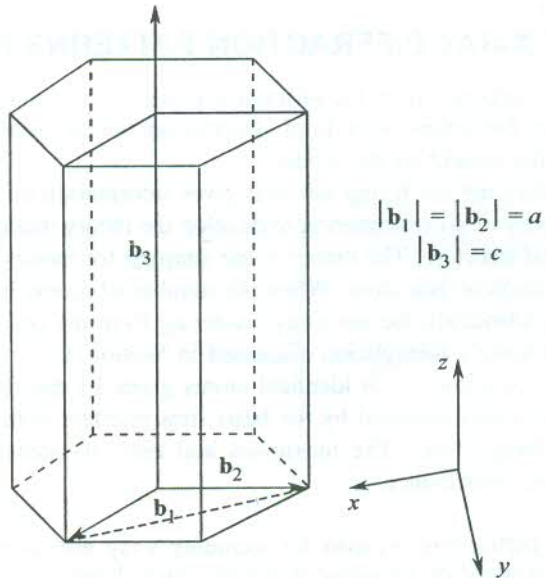


FIG. 3.12 Hexagonal space lattice— $\mathbf{b}_1$ ,  $\mathbf{b}_2$  and  $\mathbf{b}_3$  are the primitive vectors and the angle between  $\mathbf{b}_1$  and  $\mathbf{b}_2$  (on the hexagonal face) is  $120^\circ$ .

Then the primitive vectors of the corresponding reciprocal lattice are

$$\begin{aligned}\mathbf{b}_1^* &= \frac{2\pi}{a} \left( \frac{1}{\sqrt{3}} \hat{\mathbf{x}} + \hat{\mathbf{y}} \right) \\ \mathbf{b}_2^* &= \frac{2\pi}{a} \left( -\frac{1}{\sqrt{3}} \hat{\mathbf{x}} + \hat{\mathbf{y}} \right) \\ \mathbf{b}_3^* &= \frac{2\pi}{c} \hat{\mathbf{z}}\end{aligned}\quad (3.31)$$

The unit cell formed by these vectors is again a hexagonal prism as shown by Fig. 3.13. The significant point about this prism is that

$$|\mathbf{b}_3^*| < |\mathbf{b}_1^*| \text{ or } |\mathbf{b}_2^*|$$

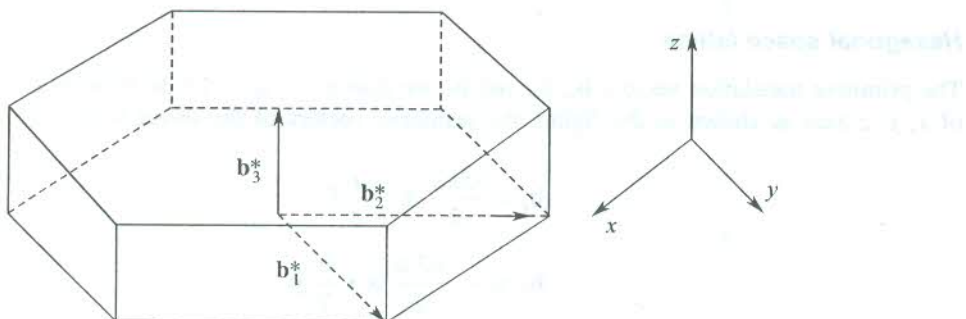


FIG. 3.13 The reciprocal lattice of the hexagonal space lattice shown in Fig. 3.12.

### 3.7 ANALYSIS OF X-RAY DIFFRACTION PATTERNS FROM CRYSTALS

The determination of crystal structure from the diffraction pattern of a crystal is a lengthy geometrical and mathematical exercise. Nevertheless, a brief description of the involved basic principles is provided in this book for the benefit of the reader.

We have to look well beyond the Bragg law that gives information on interplanar spacing. We capitalize on the Laue's theory of x-ray scattering to develop the theory that is capable of giving most of the information on crystal structure. The theory is the simplest for monatomic crystals (composed of identical atoms) with a basis of one atom. When the number of atoms in a primitive cell (basis) is more than one (all being identical), the net x-ray scattering from the cell can be treated easily by extending only slightly the Laue's formulation discussed in Section 3.3.

Let a primitive cell be composed of  $n$  identical atoms given by position vectors  $\mathbf{r}_1, \mathbf{r}_2, \dots, \mathbf{r}_n$ . The extent to which the radiations scattered by the basis sites interfere with one another determines the intensity of a certain Bragg line.<sup>†</sup> The maximum and zero of intensity occurs for complete constructive and destructive interference.

<sup>†</sup> In a modern instrument (Diffractometer) used for recording x-ray diffraction pattern of crystals the photographic recording is replaced by electronic recording which shows lines (peaks) when constructive interference takes place. See Fig. 3.15.

If the change of wavevector attributed to certain peak is

$$\mathbf{k}' - \mathbf{k} = \mathbf{g}$$

we know that the corresponding path difference between the x-rays scattered by atoms at  $\mathbf{r}_i$  and  $\mathbf{r}_j$  will be  $\mathbf{g} \cdot (\mathbf{r}_i - \mathbf{r}_j)$  and the phase factor representing the phase difference between two rays equals  $\exp[i\mathbf{g} \cdot (\mathbf{r}_i - \mathbf{r}_j)]$ .

As such, the phases of rays scattered by atoms at  $\mathbf{r}_1, \mathbf{r}_2, \dots, \mathbf{r}_n$  are in the ratios

$$e^{ig \cdot r_1}, e^{ig \cdot r_2}, \dots, e^{ig \cdot r_n}$$

This suggests that the amplitude of the x-ray beam scattered by the whole primitive cell should have a factor expressible as

$$\sum_{j=1}^n \exp(i\mathbf{g} \cdot \mathbf{r}_j)$$

The amplitude of x-rays scattered by a single primitive cell is conventionally expressed as

$$S_g = \sum_{j=1}^n f_j \exp(i\mathbf{g} \cdot \mathbf{r}_j) \quad (3.32)$$

where  $S_g$  is called the structure factor and  $f_j$  stands for the atomic form factor of the atom positioned at  $\mathbf{r}_j$ . The atomic form factor of an atom depends entirely on the internal structure of the atom. As in the present case, the primitive cell is composed of identical atoms, we can rewrite (3.32) as

$$S_g = f \sum_{j=1}^n \exp(i\mathbf{g} \cdot \mathbf{r}_j) \quad (3.33)$$

If there are  $N$  primitive cells in a crystal, the total scattering amplitude of a diffraction peak may be expressed as

$$S = NS_g \quad (3.34)$$

This Bragg peak appears because of the constructive interference of the scattered x-rays whose wavevector differs from that of the incident x-rays by reciprocal vector  $\mathbf{g}$ . Since intensity is known to be proportional to the square of amplitude, the intensity of a Bragg line is proportional to  $|S_g|^2$ . Thus, the relative intensity of Bragg lines can be obtained by calculating their  $S_g$ .

### Structure factor of a BCC crystal

Its conventional unit cell is non-primitive. But it can be pictured as a simple cubic lattice with a basis of two atoms at  $000$  and  $\frac{1}{2} \frac{1}{2} \frac{1}{2}$ . Such a lattice is primitive and we can use (3.33) for calculating the

structure factor,  $S_g$ . Thus  $\mathbf{r}_1 = 0$  and  $\mathbf{r}_2 = \frac{1}{2} a(\hat{\mathbf{x}} + \hat{\mathbf{y}} + \hat{\mathbf{z}})$ .

From (3.33), we have

$$S_g = f + f \exp\left[i\mathbf{g} \cdot \frac{a}{2} (\hat{\mathbf{x}} + \hat{\mathbf{y}} + \hat{\mathbf{z}})\right] \quad (3.35a)$$

$$\begin{aligned}
 &= f\{1 + \exp [i\pi(m_1 + m_2 + m_3)]\} \\
 &= f[1 + (-1)^{m_1 + m_2 + m_3}]
 \end{aligned} \tag{3.35b}$$

because for a simple cubic lattice, we have

$$\mathbf{g} = \frac{2\pi}{a} (m_1 \hat{\mathbf{x}} + m_2 \hat{\mathbf{y}} + m_3 \hat{\mathbf{z}}) \tag{3.36}$$

Equation (3.35b) shows that

$$S_g = 0, \quad \text{if } m_1 + m_2 + m_3 = \text{an odd integer} \tag{3.37a}$$

$$= 2f, \quad \text{if } m_1 + m_2 + m_3 = \text{an even integer} \tag{3.37b}$$

It is important to note that  $\mathbf{g} \neq 0$  though the respective  $S_g$  vanishes for an odd integral value of  $(m_1 + m_2 + m_3)$ . There cannot occur Bragg peaks for planes such as (100), (111), (120), etc. but peaks caused by reflections from planes, for example, (110), (112), (222) will appear in the diffraction pattern.

For example, in sodium metal, which has a BCC structure, the reflections from (100) plane are missing in the diffraction pattern as required by (3.37a). In a cubic crystal the phases  $(\mathbf{g} \cdot \mathbf{r}_j)$  for atoms on the bounding (100) planes are 0 and  $2\pi$ . For this phase difference, normally the (100) diffraction peak appears. But in a BCC crystal there is a plane midway between (100) planes. The phase difference between rays scattered from an atom on this plane and another atom on any of the two nearest (100) planes thus becomes  $\pi$ . As the density of atoms on the (100) and midway planes is equal, a destructive interference takes place between the rays reflected from successive (100) and midway planes. This explains why (100) reflections are not observed from sodium crystals. In fact, the destructive interference in this case is complete because of a common atomic form factor for all atoms present in the crystal.

Finally, we must recall that we have treated a BCC lattice as a simple cubic (SC) with a basis of two identical atoms. The reciprocal lattice of an SC lattice is again an SC lattice with lattice constant  $2\pi/a$ . But in accordance with (3.37a), a lattice point the sum of whose coordinates in the reciprocal lattice is an odd number should be missing in the reciprocal lattice. Every lattice point corresponds to the reflection from a certain family of parallel planes. This means that the alternate corners of a cube of side  $2\pi/a$  are non-existent. Therefore, this cube cannot be used to map the infinite reciprocal lattice and therefore, it is not the required unit cell. Interestingly, on choosing the cube of side  $4\pi/a$ , the condition (3.37a) allows all of its corners to be present along with a point at the centre of each bounding face. This arrangement of lattice points belongs to an FCC lattice, which effectively shows that the reciprocal lattice of a BCC lattice is an FCC lattice. This result has been proved earlier in Section 3.6. The conventional unit cell of an FCC lattice in reciprocal space is shown in Fig. 3.14.

### Structure factor of a monatomic FCC crystal

The unit cell in this case has four identical atoms located at its corners and at the centres of its faces. This FCC cell can as well be interpreted as SC structure whose basis is composed of four atoms. The positions of basis atoms in the SC primitive cell are: (0 0 0), (1/2 1/2 0), (1/2 0 1/2) and (0 1/2 1/2). Their position vectors as measured from a corner of the cell will be written as:

$$\mathbf{r}_1 = 0, \mathbf{r}_2 = \frac{1}{2} a(\hat{\mathbf{x}} + \hat{\mathbf{y}}); \mathbf{r}_3 = \frac{1}{2} a(\hat{\mathbf{z}} + \hat{\mathbf{x}}) \quad \text{and} \quad \mathbf{r}_4 = \frac{1}{2} a(\hat{\mathbf{y}} + \hat{\mathbf{z}})$$

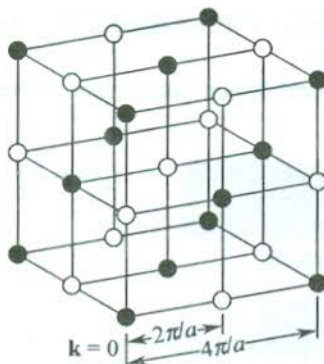


**FIG. 3.14** A cubic reciprocal lattice of side  $2\pi/a$ . The white circles represent the lattice points for which the structure factor vanishes (3.37a). When these circles are removed from the lattice, a conventional FCC lattice of side  $4\pi/a$  is obtained.

Substituting these vectors and the general reciprocal lattice vector  $\mathbf{g}$  (3.36) in (3.33), one gets the following expression for the structure factor.

$$S_g = f \left[ 1 + e^{i\pi(m_1 + m_2)} + e^{i\pi(m_3 + m_1)} + e^{i\pi(m_2 + m_3)} \right] \quad (3.38)$$

which gives

$$S_g = 4f, \text{ only if } m_1, m_2 \text{ and } m_3 \text{ are all odd or all even} \quad (3.39a)$$

$$= 0, \text{ for all odd-even combinations of } m_1, m_2 \text{ and } m_3. \quad (3.39b)$$

The result (3.39) reveals that the peaks having origin in the diffraction from planes such as (100), (110), (121) will not be observed, whereas those from the likes of (111), (200), (222) will appear in the diffraction pattern of an FCC crystal.

### Structure factor of monatomic diamond lattice

This lattice represents the crystals of diamond, germanium, silicon, grey tin, etc. Each of these is composed of identical atoms and their unit cell is interpreted as two FCC lattices displaced from one another along a body diagonal by one-fourth of the body diagonal. But it can still be treated as an FCC lattice with a basis of two identical atoms whose positions  $\mathbf{r}_j$  may be represented by

$$\mathbf{r}_1 = 0 \quad \text{and} \quad \mathbf{r}_2 = \frac{1}{4} a(\hat{\mathbf{x}} + \hat{\mathbf{y}} + \hat{\mathbf{z}}) \quad (j = 1, 2)$$

Putting direct primitive vectors from (1.4b) in set (3.26), we get the following primitive vectors of the reciprocal lattice:

$$\begin{aligned} \mathbf{a}^* &= \frac{2\pi}{a} (\hat{\mathbf{x}} + \hat{\mathbf{y}} - \hat{\mathbf{z}}) \\ \mathbf{b}^* &= \frac{2\pi}{a} (-\hat{\mathbf{x}} + \hat{\mathbf{y}} + \hat{\mathbf{z}}) \\ \mathbf{c}^* &= \frac{2\pi}{a} (\hat{\mathbf{x}} - \hat{\mathbf{y}} + \hat{\mathbf{z}}) \end{aligned} \quad (3.40)$$

A comparison with (1.4a) shows that (3.40) represent a BCC lattice the side of whose conventional cell is  $4\pi/a$ .

Using (3.40), the general reciprocal lattice vector may written as

$$\mathbf{g} = \frac{2\pi}{a} [(-m_1 + m_2 + m_3) \hat{\mathbf{x}} + (m_1 - m_2 + m_3) \hat{\mathbf{y}} + (m_1 + m_2 - m_3) \hat{\mathbf{z}}] \quad (3.41)$$

Substitution of  $\mathbf{g}$  and  $\mathbf{r}_j$  in (3.33) yields

$$S_g = f \left\{ 1 + \exp \left[ \frac{i\pi}{2} (m_1 + m_2 + m_3) \right] \right\} \quad (3.42)$$

which gives

$$S_g = f(1 \pm i), \text{ if } (m_1 + m_2 + m_3) = \text{an odd number} \quad (3.43a)$$

$$= 0, \text{ if } (m_1 + m_2 + m_3) = \text{twice an odd number} \quad (3.43b)$$

$$= 2f, \text{ if } (m_1 + m_2 + m_3) = \text{twice an even number} \quad (3.43c)$$

On lines similar to those followed for a BCC lattice, it can be shown that the reciprocal lattice of a diamond lattice is a BCC lattice with cubic cell of side  $8\pi/a$ . There will be three kinds of reciprocal lattice points in this case corresponding to the three values of the structure factor,  $f(1 \pm i)$ ,  $2f$  and  $0$  defined by (3.43). Details can be found elsewhere.\*

### Structure factor of a polyatomic crystal

Let us take the general case of a polyatomic crystal in which atoms in the basis are not identical, i.e. the crystal is composed of atoms belonging to more than one element. The structure factor of any diffraction line from this crystal is calculated by using the general relation given by (3.32).

As an example, we take the simplest case of an alloy. The binary CuZn alloy, when ordered, has CsCl structure. By ordered we mean that all nearest neighbours of a Cu atom are Zn atoms and vice versa. The lattice is simple cubic and the basis has two atoms; Cu atom at 000 and Zn atom at  $\frac{1}{2} \frac{1}{2} \frac{1}{2}$ . The structure factor is

$$\begin{aligned} S_g &= f_{\text{Cu}} + f_{\text{Zn}} \exp \left[ i \frac{2\pi}{a} (m_1 \hat{\mathbf{x}} + m_2 \hat{\mathbf{y}} + m_3 \hat{\mathbf{z}}) \cdot \frac{a}{2} (\hat{\mathbf{x}} + \hat{\mathbf{y}} + \hat{\mathbf{z}}) \right] \\ &= f_{\text{Cu}} + f_{\text{Zn}} \exp [i\pi (m_1 + m_2 + m_3)] \end{aligned} \quad (3.44)$$

In principle,  $S_g$  can never vanish since  $f_{\text{Cu}} \neq f_{\text{Zn}}$  and, therefore, all diffraction lines of the simple cubic lattice should be observed. But in practice every alloy is disordered to some extent. In the disordered structure there is an equal probability for a Cu atom and a Zn atom to be located at 000 or  $\frac{1}{2} \frac{1}{2} \frac{1}{2}$ . The relation (3.44) is found to be of tremendous value in such a situation as it can help in distinguishing between an ordered and a disordered structure. Therefore, it is prudential to talk in terms of average structure factor while discussing a disordered structure. In this case,

\* N.W. Ashcroft and N.D. Mermin, *Solid State Physics*, Chapter 6, pp. 106–107, Saunders College (1988).

$$\langle S_g \rangle = \langle f \rangle + \langle f \rangle \exp [i\pi(m_1 + m_2 + m_3)] \quad (3.45)$$

where

$$\langle f \rangle = \frac{1}{2} [f_{\text{Cu}} + f_{\text{Zn}}]$$

From (3.45) we find that the reflections, for which  $(m_1 + m_2 + m_3)$  is odd, vanish. It means that the disordered alloy will show a smaller number of diffraction lines and this fact can be used to make a distinction between an ordered and a disordered crystal in general.

Another interesting example is that of the KCl crystal. The KCl is an ionic crystal and its stable constituents are  $\text{K}^+$  and  $\text{Cl}^-$  ions both of which possess an equal number of electrons. This prompts us to expect that

$$f_{\text{K}^+} \approx f_{\text{Cl}^-}$$

The diffraction pattern really confirms our conjecture as it suggests that KCl is a monatomic simple cubic lattice of lattice constant  $a/2$ . Based on a cubic lattice of lattice constant  $a$ , we find that lines of only those planes are observed for which the sum of the plane indices  $(m_1 + m_2 + m_3)$  is an even number (Fig. 3.15). The result is of special significance as the basis is not composed of identical atoms in this case. In addition, the dependence of the atomic form factor on the internal structure of an atom/ion is established.

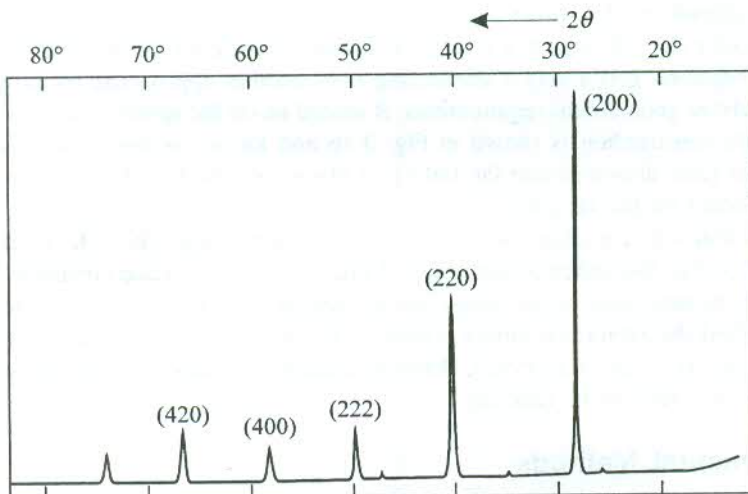


**FIG. 3.15** x-ray diffraction from KCl crystal. The ions  $\text{K}^+$  and  $\text{Cl}^-$  have an equal number of electrons characterizing them with a common form factor. This results in the vanishing of reflections from planes for which the sum  $(m_1 + m_2 + m_3)$  is an odd number. Reflections from only those planes for which this sum is an even number are present in the diffractogram.

### 3.8 MEASUREMENT OF DIFFRACTION PATTERN OF CRYSTALS

Geometries of various experimental arrangements employed for this purpose are linked with the Laue condition of diffraction. A diffraction line appears only if the tip of the incident wavevector ( $\mathbf{k}$ ) lies on a Bragg plane in  $k$ -space. The Bragg plane is only the family of parallel planes which meets the

requirements of constructive interference for reflections of the incident radiation  $\mathbf{k}$ . For this family of planes the direction of  $\mathbf{k}$  is also specific in order to observe the diffraction peak. One diffraction line or one lattice point in the reciprocal space corresponds to one family of planes. Obviously, there are many other families of planes composing the crystal. The whole reciprocal lattice or the diffraction pattern can be completed by making the constructive interference possible for reflections from all of these planes. In practice, it is done by having provisions for:

- (i) Varying the direction of  $\mathbf{k}$  which can be done by rotating the crystal.
- (ii) A continuous x-ray beam whose varying set of wavelengths may find appropriate allies among various crystal planes in order to satisfy the Laue condition for their direction of incidence.

The provisions mentioned above give rise to a number of experimental geometries which we will describe later in this section. But, before doing so, we will discuss one of the most beautiful geometrical constructions known as the Ewald construction.

### 3.8.1 The Ewald Construction

Ewald gave the following simple geometrical construction that guided experimentalists to develop various methods for deducing the crystal structure from the observed diffraction pattern.

Draw a sphere of radius  $k$  in the reciprocal space with centre at  $A$  (Fig. 3.16). Let  $\mathbf{k}$  represent the wavevector of the incident x-ray beam terminating at the origin of the reciprocal lattice  $O$ . The direction and magnitude of the wavevector of reflected x-rays (say given by  $\mathbf{k}'$ ) will be such that change in wavevector ( $\mathbf{k}' - \mathbf{k}$ ) equals a reciprocal lattice vector  $\mathbf{g}$  on the demand of Laue condition for diffraction. Therefore,  $\mathbf{g}$  is a vector connecting  $O$  to another appropriate reciprocal lattice point  $B$ . To satisfy the above geometrical requirements,  $B$  should lie on the sphere's surface and  $\mathbf{k}'$  be given by  $AB$ . The whole construction is shown in Fig. 3.16 and known as the Ewald construction. The equidistant parallel lines drawn denote the family of planes involved in the reflection shown. These planes are represented by the reciprocal lattice point  $B$ .

The Ewald construction implies the elastic x-ray scattering, since  $|\mathbf{k}| = |\mathbf{k}'|$  (= the radius of the Ewald sphere). With this, the vector relationships of Fig. 3.16 give the Laue condition  $2\mathbf{k} \cdot \mathbf{g} = \mathbf{g}^2$  that has been shown to be equivalent to the Bragg law in Section 3.3. The construction clearly establishes how rare it is to find the reciprocal lattice points on the surface of the Ewald sphere to get Bragg reflections from various planes of a crystal. Different methods are used to create situations that render the recording of these reflections feasible.

### 3.8.2 Experimental Methods

In this section we describe in brief the three main techniques employed for the determination of crystal structure.

#### *The Laue method*

This method produced the first ever recorded x-ray diffraction photograph of a crystal. The Laue photograph is historic in this sense. The Laue condition given by (3.15) can be written as

$$\Delta\mathbf{k} = \mathbf{g} \quad (3.46)$$

where  $\mathbf{g}$  is defined by (3.7).

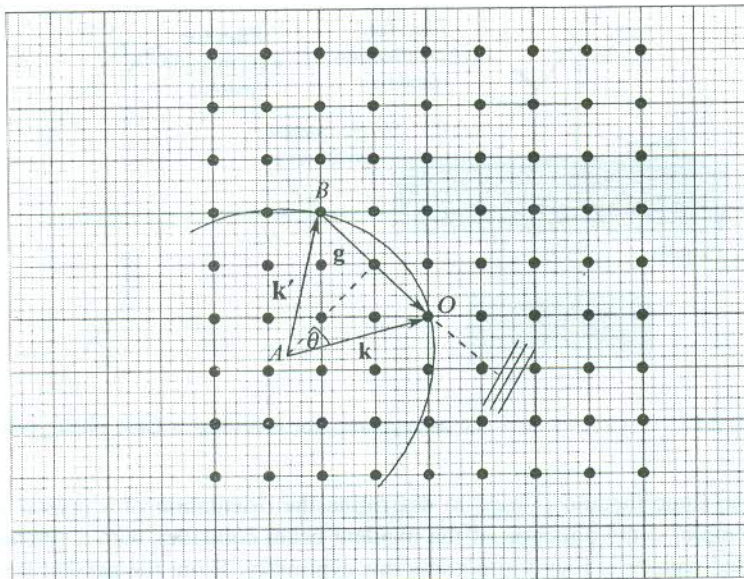


**FIG. 3.16** Ewald construction for Bragg reflections. The change in wavevector on reflection is equal to a reciprocal lattice vector  $\mathbf{g}$ . The  $\mathbf{g}$  terminates at a reciprocal lattice point falling on the Ewald sphere.

Taking the scalar product of direct lattice primitive vectors  $\mathbf{a}$ ,  $\mathbf{b}$ ,  $\mathbf{c}$  with both sides of (3.46), we have

$$\begin{aligned}\mathbf{a} \cdot \Delta\mathbf{k} &= 2\pi m_1 \\ \mathbf{b} \cdot \Delta\mathbf{k} &= 2\pi m_2 \\ \mathbf{c} \cdot \Delta\mathbf{k} &= 2\pi m_3\end{aligned}\quad (3.47)$$

Relations (3.47), called the Laue equations, indicate that  $\Delta\mathbf{k}$  lies on the surface of each of the three separate cones formed about  $\mathbf{a}$ ,  $\mathbf{b}$  and  $\mathbf{c}$ . This implies that the three cones intersect each other along a common line along  $\Delta\mathbf{k}$ . It is in fact a modified form of the Laue condition which can in practice be satisfied by using the x-ray beam with a wide range of wavelength and sweeping through crystal orientations. The condition getting fulfilled by sheer accident, however, cannot form the basis for any experiment. Laue's technique does make use of a continuous source of x-rays which simplifies the problem to a large extent. If the wavelength ranges from  $\lambda_1$  to  $\lambda_2$ , the reciprocal points that may be

searched will be in the region between the spheres of radii  $\mathbf{k}_1 \left(= \frac{2\pi}{\lambda_1} \hat{\mathbf{n}}\right)$  and  $\mathbf{k}_2 \left(= \frac{2\pi}{\lambda_2} \hat{\mathbf{n}}\right)$ ,

respectively. The larger the difference,  $(\lambda_1 - \lambda_2)$ , the larger the region into which the Ewald sphere expands.

A schematic illustration of the Laue's set-up or Laue camera is made in Fig. 3.17. A well-collimated beam of x-rays is obtained with the help of a pinhole arrangement. A typical range of the source wavelength is from 0.2 Å to 2 Å. There is no critical limitation on crystal dimensions. Two flat films are used; one to record the diffraction of reflected x-rays and the other to record the pattern produced by transmitted x-rays. The diffraction pattern is an array of spots as shown in Fig. 3.1 for a CdTe crystal.

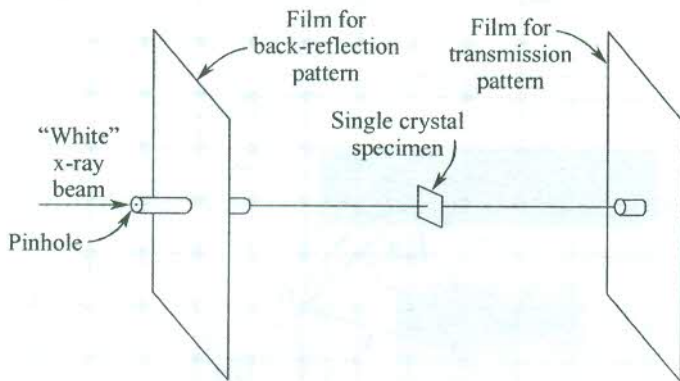


**FIG. 3.17** A Laue camera: the arrangement for recording a Laue photograph.

In practice, the Laue method is used to determine the orientation of a crystal whose structure is known. For example, if the direction of the incident beam coincides with a symmetry axis of the crystal, the recorded pattern is found to possess this symmetry. From the present status of the Laue technique we must not infer that the crystal structure cannot be deduced from the Laue photograph. This method is not used simply because it is tedious involving the complicated construction of several geometrical projections.

#### *The oscillation (rotation) method*

In this method monochromatic x-rays ( $\lambda$  kept at a constant value) are incident on a crystal rotating about an axis. The rotation of the crystal enables the variation of the angle of incidence with the Bragg plane. Whenever a set of  $\lambda$ ,  $\theta$  and  $d$  satisfies the Bragg condition (3.9), the corresponding Bragg peak appears. In a complete rotation some of the planes are repeated and thus overlapping of spots occurs. Therefore, the crystal is actually oscillated through a limited angular range to reduce overlapping. A crystal-rotating camera is shown in Fig. 3.18.

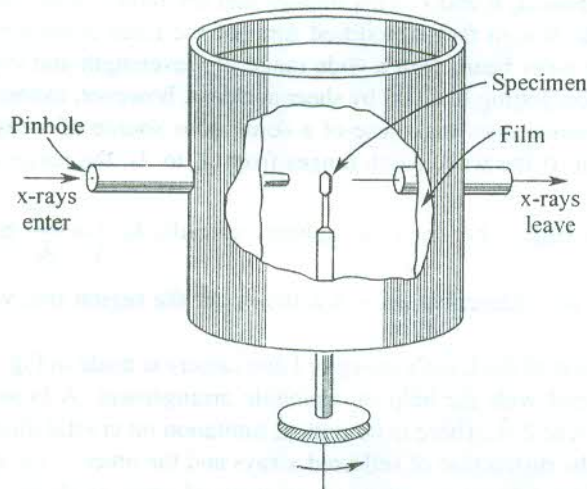


**FIG. 3.18** A camera used in the oscillation method.

The basis of diffraction spots on the film is excellently explained in the Ewald picture. On fixing the direction of the monochromatic x-ray (i.e.  $\mathbf{k}$ ), the location of the Ewald sphere in  $k$ -space gets fixed. The rotation of a crystal is equivalent to the rotation of the corresponding reciprocal lattice. So while the reciprocal lattice is under rotation, every reciprocal lattice point generates a circular path about the rotation axis. As soon as this circle intersects the fixed Ewald sphere, a diffraction peak occurs.

This method is in extensive use as it is relatively fast. But a noteworthy drawback in this method is that reflections corresponding to a three-dimensional lattice net are recorded on a two-dimensional photographic film, recording thereby a two-dimensional network of the reciprocal lattice. The problem is handled well in moving film methods. One such method, known as Weissenberg method, is almost the most used technique today. For details the reader is advised to consult Buerger's book.\*

### **The powder method**

This technique in principle provides for the variation of the axis of rotation over all possible orientations of a rotating crystal. This is practically achieved by using a powdered sample instead of a single piece of crystal. The powdered sample is filled in a glass capillary which is rotated about its length. Particles in the powder, though small, are yet substantially large on atomic scale and as such each of them can be treated as a tiny crystal. The capillary filled with the powdered sample serves as a collective unit of a large number of tiny crystals in all possible orientations. The rotation of this unit is equivalent to the rotations described in the beginning of this paragraph. The design of the Debye-Scherrer camera which is used in this method is explained in Fig. 3.19.

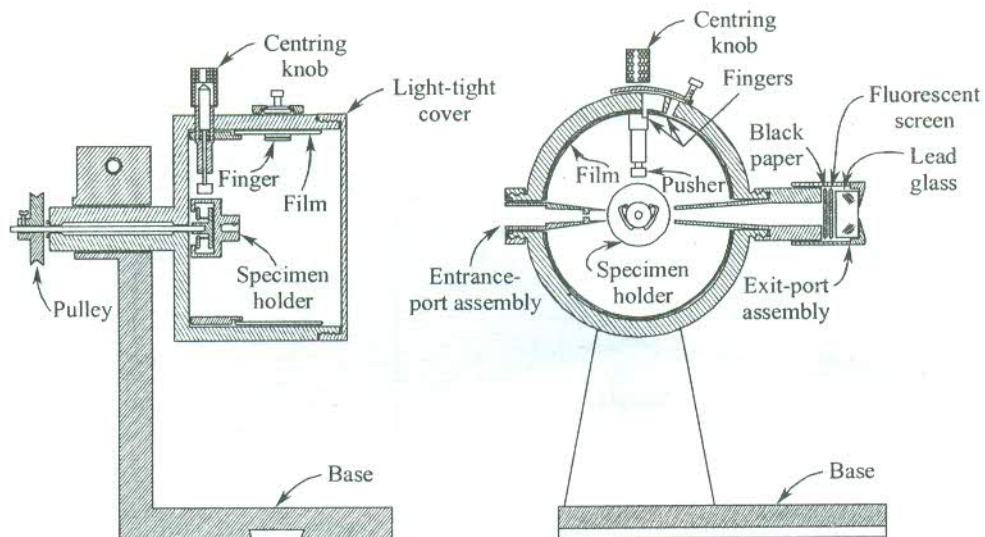


FIG. 3.19 Sectional views of a Debye-Scherrer camera used in the powder method.

This method is known to be the most fast and accurate for the determination of lattice constants. Its another important use is in the study of phase diagrams of alloy systems. Since lattice constants

\* M.J. Buerger, *X-Ray Crystallography*, John Wiley & Sons (1942).

are unique for a material, this method is widely used for the identification of materials. Further, it is the only method which works for all crystalline materials. In view of this fact we have chosen this technique for a complete description of its use for determining the lattice constants.

The nature of the diffraction pattern produced by the present technique can be visualized more easily in the Bragg formulation. For the interpretation involving Ewald construction, the reader is advised to consult the book by Ashcroft and Mermin.\*

As is evident from Fig. 3.20, the diffracted rays leave the sample along the generators of cones concentric with the incident beam. An angle of  $2\theta$  is formed between the generators and the direction of the incident beam where  $\theta$  denotes the usual Bragg angle given by

$$\sin \theta = \left( \frac{n\lambda}{2d_{hkl}} \right) \quad (3.48)$$

There exists one cone for each solution of the Bragg equation (3.48). In a perfect experimental set-up, the number of diffracted rays is enormously large and they outline the curved surface of the cone very densely. Figure 3.20 shows that these rays cut the photographic film in a continuous circle provided they are sufficiently dense. All such circles each of which corresponds to a certain Bragg plane are truncated by the edges of the film because of its limited width (see Fig. 3.21). The figure shows two sets of concentric rings with centres on the film coinciding with the entrance and exit

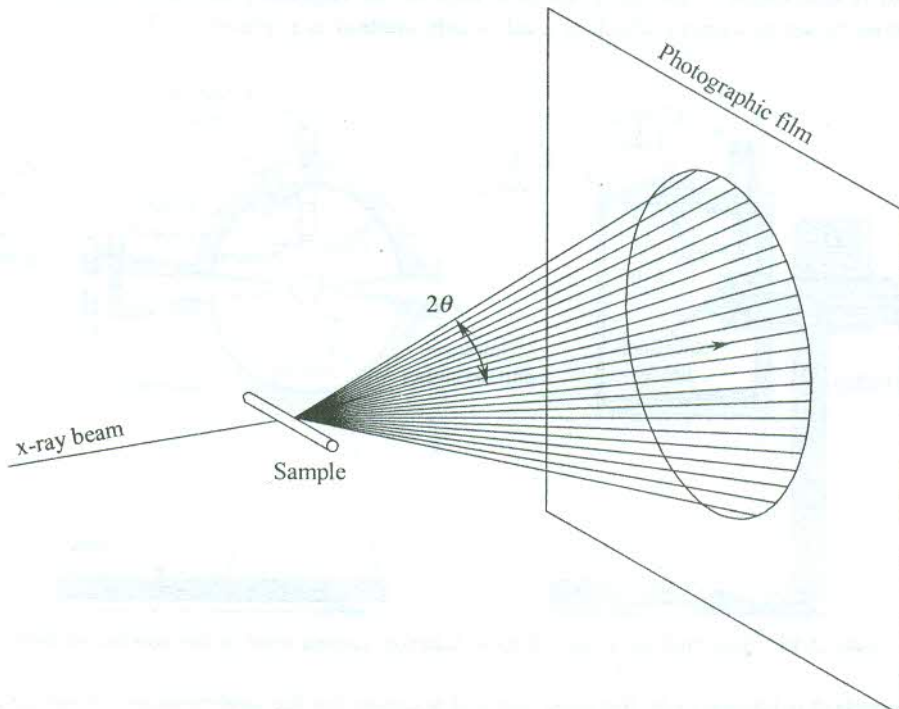


**FIG. 3.20** The diffracted rays lie on the curved surface of a cone. The photographic film intercepts the cone such that the axis of the cone is perpendicular to the plane of the film.

\* Ibid, pp. 102–104.

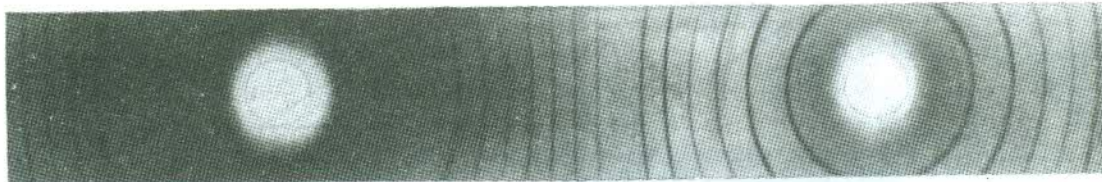


FIG. 3.21 Powder photograph of PbTe, cubic,  $a = 6.439 \text{ \AA}$ .

pinholes of the camera. The fainter set of rings represents back-reflections which occur for large values of  $\theta$ . If  $S$  is the diameter of a certain circle (Fig. 3.21), then using Fig. 3.20 the  $\theta$  for the respective diffraction line is expressed as

$$\theta(\text{radians}) = \frac{S}{4R} \quad (3.49)$$

where  $R$  is the radius of the camera. Using (3.48) and (3.49), the interplanar spacing  $d_{hkl}$  is calculated.

It is a matter of great significance to note that diffraction lines produced by back-reflections, though weak in intensity, yield more accurate results. On differentiating the Bragg equation (3.48) at constant wavelength (since monochromatic x-rays are used), we get

$$\frac{\Delta\theta}{\Delta d} = -\frac{\tan \theta}{d} \quad (3.50)$$

The relation (3.50) indicates that the change in  $\theta$  for a given change in  $d$  is the largest as  $\theta$  approaches  $90^\circ$ . Since reflections take place at  $2\theta$  from the direction of the incident beam, the highest sensitivity as defined by (3.50) refers to the back-reflections.

### 3.9 DETERMINATION OF LATTICE CONSTANTS

With knowledge of interplanar spacings ( $d_{hkl}$ ), lattice constants of a crystal can be determined using the mathematical relation valid for the symmetry of the crystal. The derivation of the relationship between the unit cell dimensions and the interplanar spacing when the edges of cells make general angles with one another is a difficult exercise. Relations for crystals with well-known symmetries can be found in standard books on crystallography. Given below is the treatment for crystal systems with orthogonal axes. A unit cell with orthogonal edges,  $a, b, c$ , is shown in Fig. 3.22. A family of parallel planes ( $hkl$ ) with a common interplanar spacing  $d_{hkl}$  intersects  $a, b, c$  axes into  $h, k, l$  parts, respectively. Supposing that the first plane of this family passes through the origin  $O$  and the next plane intersects the  $a, b, c$  axes at  $P, Q, R$ , respectively, and

$$OP = n_1a; \quad OQ = n_2b; \quad OR = n_3c \quad (3.51)$$

Then,

$$h = \frac{1}{n_1}; \quad k = \frac{1}{n_2}; \quad l = \frac{1}{n_3} \quad (3.52)$$

Therefore,

$$OP = \frac{a}{h}; \quad OQ = \frac{b}{k}; \quad OR = \frac{c}{l} \quad (3.53)$$

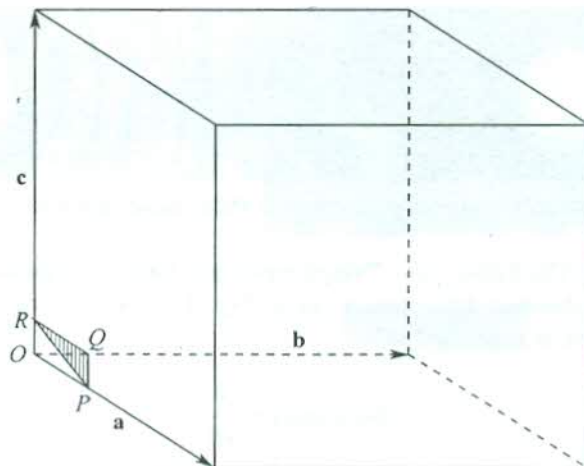


**FIG. 3.22** A plane  $PQR$  of the family of planes  $(hkl)$  in a crystal with orthogonal axes.

Figure 3.23 gives an enlarged geometry of the region of the first two planes of the family  $(hkl)$ . Let us perform a geometrical construction of drawing a plane perpendicular to the planes  $(hkl)$  such that it contains the  $c$ -axis. This plane intersects the planes  $(hkl)$  in the line  $RS$ , and the plane  $POQ$  in the line  $OS$ . The perpendicular  $OM$  dropped from  $O$  on the plane  $PQR$  obviously measures the interplanar spacing (i.e.  $OM = d_{hkl}$ ). The plane  $POQ$  is drawn separately in Fig. 3.24. It should be noted that  $OS$  is perpendicular to  $PQ$  and triangles  $POQ$  and  $PSO$  are similar. Therefore,

$$\frac{OP}{OS} = \frac{PQ}{OQ} \quad (3.54)$$

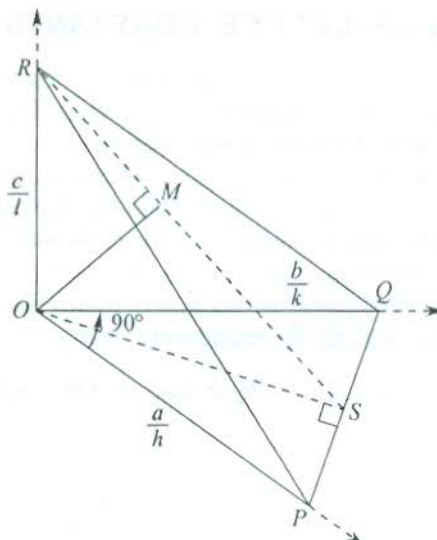


**FIG. 3.23** An enlarged view of the region of the plane  $PQR$ . It is assumed that the first member of the family of planes  $(hkl)$  passes through the origin ( $O$ ) and  $PQR$  is the second member of the family. The  $ROS$  represents an imaginary plane that is perpendicular to  $PQR$  and contains the  $c$ -axis. The perpendicular  $OM$  is equal to the interplanar spacing ( $d_{hkl}$ ).

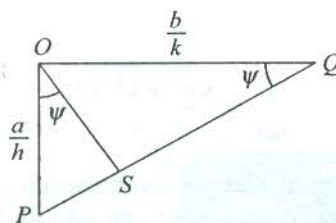


FIG. 3.24 The  $\Delta POQ$  is redrawn to show that  $\Delta s POQ$  and  $PSO$  are similar.

Placing the values of these lengths from (3.53), we have

$$\frac{1}{p^2} = \frac{h^2}{a^2} + \frac{k^2}{b^2} \quad (3.55)$$

where we have used  $OS = p$ .

Similarly, for the plane  $ROS$  shown in Fig. 3.25,  $OM$  is perpendicular to  $SR$ , and triangles  $SOR$  and  $SMO$  are similar. Hence,

$$\frac{OS}{OM} = \frac{SR}{OR} \quad (3.56)$$

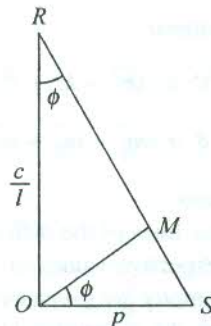


FIG. 3.25 The  $\Delta ROS$  is redrawn to show that  $\Delta s SOR$  and  $SMO$  are similar.

giving

$$\frac{1}{d_{hkl}} = \sqrt{\frac{1}{p^2} + \frac{l^2}{c^2}} \quad (3.57)$$

or

$$\frac{1}{d_{hkl}} = \sqrt{\frac{h^2}{a^2} + \frac{k^2}{b^2} + \frac{l^2}{c^2}} \quad [\text{using (3.55)}] \quad (3.58)$$

Equation (3.58) represents the relationship for an orthorhombic crystal.

For a tetragonal system ( $a = b \neq c$ ):

$$\frac{1}{d_{hkl}} = \sqrt{\frac{h^2 + k^2}{a^2} + \frac{l^2}{c^2}} \quad (3.59)$$

For a cubic system ( $a = b = c$ ):

$$\frac{1}{d_{hkl}} = \frac{\sqrt{h^2 + k^2 + l^2}}{a} \quad (3.60)$$

The simple form of (3.60) suggests that the determination of lattice constant of a cubic metal like copper can be one of the easiest exercises we can take up for learning the ideas discussed in this section.

### **Identification of cubic crystal structures**

We have now developed sufficient background to enable us to identify a cubic crystal structure from the analysis of its diffraction pattern.

Combining (3.60) with (3.9) for the first order of diffraction,

$$\sin \theta = \frac{\lambda}{2a} \sqrt{h^2 + k^2 + l^2}$$

or  $\sin^2 \theta = \frac{\lambda^2}{4a^2} (h^2 + k^2 + l^2)$  (3.61)

Therefore, for a certain diffraction pattern

$$\sin^2 \theta \propto (h^2 + k^2 + l^2)$$

or  $\sin^2 \theta \propto (m_1^2 + m_2^2 + m_3^2)$  (3.62)

where  $m_1$ ,  $m_2$  and  $m_3$  have a common factor.

One can measure  $\sin^2 \theta$  for the first few lines of the diffraction pattern. According to (3.62), their values must be in the same ratio as the respective values of  $(m_1^2 + m_2^2 + m_3^2)$ . The values of  $m_1$ ,  $m_2$  and  $m_3$  that are permitted for a crystal symmetry are given by the conditions for its non-zero structure factor derived in Section 3.7. In this way the symmetry of the crystal is determined.

### **SC crystal**

All possible values of  $m_1$ ,  $m_2$  and  $m_3$  allowed.

Ratio of  $\sin^2 \theta$  1 : 2 : 3 : 4 : 5 : 6 : 7 ...

### **BCC crystal**

$(m_1 + m_2 + m_3) =$  an odd integer, not allowed

$(m_1 + m_2 + m_3)$	Planes	$(m_1^2 + m_2^2 + m_3^2)$	$(\sin^2 \theta / \text{constant})$
2	(110)	2	1
	(200)	4	2
4	(112)	6	3
	(220)	8	4
6	(130)	10	5
	(222)	12	6
	(123)	14	7

**FCC crystal**

Values of  $m_1, m_2, m_3$  : all odd or all even integers, allowed

$(m_1 + m_2 + m_3)$	Planes	$(m_1^2 + m_2^2 + m_3^2)$	$(\sin^2 \theta/\text{constant})$
3	(111)	3	3
2	(200)	4	4
4	(220)	8	8
5	(131)	11	11
6	(222)	12	12
7	(133)	19	19

**Diamond structure**

$(m_1 + m_2 + m_3) = \text{an odd integer or twice an even integer, allowed}$

$(m_1 + m_2 + m_3) = \text{twice an odd integer, not allowed}$

$(m_1 + m_2 + m_3)$	Planes	$(m_1^2 + m_2^2 + m_3^2)$	$(\sin^2 \theta/\text{constant})$
3	(111)	3	3
4	(220)	8	8
5	(113)	11	11
4	(400)	16	16
7	(133)	19	19

### 3.10 SELECTION OF INCIDENT BEAM

The diffraction phenomenon exhibited by crystals was presumed all through our discussion to have been produced using the incident beam of x-rays. But in practice it is not always so. The main requirement on incident beam (according to the Bragg law) is that the wavelength of radiation should be of the order of interatomic separation in the crystal or less than that. The x-rays are electromagnetic waves. In de Broglie picture, every moving particle is treated as a wave with a finite wavelength. The wavelength of a particle can be manipulated by varying its energy or momentum ( $\lambda = h/p$ ), where  $p$  is the momentum. When this wavelength is of the order of a few Å, a beam of corresponding particles can be used to produce diffraction from crystals. Neutrons and electrons are two such particles whose beams have been widely used for the study of crystal structure. The purpose of this discussion is to emphasize that the use of one specific source for the study of a certain class of materials has an added advantage. We discuss below this aspect of compatibility with reference to x-rays, neutrons and electrons, separately.

#### X-rays

These are electromagnetic waves and their wavelength is expressed as  $\lambda = hc/\varepsilon$ , where  $\varepsilon$  is the photon energy. For  $\lambda$  to be of the order of a few angstrom units, the energy  $\varepsilon$  should be in the range from 10 to 50 keV which can be manipulated in an x-ray generator. The adjustment of wavelength of the outgoing beam is made by an appropriate choice of the target in the x-ray tube. For example,  $K_{\alpha 1}$

line from copper target is at  $1.541 \text{ \AA}$  and  $K_{\alpha 1}$  from molybdenum is at  $0.709 \text{ \AA}$ . The x-rays are the most commonly used source of radiation for all kinds of crystals. But all materials cannot be studied using a single target. For an accurate measurement, an appropriate target is selected on the basis of interatomic separation (guessed from rough data or some other measurement) in the crystal. Crystal monochromators are used to get discrete wavelengths.

### **Neutrons**

A neutron beam has a distinct advantage over x-rays in studying the structure of magnetic materials. Neutron itself has a magnetic moment and, therefore, its scattering pattern carries information about the magnetic moment (in both magnitude and direction) of constituent magnetic atoms of the crystal under study. This happens because of the interaction between neutron and atomic magnetic moments, the details of which form the subject matter of the chapters on magnetism. The size of the unit cell of magnetically ordered materials turns out to be very different when determined by using x-rays and neutrons, separately. The reason will be discussed while dealing with ordered magnetic materials.

In the light of the de Broglie hypothesis on wave nature of particles duly confirmed by Davisson and Germer experiments, we express the wavelength of a neutron as

$$\frac{h}{p} = \frac{h}{\sqrt{2M_n \epsilon}}$$

where  $M_n$  is the neutron mass ( $1.675 \times 10^{-27} \text{ kg}$ ) and  $\epsilon$  its energy.

It is simple to see that for  $\lambda = 1 \text{ \AA}$ ,

$$\epsilon \equiv 0.08 \text{ eV}$$

This value is of the order of energy of slow neutrons produced in a nuclear reactor. It indicates that the extra neutrons of a reactor may be used for doing the diffraction experiment. This is really the case; the neutron diffraction experiment is arranged around a nuclear reactor where all precautions are taken in the most strict sense on account of neutrons being a potent source of health hazard. Neutrons can be used for all materials as in non-magnetic materials they interact with the nuclei of constituent atoms.

### **Electrons**

The wave nature of particles was in fact established through experiments with electron beams. Thompson observed diffraction effects when he passed a narrow electron beam through crystalline films. Elastically scattered electrons have proved more suitable than x-rays for the study of surfaces because the penetrating power of electrons is limited by repulsion from electrons of the constituent atoms. Therefore, an electron beam is very frequently used to investigate the structure of thin crystals, layers, films, surfaces and gases in particular.

Substituting the electron mass ( $9.11 \times 10^{-31} \text{ kg}$ ) in the relation for de Broglie wavelength, we find that an electron beam of a few hundred electron volt energy has the appropriate wavelength for obtaining the desired diffraction pattern.

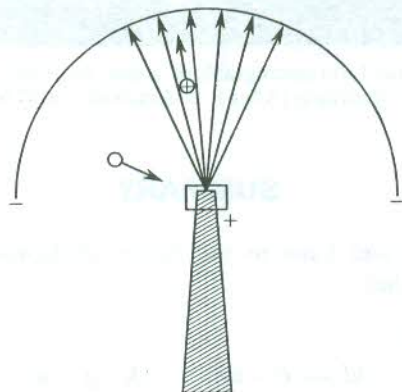
$$\text{For } \lambda = 1 \text{ \AA}, \quad \epsilon = 144 \text{ eV}$$

This energy is very low compared to that of an x-ray photon. It is for this reason that this method is called 'low-energy electron diffraction (LEED) technique'.

### 3.11 FIELD ION MICROSCOPY (FIM)

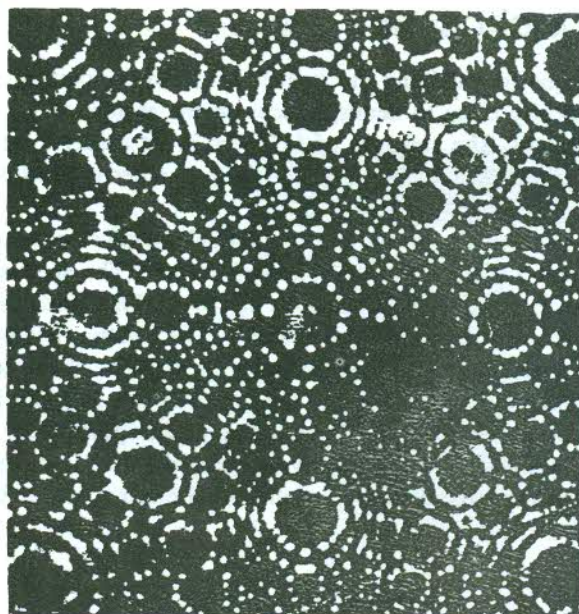
It is an excellent technique for studying the surface of a sharply-pointed specimen. The shape of the surface should be ideally close to hemispherical on the atomic scale, with radius of the order of a few thousand angstroms. The elegance of FIM lies in its ability to reveal the structure of the surface charge density in real space. The LEED, like any other diffraction method, provides this information in  $k$ -space.

Figure 3.26 gives the schematic representation of a field ion microscope. A large voltage is applied between the specimen and a plate with hemispherical surface. The specimen is given the positive polarity and the plate made to serve as the negative electrode. The whole assembly is evacuated and then neutral helium atoms are allowed into the chamber. The electric field polarizes the atoms which consequently acquire induced electric dipole moment. On account of the sustained interaction with the electric field, the helium atoms are swept to the region of the strongest field. When any of these atoms comes within a few atomic spacings above the tip of the specimen, it is ionized by the electric field which is strongest in this region. The positively charged helium ions feel the repulsion from the pointed surface and move along the directions of the radial electric field to be finally collected at the plate.



**FIG. 3.26** Schematic geometry of a field ion microscope. The radial arrows indicate the direction of the electric field. The specimen (hatched cone) is given a high positive potential and a plate (represented by the semicircle) serves as the negative electrode. The empty circle denotes a neutral helium atom and the circle marked with a plus sign represents an ionized helium atom.

The field strength is maintained at such a high value as to cause the ionization of helium atoms in the close vicinity of the specimen's surface. In this condition the angular distribution of helium ions collected at the plate can be correlated with the microscopic structure of the surface whose picture on the micrograph is magnified by the ratio of the radius of curvature of the plate to the radius of curvature of the tip of the specimen. The field ion micrograph shows the actual positions of individual atoms, in addition to reflecting the complete symmetry of a crystalline sample. One such micrograph of a gold tip is shown by Fig. 3.27.



**FIG. 3.27** The figure shows the field ion micrograph of a gold tip. Instead of helium atoms, Au atoms were used for imaging in this recording [After R.S. Averbach and D.N. Seidman, *Surface Science*, **40**, 249 (1973)].

## SUMMARY

1. Approaches of Bragg and Laue to the theory of diffraction produced by crystals are equivalent to one another.
  2. Forms of Bragg law are:
- $$2d \sin \theta = n\lambda; \quad 2\mathbf{k} \cdot \mathbf{g} = g^2$$
3. The reciprocal lattice point, representing a family of parallel planes with a common interplanar spacing, lies along the common normal of planes drawn from the origin in the reciprocal space.
  4. Primitive translation vectors  $\mathbf{a}$ ,  $\mathbf{b}$ ,  $\mathbf{c}$  of a crystal lattice are related to primitive translation vectors  $\mathbf{a}^*$ ,  $\mathbf{b}^*$ ,  $\mathbf{c}^*$  of its reciprocal lattice through

$$\mathbf{a}^* = 2\pi \frac{\mathbf{b} \times \mathbf{c}}{\mathbf{a} \cdot \mathbf{b} \times \mathbf{c}}; \quad \mathbf{b}^* = 2\pi \frac{\mathbf{c} \times \mathbf{a}}{\mathbf{a} \cdot \mathbf{b} \times \mathbf{c}}; \quad \mathbf{c}^* = 2\pi \frac{\mathbf{a} \times \mathbf{b}}{\mathbf{a} \cdot \mathbf{b} \times \mathbf{c}}$$

5. Each of the primitive translation vectors  $\mathbf{a}^*$ ,  $\mathbf{b}^*$ ,  $\mathbf{c}^*$  is orthogonal to two crystal axis vectors, stated as

$$\mathbf{i}^* \cdot \mathbf{j} = 2\pi\delta_{ij}$$

where  $\mathbf{i}, \mathbf{j} = \mathbf{a}, \mathbf{b}, \mathbf{c}$  and  $\delta_{ij}$  is the usual delta function.

6. The general form of a reciprocal lattice vector is

$$\mathbf{g} = m_1 \mathbf{a}^* + m_2 \mathbf{b}^* + m_3 \mathbf{c}^*$$

If  $m_1$ ,  $m_2$  and  $m_3$  have a common factor say  $n$ , then the Miller indices  $h$ ,  $k$ ,  $l$  of the family of planes represented by  $\mathbf{g}$  are

$$h = \frac{m_1}{n}; \quad k = \frac{m_2}{n}; \quad l = \frac{m_3}{n}$$

**7. Direct lattice**

SC	SC
BCC	FCC
FCC	BCC
Hexagonal	Hexagonal

**Corresp. reciprocal lattice**

**8. The Laue condition of diffraction can be written as**

$$\Delta\mathbf{k} = \mathbf{g}$$

The Laue equations can be expressed as

$$\begin{aligned}\mathbf{a} \cdot \Delta\mathbf{k} &= 2\pi m_1 \\ \mathbf{b} \cdot \Delta\mathbf{k} &= 2\pi m_2 \\ \mathbf{c} \cdot \Delta\mathbf{k} &= 2\pi m_3\end{aligned}$$

with  $\mathbf{g} = m_1\mathbf{a}^* + m_2\mathbf{b}^* + m_3\mathbf{c}^*$ .

**9. The structure factor for a crystal is**

$$S_{\mathbf{g}} = \sum_{j=1}^n f_j \exp(i\mathbf{g} \cdot \mathbf{r}_j)$$

with  $j$  running over all atoms in the primitive cell, and where  $f_j$  denotes the form factor of an atom whose position vector is  $\mathbf{r}_j$ .

**10. A general relation for crystals with orthogonal axes is**

$$\frac{1}{d_{hkl}} = \sqrt{\frac{h^2}{a^2} + \frac{k^2}{b^2} + \frac{l^2}{c^2}}$$

**11. Symmetry**

**Ratio of  $\sin^2\theta$**

SC	1 : 2 : 3 : 4 : 5 : 6 ...
BCC	1 : 2 : 3 : 4 : 5 : 6 ...
FCC	3 : 4 : 8 : 11 : 12 : 19 ...
Diamond	3 : 8 : 11 : 16 : 19 ...

## PROBLEMS

- 3.1 Calculate the energy carried by an e.m. wave of wavelength 1 Å (i) in eV and (ii) in kelvin. Explain why no Bragg diffraction is observed for visible light.
- 3.2 The Bragg angle for reflection from (111) planes in Al is 19.2° for an x-ray beam of wavelength 1.54 Å. Calculate (a) the lattice constant of Al and (b) the interplanar spacing for these planes.

- 3.3** A two-dimensional direct lattice is formed by repeating a parallelogram of size 4 cm  $\times$  3 cm. If one of the angles of the parallelogram be  $\pi/3$ , determine the primitive vectors of the reciprocal lattice.

- 3.4** Prove that the reciprocal lattice vector

$$\mathbf{g} = h\mathbf{a}^* + k\mathbf{b}^* + l\mathbf{c}^* \text{ is perpendicular to the plane } (hkl).$$

- 3.5** Calculate the angle between the reciprocal lattice vectors  $\mathbf{g}_{100}$  and  $\mathbf{g}_{111}$  of a simple cubic crystal. Find out the plane in the direct lattice to which  $(\mathbf{g}_{100} \times \mathbf{g}_{111})$  is perpendicular.

- 3.6** Show that for BCC structure with the basis of one atom, a scheme of assigning 1/8 of each corner atom at its respective cell coordinate location to the unit cell plus the body centre atom in the central position leads to the same result for the geometrical structure factor for this lattice as the relation (3.35b).

- 3.7** Derive a relation for the geometrical structure factor of a crystal with CsCl structure. Would you expect (100) reflections to be present in the diffraction pattern?

- 3.8** Find the geometrical structure factor for an FCC crystal of monatomic basis. Which of the following reflections, (100), (110), (111), (200), (220), (222), (211), (221) and (123) would be missing in the diffraction pattern?

- 3.9** Show that the structure factor for a monatomic HCP structure can have any of the six values

$f \left[ 1 + \exp\left(\frac{in\pi}{3}\right) \right]$  with  $n = 1, \dots, 6$  as the reciprocal lattice vector ranges through the points of the simple hexagonal reciprocal lattice.

- 3.10** Cuprous oxide has a cubic unit cell with oxygen atoms at the centre (0, 0, 0) and at the corners  $a(\pm 1, \pm 1, \pm 1)$ . The copper atoms are arranged in a tetrahedron around the central oxygen, at  $1/2a (1,1,1)$ ,  $1/2a (1,-1,-1)$ ,  $1/2a (-1,1,-1)$ , and  $1/2a (-1,-1,1)$ . Calculate the structure factor and show that some reflections are determined only by the copper, others only by the oxygen atoms.

- 3.11** Powder diffraction patterns of three monatomic cubic crystals with BCC, FCC and diamond structures are recorded using a Debye-Scherrer camera. The angles  $2\theta$  in degrees of the first four diffraction lines for the three samples marked as A, B, C are as under:

A	B	C
42.2	28.8	42.8
49.2	41.0	73.2
72.0	50.8	89.0
87.3	59.6	115.0

- (a) Determine the structure type of each sample.

- (b) What is the size of the cubic cell in each case?

Take the wavelength of incident x-rays as  $1.5 \text{ \AA}$ .

- 3.12** For a cubic crystal the diffraction line from the planes with  $(h^2 + k^2 + l^2) = 8$  is observed at the angle of diffraction  $10.23^\circ$ . If only one line is observed at an angle lower than this, what is the crystal structure? Assuming the wavelength of x-rays used as  $0.71 \text{ \AA}$ , calculate the lattice parameters.

- 3.13** The  $S$  values for the first three lines in the powder pattern of a cubic crystal are 34.88, 40.36 and 54.40 mm respectively. Given that the wavelength of x-rays used is 0.71 Å and the camera radius as 57.30 mm, find out the crystal structure and the lattice parameter.
- 3.14** Rock salt (sodium chloride) has lattice parameter of 5.63 Å. When the  $K_{\alpha 1}$  line from copper target ( $\lambda = 1.54$  Å) is used with a powder camera, what would be the first three  $S$  values? Take the camera diameter as 57.30 mm.

## SUGGESTED FURTHER READING

- Barrett, C.S. and T.B. Massalski, *Structure of Metals: Crystallographic Methods, Principles, Data*, 3rd ed. (McGraw-Hill, 1966).
- Buerger, M.J., *Contemporary Crystallography* (McGraw-Hill, 1970).
- Vainshtein, B.K., Modern Crystallography I, *Springer Ser. in Solid State Sci.*, Vol. 15 (Springer, 1981).

# Lattice Vibrations

The basis of crystal structures is often described in terms of ions for the interpretation of the properties of solids. The valence electrons are considered to have been placed in the force field of the lattice of ions. The word *ions* when used in this general way stands for ions in ionic crystals, ion cores in metals and covalent crystals, and atoms in a rare gas solid. The roles of ionic and electronic motions are crucial to the determination of the properties of solids. While some properties depend heavily on the electronic motion, several others are closely linked to the ionic dynamics. Lattice heat capacity, thermal expansion and hardness are some examples of properties that belong to the latter class. In the present chapter, a classical theory will be developed to describe small vibrations of atoms in crystalline solids in terms of normal modes (independent motions of characteristic frequency) of motion of constituent ions. In a normal mode all the ions move with well-defined amplitude and phase. A normal mode has the same amplitude in each cell, but varies from one unit cell to the other across the crystal like a wave with a certain wavevector. Such a wave is called *lattice wave* and the vibration\* with which it is associated is commonly known as *lattice vibration*.

The analysis of lattice vibrations is faced with the major difficulty of finding a way to treat the motion of ions that are heavy, separately from that of the light electrons. This is accomplished by working in the so-called ‘adiabatic approximation’ which in the context of molecules is famous as the ‘Born–Oppenheimer approximation’. We will realize in Chapter 6 that the significant electron velocity is the one at the Fermi level,  $v_F \approx 10^6 \text{ m s}^{-1}$ . On the other hand, the typical ionic velocities as derived from the analysis of vibration frequencies are found at the most of the order of  $10^3 \text{ m s}^{-1}$ . Therefore, no meaningful error can be introduced by assuming that the electrons remain in their ground state at any moment for the respective ionic configuration, because the ions move so slowly on the scale of velocities of relevance to electrons. This simplifies the calculation of the potential energy of ions, enabling us to write the equations of motion of ions that are crucial to the determination of the normal modes of vibration.

Our immediate concern is to develop the mathematical structure of a simple classical theory, that is, that of lattice vibrations. We approach the task on the basis of a mechanical model of crystals, which is described below.

## 4.1 THE ‘BALLS AND SPRINGS’ MODEL OF A HARMONIC CRYSTAL

We discussed all types of binding in Chapter 2 and observed that the equilibrium interionic separation in a crystal is determined by the balance between the attractive force (at large separations) and the repulsive force (at small separations). When thermal agitations displace ions from their equilibrium

\* Localized vibrations such as the internal oscillations of a  $\text{SO}_4^{2-}$  ion in a crystal do not produce a lattice wave.

positions, each of them experiences a net force in the form of a restoring force. This force tends to bring the ions back to their equilibrium positions and accounts for the elastic property of solids. In a simple mechanical model we visualize a crystal as a three-dimensional periodic array of balls each of which is connected to its neighbours by massless springs. The balls and the springs are, respectively, the representations for the ions and the coupling bonds of the real crystal. The force on an ion in the crystal is calculated by drawing an analogy between the crystal and its mechanical model. For small contractions or extensions of springs, the Hooke's law is applicable to the mechanical model. Accordingly, the force on an ion is supposed to be linearly proportional to the small contractions or extensions of its nearest-neighbour distances and not at all on the more remote neighbours. At first sight this model appears to do little justice to the quantum mechanical picture of coupling between ions. But experiments confirm that small displacements in most of the solids do conform to linear Hooke's law force dependence.

Each ion inside the crystal moves in a potential well of the force field of its neighbouring ions. For small displacements or small deviations from the equilibrium value of separation of ions, the potential energy curve is parabolic, as is evident from Fig. 2.1(a) drawn for a pair of ions. Since this form of potential energy is a well-known attribute of simple harmonic motion, the ionic motion involving small displacements may be treated as simple harmonic in nature. In this book, we shall conduct discussions on lattice vibrations only within the domain of the harmonic approximation. In fact, the harmonic approximation is the starting point for all theories of lattice dynamics. For completeness it must be remarked that the harmonic approximation is known to break down in some materials of which solid helium is the best example. In solid helium the displacement of an atom from its equilibrium position in a vibration may be as large as 40 per cent of the interatomic separation. Solid helium has established its identity as a quantum solid. Its vibrational properties are described by a sophisticated theory with quantum mechanical basis.

Some of the rough estimates made below demonstrate that the harmonic approximation is generally acceptable in solids.

When the separation of a pair of ions changes by  $\delta a$  from the equilibrium value  $a$ , the change in the potential energy of the ions is written as

$$\delta U = \frac{1}{2} f(\delta a)^2$$

where  $f$  is called the force constant or the spring constant associated with the massless spring joining the two ions viewed as the harmonic oscillators.

For  $\delta a = 0.1 \text{ \AA}$ , Fig. 2.1(a) gives the value of  $\delta U$  as 0.01 eV, yielding  $f = 32 \text{ N m}^{-1}$ . Using this value of  $f$  for a simple cubic crystal, we can readily deduce the macroscopic elastic modulus  $E$  for extension along one edge of the crystal. Thus we have

$$E = \frac{f(\delta a)/a^2}{(\delta a)/a} = \frac{f}{a} \simeq 10^{11} \text{ N m}^{-2} \quad (\text{for } a = 3 \text{ \AA})$$

This value of  $E$  is typically of the order of Young's modulus, identified alternatively as a stiffness constant. By ignoring the fact that an ion is coupled to several other ions, let us calculate the frequency of vibration of an ion attached to a spring whose other end is rigidly fixed. We find that the order of magnitude of frequency for  $f = 30 \text{ N m}^{-1}$  refers to the infrared region which indeed represents the region of vibration frequencies of solids.

Another important aspect is the propagation of long waves in solids. To these waves such as sound waves, a crystal behaves as an elastic continuum. It enables us to estimate the velocity  $v_s$  of these acoustic waves as

$$v_s = \sqrt{\frac{E}{\rho}} = a \left( \frac{f}{M} \right)^{1/2}$$

where  $\rho$  is the density,  $M/a^3$ , of a simple cubic crystal with  $M$  as the ionic mass.

The above relation gives  $v_s \approx 10^4 \text{ m s}^{-1}$ , which is a correct order of magnitude; most of the solids have  $v_s$  in the range  $1\text{--}10 \text{ km s}^{-1}$ . This calculation, though rough, also underlines the importance of stiffness constants in the continuum approach to wave propagation in solids. In a commonly employed technique\* for measuring stiffness constants, an ultrasonic pulse is sent through the crystal. The ultrasonic waves whose wavelength ( $\sim \mu\text{m}$ ) measures several thousand times the atomic spacing treat the crystal as a continuum.

## 4.2 NORMAL MODES OF A ONE-DIMENSIONAL MONATOMIC CHAIN

Let us consider the simplest crystal which can be a linear chain of  $N$  identical atoms (Fig. 4.1). This is equivalent to a linear chain of  $N$  primitive cells, with one atom in each of them. If we wish to describe the vibrations of the chain we are confronted with the problem of accounting appropriately the motion of ions in the middle and the motion of two ions at the ends. The broad feature of the motion may still be obtained by considering only the nearest neighbour interactions and ignoring the ends. The results of such a calculation are most acceptable when the number of atoms is large. If we denote the displacement of an ion at any moment from its site  $l$  in the static lattice by  $s_l$ , the effective potential energy of a chain of interionic separation,  $a$ , in the harmonic approximation is

$$U^{\text{eff}} = \sum_l \frac{1}{2} f(s_l - s_{l+a})^2 \quad (4.1)$$

where only the nearest neighbour interactions are included.

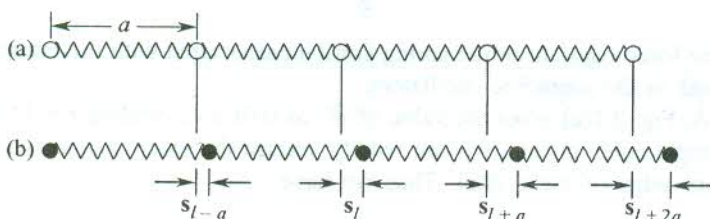


FIG. 4.1 The displacement of ions in a linear chain of identical ions connected by springs.

The restoring force on the ion situated in the static lattice at the site  $l$  can be expressed as

$$\begin{aligned} M\ddot{s}_l &= -f[(s_l - s_{l+a}) + (s_l - s_{l-a})] \\ &= -f(2s_l - s_{l+a} - s_{l-a}) \end{aligned} \quad (4.2)$$

\* R.F.S. Hearmon, *Rev. Mod. Phys.*, **18**, 409 (1946).

The preceding equation represents the equation of motion of a single ion in the chain. We expect from symmetry a normal mode solution in the form

$$s_l = s_0 \exp [i(\mathbf{k} \cdot \mathbf{l} - \omega t)] \quad (4.3)$$

which is a wave with wavevector  $\mathbf{k}$  varying as  $\exp(i\mathbf{k} \cdot \mathbf{x})$  along the line of ions (the  $\mathbf{x}$  direction) with amplitude  $s_0$ .

Substituting  $s_l$  from (4.3) in (4.2), we get

$$M\omega^2 = f[2 - \exp(ika) - \exp(-ika)]$$

or

$$\omega^2 = \frac{2f}{M} (1 - \cos ka) = \frac{f}{M} 4 \sin^2 \left( \frac{1}{2} ka \right)$$

which gives the angular frequency of oscillations as

$$\begin{aligned} \omega(k) &= 2 \sqrt{\frac{f}{M}} \left| \sin \left( \frac{1}{2} ka \right) \right| \\ &= \omega_m \left| \sin \left( \frac{1}{2} ka \right) \right| \end{aligned} \quad (4.4)$$

if the positive root is chosen.

$\omega_m$  is the frequency maximum  $\left( 2\sqrt{\frac{f}{M}} \right)$  observed at  $k = \pm \pi/a$ . It must be noted that  $l$  does not figure in (4.4), indicating that the equation of motion of every ion gives the same algebraic relation between  $\omega$  and  $k$ . This shows that the trial function  $s$  is indeed a solution of (4.2). Relation (4.4) is the required dispersion relation and the  $\omega$  versus  $k$  plot derived from this is known as the *dispersion curve*.

Another important observation is that we started with equations of  $N$  coupled harmonic oscillators (4.2), implying that if one ion starts vibrating it does not continue with constant amplitude, but transfers energy to others in a complicated way. Thus the vibrations of individual ions are not simple harmonic on account of this energy exchange. Our solutions, on the other hand, are uncoupled oscillations called normal modes. They represent independent non-interacting modes in harmonic approximation. Any pattern of displacement of the atoms can be written as a superposition of the normal modes just as any vector in three dimensions is a superposition of three independent (i.e., orthogonal) unit vectors along  $x$ ,  $y$  and  $z$  axes.

#### 4.2.1 The Periodic Boundary Condition

The dispersion relation (4.4) shows that  $\omega = 0$  at  $k = 0$  and  $\omega = \omega_m$  at  $k = \pm \pi/a$ . This indicates that all the normal mode frequencies lie in the range of  $k$ -values from  $-\pi/a$  to  $+\pi/a$ , defining the extent of the first Brillouin zone of a linear lattice as described in Chapter 3. The complete spectrum of normal modes is usually determined by invoking the periodic boundary condition, originally given by Born and von Karman for the electron gas. The condition requires the two ends of the crystal to be joined.

It is appreciated most easily in the case of the electronic conduction. The electrical conductivity depends on the details of electronic motion within the crystal. It implies as if an electron enters the crystal at one end as soon as it leaves the other end. The fact is equivalent to stating that the two ends of the crystal behave as being in contact. In the present case the ions at the ends of the linear chain are imagined to have been joined by an additional spring which is identical with those considered to couple the successive ions in the chain. The linear chain is thus transformed into a ring as shown in Fig. 4.2.

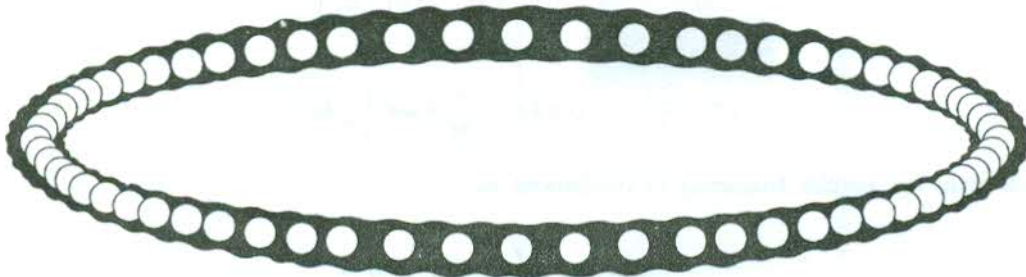


**FIG. 4.2** The Born-von Karman periodic boundary condition for a linear chain of  $N$  identical ions. If  $s_l$  denotes the magnitude of displacement of an ion at site  $l$ ,  $s_l = s_{l+Na}$ ;  $a$  is the interatomic spacing when the ions are at rest.

When we move away from a certain ion along the ring and take  $N$  steps, each of length  $a$  (the interatomic spacing), we are back to the same ion. Then, we require that

$$s_l = s_{l+Na} \quad (4.5)$$

where

$$l = pa, p \text{ being an integer}$$

$$Na = \text{the length of the chain } L.$$

Using the solution (4.3) in the condition given by (4.5), we have

$$\exp(ik \cdot Na) = 1 = \exp(i2\pi n) \quad (4.6)$$

or

$$\begin{aligned} k &= \frac{2\pi}{a} \cdot \frac{n}{N} \\ &= n \cdot \frac{2\pi}{L} \end{aligned} \quad (4.7)$$

where  $n$  is an integer.

So, the allowed values of  $k$  are given by

$$k = 0, \pm \frac{2\pi}{L}, \pm 2 \frac{2\pi}{L}, \dots \quad (4.8)$$

From (4.3) it is evident that if  $k$  changes by  $2\pi/a$  and or by its multiples, the solution remains unchanged. But such changes ( $2\pi n/a$ ) in  $k$  denote the reciprocal lattice vectors of the one-dimensional lattice under discussion. As such a root of frequency  $\omega$  corresponding to a certain  $k$ -value repeats

whenever the  $k$ -value is changed by a reciprocal lattice vector. This result forms one of the founding principles of the theory of solid state. The range of the first Brillouin zone is from  $-\pi/a$  to  $\pi/a$ , totalling  $2\pi/a$  in width. Therefore, for every  $k$ -value in the second, third or any other zone, there is a  $k$ -value in the first zone such that the vibration frequency for the two  $k$ -values is common. It happens so because the points of  $k$ -values in the set are connected by the reciprocal lattice vectors (see Fig. 4.3). This leads to a conclusion of great significance that all unique values of  $k$  that satisfy the solutions (4.3) lie within the first zone and we need not search for the  $k$ -values in other zones as they yield no new roots of  $\omega$ .

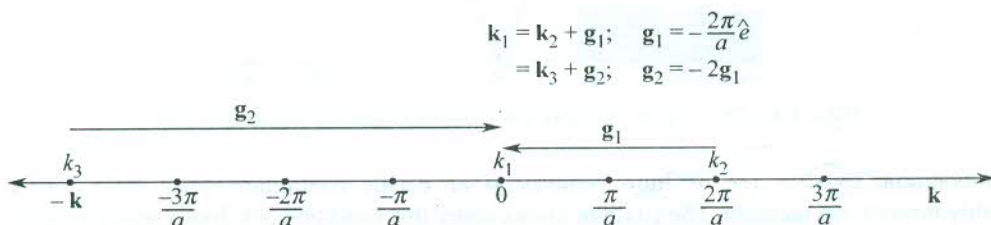


**FIG. 4.3** Brillouin zones of a one-dimensional crystal of lattice constant  $a$ . Wavevectors  $\mathbf{k}_2$  (extending to the second zone) and  $\mathbf{k}_3$  (extending to the third zone) are connected to wavevector  $\mathbf{k}_1$  (within the first zone) by reciprocal lattice vectors  $\mathbf{g}_1$  and  $\mathbf{g}_2$ , respectively. The form of the solution to the equation of motion is such as to yield the same value of vibration frequency for  $\mathbf{k}_1$ ,  $\mathbf{k}_2$  and  $\mathbf{k}_3$ . Thus all important  $\mathbf{k}$ -values (known as unique values) lie within the first zone.

Now, we are in a position to fix the last term in the set of the allowed  $k$ -values given by (4.8) and rewrite the set as

$$k = 0, \pm \frac{2\pi}{L}, \pm 2 \frac{2\pi}{L}, \dots, \frac{N}{2} \frac{2\pi}{L} \left( = \frac{\pi}{a} \right) \quad (4.9)$$

The last term coincides with the boundary  $\pi/a$  of the first Brioullin zone. The negative sign is dropped since  $-\pi/a$  is not independent on account of being connected to  $\pi/a$  by the shortest reciprocal lattice vector of magnitude  $2\pi/a$ . The total number of unique  $k$ -values in the allowed set is  $N$  and so will be the total number of normal modes.

#### 4.2.2 Salient Features of the Dispersion Curve

The dispersion relation (4.4) and the dispersion curve displayed in Fig. 4.4 show only the nearest neighbour interactions. In this spirit a monatomic linear chain may be considered to act as a low pass filter. The features of the dispersion curve are further revealing in the extreme limit of the wavevector  $\mathbf{k}$ . In the limit of small  $k$ -values, more often referred to as the long wavelength limit,  $\sin(ka/2)$  in relation (4.4) may be replaced with  $ka/2$  in the first approximation. The dispersion relation would then read as

$$\omega(k) = \sqrt{\frac{f}{M}} ka \quad (4.10)$$

From (4.10) we infer that the frequency varies linearly with the wavevector for small wavevectors. This behaviour is clearly evident in Fig. 4.4. The behaviour of elastic waves in continuum is of exactly similar nature. In the long wavelength limit of the waves where the wavelength is much larger than

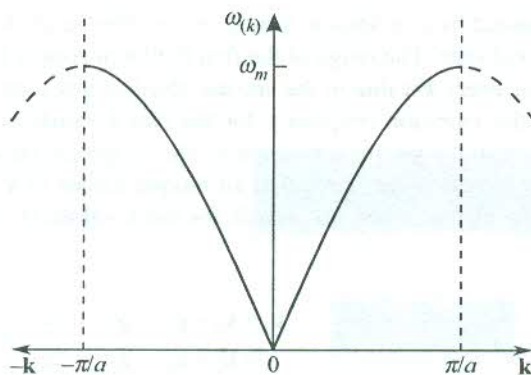


**FIG. 4.4** The dispersion curve for a one-dimensional monatomic chain.

the interatomic spacing, the medium behaves as an elastic continuum since these waves pass smoothly through the medium. The chain of atoms under this condition acts like a heavy elastic string.

In this limit the group velocity  $d\omega/dk$  and the phase velocity  $\omega/k$  of the elastic waves (or sound waves) are equal and both become independent of frequency. But as  $k$  changes to larger values, the discreteness of the medium begins to show up and at the zone boundary ( $k = \pm \pi/a$ ), the tangent to the dispersion curve is horizontal showing thereby that the group velocity is zero here. This refers to the total dispersion and no waves propagate through the crystal indicating that it acts as a discrete medium in this situation. This sounds perfectly logical as at  $k = \pm \pi/a$ , the wavelength is twice the interatomic spacing ( $\lambda = 2a$ ) for which the crystal cannot be treated as a continuous medium. The zero value of the group velocity also shows that the motions of the neighbouring atoms are out of phase and the elastic waves suffer Bragg reflection at this point in the  $k$ -space. This behaviour is consistent with the condition for Bragg reflection (discussed in Chapter 3) in a one-dimensional crystal. The elastic waves are no more the travelling waves defined by (4.3) and get transformed into standing waves at the zone boundary.

### 4.3 NORMAL MODES OF ONE-DIMENSIONAL DIATOMIC CHAIN

This chain is different from the earlier one in the sense that there are two different types of atoms whose positions alternate along its length (Fig. 4.5). The chain may be viewed as a one-dimensional crystal whose primitive cell contains two atoms of different masses  $M$  and  $m$ . The relevance of treating one-dimensional atomic chains as against the reality of crystals being three-dimensional may be questioned. But these calculations bring out a few broad features of the vibrations of real crystals,

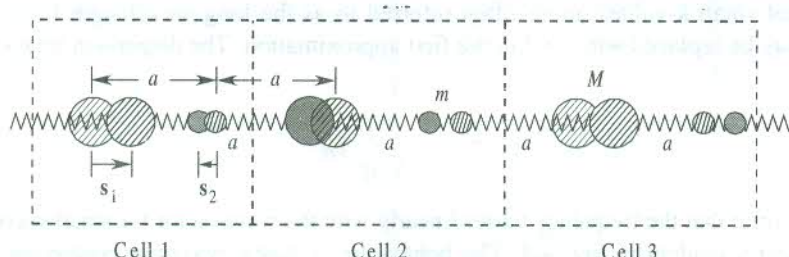


**FIG. 4.5** The displacement of ions in three consecutive unit cells of a one-dimensional diatomic crystal.

as seen in the earlier section. In other words, it suffices to acknowledge that these exercises introduce us to the basics of lattice dynamics using simple mathematics.

From Fig. 4.5 we see that the springs are identical. Therefore, if we consider only the nearest neighbour interactions, a single force constant (say,  $f$ ) will be involved in the equations of motion. Supposing that the heavy ion ( $M$ ) occupies the site 1 and the light one ( $m$ ) is at the site 2 in each primitive cell, we obtain the following equations of motion for these ions in that order:

$$M\ddot{s}_{1n} = -f(2s_{1n} - s_{2n} - s_{2,n-1}) \quad (4.11)$$

$$m\ddot{s}_{2n} = -f(2s_{2n} - s_{1n} - s_{1,n+1}) \quad (4.12)$$

where  $s_{1n}$  stands for the displacement of the ion at site 1 in the primitive cell  $n$ .

We seek the following solutions to the above equations:

and

$$\begin{aligned} s_{1n} &= u \exp [i(kna - \omega t)] \\ s_{2n} &= v \exp [i(kna - \omega t)] \end{aligned} \quad (4.13)$$

Substituting these solutions in (4.11) and (4.12), we have

$$\begin{aligned} (2f - M\omega^2)u - f[1 + \exp(-ika)]v &= 0 \\ -f[1 + \exp(ika)]u + (2f - m\omega^2)v &= 0 \end{aligned} \quad (4.14)$$

where  $u$  and  $v$  (the amplitudes) are unknowns in the above homogeneous equations. The equations have solutions only if the determinant of the coefficients of  $u$  and  $v$  in them vanishes. That is,

$$\begin{vmatrix} (2f - M\omega^2) & -f[1 + \exp(-ika)] \\ -f[1 + \exp(ika)] & (2f - m\omega^2) \end{vmatrix} = 0 \quad (4.15)$$

or

$$Mm\omega^4 - 2f(M+m)\omega^2 + 2f^2(1 - \cos ka) = 0 \quad (4.16)$$

Based on our experience with the monatomic lattice it is advisable to solve (4.16) for small  $k$  (i.e. long wavelength limit) and for the largest  $k$ , i.e. at the first zone boundary. These describe the distinct features of the dispersion curves.

For small values of  $k$ , we have

$$\cos ka = 1 - \frac{1}{2!} (ka)^2 + \dots$$

Retaining the first two terms of the series and putting this value of  $\cos ka$  in (4.16), we get the following two roots:

$$\omega^2 \cong 2f \left( \frac{1}{M} + \frac{1}{m} \right) \quad (4.17)$$

and

$$\omega^2 = \frac{\frac{1}{2}f}{M+m} k^2 a^2 \quad (4.18)$$

The dispersion curve obtained from (4.17) is called *optical branch* while the one from (4.18) is known as *acoustical branch*.

For the maximum value of  $k$ , i.e. at  $k = \pm \pi/a$ , the roots are

$$\omega^2 = \frac{2f}{m} \quad (\text{optical branch}) \quad (4.19)$$

and

$$\omega^2 = \frac{2f}{M} \quad (\text{acoustical branch}) \quad (4.20)$$

### 4.3.1 Salient Features of the Dispersion Curves

The most prominent feature of the dispersion curves shown in Fig. 4.6 is the manifestation of a frequency gap between the acoustical and optical branches. This brings out the fact that a diatomic linear chain acts as a band pass filter. It contrasts the behaviour of a monatomic linear chain which was shown to act as a low pass filter (see Section 4.2). Other features of the observed two branches representing two different types of normal modes are discussed below.

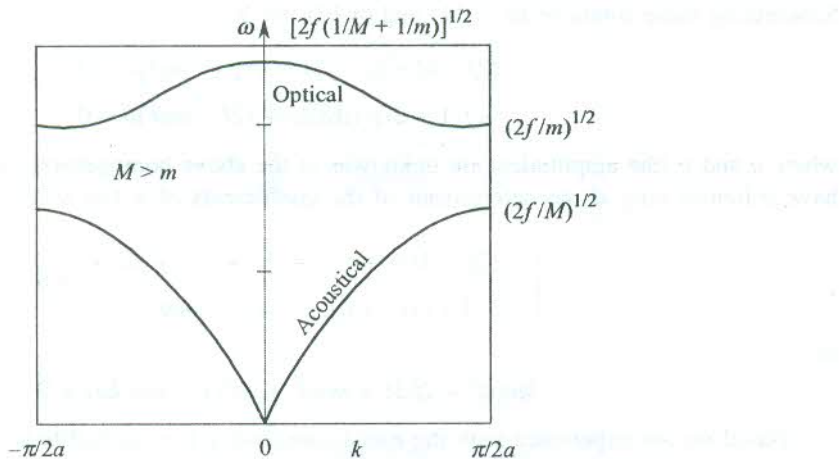


**FIG. 4.6** Optical and acoustical branches of dispersion curves for a one-dimensional diatomic crystal of lattice constant  $a$ . The frequency extrema for two branches are given.

The frequency of the optical branch is nearly constant in the limit  $k \rightarrow 0$  as made out by the approximate nature of (4.17). But it decreases slowly as  $k$  increases, dropping to the value  $2f/m$  at the zone boundary. The acoustic branch corresponds to the single branch, obtained for the linear chain of monatomic atoms of Section 4.2. The linear behaviour of  $\omega$  with  $k$  in the limit of small  $k$  (or long wavelength) is in the limit of sound waves which are longitudinal and treat the crystal as elastic continuum.

We may, further, exploit the above treatment to derive the state of ionic motions in the two branches, again for the same two limiting cases.

Substituting  $\omega^2$  from (4.17) in (4.14), at  $k = 0$ , we have for the optical branch,

$$\frac{u}{v} = -\frac{m}{M}$$

or

$$Mu = -mv \quad (4.21)$$

Relation (4.21) shows that the movements of the heavy and light ions are out of phase, i.e. they move towards each other or away from each other such that their centre of mass remains at rest. This refers to the situation in ionic crystals where such a motion of positive and negative ions may displace the centre of positive charges with the centre of negative charges creating an electric dipole. The oscillating electric dipole on interaction with the electromagnetic radiation may absorb the radiation. From a rough calculation we can find that the frequency of vibration of ionic crystals (e.g. NaCl, KBr, LiF etc.) lies in the infrared region. That is why ionic crystals are known to absorb infrared light. This forms the basis for giving the name *optical branch* to the branch under discussion. The relevance of treating a diatomic linear chain is thus amply justified. The results can be only instructive as we have allowed the linear chain to produce only longitudinal waves. In real crystals, there can be two transverse waves for each longitudinal wave. Generally, the frequencies of all the modes are different with the exception that the two transverse modes along directions of high symmetry in the crystal are degenerate (see Fig. 4.10). The longitudinal and transverse vibrational modes of a crystal can be clearly separated only in certain symmetry directions of crystals. The modes for any arbitrary direction are mixed in character.

For acoustical branch at  $k = 0$ , we obtain

$$\frac{u}{v} = \frac{m}{M} \quad (4.22)$$

which shows that the two ions move in phase.

The state of motions of the ions in the optical and acoustical branches is illustrated for a transverse wave in Fig. 4.7. The example of a transverse wave is chosen since the difference between the motions of ions in the two branches is more striking in appearance for the transverse motion. Though this motion is not allowed in the linear chain, it is present in all real crystals.

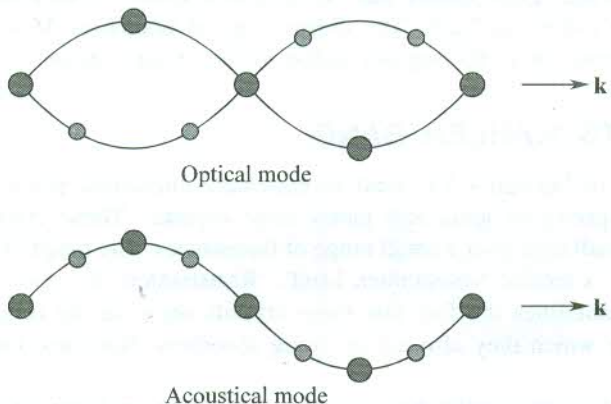


**FIG. 4.7** Illustration of the movement of ions in the transverse optical and acoustical modes at equal wavelength in a diatomic linear crystal.

The variation of the amplitude ratio  $u/v$  with the wavevector can be seen in Fig. 4.8. The state of motion at the zone end ( $k = \pm \pi/a$ , the maximum  $k$ ) can be interpreted with the help of this figure. The light ions are at rest in the acoustical mode while the heavy ions are at rest in the optical mode.

Another significant feature of the dispersion curves is that the gap at the zone end decreases with the decrease in the mass of heavy ion and approaches zero as  $M \rightarrow m$ . But it would surprise us to know that we have still two different branches though  $M = m$  which should give only the

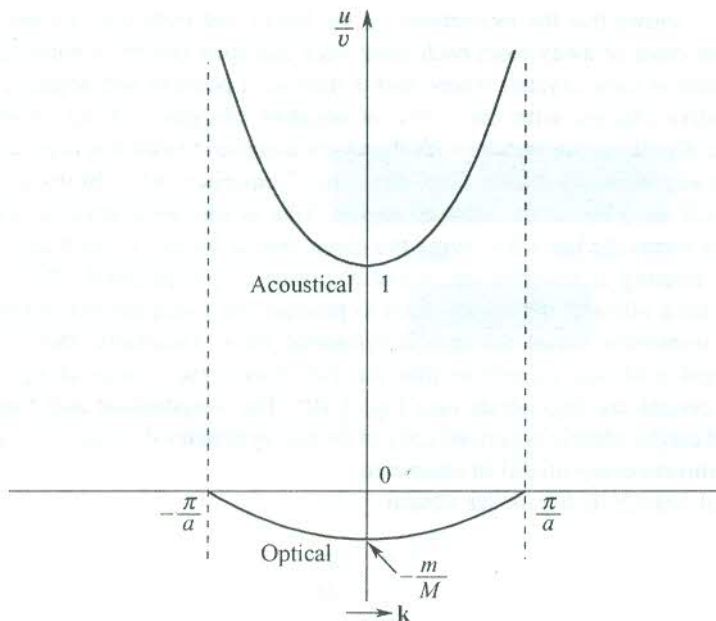


**FIG. 4.8** The amplitude ratio  $u/v$  as a function of the wavevector  $k$  for the acoustical branch (upper curve) and the optical branch (lower curve);  $u$  belongs to  $M$  and  $v$  to  $m$  ( $M > m$ ).

acoustical branch. For the present chain, if we have monatomic basis, we need to correct the size of the first zone which will now be double in size owing to the interionic spacing or the lattice constant being halved  $a/2$ . This ensures that the acoustical branch is continuous over whole region of the modified zone ( $-2\pi/a$  to  $2\pi/a$ ). The illusory optical branch of  $M = m$  in the original zone gets effectively reflected on to the regions added to the original zone.

#### 4.4 THE RESTSTRAHLEN BAND

We apply the theory of Section 4.3 to treat an extremely interesting phenomenon observed in the infrared absorption spectra of ionic and partly ionic crystals. These crystals show very intense reflection of infrared radiation over a small range of frequencies. The range of frequencies over which this reflection occurs is termed ‘reststrahlen band’. ‘Reststrahlen’ is a German word which means residual rays. This underlines the fact that these crystals show strong reflection to a radiation of certain frequency, for which they also act as strong absorbers. NaCl and GaAs are good examples of such crystals.

It was mentioned a little earlier how an optical mode in an ionic crystal is excited when an electromagnetic radiation is incident on its surface. The transverse electric field of the radiation does the trick by exerting force on cations and anions in opposite directions. The strong absorption (resonance) takes place when the frequency of radiation matches the frequency of a transverse optical mode of the crystal. A proper explanation to the reststrahlen phenomenon follows from the theory of optical constants to be discussed in Chapter 10. According to this theory, when

$$\omega_T < \omega < \left( \frac{\epsilon_s}{\epsilon_\infty} \right)^{1/2} \omega_T \quad (4.23)$$

no wave can propagate through the crystals.

Here  $\omega_T$  is the frequency of a transverse optical mode,  $\omega$  the frequency of the incident radiation and  $\epsilon_s$  and  $\epsilon_\infty$  are the static dielectric constant and the dielectric constant at high frequencies respectively. In the above condition we have an evanescent wave that decays exponentially with the increasing distance in the crystal. Therefore, in the specified range of frequencies the radiation incident on the crystal from outside suffers total external reflection. This is what we know as the reststrahlen phenomenon. The range of frequencies over which this occurs is called the *reststrahlen band*.

Now we make an estimate of  $\omega_0$ , the frequency at which the strong absorption occurs using equations of motion set up in Section 4.3 for a diatomic lattice. This also gives the measure of the reststrahlen frequency which is the same as  $\omega_0$ . For NaCl crystal, the lattice constant  $a$  is equal to 5.63 Å. With  $\lambda = 2a$ , we get the maximum cut-off wavevector  $k_m = 2\pi/\lambda \approx 10^{10} \text{ m}^{-1}$ . The wavevector associated with a typical infrared radiation of wavelength 10,000 Å is about  $10^6 \text{ m}^{-1}$ . Therefore, the vibration with these relatively small wavevectors in the optical branch can be determined in the limit  $k \rightarrow 0$ . In this limit, relations (4.14) reduce to

$$\begin{aligned}-M\omega^2 u &= 2f(v - u) \\ -m\omega^2 v &= -2f(v - u)\end{aligned}\quad (4.24)$$

Relations (4.24) essentially give the force on masses  $M$  and  $m$ , respectively. When an electromagnetic radiation with the transverse electric field  $E = E_0 \exp(i\omega t)$  is incident, these force terms get corrected by  $\mp eE_0$ . Then relations (4.24) reduce to

$$\begin{aligned}-M\omega^2 u &= 2f(v - u) - eE_0 \\ -m\omega^2 v &= -2f(v - u) + eE_0\end{aligned}\quad (4.25)$$

Relations (4.25) give the two amplitudes of vibration as

$$u = \frac{-\frac{eE_0}{M}}{\omega_0^2 - \omega^2} \quad (4.26)$$

$$v = \frac{\frac{eE_0}{m}}{\omega_0^2 - \omega^2}$$

with

$$\omega_0^2 = 2f\left(\frac{1}{M} + \frac{1}{m}\right) \quad (4.27)$$

Though relations (4.26) indicate a single frequency at which the maximum absorption should occur, experiments show that there is a small range of frequencies of the electromagnetic radiation showing the reststrahlen phenomenon. This small range of frequencies forms the reststrahlen band. The frequency  $\omega_0$  is referred to as the *reststrahlen frequency*.

## 4.5 GENERAL THEORY OF HARMONIC APPROXIMATION

Consider a primitive cell as shown in Fig. 4.9. Let us use  $n$  to index the primitive cells with  $\mathbf{n} = (n_1, n_2, n_3)$ , where  $n_1, n_2$  and  $n_3$  form a triplet of integers that mark the cells along the primitive

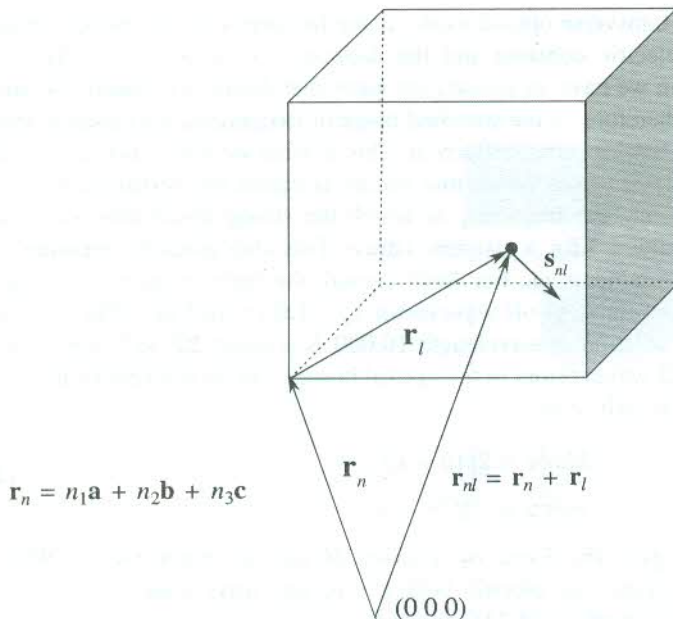


**FIG. 4.9** The picture explains the relationship between the position vectors ( $\mathbf{r}_{nl}$  and  $\mathbf{r}_l$ ) of an atom at site  $l$  within the  $n$ th unit cell as measured from the origin  $(0, 0, 0)$  fixed at a lattice point and from a corner of the unit cell  $\mathbf{n} = (n_1, n_2, n_3)$  respectively.  $\mathbf{s}_{nl}$  denotes the displacement vector of the atom from its equilibrium position.

axes. We measure the position vector of an ion within a cell from one of its corners, identified as the origin of the cell. Thus the position vector of an ion at site  $l$  within the cell  $\mathbf{n}$  may be given by

$$\mathbf{r}_{nl} = \mathbf{r}_n + \mathbf{r}_l$$

where

$$\mathbf{r}_n = n_1 \mathbf{a} + n_2 \mathbf{b} + n_3 \mathbf{c} \quad (4.28)$$

Assume that the average position of the ion at site  $l$  is still given by  $\mathbf{r}_l$  when the ion vibrates. Thus the symmetry of the Bravais lattice is supposed to remain unchanged in a vibrating crystal. Further, it is assumed that the displacement or deviation ( $\mathbf{s}_{ln}$ ) of the ion from its equilibrium position is much small in comparison with the interionic distance.

Small values of the atomic displacements allow us to expand the total potential energy about its equilibrium value in a Taylor's series. This makes the exercise of obtaining the equation of motion quite straightforward, which is otherwise extremely tedious.

The kinetic energy  $T$  of the crystal can be written as

$$T = \sum_{ln} \frac{1}{2} M_l |\dot{\mathbf{s}}_{ln}|^2 \quad (4.29)$$

where  $M_l$  is the mass of the ion at site  $l$  and  $n$  stands for the unit cell running through all the unit cells.

And the potential energy  $U$  is defined by its Taylor's expansion as

$$U = U_0 + \sum_{lnj} \mathbf{s}_{lnj} \left( \frac{\partial U}{\partial s_{lnj}} \right)_0 + \frac{1}{2} \sum_{ll', nn', jj'} \mathbf{s}_{lnj} \mathbf{s}_{l'n'j'} \left[ \frac{\partial^2 U}{\partial s_{lnj} \cdot \partial s_{l'n'j'}} \right]_0 + \dots \quad (4.30)$$

where index  $j$  denotes the three Cartesian  $x, y, z$  components.

The first term  $U_0$  refers to the potential energy at equilibrium which is a constant. It can be dropped from the expression as it is the changes in potential energy from  $U_0$  that determine the vibration spectrum of a crystal. The coefficient of  $s_{lnj}$  in the linear term is equal to the magnitude of the net force on the ion at site  $l$  exerted by all the other ions when each of the ions is at its equilibrium position. At equilibrium, this force vanishes and so should the linear term. The terms of higher orders beyond the third term are not considered in the harmonic approximation. Therefore, the lone non-vanishing third term in the expansion expresses the effective potential energy of the crystal in the harmonic approximation. That is,

$$U^{\text{eff}} = \frac{1}{2} \sum_{ll', nn', jj'} \mathbf{s}_{lnj} \mathbf{s}_{l'n'j'} \left( \frac{\partial^2 U}{\partial s_{lnj} \cdot \partial s_{l'n'j'}} \right)_0 \quad (4.31)$$

We combine (4.29) and (4.31) to write the usual Lagrange's equation from the equations of motion for the Cartesian components obtained in the form

$$M_l \ddot{\mathbf{s}}_{lnj} = - \sum_{l', n', j'} \left( \frac{\partial^2 U}{\partial s_{lnj} \cdot \partial s_{l'n'j'}} \right) \mathbf{s}_{l'n'j'} \quad (4.32)$$

Relation (4.32) represents the  $j$ th component (which could be the  $x$ -,  $y$ - or  $z$ -component) of the net force on the ion at site  $l$  in the unit cell  $n$  owing to the rest of the atoms in the crystal. This equation marks the beginning of all theories of lattice dynamics.

In view of the elastic nature of crystals, the coupling between any two atoms is customarily represented in the material form of a spring. Each spring in a crystal is assigned a constant, whose value is characteristic of the nature of the ions being coupled. In classical mechanics, this constant is called by the name *spring constant* or *force constant*.

A comparison of (4.32) with the equation of motion of a particle executing simple harmonic motion shows that the derivatives in (4.32) serve as force constants in these equations of motion. For convenience, we will use from now onwards a shorter notation for these derivatives given by

$$\left( \frac{\partial^2 U}{\partial s_{lnj} \cdot \partial s_{l'n'j'}} \right) = U_{lnj}^{l'n'j'} \quad (4.33)$$

The equation of motion (4.32) then reads as

$$M_l \ddot{\mathbf{s}}_{lnj} = - \sum_{l'n'j'} U_{lnj}^{l'n'j'} \mathbf{s}_{l'n'j'} \quad (4.34)$$

Equation (4.34) is the general equation of motion for ions in crystals. It is to be observed that the equations of motion for the linear chains of monatomic basis (4.2) and diatomic basis [(4.11) and

(4.12)] are only the special cases of this equation with  $U_{lnj}^{l'n'j'}$  having the dimensions of force constants. They denote the generalized force constants of a system with many degrees of freedom. The isotropy of space, the translational invariance and the point group symmetry require the coupling constants to satisfy certain conditions.

It must be noted that each term within the summation in (4.32) denotes a force that depends on the relative position of unit cells  $n$  and  $n'$  and not on their absolute position. It is the consequence of the translation invariance which effectively requires that

$$U_{lnj}^{l'n'j'} = U_{loj}^{l'(n'-n)j'} \quad (4.35)$$

We have, now, come to grips with the basic workable technique of solving the equations of motion in crystals.

## 4.6 NORMAL MODES OF REAL CRYSTALS

This exercise concerns real crystals which are three-dimensional and in general may have a polyatomic basis having atoms of different elements. The problem is most general and, therefore, the task of finding its solution is bound to be tedious. But, in principle, the solution is tractable. We give below the procedure for calculating the frequencies of normal modes in the framework of a theory based on the harmonic approximation.

The equation of motion of an ion, whose site in the unit cell  $n$  is denoted by the position vector  $\mathbf{r}_n$ , is given by (4.34). If the crystal is composed of  $N$  unit cells with  $p$  atoms in a unit cell, we get in total  $3pN$  equations analogous to (4.34). It is proper to write the solutions or the displacement  $\mathbf{s}_{lnj}$  in terms of a plane wave with respect to the cell coordinates. That is,

$$\mathbf{s}_{lnj} = \frac{1}{\sqrt{M_l}} \mathbf{u}_{lj}(\mathbf{k}) \exp[i(\mathbf{k} \cdot \mathbf{r}_n - \omega t)] \quad (4.36)$$

This plane wave is defined only at the lattice sites, unlike a normal plane wave.

Using this solution for (4.34), we have

$$-\omega^2 \mathbf{u}_{lj}(\mathbf{k}) + \sum_{l'j'} \sum_{n'} \frac{1}{\sqrt{M_l M_{l'}}} U_{lnj}^{l'n'j'} \exp[i(\mathbf{k} \cdot (\mathbf{r}_{n'} - \mathbf{r}_n))] \cdot \mathbf{u}_{l'j'}(\mathbf{k}) = 0 \quad (4.37)$$

Let us write (4.37) as

$$-\omega^2 \mathbf{u}_{lj}(\mathbf{k}) + \sum_{l'j'} D_{lj}^{l'j'}(\mathbf{k}) \mathbf{u}_{l'j'}(\mathbf{k}) = 0 \quad (4.38)$$

where

$$D_{lj}^{l'j'}(\mathbf{k}) = \sum_{n'} \frac{1}{\sqrt{M_l M_{l'}}} U_{lnj}^{l'n'j'} \exp[i(\mathbf{k} \cdot (\mathbf{r}_{n'} - \mathbf{r}_n))] \quad (4.39)$$

According to (4.35), the terms in the sum of the above equations depend only on the difference  $(n' - n)$  and not on the absolute values of  $n$  and  $n'$ . The quantity  $D_{lj}^{l'j'}(\mathbf{k})$ , which is obtained by summing over  $n'$ , is independent of  $n$ . It is instructive to note that it couples amplitudes with each

other without having to depend on  $n$ . This also explains why the amplitudes in (4.13) appear without index  $n$ . A very common term in lattice dynamics known as the *dynamical matrix* is formed by the quantities defined by (4.39). The set of equations (4.38) belongs to a set of linear homogeneous set of order  $3p$ . The set of linear homogeneous equations has a solution only if the

$$\text{determinant: } \{ D_{lj}^{l'j'}(\mathbf{k}) - \omega^2 \} \text{ vanishes.} \quad (4.40)$$

The above equation gives  $3p$  different solutions, i.e. for one value of  $\mathbf{k}$  there are  $3p$  values of  $\omega$ , each of which lies on a separate branch. A branch is characterized by its dispersion relation. Thus, there are in total  $3p$  branches out of which three are acoustical—one longitudinal (LA) and two transverse (TA). The number of acoustical branches is three in all crystals as it does not depend on the number of atoms. The rest ( $3p - 3$ ) belong to the optical branches;  $(p - 1)$  longitudinal (LO) and  $2(p - 1)$  transverse (TO). Since there are  $N$  (the number of unit cells) unique values of  $\mathbf{k}$  for each branch, the total number of vibrational modes comes to  $3pN$ .

A complete description of the normal modes of a crystal requires the knowledge of directions along which the ions move for a certain value of  $\mathbf{k}$ . These directions are known as the directions of *polarization*. In an isotropic crystal one mode will have ions moving in the direction of  $\mathbf{k}$ . This determines the longitudinal branch. The two transverse branches are degenerate. We can choose any two orthogonal directions in a plane perpendicular to  $\mathbf{k}$  that represent the polarization of the two independent transverse modes. The picture in anisotropic crystals is not so straightforward. We can describe the dispersion curves of these crystals in terms of longitudinal and transverse branches, only if  $\mathbf{k}$  lies along any  $n$ -fold axis of rotation permitted by the crystal symmetry. In such a case the longitudinal mode is polarized along  $\mathbf{k}$ , and transverse modes, that are degenerate, along directions perpendicular to  $\mathbf{k}$ .

It can now well be imagined that the picture of dispersion curves for crystals with polyatomic basis will be fairly complex. We take a relatively simple example of diamond whose primitive cell has two identical atoms. The dispersion curves plotted from the experimental data\* are shown in Fig. 4.10 and refer to the propagation of waves along two important directions [100] and [111]. The wavevector is expressed as a dimensionless quantity,  $q = k(2\pi/a)$ , called the reduced wavevector as measured from the centre of the Brillouin zone. In principle, there should be six branches in total. But we observe only four, as the transverse modes along [100] and [111] directions are degenerate in the acoustical and the optical branches, separately. The other important point exhibited by the curves is that the LA and LO modes at the zone boundary are degenerate. This confirms the zero gap between the acoustical and the optical branches at this point as derived in Section 4.3 for the linear chain of a diatomic lattice composed of identical atoms.

## 4.7 QUANTIZATION OF LATTICE VIBRATIONS

The energy of lattice waves is quantized the same way as that of the electromagnetic waves. In a harmonic crystal, the atomic oscillators are treated analogous to the Planck's radiation oscillators. The energy of a vibrational mode of angular frequency  $\omega$  with wavevector  $\mathbf{k}$  in the branch  $s$  is expressed

as  $\left( n_{ks} + \frac{1}{2} \right) \hbar\omega_s(\mathbf{k})$ , where  $n_{ks}$  is an integer denoting the excitation number or the order of the

\* J.L. Warren, R.G. Wenzel and J.L. Yarnell, *Inelastic Scattering of Neutrons* (Vienna, International Atomic Energy Agency, 1965).

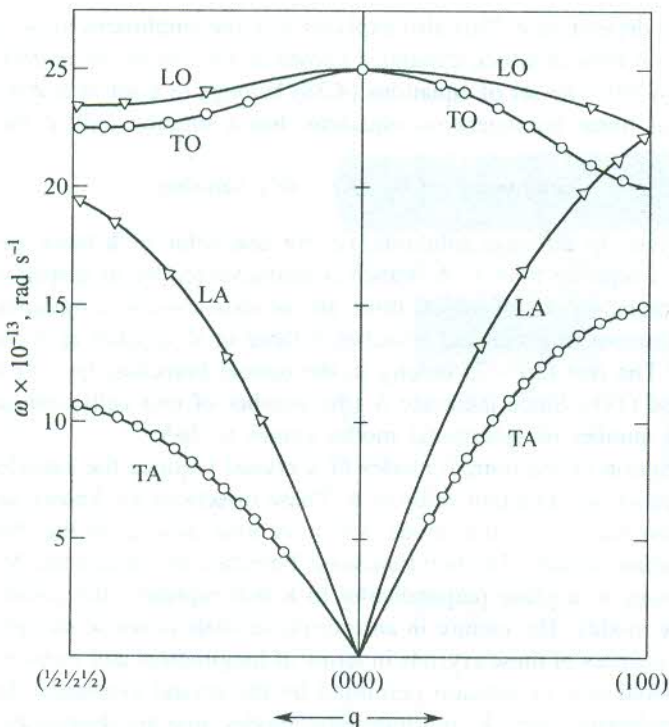


**FIG. 4.10** Dispersion curve for diamond crystal (after J.L. Warren, R.G. Wenzel and J.L. Yarnell, *Inelastic Scattering of Neutrons* (Vienna, International Atomic Energy Agency, 1965).

excitation state of the classical normal mode. The fact of the normal mode being in its  $n_{ks}$  excited state is expressed in the language of quantum theory by saying that there are  $n_{ks}$  phonons of wavevector  $\mathbf{k}$  in branch  $s$ . The usage of the term *phonon* is analogous to the term *photon* for the electromagnetic radiation. Phonon is the corpuscular representation for a quantum of vibration of energy  $\hbar\omega_s(\mathbf{k})$  carried by a sound wave in the same way as photon represents a quantum of radiation in an electromagnetic wave. The  $n_{ks}$  is also defined as the phonon occupancy expressed by the Planck's distribution function which is a function of  $\omega_s(\mathbf{k})$  and  $\mathbf{k}$ .

The thermal energy of a harmonic crystal is given by

$$E = \sum_{\mathbf{k}s} \left( n_{ks} + \frac{1}{2} \right) \hbar\omega_s(\mathbf{k}) \quad (4.41)$$

Relation (4.41) shows that the energy of an oscillator is not zero even in the lowest vibration state ( $n = 0$ ) and has a value  $\frac{1}{2} \hbar\omega_s(\mathbf{k})$ . It indicates that even the lowest state is not vibrationless. This is known as zero point motion and finds its interpretation only with the use of quantum mechanics. The quantity  $\frac{1}{2} \hbar\omega_s(\mathbf{k})$  is called the *zero point energy*.

We must appreciate that phonon is the particle name of a quantized lattice vibration. In this nomenclature, the vibration spectra of crystals are frequently addressed as the phonon spectra. In

the quantum picture, its momentum is expressed as  $\hbar\mathbf{k}$ . The phonon momentum is often required for the description of several physical properties of solids.

## 4.8 MEASUREMENT OF PHONON DISPERSION BY INELASTIC NEUTRON SCATTERING

The experiments performed to obtain the phonon dispersion curves are based on the exchange of energy between lattice vibrations and a probe. In principle, x-rays or thermal neutrons can be used as the probe in these experiments. The energy of thermal neutrons is  $\sim 0.025$  eV, which is of the order of their average thermal energy ( $k_B T$ ) at room temperature. Because of small energy, neutrons show an appreciable change in their energy on being scattered while exchanging the energy of a vibrational quantum. This change in energy is easily measurable on the respective energy scale. On the other hand, the energy of x-rays is much high ( $\sim$  keV). The energy change for such an energetic photon is only 1 part in  $10^6$  which is difficult to measure on the scale of the photon energy. On account of this reason, thermal neutrons, also known as slow neutrons, are preferred for the measurement of phonon spectra. The assembly of apparatus used for this purpose is called a triple-axis spectrometer. Its schematic diagram is shown in Fig. 4.11. The experiment is generally performed around a nuclear reactor which acts as the source of thermal neutrons. The term *slow neutrons* used for these neutrons is only relative on the energy scale as the typical order of their velocity is  $10^5 \text{ cm s}^{-1}$ , which is large compared to the motion of material objects in our daily life.

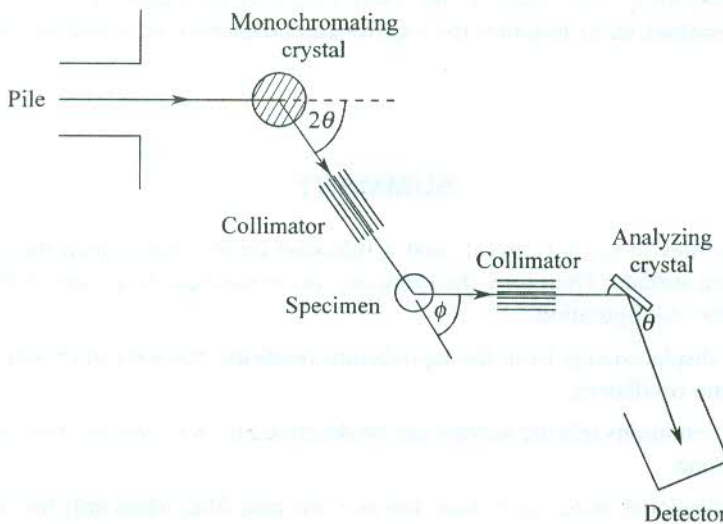


**FIG. 4.11** Outlines of the experimental set-up for measuring phonon spectra using a triple-axis neutron spectrometer.

The information from the inelastically scattered neutrons is extracted mainly by exploiting the consequences of the momentum and the energy conservation laws. If a neutron of a wavevector  $\mathbf{K}$  is scattered to a state of  $\mathbf{K}'$  and a phonon of wavevector  $\mathbf{k}_s$  is created or destroyed in the process, the momentum conservation requires that

$$\mathbf{K} - \mathbf{K}' = \pm \mathbf{k}_s + \mathbf{g} \quad (4.42)$$

where (+) and (-) signs refer respectively to the creation and destruction of a phonon of energy  $\hbar\omega_s(\mathbf{k})$ . The symbol  $s$  stands for the branch.

The reciprocal lattice vector  $\mathbf{g}$  appears for the reason that phonons are plane waves that are modified for a crystalline medium on the ground of its periodic character. The value of  $\mathbf{k}_s$  in (4.42) lies within the first Brillouin zone.

According to the principle of energy conservation,

$$\frac{\hbar^2 \mathbf{K}^2}{2 m_n} = \frac{\hbar^2 \mathbf{K}'^2}{2 m_n} + \hbar\omega_s(\mathbf{k}) \quad (4.43)$$

where  $m_n$  is the neutron mass.

The monochromator crystal which rotates about the first axis of the triple axis spectrometer fixes the energy and direction of the incident neutron beam and hence the value of  $\mathbf{K}$ . The second axis is used to rotate the crystal. This rotates the reciprocal lattice relative to  $\mathbf{K}$ . For each position of the crystal, the energy of the scattered neutron is obtained by rotating the analyzer crystal about the third axis. The analyzer crystal then gives the direction and magnitude of  $\mathbf{K}'$ . If we take the origin of the reciprocal lattice and draw two vectors  $\mathbf{K}$  and  $\mathbf{K}'$ , the difference  $(\mathbf{K} - \mathbf{K}')$  gives the wavevector of the phonon responsible for the scattering. But this vector may lie outside the first Brillouin zone. By convention we take the phonon wavevector to be within the first Brillouin zone. Hence, we add a reciprocal lattice vector  $\mathbf{g}$  to the phonon wavevector  $\mathbf{k}_s$  to get it in the first Brillouin zone (4.42). The difference in the incoming and scattered neutron energies gives  $\hbar\omega$ , where  $\omega$  is the frequency of phonon of wavevector  $\mathbf{k}_s$ . This leads to the determination of the dispersion. An elegant treatment of the theory that enables us to interpret the experimental data may be found in the book authored by David Pines\*.

## SUMMARY

1. Ionic velocities in crystals are at least a thousand times smaller than the electron velocity at the Fermi surface. Therefore, the electrons can be assumed to remain in their ground state for an ionic configuration.
2. For small displacements from the equilibrium positions, the ions in crystals may be treated as harmonic oscillators.
3. All lattice vibrations (elastic waves) can be described by wavevectors that lie within the first Brillouin zone.
4. A one-dimensional monatomic chain acts as a low-pass filter when only the nearest neighbour interactions are considered.
5. A one-dimensional diatomic chain acts as a band-pass filter by virtue of a frequency gap occurring between the acoustical and optical branches.

\* David Pines, *Elementary Excitations in Solids* (Benjamin, 1963).

6. The reststrahlen frequency for an ionic crystal containing ions of masses  $M$  and  $m$  is

$$\omega_0^2 = 2f \left( \frac{1}{M} + \frac{1}{m} \right)$$

where  $f$  denotes the force constant.

7. For a crystal with  $p$  atoms in the primitive cell:

$$\begin{aligned}\text{Number of acoustical branches} &= 3(\text{independent of } p) \\ &= 1(\text{LA}) + 2(\text{TA})\end{aligned}$$

$$\begin{aligned}\text{Number of optical branches} &= 3(p - 1) \\ &= (p - 1) \dots (\text{LO}) + 2(p - 1) \dots (\text{TO})\end{aligned}$$

8. A quantized crystal vibration or the quantum unit of a crystal vibration is called a *phonon*. Its energy is given by  $\hbar\omega$ , where  $\omega$  is the angular frequency of a crystal vibration.

9. The thermal energy of a harmonic crystal is given by

$$E = \sum_{ks} \left( n_{ks} + \frac{1}{2} \right) \hbar\omega_s(\mathbf{k})$$

where  $n_{ks}$  denotes the number of phonons with frequency  $\omega$  and wavevector  $\mathbf{k}$  in the branch  $s$ ; and  $\frac{1}{2}\hbar\omega_s(\mathbf{k})$  is the zero point energy.

10. When in a crystal a neutron of wavevector  $\mathbf{K}$  is inelastically scattered to a state of wavevector  $\mathbf{K}'$  and a phonon of wavevector  $\mathbf{k}_s$  is created or destroyed in the process, the momentum conservation requires that

$$\mathbf{K} - \mathbf{K}' = \pm \mathbf{k}_s + \mathbf{g}$$

where (+) and (-) signs refer respectively to the creation and destruction of a phonon of energy  $\hbar\omega_s(\mathbf{k})$ ; and  $\mathbf{g}$  is a reciprocal lattice vector.

## PROBLEMS

- 4.1 Localized vibrations in a crystal can be represented by a superposition of phonon modes with different wavevectors. Show that the centre of gravity of such a wave packet moves with the group velocity

$$\mathbf{v}_g = \frac{d\omega}{d\mathbf{k}}$$

- 4.2 In a linear monatomic chain of four atoms, the end atoms are fixed. Considering only the nearest neighbour interaction and assuming that the force between any two atoms is proportional to their relative displacement, set up the equations of motion for longitudinal vibrations of the free atoms. Show that the frequencies of the two normal modes are related as

$$\omega_1^2 = 3\omega_2^2$$

- 4.3 Calculate the minimum wavelength of a wave travelling along the (i) [100] direction, (ii) [111] direction in an FCC crystal. Take the lattice constant as 4.08 Å.
- 4.4 Show that the total momentum of the vibrating linear chain considered in Section 4.2 is given by

$$\mathbf{p}(\mathbf{k}) = -i\omega M s_0 \exp(-i\omega t) \sum_{n=1}^N \exp(ikna)$$

and hence that with periodic boundary conditions  $s_{N+n} = s_n$ ,  $\mathbf{p}(\mathbf{k}) \equiv 0$  for  $\mathbf{k} \neq 0$ , i.e. a phonon carries no momentum. For  $\mathbf{k} = 0$ ,  $\mathbf{p}(\mathbf{k}) \neq 0$  if  $\lim_{\omega \rightarrow 0} (\omega s_0) \neq 0$ , describe the motion of the linear chain.

- 4.5 In a linear chain of alternate atoms having mass  $m_1$  and  $m_2$ , suppose that only nearest neighbours interact.

- (a) Show that the dispersion relation for the normal mode is

$$\omega^2 = \frac{f}{m_1 m_2} (m_1 + m_2 \pm \sqrt{m_1^2 + m_2^2 + 2m_1 m_2 \cos ka})$$

- (b) Discuss the nature of the normal modes and the form of the dispersion relation if  $m_1 \gg m_2$ .
- (c) How does the dispersion relation compare with that of the monatomic chain when  $m_1 \simeq m_2$ ?

- 4.6 In a linear chain all the atoms have equal mass but are connected alternatively by springs of force constants,  $f_1$  and  $f_2$ . Derive the frequency–wavevector relation for this chain. Are there still two branches? Explain.

- 4.7 In Problem 4.6, if  $\omega_1$ ,  $\omega_2$  and  $\omega_3$  are, respectively, the maximum frequency of the acoustic branch and minimum and maximum frequencies of the optical branch, show that for  $f_1 > f_2$ ,

$$\omega_1 = \sqrt{\frac{2f_2}{M}}, \quad \omega_2 = \sqrt{\frac{2f_1}{M}} \quad \text{and} \quad \omega_3 = \sqrt{\frac{2(f_1 + f_2)}{M}}$$

- 4.8 The lattice constant of NaCl is 5.6 Å and its Young's modulus in the [100] direction is  $5 \times 10^{10}$  N m<sup>-2</sup>. Calculate the wavelength at which the e.m. radiation is strongly reflected from a NaCl crystal. State the assumptions under which your calculation is valid. Take the atomic weights of Na and Cl as 23 and 37 respectively.

(Hint: Young's modulus =  $f/a$ ).

- 4.9 Consider a longitudinal wave

$$s_n = s_0 \cos(\omega t - nka)$$

which propagates in a monatomic linear lattice of atoms of mass  $M$ , spacing  $a$  and the force constant  $f$ .

- (a) Show that the total energy of the wave is

$$\varepsilon = \frac{1}{2} M \sum_n \left( \frac{ds_n}{dt} \right)^2 + \frac{1}{2} f \sum_n (\mathbf{s}_n - \mathbf{s}_{n+1})^2$$

where  $n$  runs over all atoms.

- (b) By substituting  $\mathbf{s}_n$  in this expression and using the dispersion relation (4.4), show that the time-average total energy per atom is

$$\frac{1}{4} M \omega^2 s_0^2 + \frac{1}{2} f(1 - \cos ka) s_0^2 = \frac{1}{2} M \omega^2 s_0^2$$

## SUGGESTED FURTHER READING

- Ashcroft, N.W. and N.D. Mermin, *Solid State Physics* (Saunders College, 1988).  
 Bottger, H., *Principles of the Theory of Lattice Dynamics* (Physik Verlag, 1983).  
 Ghatak, A.K. and L.S. Kothari, *An Introduction to Lattice Dynamics* (Addison-Wesley, 1972).  
 Maradudin, A.A., E.W. Montroll, G.H. Weiss, and I.P. Ipatova, *Theory of Lattice Dynamics in the Harmonic Approximation*, 2nd ed. (Academic Press, 1971).  
 Ziman, J.M., *Principles of the Theory of Solids* (Cambridge, 1972).

# Thermal Properties of Solids

In this chapter we discuss the contribution of lattice vibrations to the thermal properties of solids. For our convenience, we classify the properties into two groups:

- Properties whose broad features can be explained in the harmonic approximation.
- Properties whose broad features cannot be explained without considering the anharmonic effects.

From group 1 we choose ‘heat capacity’ and from group 2, ‘thermal conductivity’ and ‘thermal expansion’ for a proper treatment of the thermal properties of solids.

## 5.1 CLASSICAL LATTICE HEAT CAPACITY

The major contribution to the heat capacity of solids comes from lattice vibrations. In non-magnetic insulators, lattice vibrations are the only contributors. Other contributions come from conduction electrons in metals and the ordering in magnetic materials. In this chapter, as already stated, we deal with lattice vibrations only.

In classical theory, the energy of a solid can be expressed as

$$\varepsilon = \varepsilon_s + \varepsilon_v \quad (5.1)$$

where

$\varepsilon_s$  is the energy of the static lattice

$\varepsilon_v$  is the vibration energy of the solid.

The classical equipartition energy of vibration of an atom is  $k_B T$  at temperature  $T$ ,  $k_B$  being the Boltzmann constant. This gives the total vibrational energy  $3Nk_B T$  if there are  $N$  atoms in the solid. Substituting this in (5.1), we get

$$\varepsilon = \varepsilon_s + 3Nk_B T \quad (5.2)$$

At  $T = 0$ ,  $\varepsilon = \varepsilon_s$  which does not include zero point energy, as in classical physics there is no concept of zero point motion. The heat capacity is defined as (the value at constant volume)

$$C_V = \left( \frac{\partial \varepsilon}{\partial T} \right)_V \quad (5.3)$$

Using (5.2), we obtain

$$C_V = 3Nk_B \quad (5.4)$$

The experimentally measured value of heat capacity is referred to as the heat capacity at constant pressure  $C_p$ . But for a harmonic solid  $C_V = C_p$ , since the difference between the two is known to depend on the square of the temperature coefficient of linear expansion which is zero for a harmonic crystal. It will be shown later that the expansion of solids occurs because of the anharmonic motion of atoms.

The equation for heat capacity as given by (5.4) was originally derived by Dulong and Petit in the year 1869. This is now known as the Dulong–Petit law. According to this law, heat capacity is constant for a solid and independent of temperature. The measured value of heat capacity approaches this value at high temperatures and remains almost constant thereafter in the solid state (Fig. 5.1). This is how Dulong and Petit explained the behaviour of solids at high temperatures. The Dulong–Petit law, however, fails to explain the variation of heat capacity with temperature. Most significantly, the heat capacity drops to zero as the temperature approaches 0 K. But by no means the limited success of the Dulong–Petit law can be considered a mean achievement because the behaviour it fails to account for is explained only with the use of quantum theory which came much later.

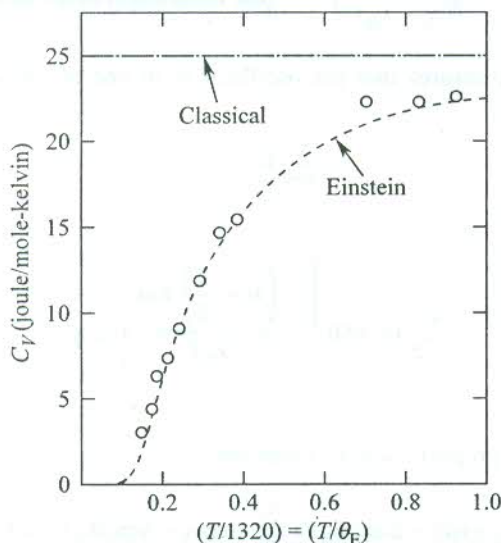


FIG. 5.1 A comparison of the experimental curve (represented by the circles) with the Einstein's theoretical curve (dotted) for molar heat capacity of diamond with  $\theta_E = 1320$  K. The horizontal dotted line gives the classical Dulong–Petit value. [After A. Einstein, *Ann. Physik*, 22, 180 (1907).]

## 5.2 QUANTUM THEORY OF LATTICE HEAT CAPACITY

In this section we build up the structure for calculating lattice heat capacity capitalizing on the principles of quantum theory. Since lattice vibrations are pictured as quantized in this theory, the term phonon heat capacity sounds more appropriate than the conventional term. The calculation of phonon heat capacity is concerned mainly with the evaluation of the average thermal energy, which in turn requires the knowledge of the vibration spectrum of the solid under study. Since we have decided to work within the harmonic approximation, our first attempt would be to calculate the average thermal energy of a harmonic oscillator and then see how to proceed further.

### 5.2.1 Average Thermal Energy of a Harmonic Oscillator

The energy levels of a quantum harmonic oscillator as already defined in Chapter 4 are given by

$$\varepsilon_n = \left( n + \frac{1}{2} \right) \hbar\omega \quad (5.5)$$

where  $\omega$  is the angular frequency of the oscillator and other indices are ignored. The average thermal energy of the oscillator  $\varepsilon$  in thermal equilibrium at temperature  $T$  is written as

$$\varepsilon = \sum_n p_n \varepsilon_n \quad (5.6)$$

where  $p_n$  represents the probability of finding the oscillator in the energy level  $\varepsilon_n$ . It is given by

$$p_n \propto \exp \left( -\frac{\varepsilon_n}{k_B T} \right) \quad (\text{the Boltzmann distribution}) \quad (5.7)$$

The proportionality constant ensures that the oscillator is in one of allowed levels. Therefore,

$$\sum_{n=0}^{\infty} p_n = 1 \quad (5.8)$$

or

$$\sum_{n=0}^{\infty} p_0 \exp \left[ -\frac{\left( n + \frac{1}{2} \right) \hbar\omega}{k_B T} \right] = 1$$

where  $p_0$  is the constant of proportionality. Therefore,

$$p_0 \exp(-\hbar\omega/2k_B T) \sum_{n=0}^{\infty} \exp(-\hbar\omega n/k_B T) = 1$$

or

$$p_0 = \exp \left( \frac{\hbar\omega}{2k_B T} \right) \cdot \left( 1 - \exp \left( -\frac{\hbar\omega}{k_B T} \right) \right) \quad (5.9)$$

Therefore,

$$p_n = \exp(-n\hbar\omega/k_B T) (1 - \exp(-\hbar\omega/k_B T)) \quad (5.10)$$

Substituting  $p_n$  from (5.10) in (5.6), we get

$$\varepsilon(\omega, T) = [1 - \exp(-\hbar\omega/k_B T)] \hbar\omega \sum_{n=0}^{\infty} \left( n + \frac{1}{2} \right) \exp(-\hbar\omega n/k_B T)$$

Putting  $\exp(-\hbar\omega/k_B T) = x$ , we obtain

$$\begin{aligned}\varepsilon(\omega, T) &= (1-x)\hbar\omega \left[ \sum_{n=0}^{\infty} (nx^n) + \frac{1}{2(1-x)} \right] \\ &= \frac{1}{2}\hbar\omega + (1-x)\hbar\omega \sum_{n=0}^{\infty} nx^n\end{aligned}\quad (5.11)$$

Since

$$\sum_{n=0}^{\infty} x^n = \frac{1}{1-x} \quad (5.12)$$

on differentiating (5.12) and then multiplying both sides by  $x$ , we get

$$\sum_{n=0}^{\infty} nx^n = \frac{x}{(1-x)^2} \quad (5.13)$$

From (5.13) and (5.11), we have

$$\varepsilon(\omega, T) = \left( \frac{1}{2} + \frac{1}{\exp(\hbar\omega/k_B T) - 1} \right) \hbar\omega \quad (5.14)$$

or

$$\varepsilon(\omega, T) = \left( \langle n \rangle + \frac{1}{2} \right) \hbar\omega \quad (5.15)$$

where

$$\langle n \rangle = \frac{1}{\exp(\hbar\omega/k_B T) - 1} \quad (5.16)$$

The comparison of (5.15) with (4.41) shows that  $\langle n \rangle$  must denote the phonon occupancy, also known as the Planck's distribution function obtained by Planck for the radiation oscillators. The above exercise is a simple demonstration of the fact that lattice vibrations are quantized the same way as the radiation oscillators.  $\langle n \rangle$  stands for the occupancy of phonons in the energy level  $\varepsilon_n$  which is also interpreted as the expected number of phonons in the energy state  $\varepsilon_n$  of an oscillator in thermal equilibrium at temperature  $T$ .

The calculation of total thermal energy of a solid is, however, not straightforward. Practically, it is done by making use of dispersion curves which provide the valuable information on the number of modes per unit frequency interval. The term giving this information is known as the density of states. It is a concept of central importance in solid state physics as it is concerned with the theory of several forms of excitations. We deliberately postpone for a while the proper treatment of the density of states to discuss a model in which the total thermal energy is obtained by an alternative method based on some extreme assumption. The oversimplification of the theory surprisingly does not prove to be of any serious consequence as the results of the calculation explain most of the qualitative features of phonon heat capacity. This model, proposed by Einstein, serves as a landmark in the progress of theory of phonon heat capacity.

### 5.2.2 Einstein Model

Einstein assumed that all the atoms in a solid (say  $N$ ) vibrate with the same frequency independently. In other words, the frequency of vibration for all the  $3N$  normal modes is common and the atoms oscillate independent of each other. Einstein treated the atomic harmonic oscillators as similar to the radiation oscillators of the Planck's theory of blackbody radiation and carried out the quantization of energy levels on parallel lines:

$$\varepsilon_n = n\hbar\omega \quad (n = 0, 1, 2, 3, \dots) \quad (5.17)$$

where  $\varepsilon_n$  represents the vibrational energy of the oscillator in its  $n$ th state of excitation. According to (5.15), the average thermal energy of the solid for a single polarization of the normal mode is equal to  $N\hbar\omega\langle n \rangle$ . The factor  $\frac{1}{2}\hbar\omega$  for the zero point energy was not known to Einstein as this factor arises on the requirement of quantum mechanics which was formulated about twenty years later. Moreover, its omission does not affect the value of heat capacity since  $C_V = (\partial\varepsilon/\partial T)_V$  and the omitted factor is not a function of temperature.

Therefore, in the Einstein model the thermal energy (or internal energy) of a solid containing  $N$  atoms is expressed as

$$= 3N\hbar\omega\langle n \rangle \quad (5.18)$$

which includes the vibrational energy in all the three polarizations of the normal mode.

The phonon heat capacity is given by

$$C_V = \left( \frac{\partial\varepsilon}{\partial T} \right)_V = 3Nk_B \left( \frac{\hbar\omega}{k_B T} \right)^2 \frac{\exp\left(\frac{\hbar\omega}{k_B T}\right)}{\left[\exp\left(\frac{\hbar\omega}{k_B T}\right) - 1\right]^2} \quad (5.19)$$

The plot of the above equation for diamond is shown in Fig. 5.1 which also shows the measured values at different temperatures. It shows a good agreement between the theoretical and experimental curves at high temperatures, and the value of heat capacity approaches its value in the classical limit. The two curves tend to be separated at low temperatures. An overall view indicates that there is an agreement between the theory and the experiment for most of the temperature range excepting the low temperatures. The value of  $C_V$  in the limit of high temperatures as evaluated from (5.19) is  $3Nk_B$ , the classical value given by the Dulong and Petit law. In the low temperatures limit it is found to decrease as  $\exp(-\hbar\omega/k_B T)$  and drops to zero at  $T = 0$  K. The experimental value also approaches zero as  $T \rightarrow 0$  K. Therefore, the biggest achievement of the Einstein model lies in its ability to demonstrate quickly that the heat capacity drops to zero at 0 K. However, the experimental curve (see Fig. 5.1) shows that the drop is faster than that of the exponential. The curve fits with a  $T^3$  dependence in the low temperature region. For every solid there is a characteristic temperature above which the model works and well below this temperature the model fails. This temperature is known as Einstein characteristic temperature  $\theta_E$  and defined by

$$\theta_E = \frac{\hbar\omega_E}{k_B} \quad (5.20)$$

where  $\omega_E$  is called the Einstein characteristic frequency.

The failure of the Einstein model at low temperatures exposes its inadequacy. The model is physically unrealistic because all vibrational modes cannot have a common frequency unless all the atoms in the solid vibrate in a manner independent of each other. The movements of adjacent atoms always tend to be correlated because of the coupling forces within the solid. Therefore, the drawback lies with the basic assumption on which the model is based. In an effort to explain the low temperature behaviour of phonon heat capacity, Debye put forward another approach in which he used an interpolation scheme to calculate the effective contribution from the frequency spectrum of a solid. The Debye model enjoys an overall success with its special achievement in the form of the Debye  $T^3$ -law that fits the low temperature heat capacity data reasonably well.

### 5.2.3 Phonon Density of States

As emphasized at the end of Section 5.2.1, the knowledge of density of states of normal modes is a prerequisite to the determination of thermal energy of a solid. Consider a cube of a periodic solid of side  $L$ . Let there be  $N^3$  primitive cells within the volume of the cube. On applying the periodic boundary condition [given by (4.5)] over these cells for a three-dimensional crystal, we have

$$\exp i(k_x x + k_y y + k_z z) = \exp i[k_x(x+L) + k_y(y+L) + k_z(z+L)] \quad (5.21)$$

where  $(x, y, z)$  are the Cartesian coordinates of any lattice site. Equation (5.21) is valid for the following restricted set

$$k_x, k_y, k_z = 0; \pm \frac{2\pi}{L}; \pm \frac{4\pi}{L}; \dots; \frac{N\pi}{L} \quad (5.22)$$

analogous to the one expressed by (4.9) for a one-dimensional crystal.

The set (5.22) shows that there lies one allowed value of  $k$  within a volume of  $(2\pi/L)^3$  in  $k$ -space. Thus the number of allowed  $k$ -values per unit volume of  $k$ -space is

$$\left(\frac{L}{2\pi}\right)^3 = \frac{V}{(2\pi)^3} \quad (5.23)$$

where  $V$  denotes the volume of the crystal. If we represent the density of the allowed  $k$ -values or the density of phonon modes by  $D(\omega)$ , the number of modes lying within the interval of frequency  $\omega$  and  $\omega + d\omega$  is given by

$$\begin{aligned} D(\omega)d\omega &= \frac{V}{(2\pi)^3} \cdot (\text{volume enclosed between } k\text{-surfaces,} \\ &\quad \omega(\mathbf{k}) = \text{constant and } \omega(\mathbf{k}) + d\omega = \text{constant}) \\ &= \frac{V}{(2\pi)^3} \int_{\omega}^{\omega+d\omega} d^3 k \end{aligned} \quad (5.24)$$

Let  $d\mathbf{s}_{\omega}$  denote a small surface element of  $\omega(\mathbf{k}) = \text{constant}$  and  $d\mathbf{k}_{\perp}$  be a vector normal to it (Fig. 5.2) with its tip touching the surface,  $\omega(\mathbf{k}) + d\omega = \text{constant}$ . Then

$$D(\omega)d\omega = \frac{V}{(2\pi)^3} \int_{\omega(\mathbf{k})=\text{const.}} d\mathbf{s}_{\omega} \cdot d\mathbf{k}_{\perp} \quad (5.25)$$

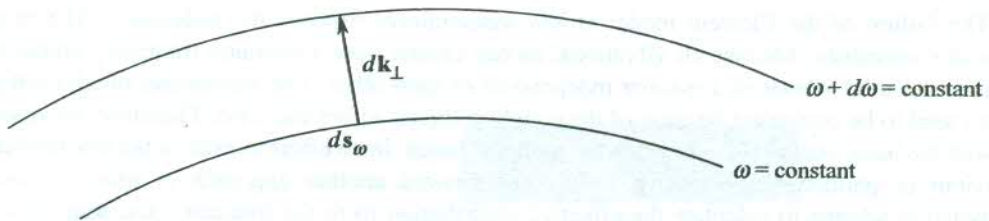


**FIG. 5.2** Neighbouring constant energy surfaces  $\omega(\mathbf{k}) = \text{constant}$  and  $\omega + d\omega(\mathbf{k}) = \text{constant}$  being connected by a vector  $d\mathbf{k}_\perp$  normal to the surface element  $ds_\omega$  of the lower energy surface.

With  $d\omega = |\text{grad}_{\mathbf{k}} \omega| d\mathbf{k}_\perp$ , we have

$$D(\omega) d\omega = \frac{V}{(2\pi)^3} d\omega \int_{\omega(\mathbf{k}) = \text{const.}} \frac{ds_\omega}{|\text{grad}_{\mathbf{k}} \omega|} \quad (5.26)$$

and

$$D(\omega) = \frac{V}{(2\pi)^3} \int_{\omega(\mathbf{k}) = \text{const.}} \frac{ds_\omega}{|\text{grad}_{\mathbf{k}} \omega|} \quad (5.27)$$

The frequency derivative of the density of states has singularities (known as van Hove singularities) at points where the group velocity is zero or the tangents on the dispersion curve are horizontal. The one-dimensional crystal is a special case for which the density of states  $D(\omega)$  itself is singular. The variation of phonon density of states with frequency for silicon is shown in Fig. 5.3.

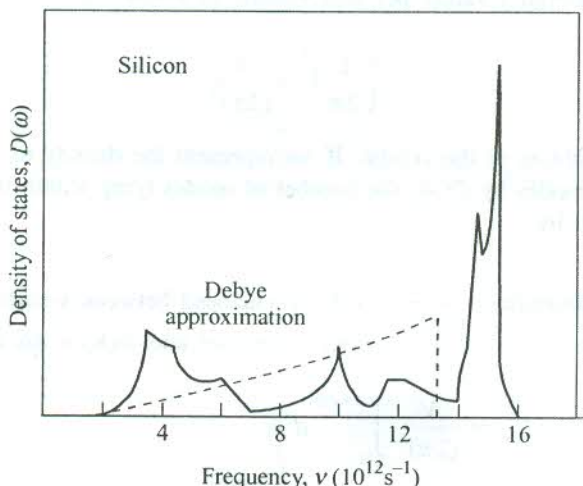


**FIG. 5.3** Behaviour of the phonon density of states in silicon. The dotted curve belongs to an isotropic medium of elastic continuum for  $\theta_D = 640$  K. [After G. Dolling and R.A. Cowley, *Proc. R. Soc., London*, **88**, 463 (1966).]

### 5.2.4 Debye Continuum Model

In the Debye model a crystal is treated as an isotropic elastic continuum in which the velocity of sound is constant ( $c = \omega/k$ ). It takes into consideration only the three acoustical branches with different sound velocities for longitudinal and transverse waves. In this case the surface  $\omega(\mathbf{k}) = \text{const.}$  is spherical and the velocity  $|\text{grad}_{\mathbf{k}} \omega|$  is equal to the sound velocity. Let  $c_i$  denote the sound velocity in the branch  $i$ . Being independent of  $\mathbf{k}$ , it can be taken outside the integral of the relation (5.27) and the surface integral becomes

$$\int_{\omega(\mathbf{k}) = \text{const.}} d\mathbf{s}_\omega = 4\pi k^2 \quad (5.28)$$

Using (5.28), the relation for the density of states (5.27) is put down as

$$D_i(\omega) = \frac{V}{2\pi^2} \cdot \frac{k^2}{c_i}$$

or

$$D_i(\omega) = \frac{V}{2\pi^2} \cdot \frac{\omega^2}{c_i^3} \quad (5.29)$$

The total phonon density of states is then given by

$$D(\omega) = \frac{V}{2\pi^2} \left( \frac{1}{c_L^3} + \frac{2}{c_T^3} \right) \omega^2 \quad (5.30)$$

where  $c_L$  and  $c_T$  are the velocities of longitudinal and transverse waves respectively.

Debye put a cut-off at the upper limit of frequency to ensure that the waves are long enough to have a smooth passage through the crystal which could then be justifiably treated as an elastic continuum. The cut-off frequency is denoted by  $\omega_D$ . The density of states function of this model is plotted as a function of frequency for silicon in Fig. 5.3. At  $\omega_D$  it drops from the maximum to the zero value giving a sharp cut-off. The total thermal energy of the crystal in thermal equilibrium, i.e. the internal energy  $U(T)$  may be written as

$$U(T) = \int_0^{\omega_D} D(\omega) \varepsilon(\omega, T) d\omega \quad (5.31)$$

where  $\varepsilon(\omega, T)$  is the average thermal energy stored in the mode of frequency  $\omega$  at temperature  $T$ .

Substituting for  $D(\omega)$  from (5.30) in (5.31), we have

$$U(T) = \frac{V}{2\pi^2} \left( \frac{1}{c_L^3} + \frac{2}{c_T^3} \right) \int_0^{\omega_D} \omega^2 \varepsilon(\omega, T) d\omega \quad (5.32)$$

Fixing the cut-off at a common frequency for longitudinal and transverse waves is not supported

by reason. But, to our surprise it gives a better agreement with the measured value of heat capacity than when separate cut-off values are chosen for calculations.

The phonon heat capacity may be expressed as

$$C_V(T) = \left( \frac{\partial U}{\partial T} \right)_V = \frac{V}{2\pi^2} \left( \frac{1}{c_L^3} + \frac{2}{c_T^3} \right) \int_0^{\omega_D} \omega^2 \frac{\partial}{\partial T} \varepsilon(\omega, T) d\omega \quad (5.33)$$

We determine the Debye cut-off frequency by applying the condition that the total number of modes or states be equal to  $3N$ , where  $N$  is the total number of atoms in the crystal. Applying this condition, we have

$$\int_0^{\omega_D} D(\omega) d\omega = 3N \quad (5.34)$$

or

$$\frac{V}{2\pi^2} \left( \frac{1}{c_L^3} + \frac{2}{c_T^3} \right) \int_0^{\omega_D} \omega^2 d\omega = 3N$$

or

$$\frac{V}{2\pi^2} \left( \frac{1}{c_L^3} + \frac{2}{c_T^3} \right) = \frac{9N}{\omega_D^3} \quad (5.35)$$

Using (5.35) and taking the value  $\varepsilon(\omega, T)$  as  $\langle n \rangle \hbar\omega$ , we have from (5.33)

$$C_V = \frac{9N}{\omega_D^3} \frac{\partial}{\partial T} \int_0^{\omega_D} \frac{\hbar\omega^3}{\exp(\hbar\omega/k_B T) - 1} d\omega \quad (5.36)$$

The Debye continuum model is most relevant at low temperatures where only low frequencies can be excited and, therefore, waves of only long wavelength will be present. Thus a Debye characteristic temperature  $\theta_D$  is defined below, for which the model is valid. It is given by

$$\theta_D = \frac{\hbar\omega_D}{k_B} \quad (5.37)$$

Using (5.37) and the substitution,  $\hbar\omega/k_B T = x$  in the relation (5.36), we get

$$C_V = 9Nk_B \left( \frac{T}{\theta_D} \right)^3 \int_0^{\theta_D/T} \frac{x^4 e^x}{(e^x - 1)^2} dx \quad (5.38)$$

The behaviour of phonon heat capacity in the extreme limits of temperature can be deduced from (5.38) by evaluating the integral between these limits.

At high temperatures,

$$T \gg \theta_D$$

In this limit ( $k_B T \gg \hbar\omega_D$ ),  $C_V$  as expressed by (5.38) approaches the classical value  $3Nk_B$ .

At very low temperatures,

$$T \ll \theta_D$$

The upper limit of the integral in (5.38) approaches infinity and we obtain the value of the integral as  $4\pi^4/15$ . This gives

$$C_V = \frac{12\pi^4}{5} Nk_B \left( \frac{T}{\theta_D} \right)^3 \quad (5.39)$$

The relation (5.39) expresses the Debye  $T^3$ -law that explains the temperature dependence of the experimental data at low temperatures. The variation of phonon heat capacity in the Debye model together with the experimental curve for yttrium is shown in Fig. 5.4. A comparative study in low temperature region demonstrates that the drop of heat capacity in the Debye curve is faster than that given by the Einstein curve (Fig. 5.5) and matches the experimental curve characterized by  $T^3$  behaviour.

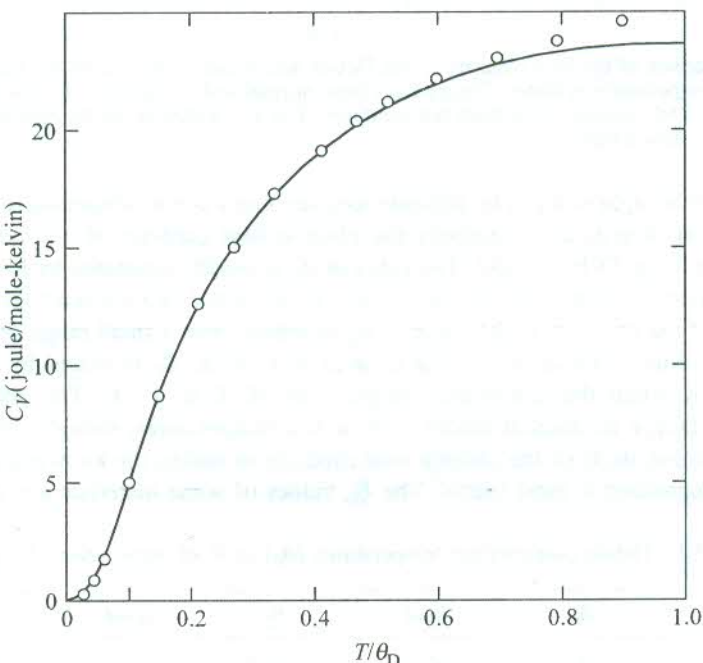


**FIG. 5.4** Debye curve of heat capacity for yttrium for  $\theta_D = 200$  K. The experimental points (circles) are above the Debye curve at high temperatures. For fitting points at lower temperatures, a slightly higher  $\theta_D$  is required. [After L.D. Jennings, R.E. Miller, and F.H. Spedding, *J. Chem. Phys.*, 33, 1849 (1960).]

According to the Debye model, the  $T^3$ -law is expected to be valid in the temperature range  $T \leq 0.1\theta_D$ . But the experimental reports suggest a much lower temperature range,  $T \leq \frac{\theta_D}{50}$ . Though the success of the Debye model is largely accepted, the departure from the theoretically predicted

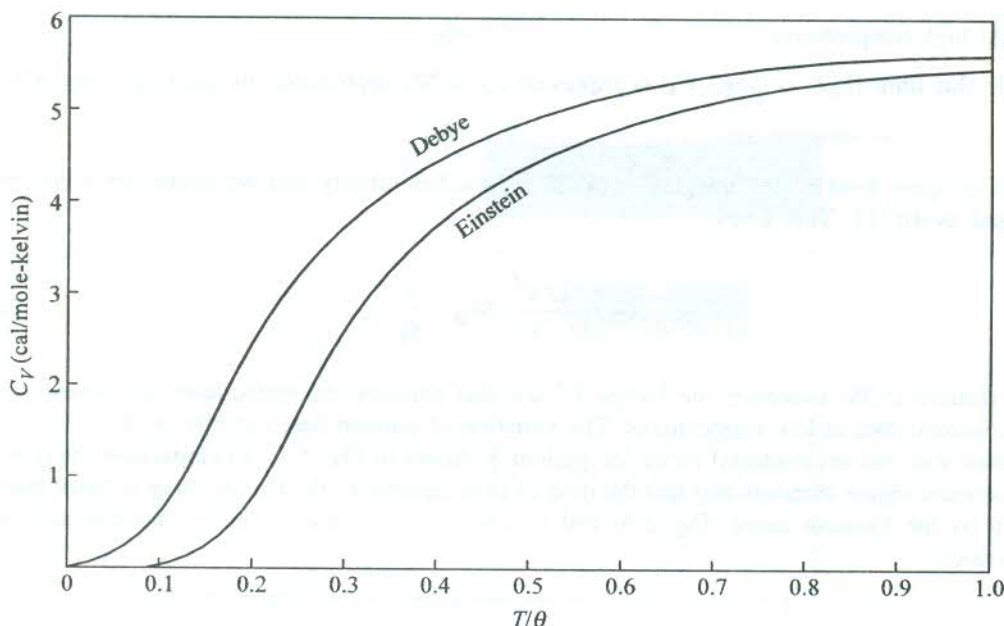


FIG. 5.5 A comparison of the heat capacity in the Debye and Einstein models. In the Debye model, the drop at low temperatures is faster. Curves have been normalized to approach the classical value (Dulong-Petit) of 5.96 cal/mole-K at high temperatures. The  $\theta$  is either  $\theta_D$  or  $\theta_E$  depending on which curve is under consideration.

behaviour has been brought to focus by accurate measurements at low temperatures. The characteristic temperature  $\theta_D$  that determines completely the phonon heat capacity of a solid plays the role of central importance in the Debye model. The value of  $\theta_D$  is usually estimated by feeding the measured value of heat capacity in relation (5.39). In  $T^3$ -law,  $\theta_D$  is treated as a constant which does not sound realistic because of the variation in the value of  $\theta_D$  estimated over a small range of low temperatures. For example, in sodium chloride on cooling from 20 K to 10 K,  $\theta_D$  increases by 20 K; in lithium it decreases by 28 K when the temperature drops from 30 K to 15 K. This data jeopardizes the soundness of the Debye continuum model even at low temperatures, though only marginally.

For a comparative study of the phonon heat capacity of solids, the knowledge of the respective characteristic temperatures is most useful. The  $\theta_D$  values of some materials are given in Table 5.1.

Table 5.1 Debye characteristic temperatures ( $\theta_D$ ) in K of some selected materials\*

Solid	$\theta_D$	Solid	$\theta_D$	Solid	$\theta_D$
Li	344	Hg	71.9	C	2230
Na	158	Pb	105	Si	645
Cs	38	Fe	467	Ge	374
In	108	Ni	450	ZnS	315
Te	153	Mo	450	LiF	732
Cu	343	W	400	LiCl	422
Ag	225	Ar	93	NaCl	321
Au	165	Kr	72	KCl	235

\*From American Institute of Physics Handbook, 3rd ed., McGraw-Hill, New York, 1972.

### 5.3 ANHARMONIC EFFECTS

While dealing with lattice vibrations, the harmonic approximation has been the basis of discussion so far. Notwithstanding its success in handling most of the solids at temperatures well below the melting point, it would be totally misleading to conclude that corrections to the approximation make sense only in calculations where high precision is required. Keeping aside the exceptions like solid helium in which the harmonic approximation is not applicable, we come across a number of interesting physical phenomena that cannot be explained without relaxing the approximation. Some of these are:

- (i) Thermal expansion
- (ii) Thermal conductivity has a finite value
- (iii) The temperature dependence of elastic constants
- (iv) The failure of Debye heat capacity to attain the classical value at high temperatures ( $T \gg \theta_D$ )
- (v) The line broadening or the measurable width of one phonon peaks in the neutron inelastic scattering pattern

The cause of failure of the harmonic approximation in explaining the above phenomena rests in the questionable relevance of its two basic assumptions:

1. Vibrations of atoms may be treated as small oscillations in which the displacement of atoms from their respective equilibrium positions are small.
2. Only the leading non-vanishing term in the expansion of potential energy about its equilibrium value is retained.

The validity of the first assumption is always questionable at high temperatures where the amplitude of vibration is large. And when the displacements become large, we can ill-afford to ignore the higher order terms in displacement beyond the quadratic term in the potential energy expansion. In this situation both the assumptions become irrelevant. This is indicated by the shape of the potential energy curve at large interatomic separations (Fig. 5.6) where it is more asymmetric, showing thereby deviation from the harmonic nature. This is understandable as atoms can never oscillate like independent harmonic oscillators in a real crystal because the motion of adjacent atoms is always correlated. In general, we must accept the presence of anharmonicity to a certain degree in the vibrations of a solid. The physical phenomena stated earlier are explained successfully when corrections on the requirement of anharmonicity are included in the calculations.

The anharmonic effects are most reasonably accounted when the potential energy expansion is truncated not before the quartic term. Dropping the constant equilibrium term, we write the potential energy as

$$U(x) = fx^2 - gx^3 - hx^4 \quad (5.40)$$

where  $x$  is the deviation from the equilibrium separation at absolute zero and all the coefficients  $f$ ,  $g$  and  $h$  are positive.

The first term in (5.40) is the usual harmonic component and the other two refer to the anharmonic effects. The cubic term stands for the asymmetry of the mutual repulsion of the atoms and the quartic term represents the softening of the vibration at large amplitudes.

As the applications of the anharmonic potential, we will deal with the first two of the phenomena cited earlier as examples. While the thermal expansion refers to an equilibrium property, the thermal conductivity is a well-known transport phenomenon.

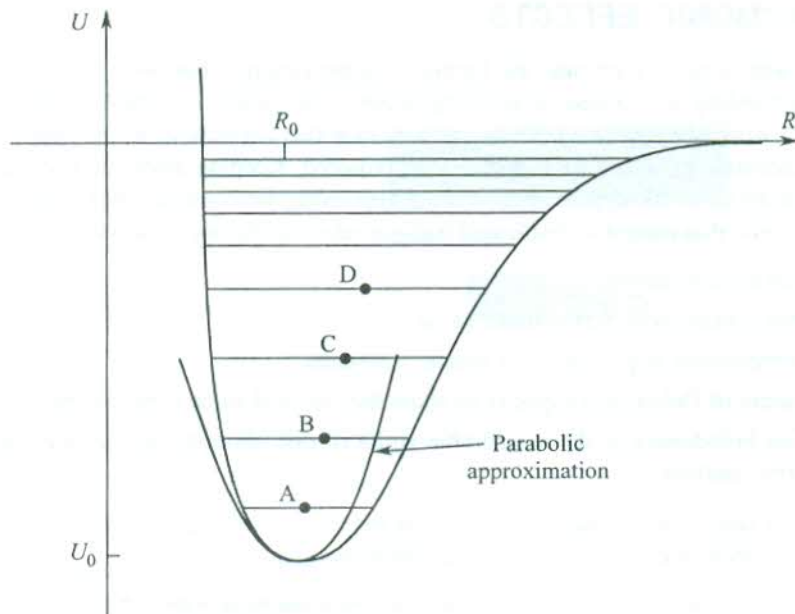


**FIG. 5.6** An exaggerated potential energy curve based on Lennard-Jones potential for real crystals. The asymmetrical nature of the curve at higher energies does not allow the motion to be interpreted in parabolic approximation. The increase in the interatomic separation  $R$  at high energies (excited at high temperatures) produces thermal expansion. The  $R_0$  is the interatomic distance in the ground state. Because of anharmonicity, the vibration quantum (the spacing between vibrational levels) does not remain constant. It decreases with increase in energy.

### 5.3.1 Thermal Expansion

It is an established fact that solids expand on heating. In the harmonic approximation, all atoms vibrate about their equilibrium position within a perfectly symmetric well (parabola) of interatomic interaction. But the potential energy curve (see Fig. 5.6), as derived from a Lennard-Jones potential type for real solids, matches this behaviour only in the range of low thermal excitations that correspond to low temperatures. We may thus conclude that the harmonic approximation is strictly valid only at low temperatures.

The potential well gets asymmetrical for larger interatomic separations (see Fig. 5.6) occurring at higher energies. The mean interatomic separations at a few vibrational energies taken in increasing order are denoted by points A, B, C, D respectively. The values represented by these points are in increasing order as shown by the trend of shift toward larger values relative to the mean equilibrium separation  $R_0$  in the ground state. It is then imperative that at higher temperatures when higher vibrational states are sufficiently populated, solids would show expansion. The range of vibration frequencies of solids is such as can be excited by the thermal energy. These arguments explain the thermal expansion of solids. Since this property follows from the anharmonic nature of the potential energy curve, the thermal expansion is attributed to the presence of anharmonicity in atomic vibrations.

Now we use (5.40) to calculate the thermal expansion in terms of the mean displacement  $\langle x \rangle$  of the atoms in a solid. It is non-zero because of the cubic term. A crude way of determining  $\langle x \rangle$  is to use the condition,

$$\frac{\partial U}{\partial x} = 0$$

and ignore the term in  $h$ . This gives

$$\langle x \rangle = \frac{3g \langle x^2 \rangle}{2f} \quad (5.41)$$

If the mean square displacement is calculated classically in the harmonic approximation, we get

$$\langle x^2 \rangle = \frac{\int_{-\infty}^{+\infty} x^2 \exp(-fx^2/k_B T) dx}{\int_{-\infty}^{+\infty} \exp(-fx^2/k_B T) dx} = \frac{\frac{k_B T}{4f} \sqrt{\frac{\pi}{f/k_B T}}}{\frac{1}{2} \sqrt{\frac{\pi}{f/k_B T}}} = \frac{k_B T}{2f}$$

or

$$\langle x^2 \rangle = \frac{k_B T}{2f} \quad (5.42)$$

Substituting (5.42) in (5.41), we express the mean displacement as

$$\langle x \rangle = \frac{3g k_B T}{4f^2} \quad (5.43)$$

The relation (5.43) shows an increase in the interatomic separations and, therefore, a thermal expansion of the solid.

We may define the coefficient of linear expansion  $\alpha$  as

$$\alpha = \frac{\partial \langle x \rangle}{\partial T} \quad (5.44)$$

Using (5.43), we get

$$\alpha = \frac{3g k_B}{4f^2} \quad (5.45)$$

Though changes in size because of the thermal expansion are small in solids, the knowledge of their expansion coefficients is nonetheless of great practical value in industry where even simple jobs like making a permanent joint between two materials have their tactical importance.

Another striking feature, that is associated with the thermal expansion, has reference to the change of the characteristic frequency in a solid. The levels of vibrational energy come closer at high energy values (see Fig. 5.6). In the harmonic approximation the levels are expected to remain evenly spaced and unaffected by the change of temperature. The spacing can alter only if the energy quantum  $\hbar\omega$  changes. By taking anharmonic considerations into account with the use of (5.40), it can be shown that the characteristic frequency  $\omega$  decreases with the increase in temperature. This is consistent with the observation of closer energy levels at high energies to which the thermal excitation can be made by raising the temperature. We must appreciate that the anharmonic contributions at these values of energy and temperature are at their maximum.

The above frequency effect may as well be interpreted as the change in characteristic frequencies in a solid because of the change in its volume. It is conventionally put in the form of an assumption

that allows both the characteristic frequencies and the volume  $V$  to suffer the same relative change. That is,

$$\frac{\Delta\omega}{\omega} \propto \frac{\Delta V}{V}$$

or

$$\frac{\Delta\omega}{\omega} = \gamma \frac{\Delta V}{V} \quad (5.46)$$

where the proportionality constant  $\gamma$  is called the Grüneisen constant. It is a measure of the anharmonic coupling.

This anharmonic effect, though small, may be studied by neutron scattering measurements that provide the change in characteristic frequencies with temperature.

An exact treatment of the anharmonic effects is unfortunately not easy. We have to take recourse to some approximate method like perturbation method of quantum mechanics. As a first approximation to the true solution, we start with the solutions of harmonic potential (the phonons). Obviously, the phonons are not the exact eigensolutions to the equations of motion. The description of a state of motion in an anharmonic solid in terms of a phonon or a plane wave changes with time and the accuracy of the description drops progressively. For an accurate description with time, it is required to recognize the status of a spectrum of some other phonons. It means that the anharmonic phonons, unlike the harmonic ones, have only a limited lifetime after which they merge or decay to produce new phonons. In the next section, we discuss these phonon processes as they enable us to explain the basis for thermal resistance and related features.

### 5.3.2 Phonon Collision Processes

An exact quantum mechanical treatment based on the first order perturbation theory shows that:

- (a) The cubic term in the potential energy accounts for the following processes:
  - (i) one phonon decays into two
  - (ii) two phonons merge into one
- (b) The quartic term in the potential energy accounts for the following processes:
  - (i) one phonon decays into three
  - (ii) two phonons get converted into two others
  - (iii) three phonons merge into one

We observe that the cubic term is related to the three-phonon processes and the quartic to the four-phonon processes. It is now necessary to examine the probable collision processes, especially in the context of thermal resistance which is on our plan for discussion. Let us consider the collision involving three phonons. The use of the term collision should not be objectionable as phonons are treated here as particles. If two phonons of wavevectors  $\mathbf{k}_1$  and  $\mathbf{k}_2$  collide or merge to produce a new phonon with wavevector  $\mathbf{k}_3$ , the momentum conservation requires that

$$\mathbf{k}_1 + \mathbf{k}_2 = \mathbf{k}_3 \quad (5.47)$$

The total energy of the initial phonons is completely held by the final phonon. The net phonon momentum is written as

$$\mathbf{j} = \sum_{\mathbf{k}_s} n_{\mathbf{k}_s} \hbar \mathbf{k}_s \quad (5.48)$$

where  $n_{\mathbf{k}_s}$  is the number of phonons with wavevector  $\mathbf{k}$  in the branch  $s$ .

The net phonon momentum  $\mathbf{j}$  constitutes the phonon thermal current in a solid between whose two ends a difference of temperature is maintained. In view of (5.47), the net phonon momentum is a constant and, therefore, the phonon current  $\mathbf{j}$  remains unchanged. The distribution of phonons (or the distribution function) at any stage when  $\mathbf{j} \neq 0$  tends to approach its equilibrium value (condition of zero temperature). But in the present case it is not permitted as  $\mathbf{j}$  has to remain unaffected. Any distribution of phonons flows down the solid unhindered as if the phonon mean free path were infinite. Consequently, the thermal resistance, a measure of the rate at which the equilibrium distribution is approached, becomes zero. This gives an infinite value of thermal conductivity—an unacceptable result. Therefore, the collision processes described by (5.47) do not give rise to thermal resistance. These processes are called ‘normal processes’ or simply ‘N-processes’. Figure 5.7(a) shows a normal process of collision in a two-dimensional square lattice.

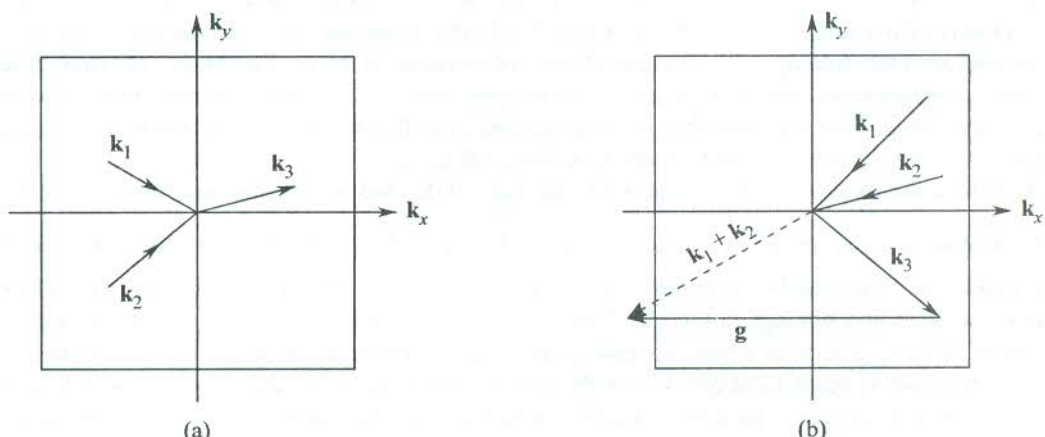


**FIG. 5.7** Phonon scattering processes in  $k$ -space for a two-dimensional square lattice: (a) normal process, (b) Umklapp process—two phonons with wavevector  $\mathbf{k}_1$  and  $\mathbf{k}_2$  merge into  $\mathbf{k}_3$  with the help of a reciprocal lattice vector  $\mathbf{g}$  ( $= 2\pi/a$  in this case). Note that the direction of the  $x$ -component of the phonon flux has been reversed.

It should be, however, surprising to note that N-processes explain the conduction of heat in gases where we deliberately impose the condition that no mass transport of particles takes place. In this picture, the hot particles while moving along one direction lose their energy to the cold particles moving in the opposite direction [Fig. 5.8(a)]. But these ideas are not tenable in the case of phonon gas where there is no net particle conservation in the true picture. The phonons that carry heat from the hot end are destroyed at the cold end [Fig. 5.8(b)].

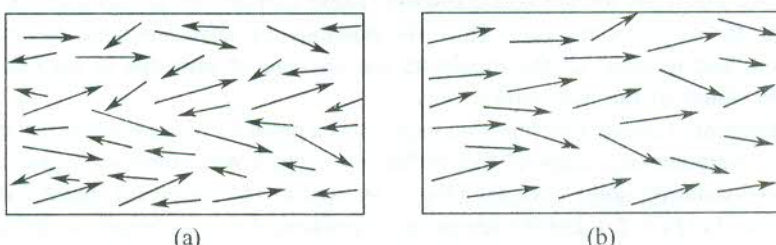


**FIG. 5.8** (a) Conduction of heat in a gas: hot electrons moving in one direction lose their energy to cold electrons moving in the opposite direction. During the conduction process the number of electrons is conserved. (b) Conduction of heat by phonons in a solid: There is no net particle conservation. Phonons carrying heat from the hot end get destroyed at the cold end.

The phonons could also suffer collisions with the immobile imperfections and the crystal bounding surface. But these collisions are known to be elastic in nature, meaning thereby that the collisions do not change the frequency of the individual phonons. This makes impossible for an equilibrium distribution of phonons to be established locally.

The puzzle of thermal resistance is solved by a different kind of collisions expressed as

$$\mathbf{k}_1 + \mathbf{k}_2 = \mathbf{k}_3 + \mathbf{g} \quad (5.49)$$

where  $\mathbf{g}$  is a reciprocal lattice vector.

Since in a periodic lattice the energy of a phonon with wavevector  $(\mathbf{k}_3 + \mathbf{g})$  is the same as that for a phonon with wavevector  $\mathbf{k}_3$ , the phonon  $\mathbf{k}_3$  in (5.49) must be carrying the total energy. The special feature of (5.49) is that it destroys the momentum  $\hbar\mathbf{g}$  and changes the direction of energy flow as shown in Fig. 5.7(b). The  $x$ -components of  $\mathbf{k}_1$  and  $\mathbf{k}_2$  are directed opposite to the  $x$ -component of  $\mathbf{k}_3$ . Peierls called such collisions by the name ‘Umklapp processes’ or ‘U-processes’. Umklapp is the German term for ‘folding over’. Because of non-conservation of the net momentum, the equilibrium distribution of phonons can be restored by these processes at a certain rate that determines the thermal resistance. This confirms that the U-processes of collisions give rise to thermal resistance, limiting the value of thermal conductivity to a finite value.

For the condition (5.49) to be satisfied, the sum of  $\mathbf{k}_1$  and  $\mathbf{k}_2$  must extend beyond the first Brillouin zone and the individual values should not be less than  $\frac{1}{2}\mathbf{g}$ . The sum  $(\mathbf{k}_1 + \mathbf{k}_2)$  can be translated to the first zone by reciprocal lattice vector  $-\mathbf{g}$  [Fig. 5.7(b)]. The  $\mathbf{k}_3$  is called the reduced value of  $(\mathbf{k}_3 + \mathbf{g})$  and belongs to the set of unique  $k$ -values defined by (4.9) in Chapter 4. We will talk more about U-processes while discussing the effect of temperature on thermal conductivity.

It is desirable to make some remarks on the terminology followed in the above discussion. In the refined theoretical picture, a phonon collision is referred to as the scattering of phonons because of phonon–phonon interaction. This is only to avoid confusion to the reader as we may inadvertently be using sometimes a mixed terminology.

### 5.3.3 Phonon Thermal Conductivity

Metals are good conductors of heat and electricity. The energy is transported mainly by free electrons. But it must not be construed that thermal conductivity depends entirely on the number of available free electrons. Some of the insulators, for example, the crystalline sapphire ( $\text{Al}_2\text{O}_3$ ) and quartz ( $\text{SiO}_2$ ) possess higher thermal conductivity than copper at low temperatures. The maximum value of thermal conductivity of sapphire is  $200 \text{ W cm}^{-1} \text{ K}^{-1}$  as against the corresponding value,  $100 \text{ W cm}^{-1} \text{ K}^{-1}$ , of copper. The observations indicate to the involvement of some other carriers in addition to the free electrons for the heat transport. These carriers are phonons as confirmed by the theory explaining the experimental data. Thus, the phonons are unambiguously the main carriers of heat in insulators, and in some of the insulators the passage of phonons is smooth enough so as to result in large values of thermal conductivity.

An exact treatment of phonon thermal conductivity is a problem of great mathematical complexity. We give below an elementary classical theory based on the kinetic theory of gases.

Consider an insulating solid cylinder (Fig. 5.9) whose two ends are maintained at different temperature  $T_1$  and  $T_2$  ( $T_2 > T_1$ ). Let the temperature gradient down its length be defined as  $-\partial T/\partial x$ . At steady state, there is a steady flow of heat from the hot end to the cold end maintaining the temperature difference  $(T_2 - T_1)$  at a constant value. It is observed that the thermal energy flowing

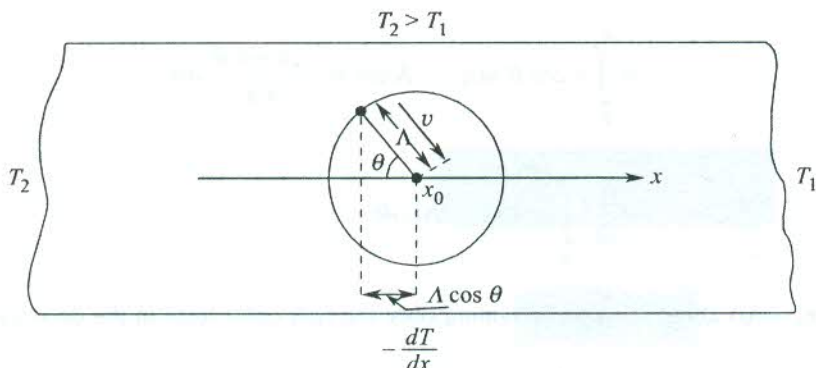


**FIG. 5.9** Conduction of heat by phonons in an insulating solid cylinder along its length when a temperature gradient is maintained between the two ends of the cylinder. Phonons approaching the point  $x_0$  at an angle  $\theta$  with the cylinder's axis ( $x$ -direction) and moving with velocity  $v$  make a collision at the point. The temperature at the point is  $T$ .

down the cylinder per unit of its circular cross-section per unit time  $j$  is proportional to the temperature gradient  $-\partial T/\partial x$ . That is,

$$\mathbf{j} \propto - \frac{\partial T}{\partial x} \quad (5.50)$$

or

$$\mathbf{j} = - K_{ph} \left( \frac{\partial T}{\partial x} \right) \quad (5.51)$$

where  $K_{ph}$  is called the thermal conductivity and  $|\mathbf{j}|$  is the thermal flux per unit time.

The flow of heat thus cannot be linear, as in that case  $\mathbf{j}$  would have been proportional to  $T$ . The heat energy diffuses from the hot end to the cold end through a random process. As we consider here only the phonons as the heat carriers, the random process involves mainly the phonon-phonon collisions. The extra phonons created at hot end are destroyed at the cold end. This picture of phonon gas is better suited to be treated by the kinetic theory of molecular gases.

Frequent collisions among phonons limit the phonon mean free path. In a rigorous theory the mean path is treated as a function of the temperature and the phonon frequency. But we take an average value ( $\Lambda$ ) over the length of the solid cylinder. Let the non-equilibrium energy density contributed by phonons coming out of collisions at the point  $x$  be denoted by  $u(x)$ . If  $T$  be the temperature at  $x$ ,  $u(x)$  is supposed to be proportional to the equilibrium energy density  $u[T(x)]$ . Then, the contribution to thermal current density  $j$  from a single phonon is  $v_x u(x)$ , where  $v_x$  is the  $x$ -component of the phonon velocity  $v$ .

Figure 5.9 shows that the collision at  $x_0$  involves the phonons approaching it at angle  $\theta$  with the  $x$ -axis. The immediate last collision of these phonons on the average should have occurred at a point whose  $x$ -coordinate is shorter by  $\Lambda \cos \theta$ , i.e. at  $x = (x_0 - \Lambda \cos \theta)$ . The net thermal current  $j$  can be calculated by using the fact that  $j$  is proportional to the product  $v_x \cdot u(x_0 - \Lambda \cos \theta)$  averaged over all solid angles. Accordingly,

$$j = \langle v_x \cdot u(x_0 - \Lambda \cos \theta) \rangle$$

$$\begin{aligned}
 &= \int_0^\pi v \cos \theta u(x_0 - \Lambda \cos \theta) \frac{2\pi \sin \theta}{4\pi} d\theta \\
 &= \frac{1}{2} \int_{-1}^1 vt u(x_0 - \Lambda t) dt
 \end{aligned} \tag{5.52}$$

Expanding  $u(x_0 - \Lambda t)$  about  $u(x_0)$  and retaining only the first order term in the derivative, we have

$$\begin{aligned}
 j &= \frac{1}{2} \int_{-1}^1 vt \left[ u(x_0) - \Lambda t \frac{\partial u}{\partial x} \Big|_{x_0} \right] dt \\
 &= 0 - \frac{1}{2} v \Lambda \frac{\partial u}{\partial x} \left[ \frac{t^3}{3} \right]_{-1}^1 \\
 &= -\frac{1}{3} v \Lambda \frac{\partial u}{\partial x}
 \end{aligned}$$

or

$$j = \frac{1}{3} v \Lambda \frac{\partial u}{\partial T} \left( -\frac{\partial T}{\partial x} \right) \tag{5.53}$$

Comparing (5.53) with (5.51), the contribution of phonons to the thermal conductivity may be expressed as

$$K_{\text{ph}} = \frac{1}{3} v \Lambda \frac{\partial u}{\partial T}$$

or

$$\begin{aligned}
 K_{\text{ph}} &= \frac{1}{3} C_V \Lambda v \\
 &= \frac{1}{3} C_V v^2 \tau
 \end{aligned} \tag{5.54}$$

where  $C_V$  denotes the phonon heat capacity and  $\tau$  is the relaxation time ( $v\tau = \Lambda$ ).

We can define the phonon collision frequency as  $\tau^{-1}$ . The variation of thermal conductivity with temperature in terms of the parameters  $\Lambda$  and  $C_V$  is explained below.

### **At high temperatures ( $T \gg \theta_D$ )**

In this temperature range, the thermal equilibrium phonon occupation numbers given by

$$\langle n_k \rangle = \frac{1}{\exp(\hbar\omega(k)/k_B T) - 1}$$

reduce to

$$\sim \frac{k_B T}{\hbar \omega(\mathbf{k})} \quad (5.55)$$

So, the total number of phonons is proportional to the temperature. Therefore, the higher the temperature, the more will be the collision frequency, resulting in smaller mean free paths. Since  $C_V$  approaches the constant Dulong-Petit value, the change in the thermal conductivity is predominantly controlled by the change in mean free path. Thus, the thermal conductivity decreases with increase in temperature. Though this trend is confirmed by experiments, the observed rate of fall is given by

$$K_{ph} \propto \frac{1}{T^m} \quad (5.56)$$

where  $m$  lies between 1 and 2.

### **At low temperatures ( $T \ll \theta_D$ )**

The phonon occupancy in thermal equilibrium may be taken as  $\sim \exp(-\hbar \omega(\mathbf{k})/k_B T)$ . The probability of occurrence of U-processes [as expressed by (5.49)] is written as

$$\begin{aligned} n_{\mathbf{k}_1} \cdot n_{\mathbf{k}_2} &= \exp(-\hbar \omega_{\mathbf{k}_1}/k_B T) \cdot \exp(-\hbar \omega_{\mathbf{k}_2}/k_B T) \\ &= \exp[-\hbar(\omega_{\mathbf{k}_1} + \omega_{\mathbf{k}_2})/k_B T] \\ &= \exp(-\hbar \omega_{\mathbf{k}_3}/k_B T) \end{aligned}$$

which shows that the U-processes are almost frozen at low temperatures and the thermal conductivity exponentially approaches infinity.

But, in practice, all solids have finite conductivity even in the range of lowest temperatures. Since no perfect crystal exists in nature, there may be collisions of phonons with imperfections, impurities or even with the bounding surfaces. At certain temperature the mean free path on account of these collisions becomes so large that it is comparable with the size of the sample. This being the maximum realistic value, the mean free path assumes the *temperature independent behaviour below this temperature*. This is known as the *size effect*. Then (5.54) is replaced by

$$K_{ph} = \frac{1}{3} C_V v D \quad (5.57)$$

where  $D$  stands for the size (diameter in the case of a rod).

The behaviour of thermal conductivity *in this temperature region* is mainly determined by the *Debye heat capacity* which drops as  $T^3$ . In fact, a competition between the *exponential* and the  $T^3$  terms sets in at the temperature *below which the mean free path is temperature independent*. The drop of  $T^3$  being faster than the exponential increase, the thermal conductivity is limited to a finite value.

The scattering of phonons from crystal walls was suggested by Casimir.\* The nature of the curves of Fig. 5.10 below 10 K provides a sound proof to the ideas of Casimir. The larger the cross-sectional area of the sample, the higher the conductivity. From below 10 K as the temperature rises,

\* H.B.G. Casimir, *Physica* 5, 495 (1938).

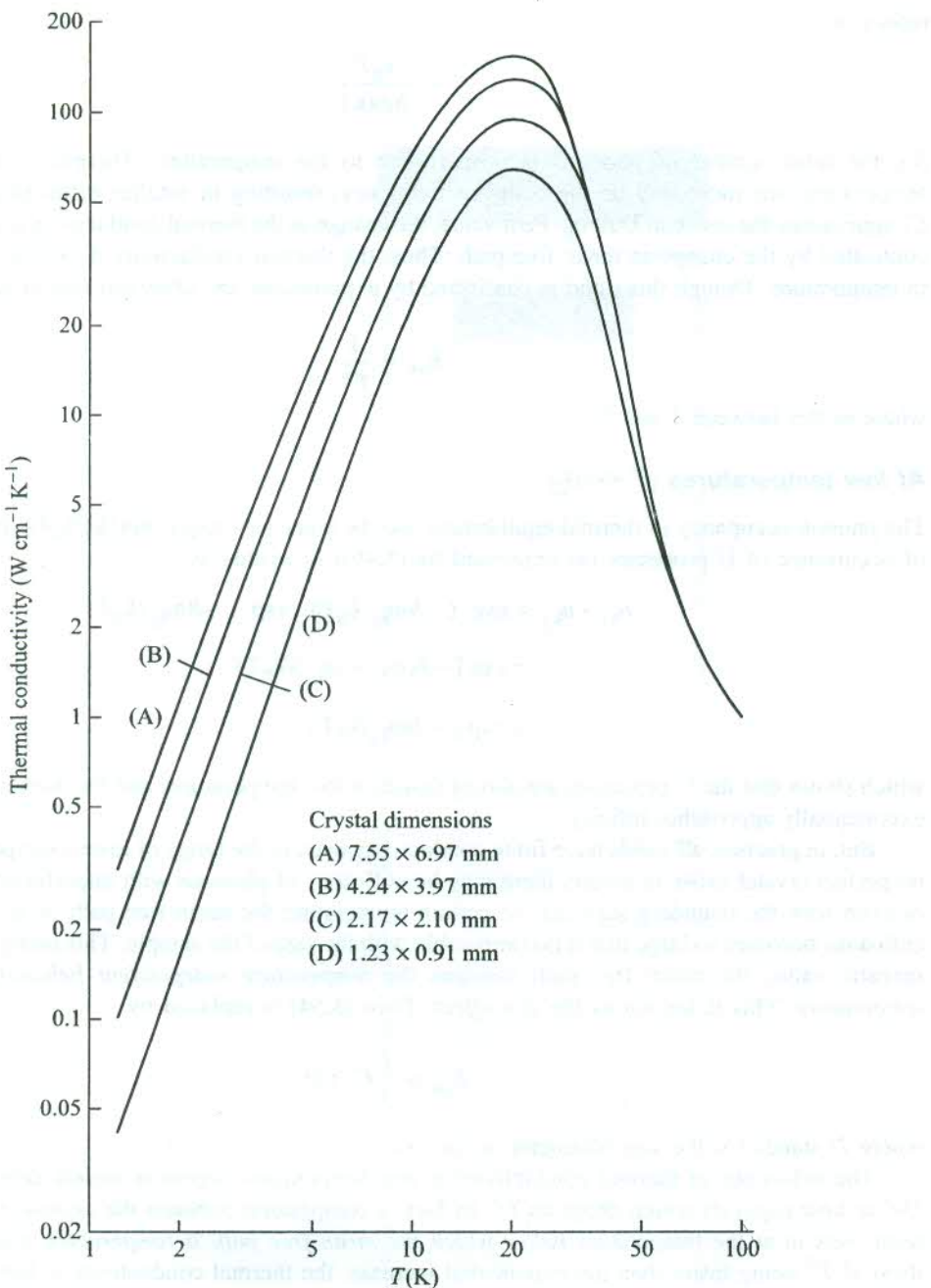


**FIG. 5.10** Thermal conductivity of isotopically pure LiF crystals as a function of temperature. The curves are the beautiful demonstration of size effect on thermal conductivity. The larger the cross-sectional area of the sample, the higher the thermal conductivity. [After P.D. Thatcher, *Phys. Rev.*, **156**, 975 (1967).]

the U-processes become more frequent and the conductivity attains its maximum value when the mean free path because of the phonon-phonon scattering becomes comparable with that owing to the scattering from the crystal's surface. With further rise in temperature the conductivity falls because of the increasing phonon-phonon scattering and assumes the expected exponential drop at higher temperatures in the low temperature regime. The fall continues in the highest temperature range but according to (5.56), because the heat capacity here tends to be on level with the constant Dulong-Petit value.

The presence of the rival phonon scattering mechanisms is found to soften the 'sharp conductivity maximum' in most of the samples, irrespective of the material. The scattering from isotopic impurities is well identified among these. Its effect is demonstrated in Fig. 5.11 by the experimental curves of two samples of LiF crystal, one of which contains a mixture of  $^6\text{Li}$  and  $^7\text{Li}$  isotopes. On cooling, the rise of conductivity is less steep in the sample having both isotopes than in the sample which is almost free from  $^6\text{Li}$  isotope. In addition, it has a lower and flatter maximum. The sharp maximum in the pure sample is almost totally contributed by U-processes in the absence of rival isotopic scattering.

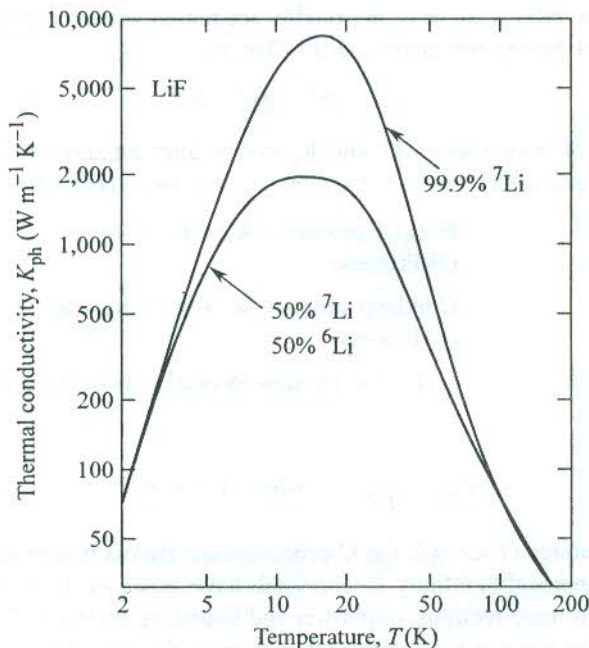


**FIG. 5.11** The influence of isotope scattering on the maximum of thermal conductivity. The phonon scattering from isotopes lowers the thermal conductivity as is observed for the sample composed of  $^7\text{Li}$  and  $^6\text{Li}$  isotopes. The other sample almost free of  $^6\text{Li}$  isotope shows a sharper and higher maximum. The presence of the rival phonon scattering mechanisms softens the sharp conductivity maximum. [After R. Berman, *Cryogenics*, 5, 297 (1965).]

Insulators characterized by large values of thermal conductivity have found wide applications in the field of low temperature physics.

## SUMMARY

- For a harmonic crystal, heat capacity at constant volume,  $C_V$  is equal to heat capacity at constant pressure  $C_P$  because the difference between the two depends on the square of the temperature coefficient of linear expansion which is zero for a harmonic solid.
- The achievements of the Einstein model of phonon heat capacity are:
  - It explains the behaviour of heat capacity at room temperature and above. In the high temperature limit, it gives the classical value  $(3Nk_B)$  which the experimental value approaches at these temperatures.
  - It shows that the heat capacity approaches zero as  $T \rightarrow 0$  K, a fact that agrees with the experiment.
- The limitation of the Einstein model of phonon heat capacity is that the heat capacity at low temperatures decreases as  $\exp(-\hbar\omega/k_B T)$  in contrast to the observed  $T^3$  dependence.  
The Debye  $T^3$ -law based on a continuum model explains very well the low temperature behaviour. The Debye model enjoys success over the entire useful temperature range.
- The anharmonic effects are most reasonably accounted when the potential energy expansion is truncated not before the quartic term. That is,

$$U(x) = fx^2 - gx^3 - hx^4$$

- Two phonons of wavevectors  $\mathbf{k}_1$  and  $\mathbf{k}_2$  may scatter against each other (or collide) and merge to produce a new phonon by either of the two types of scattering processes:

Normal process:  $\mathbf{k}_1 + \mathbf{k}_2 = \mathbf{k}_3$   
(N-Process)

Umklapp process:  $\mathbf{k}_1 + \mathbf{k}_2 = \mathbf{k}_3 + \mathbf{g}$   
(U-Process)

- At high temperatures ( $T \gg \theta_D$ ), the phonon thermal conductivity ( $K_{ph}$ ) changes according to

$$K_{ph} \propto \frac{1}{T^m} \quad \text{where } 1 < m < 2$$

At low temperatures ( $T \ll \theta_D$ ), the U-processes are almost frozen and  $K_{ph}$  for ideal crystals exponentially approaches infinity. Real crystals have, however, finite  $K_{ph}$  because of collisions of phonons with imperfections, impurities and bounding surfaces of specimens. At very low temperatures, the phonon mean free path is comparable with the size of the specimen (or a constant), so that

$$K_{ph} = \frac{1}{3} C_V v D$$

where  $D$  is the diameter in the case of a rod. Or

$$K_{ph} \propto T^3 \quad (\text{since } v \text{ and } D \text{ are constant and } C_V \propto T^3)$$

## PROBLEMS

- 5.1** The thermal conductivity maximum of a synthetic sapphire sample of 3 mm diameter is observed at 30 K. The measured maximum value is  $2.7 \times 10^4 \text{ W m}^{-1} \text{ K}^{-1}$ . If the speed of sound in sapphire is  $10^4 \text{ m s}^{-1}$ , calculate the heat capacity of the sapphire at 30 K.
- 5.2** Obtain expressions for the thermal energy and the phonon heat capacity of  
 (a) a system of two harmonic oscillators, and  
 (b) a system with two energy levels.  
 Explain the difference in the two results.
- 5.3** Derive an expression for the temperature at which the thermal lattice energy is equal to the zero point energy in the Einstein model. Write down the corresponding condition in the Debye model.
- 5.4** Using the Debye approximation for a one-dimensional monatomic lattice with atomic spacing  $a$  and sound speed  $v$ , show that

$$\omega_D = \frac{\pi v}{a} \quad \text{and} \quad \theta_D = \frac{\hbar \omega_D}{k_B}$$

- 5.5** For Problem 5.4, derive the integral expressions for the thermal energy and phonon heat capacity. Show that

$$\begin{aligned} C_V &= \frac{\pi^2 k_B}{3a} \left( \frac{T}{\theta_D} \right) \text{ per unit length at low temperatures} \\ &= \frac{k_B}{a} \text{ per unit length at high temperatures.} \end{aligned}$$

- 5.6** Solve the above problem for a two-dimensional crystal and show that at low temperatures  $C_V \propto T^2$ .
- 5.7** Consider the dispersion relation (4.4) for a one-dimensional monatomic lattice of  $N$  atoms. Show that the density of normal modes is given by

$$D(\omega) = \frac{2N}{\pi} \frac{1}{(\omega_m^2 - \omega^2)^{1/2}}$$

- 5.8** Show that for temperatures well below  $\theta_D$ , the mean free path of a phonon can be expressed as

$$\Lambda = \frac{f K_{ph} \theta_D^3}{v T^3}$$

where  $v$  is the speed of sound and  $f$  is defined in (5.40).

- 5.9** In the approximation that the heat capacity is temperature independent, prove the following for the variation of thermal expansion coefficient  $\alpha$ :

$$\frac{d\alpha}{dT} = - \frac{9g f C_V^2}{8v^4 x_0}$$

where  $x_0$  is the equilibrium interatomic separation.

- 5.10** Show that  $u = \sum_{n=1}^{\infty} a_n \exp(in\omega t)$  is an approximate solution multiples of the harmonic

frequency  $\omega = \sqrt{\frac{f}{M}}$ , to the equation of motion

$$M\ddot{\mathbf{u}} + f\mathbf{u} - \frac{1}{2} g\mathbf{u}^2 = 0$$

for an anharmonic oscillator.

- 5.11** Show that the phonon density of states  $D(\omega)$  for a diatomic linear chain diverges at the maximum frequency and at frequencies on either side of the gap while it tends to be a constant as  $\omega \rightarrow 0$ .

### SUGGESTED FURTHER READING

- Blackman, M., *Handbuch der Physik*, 7, 325 (Springer, 1955).  
 Gopal, E.S.R., *Specific Heats at Low Temperatures* (Plenum Press, 1966).  
 Ho, C.Y. and R.E. Taylor (Editors), *Thermal Conductivity* (Plenum, 1969).  
 Keesom, P.H. and N. Pearlman, *Handbuch der Physik*, 14, 282 (Springer, 1956).  
 Klemens, P.G., in F. Seitz and D. Turnbull (Editors), *Solid State Phys.*, Vol. 7 (Academic Press, 1958).  
 Launey, de J., in F. Seitz and D. Turnbull (Editors), *Solid State Phys.*, Vol. 2 (Academic Press, 1956).  
 Ziman, J.M., *Electrons and Phonons*, Chapter 8 (Oxford, 1960).

# Free Electron Theory of Metals

We know that more than a two-third of elements are metals. This shows that the natural tendency of elements is to favour the metallic state. Of the common solids most of which are insulators, metals have found the largest number of applications according them thereby a very special status. The striking physical properties that make them so attractive should emerge as natural consequences of a successful theory. It is easy to develop a theory for metals because of their relatively simple structure. Then, this theory can be extended to other solids with suitable modifications as the situation demands. As no perfect theory exists even today, we make an endeavour in this chapter to give an appropriate account of the main theoretical models proposed in order to explain the characteristic properties of metals.

The theory of metals heavily relies on the conviction that the valence electrons of metal atoms can be treated as free. The valence electrons are so loosely bound to the ion core that in the first approximation they may be considered to have freedom of moving through the volume of the metal. For example, the so called free nature of these electrons readily explains the metallic lustre as for free particles the emission of radiation immediately follows the process of absorption. The concept of free electron motion is indicated by the observed large electrical and thermal conductivities of metals. The free electrons in metals are called '*conduction electrons*' since they are responsible for the electric conduction. The collective body of conduction electrons contributed by individual metal atoms is conventionally interpreted as '*the free electron gas*' that occupies most of the volume of the metal. The fraction of volume belonging to the positive metal ions is mere 15 per cent in sodium metal. To sum up, a metallic crystal may be envisaged as the superposition of a periodic array of positive ion cores and a quasi-uniform negative charge density of the free electron gas.

The formulation of the theory of metals began well before the announcement of the Pauli principle (1926) and the advent of quantum mechanics (1925). Drude was the first to propose a model in 1900, three years after the discovery of electron by J.J. Thomson. Though the model operates in the domain of classical physics, its importance cannot be undermined in view of the amazing success it has achieved in deriving the Ohm's law and the relationship between the electrical and thermal conductivities. Its another feature of quickly demonstrating the behaviour of electrical conductivity further emphasizes the value of its contribution. A befitting account of this theory will be given in this chapter with a final word on the classical models. With the Pauli exclusion principle coming to force, the electrons in metals could no longer be treated by the classical statistics. The requirement that the electrons be subjected to the Pauli principle brought about a remarkable transformation in the theory which is now capable of addressing most of the questions left unanswered by the classical theory. This replaced the Maxwell-Boltzmann statistics by the Fermi-Dirac statistics and renamed the free electron gas as '*the free electron Fermi gas*'. Sommerfeld (1927) won the distinction of applying the related quantum mechanical ideas for the first time to explain the properties of metals. A suitable account of the Sommerfeld theory will lead us to a concluding discussion of this chapter.

## 6.1 THE DRUDE MODEL

The Drude model is essentially based on the classical kinetic theory of gases. According to Drude the metal must have two types of particles as against only one type in the simplest gases. The discovery of electrons bearing negative charge made it mandatory to accept the presence of positively charged entities (or particles) on the requirement of the charge neutrality condition. It is assumed that when metal atoms come together to form a metal, the valence electrons get liberated and move freely within the metal. The remainder of the atom is a positive ion carrying the major portion of the atomic mass. Drude took these particles as heavy and immobile. Under the action of an external electric field the free electrons referred to as conduction electrons in metals move in the background of immobile positive metal ions. In the absence of a relevant theoretical framework to deal with the free electron gas, Drude took recourse to the methods of kinetic theory of ideal gases for examining metallic conduction without getting deterred by the large electron densities ( $10^{22} \text{ cm}^{-3}$ ). It is assumed that the reader is acquainted with the postulates of kinetic theory of gases through a prior exposure, and therefore assumptions specific to only free electron gas are being given below:

1. The electron-electron and electron-ion interactions are neglected. The approach tantamounts to working in the independent electron approximation and the free electron approximation in that order. To be exact, the free electron approximation is not adhered to in strict literal sense because the electrons are considered to remain confined within the metal in the Drude Model and this is possible only if the electron-ion attractive force is active.
2. Under the action of an external electric field, electrons move opposite to the field direction and make collisions with immobile and impenetrable ion cores. An electron bumps<sup>†</sup> from ion to ion and between successive collisions moves in a straight line as determined by the Newton's equations of motion.
3. All electrons move with the RMS speed of a Maxwell-Boltzmann distribution, representing the random or thermal velocity of electrons. The average electron velocity immediately after the collision is zero.

### 6.1.1 Electrical Conductivity of Metals

#### *DC Conductivity*

We apply Drude theory first to derive an expression for dc conductivity. An external static electric field can affect electron velocity during the time interval between two successive collisions. But the gain in velocity is destroyed each time a collision occurs since the average velocity immediately after the collision is zero. A large influence of electric field is reflected in a larger mean free time or relaxation time  $\tau$ . The probability of collision per unit time is defined as  $1/\tau$ . Therefore, the probability that a collision occurs in a small time interval  $dt$  is simply  $dt/\tau$ .

Taking the acceleration of an electron of mass  $m$  as  $eE/m$ , the mean drift velocity can be written as

$$v_d = \left( -\frac{eE}{m} \right) \tau \quad (6.1)$$

<sup>†</sup> The collision involving physical contact is unrealistic. We, however, refrain from identifying the true scattering mechanism at this stage.